Mechanical integrators for constrained dynamical systems in flexible multibody dynamics

vom Fachbereich Maschinenbau und Verfahrenstechnik
der Technischen Universität Kaiserslautern
zur Verleihung des akademischen Grades
Doktor-Ingenieur (Dr.-Ing.)
genehmigte Dissertation

Dipl.-Math. techn. Sigrid Leyendecker

Preface

The work presented in this thesis has been carried out during the period 2002-2006 at the Chair of Applied Mechanics at the University of Kaiserslautern. The support of the DFG (Deutsche Forschungsgemeinschaft) within the project STE 544/17-1 entitled *'Objektive Balkenelemente für die Dynamik elastischer Mehrkörpersysteme'* is gratefully acknowledged.

My sincere gratefulness is dedicated to Professor Paul Steinmann for the constant guidance and support I was allowed to receive. I am especially thankful to Professor Peter Betsch who introduced me into the field of numerical mechanics and consequently supervised my work. And I would like to thank Professor Claus Führer very much for his interest in this work and many valuable remarks.

The working atmosphere at the Chair of Applied Mechanics is exceptionally pleasant wherefore all colleagues are sincerely thanked, in particular those who provided advise and assistance during these years.

Most of all I would like to express my deep gratitude to my family, friends and Manus for the strong support and continuous encouragement I enjoyed.

Kaiserslautern, June 2006   Sigrid Leyendecker

Contents

Nomenclature

Throughout this work, scalars as well as scalar valued functions (e.g. differential forms) and their values are denoted by small non-bold symbols. Vectors are denoted by small bold symbols, e.g. $\boldsymbol{a} = a_i \boldsymbol{e}_i$, where $\{\boldsymbol{e}_I\}$ always denotes a spatially fixed Cartesian basis of the three-dimensional inertial space. Einstein's summation convention is used to sum over repeated lower case indices. A capital symbol indexing a vector indicates that this vector belongs to a set (usually a triad) of vectors. Second order tensors are denoted by capital bold symbols. Calligraphic symbols denote sets or spaces of functions. Each $\cdot$ indicates one contraction, e.g. the scalar product of two vectors of equal dimension reads $\boldsymbol{a}^T \cdot \boldsymbol{b} = c$, a matrix product of two appropriate second order tensors reads $\boldsymbol{A} \cdot \boldsymbol{B} = \boldsymbol{C}$ and the product of a matrix with a vector reads $\boldsymbol{A} \cdot \boldsymbol{b} = \boldsymbol{c}$.

The symbol n is used twofold, first of all, it indicates the dimension of the configuration manifold and secondly, it is used as an index to represent approximations to quantities at the n-th time node t_n, e.g. $\boldsymbol{z}_n$ approximates $\boldsymbol{z}(t_n)$.

The system of equations of motion emanating from the use of the Lagrange multiplier method for the constraint enforcement is also called 'constrained formulation', similarly the corresponding time-stepping scheme is termed 'constrained scheme'. The use of the null space method leads to the 'reduced formulation' or 'd'Alembert-type formulation' of the equations of motion. Similarly, the discrete null space method gives rise to the 'reduced scheme' or 'd'Alembert-type scheme'.

In Chapter 4, 5 and 6, the numerical performance of different time-stepping schemes is compared with the help of various examples. In the corresponding tables, the order of magnitude of the constraint fulfilment and the condition number are given. In contrast to that, the number of unknowns is given exactly, while the CPU-time is specified as the ratio between the computation time for a certain number of time-steps by the specific scheme and that of the d'Alembert-type scheme with nodal reparametrisation.

Q	n-dimensional real configuration manifold (see A.1)
P	$2n$-dimensional real phase manifold
C	$(n-m)$-dimensional constraint manifold
TQ	tangent bundle (see A.3)
T^*Q	cotangent bundle (see A.3)
$\boldsymbol{q}$	configuration vector
$\dot{\boldsymbol{q}}$	velocity vector
$\boldsymbol{p}$	momentum vector
$\boldsymbol{z}$	phase vector
$\boldsymbol{\lambda}$	Lagrange multiplier
L	Lagrangian
H	Hamiltonian
T	kinetic energy
V	potential energy
P_H	extra function to treat the constraints in the Hamiltonian formalism
P_L	extra function to treat the constraints in the Lagrangian formalism
S	action integral
ω	symplectic form (see A.10)
$\mathbb{J}$	symplectic matrix
$\boldsymbol{J}$	momentum map (see A.21)
$\mathbb{F}L$	fibre derivative
X_H	Hamiltonian vector field (see A.16)
D	Jacobian (see A.4)
D_i	partial derivatives with respect to i-th argument
$\boldsymbol{d}$	exterior derivative (see A.9)
D	discrete derivative (see 3.1.1)
D^G	G-equivariant discrete derivative (see 3.1.4)
D_i	partial discrete derivative with respect to i-th argument (see 3.1.7)
d	discrete derivative on lower dimensional subspace (see 3.1.7)
$\boldsymbol{g}$	holonomic constraints
$\boldsymbol{G}$	constraint Jacobian
G	discrete derivative of the constraints
$\boldsymbol{P}$	null space matrix
P	discrete null space matrix
t	time
h	time-step
μ	penalty parameter
G	Lie group (see A.17)
$\mathfrak{g}$	Lie algebra (see A.18)
ϕ	action of a Lie group

$\boldsymbol{\varphi}$	placement of centre of mass
$\dot{\boldsymbol{\varphi}}$	translatorical velocity of placement of centre of mass
$\boldsymbol{p}_\varphi$	momentum conjugate to translatorical velocity of placement of centre of mass
$\{\boldsymbol{d}_I\}$	director triad
$\{\dot{\boldsymbol{d}}_I\}$	director velocities
$\boldsymbol{\omega}$	angular velocity
$\{\boldsymbol{p}_I\}$	momenta conjugate to director velocities
$\boldsymbol{\varrho}$	joint location with respect to body-fixed director triad
$\boldsymbol{u}_\varphi$	incremental displacement of centre of mass
$\boldsymbol{\theta}$	incremental rotation
$\mathcal{F}(P)$	set of continuously differentiable real-valued functions on P
$\mathcal{C}^k(A, B)$	set of k-times continuously differentiable functions from A to B
$\mathcal{P}^k(0, 1)^{2n}$	set of $2n$-dimensional real-valued polynomials of degree k on $[0, 1]$
δ_{ij}	Kronecker delta
ϵ_{ijk}	alternating symbol

1 Introduction

The numerical simulation of real physical processes is indispensable in all modern techno-
logical sciences, especially in mechanical engineering. It always relies on an idealisation
of the actual situation in a physical model, such that this can be described in terms of an
abstract mathematical model. In general, a mathematical model consists of (differential)
equations and side conditions. A solution of these equations represents the simulation of
the real process. The art of modelling lies in finding the balance between simplification
of the process in the physical model and veritableness of the resulting solution. As a
consequence of nonlinearities present in even the simplest useful models, an analytical
solution to the describing equations is rarely feasible. This causes the necessity for nu-
merical methods that approximate the solution of the mathematical model. Naturally
most realistic approximations are in demand which share the relevant properties of the
analytical solution while minimising the computational costs.
This work deals with the simulation of the dynamics of multibody systems consisting
of rigid and elastic components combined by joints. Typical applications are all kinds
of robot manipulators including industrial manufacturing robots or portage machinery,
as well as deployable structures such as space satellites. The simulation of multibody
dynamics combines several issues. First of all, flexible parts must be discretised in space
and a material model for their (elastic) behaviour has to be identified. Secondly, the
interconnections have to be taken into account. Typically they give rise to constraints
restricting the possible states of the system. The choice of a method to enforce the con-
straints completes the formulation of the evolution equations and side conditions in the
mathematical model. Finally these semi-discrete equations have to be discretised in time
resulting in time-stepping algorithms.

The equations of motion, which are the basis for mathematical models of dynamical pro-
cesses, can be derived in different contexts. On the one hand, force-based approaches lead
to Newton's second law. On the other hand, the Hamiltonian and the Lagrangian formal-
ism in analytical mechanics focus on the observation of energy and variational principles
which enhances their generality. The Hamiltonian formalism for instance can be used to
model classical mechanical systems as well as quantum dynamics, see [Pesk 95]. There-
fore, a representation in an abstract formalism, as introduced e.g. in [Abra 78, Hofe 94], is
necessary. A special property of the solutions of the equations of motion in Lagrangian or
Hamiltonian dynamics is the conservation of first integrals. Under certain suppositions,
the energy, momentum maps related to the system's symmetries and the symplectic form
remain unchanged along these solutions. See e.g. [Nolt 02, Gold 85] for classical intro-
ductions to analytical dynamics or [Olve 95] and references therein for a more theoretical
approach to the symmetries of differential equations and variational problems.

Flexible bodies can be modelled in the framework of nonlinear continuum mechanics [Holz 00, Mars 83, Beck 75] or nonlinear structural mechanics [Antm 95]. The spatial discretisation by finite elements divides the body into a finite number of disjoint regions – the elements. Classical introductions to the finite element method for nonlinear continuum or structural mechanics are [Zien 92, Zien 94, Bone 97, Bely 01, Wrig 01]. A fundamental requirement to the resulting semi-discrete mechanical system is objectivity (also termed frame-indifference), i.e. the resulting strain measures must be invariant with respect to superimposed rigid body motion. This restricts the possible discretisation techniques, especially in structural mechanics as pointed out in [Cris 99]. The flexible structure considered throughout this work is a geometrically exact beam, i.e. a deformable structure whose cross-sections are small compared to its length. The term geometrically exact refers to the allowance of large finite deformation requiring a geometrically nonlinear description. The modelling of geometrically exact beams as a special Cosserat continuum (which is a directed continuum, see e.g. [Antm 95]), has been the basis for many finite element formulations starting with the works of Simo [Simo 85, Simo 86b, Simo 88]. A realisation of the placements and orientations of the interior beam points in terms of translations and rotations is manifest and widely used, e.g. in [Ibra 98, Jele 98]. However, the interpolation of rotations is prone to violate the objectivity requirement. Thus the parametrisation of rotations is subject of many investigations including [Bets 98, Ibra 95, Ibra 97, Ibra 02b, Jele 99, Jele 02, Rome 04, Bott 02b, Bauc 03b]. A remedy was found independently by [Rome 02b] and [Bets 02d] in the spatial interpolation of director triads. To maintain the kinematic assumptions of the underlying continuous Timoshenko beam theory, each triad is required to stay orthonormal during motion and deformation of the beam, giving rise to so called internal constraints. The formulation of the beam dynamics as Hamiltonian system subject to internal constraints is particularly suited for a generalisation to multibody systems since rigid bodies can be described in the same way as directed constrained continua and, moreover, the interconnections to other components are modelled as external constraints which can be treated by analogy with the internal constraints.

For the enforcement of holonomic constraints, there are different methods at the disposal. The Lagrange multiplier method enlarges the number of unknowns by as many Lagrange multipliers as there are constraints. A solution of the resulting enlarged system fulfils the constraints exactly. In contrast to that, using the penalty method, the constrained motion is approximated by an unconstrained one under the influence of strong conservative forces. Thereby the magnitude of the so-called penalty parameter determines the accuracy of the solution's constraint fulfilment. The augmented Lagrange method can be interpreted as a combination of the just mentioned methods, with the difference, that the error in the constraint fulfilment is reduced below a prescribed tolerance by performing extra iterations. [Bert 95, Luen 84] offer general introductions to these three methods. A different approach to constrained systems is given by null space methods, see e.g. [Benz 05]. The main distinguishing feature is the elimination of the Lagrange multipliers (which can be interpreted as constraint forces) from the equations leading to a size reduction of the system of equations. This is accomplished by dint of a so-called null space matrix as

introduced in [Lian 87] among others. Since the null space matrix spans the null space of the constraint Jacobian, it is often referred to as natural orthogonal complement, e.g. by [Ange 89, Saha 99]. The elimination of the workless constraint forces is closely related to d'Alembert's principle (see e.g. [Arno 78]), wherefore the resulting form of the equations of motion is also termed d'Alembert-type formulation. Another way to deal with constraints is the reparametrisation of the system's description in terms of independent generalised coordinates. This method reduces the system's dimension to the minimal possible number and redundantises the constraints, see e.g. [Gold 85, Kuyp 03].

The temporal discretisation of the finite-dimensional system of nonlinear ordinary differential equations (ODEs) emanating from the spatial discretisation of a flexible body is – even without the consideration of constraints – comparatively demanding, see e.g. [Leim 04]. Especially if the resulting ODEs belong to the class of stiff equations, the design of stable time-stepping schemes is not an easy task as investigated by [Hair 96, Hair 00, Gonz 96a, Gonz 96b]. During the research of the last decades it has been recognised that the inheritance of the conservation of first integrals to the temporal discrete solution entails superior numerical performance of the specific integrator. Besides the benefit of increased numerical stability, the conservation of energy, momentum maps and the symplectic form along the discrete solution enhances its veritableness since the 'unique fingerprint of the process', i.e. its 'qualitative and structural characteristics' (see [Bott 02b]) are transferred to the discrete solution. Time-stepping schemes which inherit the (conservation) properties of the continuous mechanical system are referred to as 'mechanical integrators', according to [Mars 92]. Energy-momentum conserving schemes, relying on a direct discretisation of the ODEs, have been widely investigated, see e.g. [Bets 00a, Bets 00b, Bets 01a, Ibra 99, Ibra 02a, Arme 01a, Cris 96, Gonz 00, Hugh 78, LaBu 76a, LaBu 76b, Noel 04a, Reic 95, Simo 91a, Simo 91b, Simo 92a, Simo 94, Simo 95]. Based on the discretisation of the variational formulation behind the ODEs, symplectic-momentum integrators have been derived e.g. by [Bart 98, Hair 04, Jay 96, Leim 94, Leim 96, Lew 03, Reic 94, Kane 00, Mars 01]; see e.g. [Simo 92b, Simo 93] for a discussion on energy-momentum and symplectic schemes. Then again it is a common opinion that there are processes, e.g. highly oscillatory ones, for which stable time integration requires numerical damping, see e.g. [Arme 01a, Arme 01b, Arme 03, Bauc 96, Bott 02a, Hilb 77, Ibra 02a, Rome 02a].

The presence of constraints complicates the temporal integration of the system of equations substantially. Using the Lagrange multiplier method for the constraint enforcement results in differential algebraic equations (DAEs) of index three, see e.g. [Seil 99, Rhei 91, Deuf 00]. Due to the presence of the Lagrange multipliers, the direct application of ODE integrators leads to numerical difficulties as reported by [Petz 86, Hair 89, Gera 01]. However, well-performing integration schemes for the large dimensional DAEs have been designed recently e.g. by [Bets 01b, Bets 02b, Bets 02c, Eich 98, Fuhr 91, Arno 05, Gonz 99, Wend 97, Reic 96]. The description of the problem in terms of independent generalised coordinates by a local reparametrisation of the constraint manifold leads to highly complex ODEs for which the application of ODE integrators is generally possible but in most cases not recommendable, see [Leim 04, Rhei 84, Rhei 96, Rhei 97]. These problems can be overcome using the discrete null space method proposed by [Bets 05] which is investigated

extensively in this work – mainly and in-depth for the simulation of flexible multibody dynamics.

Time-stepping schemes for flexible multibody dynamics based on the solution of the DAEs have been developed by [Bets 02a, Bets 04, Ibra 00b, Bauc 99b, Bauc 99a, Bauc 03a]. A different procedure relying on the master-slave approach can be found in [Jele 96, Jele 01, Ibra 00a, Ibra 03]. An alternative to the semi-discretisation of elastic multibody systems using wavelets is proposed by [Diaz 03].

Main issues and outline of this work

The primary object of this work is the development of a robust, accurate and efficient time integrator for the dynamics of flexible multibody systems. Particularly a unified framework for the computational dynamics of multibody systems consisting of mass points, rigid bodies and flexible beams forming open kinematic chains or closed loop systems is developed. In addition, it aims at the presentation of (i) a focused survey of the Lagrangian and Hamiltonian formalism for dynamics, (ii) five different methods to enforce constraints with their respective relations, and (iii) three alternative ways for the temporal discretisation of the evolution equations. The relations between the different methods for the constraint enforcement in conjunction with one specific temporal discretisation method are proved and their numerical performances are compared by means of theoretical considerations as well as with the help of numerical examples.

Finite dimensional equations of motion are deduced in an abstract Lagrangian and Hamiltonian formalism in Chapter 2, providing a basis of the modelling of any dynamical process. The basic (conservation) properties of the solutions of these evolution equations are shown, in particular the conservation of energy, momentum maps related to the system's symmetries and symplecticity. The presentation of well-known classical theories on dynamics concludes with the sketch of specific momentum maps resulting from temporal, translational and rotational symmetry of the mechanical system. The second part of Chapter 2 is devoted to different methods for the enforcement of holonomic constraints: the Lagrange multiplier method, the penalty method, the augmented Lagrange method, the null space method and the reparametrisation in terms of generalised coordinates. The evolution equations resulting from the use of each method are given in Lagrangian and Hamiltonian formalism and their relations are discussed.

Chapter 3 starts with the presentation of the temporal discretisation of Hamilton's evolution equations using the concept of discrete derivatives and Galerkin-based finite elements in time, both resulting in energy-momentum conserving time-stepping schemes. Then the concept of variational integrators based on the direct discretisation of a variational principle is sketched. It leads to a symplectic-momentum conserving integrator. After a short motivation for the decision to use the Hamiltonian formalism in conjunction with the concept of discrete derivatives for the construction of an integrator, the resulting time-stepping schemes are given for all five methods to treat the constraints. Because of the relatively simple structure of the evolution equations emanating from the Lagrange multiplier method, the penalty method and the augmented Lagrange method (in particular

they contain constant mass matrices), these can be discretised easily. Furthermore the equivalence to the Lagrange multiplier scheme of the penalty scheme for penalty parameters tending to infinity and of the augmented Lagrange scheme for infinitely many iterations is proved explicitly. The d'Alembert-type equations and the evolution equations in terms of generalised coordinates contain configuration dependent mass matrices, complicating the temporal discretisation substantially. (The highly complicated configuration dependent mass matrix resulting from the description of a double spherical pendulum in generalised coordinates is given as a deterrent example in Appendix D.) However, they bear the advantageous properties of small dimensional systems (especially compared to the Lagrange multiplier system) and of exact constraint fulfilment (in contrast to the penalty system and the augmented Lagrange system, providing exact constraint fulfilment only in the limit cases). Thus despite the awkwardly complicated temporal discretisation procedure, they are promising to yield accurate and efficient time-stepping schemes. A remedy can be found in the discrete null space method which proposes a reversal of the two main steps when designing a specific numerical method. First of all, the simple structured DAEs emanating from the use of the Lagrange multiplier method are discretised in time. Then the transition to the d'Alembert-type scheme and finally the nodal reparametrisation is performed in the temporal discrete setting in complete analogy to the transition from the Lagrange multiplier formulation to the d'Alembert-type formulation and the reparametrisation in terms of generalised coordinates in the temporal continuous case. This transition involves the so-called discrete null space matrix for which different representations are ascertained. The comparison of the theoretical aspects of the five time-stepping schemes at the end of Chapter 3 shows that the d'Alembert-type scheme with nodal reparametrisation performs excellently in all relevant categories. First of all, it yields the smallest dimensional system of equations, promising lower computational costs than the other schemes. Secondly, the constraints are fulfilled exactly and thirdly, it is unconditionally well-conditioned, i.e. the condition number of the iteration matrix during the iterative solution procedure of the system of nonlinear algebraic equations is independent of the time-step. The dependence of the condition number of the specific schemes on the time-step or on other parameters is calculated generally for each scheme in Appendix C.

In Chapter 4, the performance and especially the equivalence of the different methods to treat the constraints are demonstrated illustratively for the dynamics of mass point systems and rigid bodies. For a double spherical pendulum, the time-stepping schemes emanating from the different methods for the constraint enforcement are given explicitly. The description of rigid body dynamics as Hamiltonian system subject to internal constraints serves as a basis for the objective description of spatially discretised beams in Chapter 5. Furthermore, it is shown that the d'Alembert-type formulation of the equations of rigid body motion coincides with the well-known Newton-Euler equations. Before the simulation of the motion of a heavy symmetrical top is documented at the end of Chapter 4, the treatment of boundary conditions and bearings by the null space method is outlined.

The formulation of the dynamics of a geometrically exact beam theory as Hamiltonian system subject to internal constraints is introduced in Chapter 5. A spatial discretisation using linear finite beam elements leads to objective discrete strain measures. Based on the

concept of discrete derivatives, an objective energy-momentum conserving time-stepping scheme is deduced. A numerical example illustrates the formerly developed relations between the time-stepping schemes emanating from the different constraint enforcement methods in the spatially distributed context.

The treatment of internally constrained rigid body or beam dynamics is generalised to the dynamics of multibody systems in a systematic way in Chapter 6. First of all, the enforcement of the internal and external constraints occurring in kinematic pairs using the Lagrange multiplier method and the discrete null space method with nodal reparametrisation is developed in detail. Specifically, the continuous and discrete null space matrices are given for the spherical, cylindrical, revolute, prismatic and planar pair and numerical examples are shown. Then the treatment of kinematic pairs is generalised to open kinematic chains consisting of an arbitrary number of rigid bodies and further on to closed kinematic chains, for which a numerical example is given in form of a six-body linkage. Finally the procedure is generalised to the treatment of arbitrary multibody systems consisting of rigid and elastic components. An instructive outline for the treatment of general multibody systems by the discrete null space method is given, providing a new robust, accurate and efficient integrator for flexible multibody dynamics. Finally an example of a spatial slider-crank mechanism containing flexible beams and rigid bodies is presented. After the conclusions in Chapter 7, the Appendix provides a collection of definitions of relevant notions. Moreover, it contains details concerning the implementation of the d'Alembert-type scheme and the discrete derivative in the spatially distributed case. It concludes with some historical remarks on the 'invertible cube' by Paul Schatz which is used in the example of the six-body linkage.

Einleitung

Die numerische Simulation tatsächlicher physikalischer Prozesse ist unverzichtbar in der modernen Technologie, speziell für Ingenieuranwendungen. Sie basiert immer auf der Idealisierung des vorliegenden Problems durch ein physikalisches Modell, welches wiederum durch ein abstraktes mathematisches Modell beschrieben werden kann. Im Allgemeinen besteht ein mathematisches Modell aus (Differential-) Gleichungen und Nebenbedingungen. Eine Lösung dieser Gleichungen stellt die Simulation des tatsächlichen Prozesses dar. Die Kunst des Modellierens liegt darin, ein ausgewogenes Verhältnis zwischen der Vereinfachung des Prozesses im physikalischen Modell und der Echtheit der resultierenden Lösung zu finden. Als Konsequenz von Nichtlinearitäten, die sogar in den einfachsten brauchbaren Modellen auftreten, ist das analytische Lösen der beschreibenden Gleichungen im mathematischen Modell meistens unmöglich. Daraus ergibt sich die Notwendigkeit für numerische Methoden, die diese Lösung approximieren. Natürlich sucht man nach möglichst realisitischen Approximationen, welche die relevanten Eigenschaften der tatsächlichen Lösungen innehaben und gleichzeitig den Rechenaufwand minimieren.
Die vorliegende Arbeit beschäftigt sich mit der Simulation der Dynamik von Mehrkörpersystemen, in denen starre und elastische Komponenten durch Gelenke verbunden sind. Typische Anwendungsbeispiele sind alle Arten von Robotern wie zum Beispiel Fertigungsroboter oder Beförderungsanlagen in der Industrie, aber auch ausschwenkbare Strukturen wie sie beispielsweise an Satelliten zu finden sind. Die Simulation der Dynamik flexibler Mehrkörpersysteme beinhaltet mehrere Aspekte. Zunächst müssen flexible Teile räumlich diskretisiert werden, und ein Modell für ihr (elastisches) Materialverhalten muss bestimmt werden. Des Weiteren müssen die Verbindungen zwischen den Körpern berücksichtigt werden. Typischerweise entstehen aus ihnen Zwangsbedingungen, welche die möglichen Zustände des Systems einschränken. Die Wahl einer Methode zur Realisierung dieser Zwangsbedingungen vervollständigt die Formulierung der Bewegungsgleichungen und Nebenbedingungen im mathematischen Modell. Schließlich müssen diese semi-diskreten Gleichungen auch zeitlich diskretisiert werden, damit ein Zeitschrittverfahren entsteht.

Die Bewegungsgleichungen, welche die Basis mathematischer Modelle für dynamische Prozesse bilden, können in unterschiedlichen Zusammenhängen hergeleitet werden. Auf der einen Seite führen kraftbasierte Ansätze zum zweiten Newtonschen Gesetz. Deutlich allgemeiner betrachten der Hamiltonsche und der Lagrangesche Formalismus der analytischen Mechanik Energie und Variationsprinzipien. So kann der Hamiltonsche Formalismus zum Beispiel sowohl zur Modellierung klassischer mechanischer Systeme als auch für quantendynamische Prozesse eingesetzt werden, siehe [Pesk 95]. Diese allgemeinen Ansätze bedienen sich eines abstrakten mathematischen Formalismus', wie er

z.B. in [Abra 78, Hofe 94] eingeführt wird. Eine spezielle Eigenschaft der Lösungen der Bewegungsgleichungen im Hamiltonschen und Lagrangeschen Formalismus ist die Konservierung von Erhaltungsgrößen entlang der Lösung. Unter bestimmten Voraussetzungen bleiben die Energie, Impulsabbildungen, die mit den Symmetrien des Systems zusammenhängen und die symplektische Form entlang der Lösung erhalten. Siehe z.B. [Nolt 02, Gold 85] für eine klassische Einführung in die analytische Dynamik oder [Olve 95] und Referenzen darin für eine theoretischere Herangehensweise an Differentialgleichungen mit Symmetrien und Variationsprobleme.

Flexible Körper können im Rahmen der nichtlinearen Kontinuumsmechanik [Holz 00, Mars 83, Beck 75] oder der nichtlinearen Strukturmechanik [Antm 95] modelliert werden. Die räumliche Diskretisierung mit finiten Elementen unterteilt den Körper in eine endliche Anzahl disjunkter Gebiete – die Elemente. Klassische Einführungen in die finite Elemente-Methode für nichtlineare Kontinuums- oder Strukturmechanik bieten [Zien 92, Zien 94, Bone 97, Bely 01, Wrig 01]. Eine fundamentale Bedingung an das resultierende semidiskrete System ist die Objektivität, d.h. die resultierenden Verzerrungsmaße müssen invariant gegenüber überlagerten Starrkörperbewegungen sein, was mögliche Diskretisierungstechniken einschränkt, wie in [Cris 99] gezeigt wird. In der vorliegenden Arbeit werden geometrisch exakte Balken als flexible Strukturen eingesetzt. Dies sind verformbare Körper, deren Querschnitte im Vergleich zu ihrer Länge klein sind. Sie können große endliche Verfomungen erfahren. Die Modellierung geometrisch exakter Balken als spezielles Cosserat-Kontinuum (welches ein gerichtetes Kontinuum darstellt, siehe [Antm 95]) bildet die Basis für viele finite Elemente-Formulierungen, angefangen mit den Arbeiten von Simo [Simo 85, Simo 86b, Simo 88]. Die Darstellung der Platzierungen und Orientierungen der inneren Balkenpunkte mittels Verschiebungen und Rotationen ist nahe liegend und wird weithin benutzt, z.B. in [Ibra 98, Jele 98]. Allerdings birgt die Interpolation von Rotationen die Gefahr, die Objektivitätsanforderungen zu verletzen, weshalb die Parametrisierung von Rotationen Gegenstand vieler Untersuchungen wie z.B. in [Bets 98, Ibra 95, Ibra 97, Ibra 02b, Jele 99, Jele 02, Rome 04, Bott 02b, Bauc 03b] war. Eine Möglichkeit diese Schwierigkeiten zu umgehen wurde unabhängig von [Rome 02b] und [Bets 02d] gefunden; die Darstellung des gerichteten Balkenkontinuums mit Direktortriaden erfüllt die Objektivitätsanforderungen. Um die kinematischen Voraussetzungen der Timoshenko-Balkentheorie zu erfüllen, wird verlangt, dass jede Direktortriade während der Bewegung und Verformung des Balkens orthonormal bleibt. Dies führt zu so genannten internen Zwangsbedingungen. Die Formulierung der Balkendynamik als Hamiltonsches System mit internen Zwangsbedingungen ist für eine Verallgemeinerung zu Mehrkörpersystemen besonders geeignet, da starre Körper in der selben Art und Weise als gerichtete Kontinua mit internen Zwangsbedingungen beschrieben werden können. Außerdem werden die Verbindungen zwischen den Komponenten als externe Zwangsbedingungen modelliert, welche analog zu den internen behandelt werden können.

Zur Erzwingung holonomer Zwangsbedingungen stehen verschiedene Methoden zur Verfügung. Die Lagrangesche Multiplikatoren-Methode erhöht die Anzahl der Unbekannten um so viele Lagrangesche Multiplikatoren, wie Zwangsbedingungen vorhanden sind. Eine

Lösung des resultierenden erweiterten Systems erfüllt die Zwangsbedingungen exakt. Im Gegensatz dazu approximiert die penalty-Methode das Problem mit Zwangsbedingungen durch eines ohne Zwangsbedingungen, welches dem Einfluss einer starken konservativen Kraft unterliegt. Dabei wird die Erfüllung der Zwangsbedingungen durch die Größenordnung des so genannten penalty-Parameters bestimmt. In der erweiterten Lagrangeschen Methode (welche als Kombination der gerade genannten Methoden interpretiert werden kann) wird die Verletzung der Zwangsbedingungen während einer zusätzlichen Iteration unter eine vorgegebene Toleranz reduziert. [Bert 95, Luen 84] bieten allgemeine Einführungen zu diesen drei Methoden. Eine andere Herangehensweise an Systeme mit Zwangsbedingungen stellt die so genannte Nullraum-Methode stellt dar, siehe z.B. [Benz 05]. Der Hauptunterschied besteht in der Eliminierung der Lagrangeschen Multiplikatoren (welche als Zwangskräfte interpretiert werden können), die gleichzeitig das Gleichungssystem reduziert. Diese Eliminierung wird mit Hilfe einer so genannten Nullraum-Matrix erreicht, die unter anderem in [Lian 87, Ange 89, Saha 99] eingeführt wird. Das reduzierte Gleichungssystem wird auch d'Alembertsche Formulierung genannt, da die Eliminierung der Zwangskräfte eng mit dem d'Alembertschen Prinzip zusammenhängt. Eine weitere Möglichkeit, die Zwangsbedingungen zu behandeln, ist die Reparametrisierung der Beschreibung des Problems in unabhängigen generalisierten Koordinaten. Diese reduziert das Gleichungssystem auf die minimal mögliche Dimension und macht die Zwangsbedingungen überflüssig, siehe [Gold 85, Kuyp 03].

Die zeitliche Diskretisierung des endlich-dimensionalen Systems gewöhnlicher Differentialgleichungen (ODEs), das aus der räumlichen Diskretisierung der flexiblen Körper hervorgeht, ist – auch ohne die Berücksichtigung von Zwangsbedingungen – relativ anspruchsvoll, siehe z.B. [Leim 04]. Die Entwicklung stabiler Zeitschrittverfahren ist besonders schwierig, wenn die resultierenden ODEs zur Klasse der steifen Systeme gehören, siehe [Hair 96, Hair 00, Gonz 96a, Gonz 96b]. Die Forschung der letzten Jahrzehnte hat ergeben, dass die Vererbung der Konservierung von Erhaltungsgrößen an das zeitlich diskrete System dessen numerisches Verhalten verbessert. Neben dem Vorteil der numerischen Stabilität erhöht die Konservierung von Energie, Impulsabbildung und symplektischer Form entlang der diskreten Lösung deren Echtheit, da der 'einzigartige Fingerabdruck des Prozesses', also seine 'qualitativen und strukturellen Charakteristika' (siehe [Bott 02b]) auf die diskrete Lösung übertragen werden. Solche Zeitschrittverfahren, die die (Erhaltungs-) Eigenschaften des kontinuierlichen Systems innehaben, werden nach [Mars 92] als 'mechanische Integratoren' bezeichnet. Auf der direkten Diskretisierung der ODEs basierende Energie-Impuls-erhaltende Verfahren wurden umfassend untersucht, siehe z.B. [Bets 00a, Bets 00b, Bets 01a, Ibra 99, Ibra 02a, Arme 01a, Cris 96, Gonz 00, Hugh 78, LaBu 76a, LaBu 76b, Noel 04a, Reic 95, Simo 91a, Simo 91b, Simo 92a, Simo 94, Simo 95]. Symplektisch-Impuls-erhaltende Integratoren, die auf der Diskretisierung der variationellen Formulierung beruhen, wurden z.B. in [Bart 98, Hair 04, Jay 96, Leim 94, Leim 96, Lew 03, Reic 94, Kane 00, Mars 01] hergeleitet; siehe z.B. [Simo 92b, Simo 93] für eine Erörterung Energie-Impuls-erhaltender und symplektischer Verfahren. Andererseits ist die Meinung weit verbreitet, dass für bestimmte Prozesse (wie z.B. stark oszillierende Bewegungen) numerische Dämpfung nötig ist, um stabile Zeitintegratoren zu erhalten,

siehe z.B. [Arme 01a, Arme 01b, Arme 03, Bauc 96, Bott 02a, Hilb 77, Ibra 02a, Rome 02a]. Durch die Gegenwart von Zwangsbedingungen wird die Zeitintegration der Bewegungsgleichungen wesentlich verkompliziert. Die Lagrangesche Multiplikatoren-Methode liefert ein System differential-algebraischer Gleichungen (DAEs) mit Index drei, siehe z.B. [Seil 99, Rhei 91, Deuf 00]. In [Petz 86, Hair 89, Gera 01] wird berichtet, dass die direkte Anwendung von ODE-Integratoren numerische Schwierigkeiten aufwirft. Dennoch wurden gut funktionierende Integratoren für große Systeme von DAEs in [Bets 01b, Bets 02b, Bets 02c, Eich 98, Fuhr 91, Arno 05, Gonz 99, Wend 97, Reic 96] entwickelt. Die Darstellung des Problems in unabhängigen generalisierten Koordinaten führt zu hochkomplexen ODEs (mit in der Regel konfigurationsabhängigen Massenmatrizen), für welche die Anwendung von ODE-Integratoren zwar möglich, jedoch meistens nicht zu empfehlen ist, siehe [Leim 04, Rhei 84, Rhei 96, Rhei 97]. Diese Probleme werden durch die diskrete Nullraum-Methode, welche in [Bets 05] vorgeschlagen wird, überwunden. Sie basiert auf der zeitlichen Diskretisierung der einfach strukturierten DAEs (insbesondere beinhalten diese eine konstante Massenmatrix) und der anschließenden Eliminierung der Lagrange Multiplikatoren aus dem Zeitschrittverfahren. Die diskrete Nullraum Methode wird in der vorliegenden Arbeit umfangreich untersucht – vor allem und eingehend für die Simulation flexibler Mehrkörperdynamik.

Basierend auf der Lösung der DAEs wurden Zeitschrittverfahren für flexible Mehrkörpersysteme in [Bets 02a, Bets 04, Ibra 00b, Bauc 99b, Bauc 99a, Bauc 03a] entwickelt. Ein anderes Verfahren beruht auf dem so genannten master-slave Ansatz, siehe z.B [Jele 96, Jele 01, Ibra 00a, Ibra 03]. In [Diaz 03] wird eine Alternative zur Semi-Diskretisierung elastischer Mehrkörpersysteme beschrieben, welche wavelets verwendet.

Hauptaspekte der vorliegenden Arbeit

Der Hauptanspruch der vorliegenden Arbeit ist die Entwicklung robuster, genauer und effizienter Zeitintegratoren für die Dynamik flexibler Mehrkörpersysteme. Insbesondere wird ein einheitlicher Rahmen für die numerische Dynamik von Mehrkörpersystemen bereitgestellt, in denen Massenpunkte, Starrkörper und elastische Balken sowohl offene als auch geschlossene kinematische Ketten bilden können. Außerdem werden (i) ein fokussierter Überblick über den Lagrangeschen und den Hamiltonschen Formalismus in der Dynamik, (ii) fünf verschiedene Methoden zur Realisierung von Zwangsbedingungen mit ihren Zusammenhängen und (iii) drei Alternativen für die zeitliche Diskretisierung von Bewegungsgleichungen präsentiert. Die Zusammenhänge zwischen den verschiedenen Methoden zur Zwangsbedingungsbehandlung in Verbindung mit einer bestimmten zeitlichen Diskretisierungsmethode werden bewiesen und ihre numerischen Verhaltensweisen werden anhand von theoretischen Überlegungen sowie mit Hilfe von numerischen Beispielen verglichen.

Aus den verschiedenen Methoden zur Realisierung der Zwangsbedingung hervorgehende Energie-Impuls-erhaltende Zeitschrittverfahren werden von Grund auf hergeleitet. Der Vergleich ihrer numerischen Verhaltensweisen ergibt, dass die Lagrangesche Multiplikatoren-Methode zwar direkt auf relativ komplexe Probleme angewandt werden kann, jedoch

muss dabei ein erweitertes System von DAEs gelöst werden. Dessen Lösung erfüllt die Zwangsbedingungen exakt, allerdings wird die Methode für große mechanische Systeme mit vielen Zwangsbedingungen sehr rechenaufwändig, und es treten schwerwiegende Konditionierungsprobleme auf. Die Lagrangesche Multiplikatoren-Methode liefert also genaue Lösungen, ist aber weder robust noch effizient. Problematisch bei der penalty-Methode ist, dass die Erfüllung der Zwangsbedingungen stark von der Wahl des penalty-Parameter abhängt. Während für höhere Genauigkeiten immer größere penalty-Parameter benötigt werden, wird das Gleichungssystem zunehmend steifer. Obwohl die penalty-Methode sehr genaue Ergebnisse liefern kann, wird dieser Aspekt durch die damit einhergehende schlechte Konditionierung des Gleichungssystems bzw. den hohen Rechenaufwand, der nötig ist, wenn die schlechte Konditionierung durch einen besonders kleinen Zeitschritt verbessert werden soll, negiert. Die auffallendste Eigenschaft der erweiterten Lagrangeschen Methode ist der immens hohe Rechenaufwand, welcher sie im Vergleich mit den anderen Methoden disqualifiziert. Es wird durch theoretische Analysen und durch numerische Beispiele klar, dass die diskrete Nullraum-Methode in allen Kategorien exzellent abschneidet. Diese Methode liefert genaue Lösungen – die Zwangsbedingungen sind exakt erfüllt, der Rechenaufwand ist vergleichsweise gering, da das Gleichungssystem auf seine minimal mögliche Dimension reduziert wird, und sie ist robust, da die Konditionierung des Gleichungssystems vom Zeitschritt unabhängig ist.

Das Herzstück der diskreten Nullraum-Methode ist die diskrete Nullraum-Matrix, deren Haupteigenschaften in Bemerkung 3.2.7 zusammengefasst sind. Mit ihrer Hilfe werden die Lagrangeschen Multiplikatoren aus dem zeitlich diskreten Gleichungssystem eliminiert und gleichzeitig die Dimension des Systems reduziert. Die wichtige Frage 'Wie kann eine diskrete Nullraum-Matrix gefunden werden?' wird in der vorliegenden Arbeit explizit für allgemeine flexible Mehrkörpersysteme beantwortet. Es kann festgehalten werden, dass eine explizite Darstellung der diskreten Nullraum-Matrix immer wünschenswert ist, da sie den Rechenaufwand minimiert. Solch eine explizite Darstellung kann für die meisten Anwendungsbeispiele gefunden werden, z.B. für die Massenpunktsysteme, die Starrkörperdynamik, die offenen kinematischen Ketten und für die Dynamik flexibler Balken, die in der vorliegenden Arbeit behandelt werden. Einzig bei der Simulation der Dynamik der geschlossenen Kette ist eine spezielle Vorgehensweise nötig, bei der die diskrete Nullraum-Matrix implizit konstruiert wird.

In Abschnitt 6.3.1 wird die Vorgehensweise zur Simulation der Dynamik flexibler Mehrkörpersysteme mit der diskreten Nullraum-Methode allgemein beschrieben. Sie führt zu einem neuen, robusten, genauen und effizienten Integrator für die flexible Mehrkörperdynamik. Die explizit angegebenen diskreten Nullraum-Matrizen für die internen Zwangsbedingungen in der Starrkörperdynamik und der Dynamik räumlich diskretisierter Balken sowie die angegebenen diskreten Nullraum-Matrizen für die externen Zwangsbedingungen, die sich aus der Verbindung kinematischer Paare durch Gelenke ergeben, können dabei benutzt werden.

2 Finite dimensional equations of motion

In classical analytical mechanics, the investigation of the temporal evolution of the states of a macroscopic physical system is based on the analysis of a scalar quantity, the energy. In contrast to that, a force-based approach leads to Newton's second law. Two main branches developed during the progression of analytical mechanics. The Lagrangian formulation is evolved from the observation that there are variational principles behind the fundamental laws of force balance. The Hamiltonian formalism focuses on the observation of energy and can be embedded into a certain geometrical structure. Although for most applications a representation of the formalisms in the framework of linear spaces is sufficient, a short overview of a more abstract formulation is given here as well. 'The treatment may seem unnecessarily abstract, but it is of ultimate benefit for a thorough understanding.' [Abra 78] A detailed presentation of these theories is established in [Mars 94] and a more classical approach can be found e.g. in [Gold 85].

2.1 Lagrangian mechanics

2.1.1 Euler-Lagrange equations

Consider an n-dimensional real differentiable configuration manifold (see A.1) Q with local coordinates $\boldsymbol{q} = (q^1, \ldots, q^n)$ that are at least two times continuously differentiable real-valued functions $q^i(t) : [t_0, t_1] \to \mathbb{R}$, $i = 1, \ldots, n$ on a bounded time interval. Together with the corresponding velocities $\dot{q}^i = dq^i/dt$, the tangent bundle TQ (see A.3), representing the phase space in the Lagrangian formalism, is described. Given a Lagrangian function $L : TQ \to \mathbb{R}$, the action integral $S(\boldsymbol{q}) = \int_{t_0}^{t_1} L(\boldsymbol{q}, \dot{\boldsymbol{q}}) \, dt$ is defined. Hamilton's principle of critical action states that

$$\delta S(\boldsymbol{q}) = \delta \int_{t_0}^{t_1} L(\boldsymbol{q}, \dot{\boldsymbol{q}}) \, dt = 0 \tag{2.1.1}$$

where variations amongst the paths $q^i(t)$ with fixed endpoints are taken. If (2.1.1) is to hold for arbitrary variations, the Euler-Lagrange equations

$$\frac{d}{dt} \left(\frac{\partial L(\boldsymbol{q}, \dot{\boldsymbol{q}})}{\partial \dot{\boldsymbol{q}}} \right) - \frac{\partial L(\boldsymbol{q}, \dot{\boldsymbol{q}})}{\partial \boldsymbol{q}} = 0 \tag{2.1.2}$$

are induced. Together with initial conditions $\boldsymbol{q}(t_0) = \boldsymbol{q}_0, \dot{\boldsymbol{q}}(t_0) = \dot{\boldsymbol{q}}_0$ the n-dimensional system (2.1.2) of second order differential equations defines a mechanical system's dynamics uniquely.

2.1.2 Abstract Lagrange equations

For a given Lagrangian $L : TQ \to \mathbb{R}$ the fibre derivative $\mathbb{F}L : TQ \to T^*Q$ allows the transition from the tangent bundle to its cotangent bundle T^*Q (see A.3) via

$$\mathbb{F}L(q^i, \dot{q}^i) = \left(q^i, \frac{\partial L}{\partial \dot{q}^i}\right) = (q^i, p_i) \qquad i = 1, \dots, n \tag{2.1.3}$$

Hereby L is called hyperregular if $\mathbb{F}L$ is a diffeomorphism.

Remark 2.1.1 The cotangent bundle T^*Q (see A.3) has an intrinsic symplectic structure that can be represented by the canonical symplectic form $\omega : T(T^*Q) \times T(T^*Q) \to \mathbb{R}$, $\omega = dq^i \wedge dp_i$. Thus (T^*Q, ω) is a symplectic manifold (see A.10). Then $\theta : T(T^*Q) \to \mathbb{R}$, $\theta = p_i dq^i$ constitutes the corresponding canonical one-form with $\boldsymbol{d}\theta = -\omega$ (here $\boldsymbol{d}$ denotes the exterior derivative see A.9).

By pulling these canonical forms on T^*Q back to TQ, one obtains the Lagrangian one-form $\theta_L : T(TQ) \to \mathbb{R}$ and the closed Lagrangian two-form $\omega_L : T(TQ) \times T(TQ) \to \mathbb{R}$

$$\theta_L = (\mathbb{F}L)^* \theta \qquad \omega_L = (\mathbb{F}L)^* \omega = -\boldsymbol{d}\theta_L \tag{2.1.4}$$

Defining the energy $E : TQ \to \mathbb{R}$ of a Lagrangian L as $E(q^i, \dot{q}^i) = \dot{q}^i \frac{\partial L}{\partial \dot{q}^i} - L(q^i, \dot{q}^i)$, a vector field $Y : TQ \to T(TQ)$ is called Lagrangian vector field, if

$$(\omega_L)_{\boldsymbol{v}}\left(Y(\boldsymbol{v}), \boldsymbol{w}\right) = \boldsymbol{d}E(\boldsymbol{v}) \cdot \boldsymbol{w} \quad \text{ for all } \boldsymbol{v} \in TQ \text{ and } \boldsymbol{w} \in T_{\boldsymbol{v}}(TQ) \tag{2.1.5}$$

For hyperregular Lagrangians, ω_L is symplectic, thus Y is a Hamiltonian vector field (see A.16) of E with respect to ω_L. For given initial conditions $\boldsymbol{v}(t_0) = (\boldsymbol{q}_0, \dot{\boldsymbol{q}}_0) \in TQ$, a curve $\boldsymbol{v}(t) = (\boldsymbol{q}(t), \dot{\boldsymbol{q}}(t))$ satisfies the Euler-Lagrange equations (2.1.2) if and only if it is an integral curve of Y through $\boldsymbol{v}(t_0)$. More generally, solutions of (2.1.2) can be identified with the Lagrangian flow $\boldsymbol{v} : [t_0, t_1] \times TQ \to TQ$ generated by the Lagrangian vector field Y. Note that by slight abuse of terminology, for constant $t \in [t_0, t_1]$ the map $\boldsymbol{v}_t : TQ \to TQ$ is also termed flow.

Proposition 2.1.2 (Energy conservation) *The energy E is conserved along a solution of the Euler-Lagrange equations.*

Proof: The skew-symmetry of ω_L induces

$$\begin{aligned} \frac{d}{dt}E(\boldsymbol{v}(t)) &= \boldsymbol{d}E(\boldsymbol{v}(t)) \cdot \dot{\boldsymbol{v}}(t) = (\omega_L)_{\boldsymbol{v}(t)}(Y(\boldsymbol{v}(t)), \dot{\boldsymbol{v}}(t)) \\ &= (\omega_L)_{\boldsymbol{v}(t)}(Y(\boldsymbol{v}(t)), Y(\boldsymbol{v}(t)) = 0 \end{aligned} \tag{2.1.6}$$

for integral curves $\boldsymbol{v}(t) \in TQ$ of Y. $\blacksquare$

Proposition 2.1.3 (Symplecticity) *The Lagrangian flow $\boldsymbol{v} : [t_0, t_1] \times TQ \to TQ$ preserves the symplectic form ω_L, i.e. $\boldsymbol{v}_t^* \omega_L = \omega_L$ for all $t \in [t_0, t_1]$.*

Proof: Since Y is a Hamiltonian vector field (see A.16) of E with respect to ω_L, $L_Y \omega_L = 0$ holds. Using the Lie derivative Theorem (see A.15) one gets

$$\frac{d}{dt}(\boldsymbol{v}_t^* \omega_L) = \boldsymbol{v}_t^* L_Y \omega_L = 0 \tag{2.1.7}$$

Thus $\boldsymbol{v}_t^* \omega_L$ is independent of t, and since $\boldsymbol{v}_0 = Id$, it equals ω_L. ∎

Noether's theorem states that the presence of symmetry in a mechanical system leads to a quantity's conservation along the solution of the equations of motion. If the Lie group G (see A.17) acts canonically (see A.20, A.12) on the configuration manifold Q via ϕ, this action can be extended to an action $\check{\phi} = (\phi, T\phi)$ on TQ in a natural way by tangent lift (see A.4). A Lagrangian $L : TQ \to \mathbb{R}$ is called G-invariant with respect to the action of G, if $L \circ \check{\phi}_g = L$ for all $g \in G$. Let $\mathfrak{g}$ denote the Lie algebra (see A.18) of G and $\mathfrak{g}^*$ its dual. Using the definition of the fibre derivative (2.1.3), a momentum map (see A.21) $\boldsymbol{J}_L : TQ \to \mathfrak{g}^*$ for a G-invariant Lagrangian is given by

$$\langle \boldsymbol{J}_L(\boldsymbol{v}), \xi \rangle = \langle \mathbb{F}L(\boldsymbol{v}), \xi_Q(\boldsymbol{q}) \rangle = \frac{\partial L}{\partial \dot{q}^i} \xi_Q^i(\boldsymbol{q}) \tag{2.1.8}$$

where $\xi_Q(\boldsymbol{q}) \in TQ$ is the infinitesimal generator (see A.20) of the action corresponding to $\xi \in \mathfrak{g}$.

Proposition 2.1.4 (Momentum conservation) *For a G-invariant Lagrangian, the momentum map $\boldsymbol{J}_L$ is conserved along a solution of the Euler-Lagrange equations.*

Proof: Taking the time derivative of the ξ-component of the momentum map yields

$$\frac{d}{dt} J_L^\xi = \frac{d}{dt}\left(\frac{\partial L}{\partial \dot{q}^i} \xi_Q^i(\boldsymbol{q})\right) = \left(\frac{d}{dt}\frac{\partial L}{\partial \dot{q}^i}\right) \xi_Q^i(\boldsymbol{q}) + \frac{\partial L}{\partial \dot{q}^i}\left(T\xi_Q(\boldsymbol{q}) \cdot \dot{\boldsymbol{q}}\right)^i \tag{2.1.9}$$

The G-invariance of L implies $L(T\exp(s\xi) \cdot \boldsymbol{v}) = L(\boldsymbol{v})$ corresponding to

$$\frac{\partial L}{\partial q^i} \xi_Q^i(\boldsymbol{q}) + \frac{\partial L}{\partial \dot{q}^i}\left(T\xi_Q^i(\boldsymbol{q}) \cdot \dot{\boldsymbol{q}}\right)^i = 0 \tag{2.1.10}$$

at the infinitesimal level. Insertion into (2.1.9) yields

$$\frac{d}{dt} J_L^\xi = \left(\frac{d}{dt}\frac{\partial L}{\partial \dot{q}^i} - \frac{\partial L}{\partial q^i}\right) \xi_Q^i(\boldsymbol{q}) \tag{2.1.11}$$

Thus along solutions of the Euler-Lagrange equations, (2.1.11) vanishes. Since ξ was arbitrary, it follows that the momentum map $\boldsymbol{J}_L$ is conserved by the Lagrangian flow. ∎

2.2 Hamiltonian mechanics

While the Lagrangian formalism relies on the coordinate's position and velocity in the phase space TQ, the Hamiltonian formalism considers the position and the momentum conjugate to the velocity as independent coordinates in the phase space T^*Q, which is the cotangent bundle (see A.3) to the configuration manifold Q.

2.2.1 Hamilton's equations

The fibre derivative (2.1.3) is used to perform the Legendre transformation

$$p_i = \frac{\partial L}{\partial \dot{q}^i} \qquad i = 1, \ldots, n \tag{2.2.1}$$

Then the Hamiltonian $H : T^*Q \to \mathbb{R}$ of a mechanical system is defined as

$$H(q^i, p_i) = p_j \dot{q}^j - L(q^i, \dot{q}^i) \tag{2.2.2}$$

Assuming that the transformation $(q^i, \dot{q}^i) \to (q^i, p_i)$ specified by (2.2.1) is invertible and considering the partial derivatives of the Hamiltonian yields

$$\frac{\partial H}{\partial p_i} = \dot{q}^i + p_j \frac{\partial \dot{q}^j}{\partial p_i} - \frac{\partial L}{\partial \dot{q}^j} \frac{\partial \dot{q}^j}{\partial p_i} = \dot{q}^i$$

$$\frac{\partial H}{\partial q_i} = p_j \frac{\partial \dot{q}^j}{\partial q_i} - \frac{\partial L}{\partial q^i} - \frac{\partial L}{\partial \dot{q}^j} \frac{\partial \dot{q}^j}{\partial q^i} = -\frac{\partial L}{\partial q^i} \tag{2.2.3}$$

Thus Hamilton's equations

$$\begin{aligned} \dot{\boldsymbol{q}} &= \frac{\partial H(\boldsymbol{q}, \boldsymbol{p})}{\partial \boldsymbol{p}} \\ \dot{\boldsymbol{p}} &= -\frac{\partial H(\boldsymbol{q}, \boldsymbol{p})}{\partial \boldsymbol{q}} \end{aligned} \tag{2.2.4}$$

together with initial conditions $\boldsymbol{q}(t_0) = \boldsymbol{q}_0, \boldsymbol{p}(t_0) = \boldsymbol{p}_0$ are a $2n$-dimensional system of first order differential equations, which is equivalent to the Euler-Lagrange equations (2.1.2).

2.2.2 Abstract Hamilton equations

Consider the symplectic manifold (T^*Q, ω) mentioned in Remark 2.1.1. A vector field $X : T^*Q \to T(T^*Q)$ is called Hamiltonian vector field (see A.16) of the function $H : T^*Q \to \mathbb{R}$ with respect to ω, if $\mathsf{i}_X \omega = \boldsymbol{d}H$ holds. Then X is denoted by X_H. Using the definition of the contraction i_X of a vector field and a two-form (see A.8), this condition reads more explicitly

$$(\mathsf{i}_{X_H} \omega)_{\boldsymbol{z}}(\boldsymbol{y}) = \omega_{\boldsymbol{z}}(X_H(\boldsymbol{z}), \boldsymbol{y}) = \boldsymbol{d}H(\boldsymbol{z})(\boldsymbol{y}) \quad \text{for all } \boldsymbol{z} \in T^*Q \text{ and } \boldsymbol{y} \in T_{\boldsymbol{z}}(T^*Q) \tag{2.2.5}$$

Hamilton's equations (2.2.4) can be written as the evolution equations

$$\dot{\boldsymbol{z}}(t) = X_H(\boldsymbol{z}(t)) \tag{2.2.6}$$

Remark 2.2.1 In case of (T^*Q, ω) being a $2n$-dimensional linear space, the Hamiltonian vector field can be expressed in terms of the gradient of H as

$$X_H(\boldsymbol{z}(t)) = \mathbb{J} \cdot \nabla H(\boldsymbol{z}(t)) \tag{2.2.7}$$

where the symplectic matrix $\mathbb{J}$ reads

$$\mathbb{J} = \begin{pmatrix} \boldsymbol{0} & \boldsymbol{I}_n \\ -\boldsymbol{I}_n & \boldsymbol{0} \end{pmatrix} \tag{2.2.8}$$

with $\boldsymbol{I}_n$ denoting the $n \times n$ identity matrix.

Since (2.2.4) and (2.2.6) are apparently equivalent, for given initial conditions $\boldsymbol{z}(t_0) = (\boldsymbol{q}_0, \boldsymbol{p}_0) \in T^*Q$, a curve $\boldsymbol{z}(t) = (\boldsymbol{q}(t), \boldsymbol{p}(t))$ satisfies Hamilton's equations (2.2.4) if and only if it is an integral curve of X_H through $\boldsymbol{z}(t_0)$. More generally, a solution of (2.2.4) can be identified with the Hamiltonian flow $\boldsymbol{z} : [t_0, t_1] \times T^*Q \to T^*Q$ generated by the Hamiltonian vector field X_H. Note that by slight abuse of terminology, for constant $t \in [t_0, t_1]$ the map $\boldsymbol{z}_t : T^*Q \to T^*Q$ is also termed flow.

Remark 2.2.2 (Equivalence of Hamilton's and Euler-Lagrange equations) The transition from the Lagrangian to the Hamiltonian formalism given by the fibre derivative (2.1.3) is a diffeomorphism for hyperregular Lagrangians. In this case, Hamilton's equations (2.2.6) are equivalent to the Euler-Lagrange equations (2.1.2) in the sense that the corresponding vector fields $Y : TQ \to T(TQ)$ and $X_H : T^*Q \to T(T^*Q)$ and their flow maps $\boldsymbol{v} : [t_0, t_1] \times TQ \to TQ$ and $\boldsymbol{z} : [t_0, t_1] \times T^*Q \to T^*Q$ are related via pullback by the fibre derivative

$$Y = (\mathbb{F}L)^* X_H \qquad v = (\mathbb{F}L)^{-1} \circ \boldsymbol{z} \circ \mathbb{F}L \tag{2.2.9}$$

Remark 2.2.3 (Hamiltonian and energy) Many applications are assumed to take place in an inertial frame and furthermore it is assumed that all appearing external loads are conservative. Then the Hamiltonian represents the total energy of the mechanical system.

Proposition 2.2.4 (Energy conservation) *The Hamiltonian H is conserved along a solution of Hamilton's equations.*

Proof: The skew-symmetry of ω induces

$$\begin{aligned}
\frac{d}{dt} H(\boldsymbol{z}(t)) &= \boldsymbol{d}H(\boldsymbol{z}(t)) \cdot \dot{\boldsymbol{z}}(t) = (\omega)_{\boldsymbol{z}(t)}(X_H(\boldsymbol{z}(t)), \dot{\boldsymbol{z}}(t)) \\
&= (\omega)_{\boldsymbol{z}(t)}(X_H(\boldsymbol{z}(t)), X_H(\boldsymbol{z}(t))) = 0
\end{aligned} \tag{2.2.10}$$

for integral curves $\boldsymbol{z}(t) \in T^*Q$ of X_H. ∎

Proposition 2.2.5 (Symplecticity) *The Hamiltonian flow $\boldsymbol{z} : [t_0, t_1] \times T^*Q \to T^*Q$ preserves the symplectic form ω, i.e. $\boldsymbol{z}_t^* \omega = \omega$ for all $t \in [t_0, t_1]$.*

Proof: Since X_H is a Hamiltonian vector field (see A.16) of H with respect to ω, $L_{X_H}\omega = 0$ holds. Using the Lie derivative Theorem (see A.15) one gets

$$\frac{d}{dt}(\boldsymbol{z}_t^* \omega) = \boldsymbol{z}_t^* L_{X_H} \omega = 0 \tag{2.2.11}$$

Thus $\boldsymbol{z}_t^* \omega$ is independent of t, and since $\boldsymbol{z}_0 = Id$, it equals ω. ∎

Hence the rich theory on symplectic transformations (see A.12, [Mars 94], [Mars 92], [Abra 78], [Bern 98]) can be applied to Hamiltonian flows. Some important properties of symplectic transformations are presented in the sequel. By the same argument as in the proof of Proposition 2.2.5, the following proposition can be proved:

Proposition 2.2.6 *The flow $\varphi : [t_0, t_1] \times P \to P$ of a vector field X on a symplectic manifold (P, ω) consists of symplectic transformations (i.e. $\varphi_t^* \omega = \omega$ for all $t \in [t_0, t_1]$) if and only if X is locally Hamiltonian.*

Proposition 2.2.7 *A symplectic transformation $f : P_1 \to P_2$ between symplectic manifolds (P_1, ω_1) and (P_2, ω_2) of the same dimension is volume preserving.*

Proof: Since the wedge product commutes with pull backs, the Liouville measure Λ (see A.22) is preserved, i.e. $f^* \Lambda = \Lambda$.
Alternatively for (P_1, ω_1) and (P_2, ω_2) being symplectic vector spaces, the Jacobian (see A.4) of f fulfils $Df \cdot \mathbb{J} \cdot D^T f = \mathbb{J}$, taking determinants shows that $|\det Df| = 1$. ∎

Proposition 2.2.8 states that the set of Hamiltonian vector fields is invariant under symplectic transformations:

Proposition 2.2.8 *Let $f : P_1 \to P_2$ be a symplectic transformation between the symplectic manifolds (P_1, ω_1) and (P_2, ω_2), i.e. $f^* \omega_2 = \omega_1$. Then for every function $H : P_2 \to \mathbb{R}$*

$$f^* X_H = X_K \qquad and \qquad K = H \circ f \tag{2.2.12}$$

Proof: In view of the definition of a Hamiltonian vector field (see A.16) the following equation holds

$$\mathsf{i}_{X_{H \circ f}} \omega_1 = \boldsymbol{d}(H \circ f) = f^*(\boldsymbol{d}H) = f^*(\mathsf{i}_{X_H} \omega_2) = \mathsf{i}_{f^* X_H}(f^* \omega_2) = \mathsf{i}_{f^* X_H} \omega_1 \tag{2.2.13}$$

Since ω_1 is nondegenerate, the vector fields $X_{H \circ f}$ and $f^* X_H$ must be equal. ∎

Similar to the Lagrangian formulation, Noether's theorem states that in the presence of symmetry in the mechanical system, there exists a quantity that is conserved along the solution of Hamilton's equations. The canonical action ϕ of a Lie group G (see A.17) on the configuration manifold Q induces an action $\hat{\phi}_g = (\phi_g, T^* \phi_g)$ on $P = T^* Q$ by cotangent lift (see A.6). Let $\mathfrak{g}$ denote the Lie algebra (see A.18) of G and $\mathfrak{g}^*$ its dual. If the Hamiltonian is invariant under the action of G, i.e. $H \circ \hat{\phi}_g = H$ for all $g \in G$, a momentum map $\boldsymbol{J} : T^* Q \to \mathfrak{g}^*$ (see A.21) is given by

$$\langle \boldsymbol{J}(\boldsymbol{z}), \xi \rangle = \langle \boldsymbol{z}, \xi_Q(\boldsymbol{q}) \rangle \tag{2.2.14}$$

where $\xi_Q(\boldsymbol{q}) \in TQ$ is the infinitesimal generator (see A.20) of the action corresponding to $\xi \in \mathfrak{g}$.

Proposition 2.2.9 (Momentum conservation) *For a G-invariant Hamiltonian, the momentum map $\boldsymbol{J}$ is conserved along the solution of Hamilton's equations.*

Proof: $\hat{\phi}_g$ is the flow of the vector field ξ_P that belongs to the function $J(\xi) \in \mathcal{F}(P)$. Differentiating the invariance condition $H \circ \hat{\phi}_g = H$ with respect to g at the neutral element e in the direction of ξ, one obtains

$$\frac{d}{dg}\left(H \circ \hat{\phi}_g\right)\big|_{g=e} \cdot \xi = \boldsymbol{d}H(\boldsymbol{z}) \cdot \xi_P(\boldsymbol{z}) = \{H, J(\xi)\} = 0 \quad \text{for all } \xi \in \mathfrak{g} \tag{2.2.15}$$

According to the properties of the Poisson bracket $\{\,\cdot\,,\,\cdot\,\}$ (see A.23), it follows that for each Lie algebra element ξ, $J(\xi) \in \mathcal{F}(P)$ (see A.21) is conserved along the trajectories of the Hamiltonian vector field X_H, thus the values of the corresponding $\mathfrak{g}^*$-valued momentum map $\boldsymbol{J}$ are also conserved along the solution of Hamilton's equations. ∎

2.2.3 Examples of momentum maps

A physical interpretation of the specific conserved quantity is often desirable for practical applications. Therefore, some common momentum maps are deduced in the established theoretical framework.

Remark 2.2.10 The assumption of a Lagrangian being hyperregular, such that the transition to the Hamiltonian formalism given by the fibre derivative in (2.1.3) is a diffeomorphism, is reasonable for many applications. Since in this case Hamilton's equations are equivalent to the Euler-Lagrange equations (see Remark 2.2.2) the examples of momentum maps given here in the Hamiltonian formalism can be easily transferred to the Lagrangian formalism.

Hamiltonian

The flow $\varphi : \mathbb{R} \times T^*Q \to T^*Q$ of a Hamiltonian vector field X_H on $P = T^*Q$ can be interpreted as $\mathbb{R}$-action on T^*Q, i.e. $G = \mathfrak{g} = \mathbb{R}$. According to Proposition 2.2.4, the Hamiltonian is invariant under that action. The infinitesimal generator (see A.20) of the action corresponding to $\xi \in \mathfrak{g}$ is given by

$$\xi_P(\boldsymbol{z}) = \frac{d}{ds}\varphi(\exp(s\xi), \boldsymbol{z})|_{s=0} = X_H(\varphi(0, \boldsymbol{z}))\xi = X_H(\boldsymbol{z})\xi \tag{2.2.16}$$

The condition $X_{J(\xi)}(\boldsymbol{z}) = \xi_P(\boldsymbol{z})$ (see A.21) implies that $J(\xi)(\boldsymbol{z}) = H(\boldsymbol{z})\xi$ for all $\xi \in \mathfrak{g}$ and as expected, the corresponding momentum map $J(\boldsymbol{z}) = H(\boldsymbol{z})$ equals the Hamiltonian itself.

Linear momentum

Let $Q = \mathbb{R}^n$ and let $G = \mathbb{R}^n$ operate on Q by translation, i.e. $\phi : G \times Q \to Q$ is given by

$$\phi(\boldsymbol{g}, \boldsymbol{q}) = \boldsymbol{g} + \boldsymbol{q} \tag{2.2.17}$$

Then the infinitesimal generator (see A.20) of the action corresponding to $\xi \in \mathfrak{g} = \mathbb{R}^n$ is given by

$$\xi_Q(\boldsymbol{q}) = \frac{d}{ds}\phi(\exp(s\xi), \boldsymbol{q})|_{s=0} = \xi \tag{2.2.18}$$

According to (2.2.14) a momentum map can be calculated as

$$\langle \boldsymbol{J}(\boldsymbol{z}), \xi \rangle = \boldsymbol{p} \cdot \xi \tag{2.2.19}$$

thus $\boldsymbol{J}(\boldsymbol{z}) = \boldsymbol{p}$ is the linear momentum.

Angular momentum

Let the Lie group of proper rotations $G = SO(3)$ act on the configuration space $Q = \mathbb{R}^3$ via

$$\phi(\boldsymbol{A}, \boldsymbol{q}) = \boldsymbol{A} \cdot \boldsymbol{q} \tag{2.2.20}$$

The action corresponding to the skew-symmetric matrix $\xi \in \mathfrak{g} = \mathfrak{so}(3)$ has the infinitesimal generator (see A.20)

$$\xi_Q(\boldsymbol{q}) = \frac{d}{ds}\phi(\exp(s\xi), \boldsymbol{q})|_{s=0} = \xi \cdot \boldsymbol{q} \tag{2.2.21}$$

Identifying $\mathfrak{so}(3)$ with $\mathbb{R}^3$ (equipped with the cross product) via the isomorphism $\widehat{\,\,}: \mathbb{R}^3 \to \mathfrak{so}(3)$ (see A.24), the infinitesimal generator corresponding to $\xi = \widehat{\boldsymbol{\mu}} \in \mathfrak{so}(3)$ reads

$$\xi_Q(\boldsymbol{q}) = \widehat{\boldsymbol{\mu}} \cdot \boldsymbol{q} = \boldsymbol{\mu} \times \boldsymbol{q} \tag{2.2.22}$$

Using (2.2.14), a momentum map is given by

$$\langle \boldsymbol{J}(\boldsymbol{z}), \xi \rangle = (\xi \cdot \boldsymbol{q}) \cdot \boldsymbol{p} = (\boldsymbol{\mu} \times \boldsymbol{q}) \cdot \boldsymbol{p} = (\boldsymbol{q} \times \boldsymbol{p}) \cdot \boldsymbol{\mu} \tag{2.2.23}$$

thus $\boldsymbol{J}(\boldsymbol{z}) = \boldsymbol{q} \times \boldsymbol{p}$ denotes the angular momentum.

2.3 Constrained mechanical systems

Many mechanical systems are not free to move in an n-dimensional configuration manifold since they are subject to constraints. These restrictions are expressed as specific relationships between certain coordinates, their rates of change, and possibly time. Geometric restrictions are restrictions on the configuration of the system expressed in the form

$$\boldsymbol{g} : [t_0, t_1] \times Q \to \mathbb{R}^m \tag{2.3.1}$$

and called holonomic constraints. The consistency condition that the constraints must be fulfilled at all times induces the temporal differentiated form of the constraints $\boldsymbol{f} = d\boldsymbol{g}/dt$. These are integrable kinematic restrictions of the form

$$\boldsymbol{f} : [t_0, t_1] \times TQ \to \mathbb{R}^m \tag{2.3.2}$$

Any constraint that cannot be put in the form of a geometric or integrable restriction is called nonholonomic constraint. In both cases the number of degrees of freedom is reduced, i.e. the mechanical system is constrained to a lower dimensional manifold. Furthermore, one distinguishes between rheonomic constraints that depend explicitly on time and scleronomic constraints where the time does not explicitly appear. This standard classification of constraints is discussed in books on classical mechanics like [Gold 85, Toro 00, Mars 94], examples of holonomic and nonholonomic constraints are expatiated in [Kuyp 03, Nolt 02]. In this work only scleronomic holonomic constraints are considered. Different methods for their treatment are presented in the sequel.

2.3.1 Lagrange multiplier method

Consider a mechanical system in an n-dimensional configuration manifold Q subject to holonomic scleronomic constraints $\boldsymbol{g} : Q \to \mathbb{R}^m$ requiring $\boldsymbol{g}(\boldsymbol{q}) = \boldsymbol{0}$. In this work it is always supposed that $\boldsymbol{0} \in \mathbb{R}^m$ is a regular value (see A.25) of the constraints, such that

$$C = \boldsymbol{g}^{-1}(\boldsymbol{0}) = \{\boldsymbol{q}|\boldsymbol{q} \in Q, \boldsymbol{g}(\boldsymbol{q}) = \boldsymbol{0}\} \subset Q \tag{2.3.3}$$

is an $(n-m)$-dimensional submanifold (see A.26), called constraint manifold. Just as C can be embedded in Q via $i : C \to Q$, its $2(n-m)$-dimensional tangent bundle (see A.3)

$$TC = \left\{(\boldsymbol{q}, \dot{\boldsymbol{q}})|(\boldsymbol{q}, \dot{\boldsymbol{q}}) \in T_{\boldsymbol{q}}Q, \boldsymbol{g}(\boldsymbol{q}) = \boldsymbol{0}, \boldsymbol{G}(\boldsymbol{q}) \cdot \dot{\boldsymbol{q}} = \boldsymbol{0}\right\} \subset TQ \tag{2.3.4}$$

can be embedded in TQ in a natural way by tangent lift $Ti : TC \to TQ$ (see A.4). Here and in the sequel $\boldsymbol{G}(\boldsymbol{q}) = D\boldsymbol{g}(\boldsymbol{q})$ denotes the $m \times n$ Jacobian (see A.4) of the constraints.

Lagrangian formalism

A Lagrangian $L : TQ \to \mathbb{R}$ can be restricted to $L^C = L|_{TC}\colon TC \to \mathbb{R}$. To investigate the relationship of the dynamics of L^C on TC to the dynamics of L on TQ, the following notation is used. $\mathcal{C}(Q) = \mathcal{C}([t_0, t_1], Q, \boldsymbol{q}_0, \boldsymbol{q}_1)$ denotes the space of smooth functions satisfying $\boldsymbol{q}(t_0) = \boldsymbol{q}_0$ and $\boldsymbol{q}(t_1) = \boldsymbol{q}_1$ where $\boldsymbol{q}_0, \boldsymbol{q}_1 \in C \subset Q$ are fixed endpoints. Let $\mathcal{C}(C)$ denote the corresponding space of curves in C and set $\mathcal{C}(\mathbb{R}^m) = \mathcal{C}([t_0, t_1], \mathbb{R}^m)$ to be the space of curves $\boldsymbol{\lambda} : [t_0, t_1] \to \mathbb{R}^m$ with no boundary conditions. This notation has been introduced in [Mars 01], where a large part of the theory presented here can be found.

Theorem 2.3.1 *Suppose that $\boldsymbol{0}$ is a regular value of the scleronomic holonomic constraints $\boldsymbol{g} : Q \to \mathbb{R}^m$ and set $C = \boldsymbol{g}^{-1}(\boldsymbol{0}) \subset Q$. Let $L : TQ \to \mathbb{R}$ be a Lagrangian and $L^C = L|_{TC}$ its restriction to TC. Then the following statements are equivalent:*

(i) $\boldsymbol{q} \in \mathcal{C}(C)$ *extremises the action integral* $S^C(\boldsymbol{q}) = \displaystyle\int_{t_0}^{t_1} L^C(\boldsymbol{q}, \dot{\boldsymbol{q}})\, dt$ *and hence solves the Euler-Lagrange equations for L^C.*

(ii) $\boldsymbol{q} \in \mathcal{C}(Q)$ *and $\boldsymbol{\lambda} \in \mathcal{C}(\mathbb{R}^m)$ satisfy the constrained Euler-Lagrange equations*

$$\begin{aligned} \frac{d}{dt}\left(\frac{\partial L(\boldsymbol{q}, \dot{\boldsymbol{q}})}{\partial \dot{\boldsymbol{q}}}\right) - \frac{\partial L(\boldsymbol{q}, \dot{\boldsymbol{q}})}{\partial \boldsymbol{q}} + \boldsymbol{G}^T(\boldsymbol{q}) \cdot \boldsymbol{\lambda} &= \boldsymbol{0} \\ \boldsymbol{g}(\boldsymbol{q}) &= \boldsymbol{0} \end{aligned} \tag{2.3.5}$$

(iii) $(\boldsymbol{q}, \boldsymbol{\lambda}) \in \mathcal{C}(Q \times \mathbb{R}^m)$ *extremise $\bar{S}(\boldsymbol{q}, \boldsymbol{\lambda}) = S(\boldsymbol{q}) - \langle \boldsymbol{\lambda}, \boldsymbol{g}(\boldsymbol{q})\rangle$ and hence, solve the Euler-Lagrange equations for the augmented Lagrangian $\bar{L} : T(Q \times \mathbb{R}^m) \to \mathbb{R}$ defined by*

$$\bar{L}(\boldsymbol{q}, \boldsymbol{\lambda}, \dot{\boldsymbol{q}}, \dot{\boldsymbol{\lambda}}) = L(\boldsymbol{q}, \dot{\boldsymbol{q}}) - \boldsymbol{g}^T(\boldsymbol{q}) \cdot \boldsymbol{\lambda} \tag{2.3.6}$$

The proof given in [Mars 01] makes use of the Lagrange multiplier theorem (see e.g. [Abra 88]).

Equations $(2.3.5)_1$ are often called Lagrange equations of motion of first kind like, e.g. in [Kuyp 03, Nolt 02]. Together with the constraints, they constitute a system of $n+m$ second order differential and algebraic equations (DAEs) of index three (see [Bren 96, Petz 86]), which is also called descriptor form of the equations of motion and requires non-standard methods for the numerical solution (see [Fuhr 91]). The last term in $(2.3.5)_1$ represents the constraint forces that prevent the system from deviations of the constraint manifold (2.3.3).

Hamiltonian formalism

The augmented Hamiltonian $\bar{H} : T^*(Q \times \mathbb{R}^m) \to \mathbb{R}$ corresponding to the augmented Lagrangian in (2.3.6) is given by

$$\bar{H}(\boldsymbol{q}, \boldsymbol{\lambda}, \boldsymbol{p}, \boldsymbol{\pi}) = H(\boldsymbol{q}, \boldsymbol{p}) + \boldsymbol{g}^T(\boldsymbol{q}) \cdot \boldsymbol{\lambda} \tag{2.3.7}$$

Since $\bar{L}$ is degenerate in $\boldsymbol{\lambda}$, the momentum $\boldsymbol{\pi}$ conjugate to $\boldsymbol{\lambda}$ is constrained to be zero and consequently the Legendre transform is not invertible. Pulling back the canonical form ω on T^*Q to the primary constraint set $\Pi \subset T^*(Q \times \mathbb{R}^m)$ defined by $\boldsymbol{\pi} = 0$, one obtains a closed, but possibly degenerate, two-form ω^Π. Seeking $X_{\bar{H}}$ such that $\mathrm{i}_{X_{\bar{H}}}\omega^\Pi = \boldsymbol{d}\bar{H}$ gives no equation for $\boldsymbol{\lambda}$. However, the other equations constitute the constrained Hamilton's equations

$$
\begin{aligned}
\dot{\boldsymbol{q}} &= \frac{\partial H(\boldsymbol{q}, \boldsymbol{p})}{\partial \boldsymbol{p}} \\
\dot{\boldsymbol{p}} &= -\frac{\partial H(\boldsymbol{q}, \boldsymbol{p})}{\partial \boldsymbol{q}} - \boldsymbol{G}^T(\boldsymbol{q}) \cdot \boldsymbol{\lambda} \\
0 &= \boldsymbol{g}(\boldsymbol{q})
\end{aligned}
\tag{2.3.8}
$$

forming $2n + m$ first order differential and algebraic equations, which are equivalent to (2.3.5). The general theory appropriate for degenerate systems is Dirac's theory of constraints [Dira 50], see also [Mars 94]. A major difficulty in this approach is that there is no canonical embedding of T^*C in T^*Q. However for hyperregular Lagrangians, such an embedding is given in [Mars 01].

Remark 2.3.2 (Conservation properties of constrained systems) The constrained systems (2.3.5) on TC and (2.3.8) on T^*C are standard Lagrangian and Hamiltonian systems respectively, and therefore, have the usual conservation properties. See [Mars 01] for further details.

A smooth solution $(\boldsymbol{q}, \boldsymbol{p}, \boldsymbol{\lambda})(t)$ of (2.3.8) naturally fulfils the consistency condition $d\boldsymbol{g}(\boldsymbol{q})/dt = \boldsymbol{0}$, i.e. $(\boldsymbol{q}, \boldsymbol{p})(t) \in T^*C$. Using $(2.3.8)_1$ this condition leads to the 'hidden' constraints on momentum level (also called secondary constraints, see [Dira 50, Seil 99])

$$\boldsymbol{f}(\boldsymbol{q}, \boldsymbol{p}) = \boldsymbol{G}(\boldsymbol{q}) \cdot \frac{\partial H}{\partial \boldsymbol{p}} = \boldsymbol{0} \tag{2.3.9}$$

which are (by slight abuse of notation, see (2.3.2)) also denoted by $\boldsymbol{f} : T^*Q \to \mathbb{R}^m$. They can be explicitly incorporated into the equations of motion by a further augmentation of the Hamiltonian in (2.3.7) according to

$$\bar{\bar{H}}(\boldsymbol{q}, \boldsymbol{\lambda}, \boldsymbol{\gamma}, \boldsymbol{p}, \boldsymbol{\pi}, \boldsymbol{\vartheta}) = H(\boldsymbol{q}, \boldsymbol{p}) + \boldsymbol{g}^T(\boldsymbol{q}) \cdot \boldsymbol{\lambda} + \boldsymbol{f}^T(\boldsymbol{q}, \boldsymbol{p}) \cdot \boldsymbol{\gamma} \tag{2.3.10}$$

The Hamiltonian $\bar{\bar{H}} : T^*(Q \times \mathbb{R}^m \times \mathbb{R}^m) \to \mathbb{R}$ gives rise to the $2(n+m)$-dimensional system of DAEs

$$
\begin{aligned}
\dot{\boldsymbol{q}} &= \quad \frac{\partial H(\boldsymbol{q}, \boldsymbol{p})}{\partial \boldsymbol{p}} + D_2^T \boldsymbol{f}(\boldsymbol{q}, \boldsymbol{p}) \cdot \boldsymbol{\gamma} \\
\dot{\boldsymbol{p}} &= \quad -\frac{\partial H(\boldsymbol{q}, \boldsymbol{p})}{\partial \boldsymbol{q}} - \boldsymbol{G}^T(\boldsymbol{q}) \cdot \boldsymbol{\lambda} - D_1^T \boldsymbol{f}(\boldsymbol{q}, \boldsymbol{p}) \cdot \boldsymbol{\gamma} \\
\boldsymbol{0} &= \quad \boldsymbol{g}(\boldsymbol{q}) \\
\boldsymbol{0} &= \quad \boldsymbol{f}(\boldsymbol{q}, \boldsymbol{p})
\end{aligned}
\tag{2.3.11}
$$

which is equivalent to that in (2.3.8), see e.g. [Bets 02b, Leim 04]. In this connection, partial derivatives D_1 and D_2 are associated with the usual Jacobian D (see A.4). Although being formally desirable since the configuration variable and the momentum variable are dealt with on an equal footing in the Hamiltonian formalism, the inclusion of the momentum constraints does not alter the properties of the solution of the equations of motion in the temporal continuous setting. The projection method presented in [Gear 85] constitutes a different approach based on the stabilisation of an index reduced system of DAEs.

Remark 2.3.3 (Secondary constraints / hidden constraints) In the temporal discrete setting, algorithmic solutions of (2.3.8) obtained by numerical integration do not a priori fulfil the secondary constraints (2.3.9) at the time nodes. However, the investigation of several numerical examples dealing with point mass systems, rigid bodies and geometrically exact beams (e.g. in [Bets 02d], [Bets 03]) has brought forward that the incorporation of the temporally differentiated form of the constraints has not lead to crucial advantages (besides the fulfilment of the secondary constraints themselves). This fact is also reported in [Gonz 99] and references therein. The solution of the smaller dimensional Hamiltonian system has not been influenced considerably by their fulfilment. Therefore, avoiding unnecessary computational efforts, in the sequel, the attention is restricted to the enforcement of the constraints on configuration level, although the Hamiltonian formalism allows for the incorporation of secondary constraints in an obvious systematic way.

Augmented Hamiltonian and Lagrangian formulation

The treatment of the constraints shall be represented generally by the scalar valued $\mathcal{C}^1$-function $P_{con} : \boldsymbol{g}(Q) \to \mathbb{R}$ that is required to be of the form

$$
P_{con}(\boldsymbol{g}(\boldsymbol{q})) \geq 0 \quad \text{for all } \boldsymbol{q} \in Q \qquad P_{con}(\boldsymbol{g}(\boldsymbol{q})) = 0 \iff \boldsymbol{g}(\boldsymbol{q}) = \boldsymbol{0}
\tag{2.3.12}
$$

The extra function P_{con} to treat the constraints is assumed to be composed of the functions $\boldsymbol{v} = \boldsymbol{v}(t), \boldsymbol{R} = \boldsymbol{R}(\boldsymbol{g}(\boldsymbol{q}(t)))$. The product $P_{con}(\boldsymbol{g}(\boldsymbol{q})) = \boldsymbol{v}\boldsymbol{R}(\boldsymbol{g}(\boldsymbol{q}))$ must be scalar. Further conditions on $\boldsymbol{v}, \boldsymbol{R}$ can be deduced from (2.3.12). In order to unify the domains of the functions composing H and L, the functions $P_H : T^*Q \to \mathbb{R}$ with $P_H(\boldsymbol{z}) = P_{con}(\boldsymbol{g}(\boldsymbol{q}))$ and $P_L : Q \to \mathbb{R}$ with $P_L(\boldsymbol{q}) = P_{con}(\boldsymbol{g}(\boldsymbol{q}))$ are introduced.

A deviation of the mechanical system from the constraint manifold is interpreted as a contribution to the systems potential energy. In cases of conservative mechanical systems

(see Remark 2.2.3), where the Hamiltonian and the Lagrangian function can be separated into the contribution of kinetic and potential energy, the following parametrisation is introduced

$$
\begin{aligned}
H_{aug}(\boldsymbol{z}) &= H(\boldsymbol{z}) + P_H(\boldsymbol{z}) = T_H(\boldsymbol{z}) + V_H(\boldsymbol{z}) + P_H(\boldsymbol{z}) \\
L_{aug}(\boldsymbol{q}, \dot{\boldsymbol{q}}) &= L(\boldsymbol{q}, \dot{\boldsymbol{q}}) - P_L(\boldsymbol{q}) = T_L(\dot{\boldsymbol{q}}) - V_L(\boldsymbol{q}) - P_L(\boldsymbol{q})
\end{aligned}
\tag{2.3.13}
$$

comprising the kinetic energy T and the potential energy V.

Remark 2.3.4 (Separable energies) In (2.3.13) the Hamiltonian and the Lagrangian are separated into the contributions of the kinetic energy, the potential energy and the extra function to treat the constraints. For the Lagrangian, also the dependence of the energies on either the configuration or the velocity composing the phase variable $\boldsymbol{v} = (\boldsymbol{q}, \dot{\boldsymbol{q}}) \in TQ$ is apparent. This separation is hidden for the Hamiltonian, since the unified parametrisation in the phase variable $\boldsymbol{z} = (\boldsymbol{q}, \boldsymbol{p}) \in T^*Q$ is useful for the discretisation using a G-equivariant discrete derivative described in Section 3.1.1. In the sequel it is assumed that the energy functions fulfil the following natural conditions:

(i) $\quad H_{aug}, L_{aug} \in \mathcal{C}^1(P, \mathbb{R})$ where $P \in \{T^*Q, TQ\}$

(ii) $\quad D_1 T_H(\boldsymbol{z}) = D_2 V_H(\boldsymbol{z}) = D_2 P_H(\boldsymbol{z}) = \boldsymbol{0}$

(iii) $\quad T_H(\boldsymbol{z}) \geq 0 \quad$ for all $\quad \boldsymbol{z} \in T_{\boldsymbol{q}}^* Q \quad$ and $\quad T_H(\boldsymbol{z}) = 0 \quad \Longleftrightarrow \quad \boldsymbol{p} = \boldsymbol{0}$

$\quad\quad T_L(\dot{\boldsymbol{q}}) \geq 0 \quad$ for all $\quad \dot{\boldsymbol{q}} \in TQ \quad\quad$ and $\quad T_L(\dot{\boldsymbol{q}}) = 0 \quad \Longleftrightarrow \quad \dot{\boldsymbol{q}} = \boldsymbol{0}$

$\quad\quad\quad\quad\quad\quad\quad\quad\quad\quad\quad\quad\quad\quad\quad\quad\quad\quad\quad\quad\quad\quad\quad\quad\quad\quad\quad\quad\quad\quad (2.3.14)$

(iv) $\quad V_H$ is bounded from below, i.e. $\exists V_H^*$ with $\displaystyle\inf_{\boldsymbol{z} \in T^*Q} V_H(\boldsymbol{z}) \geq V_H^* > -\infty$

$\quad\quad V_L$ is bounded from below, i.e. $\exists V_L^*$ with $\displaystyle\inf_{\boldsymbol{q} \in Q} V_L(\boldsymbol{z}) \geq V_L^* > -\infty$

According to the method used to treat the constraints, the additional function P_{con} takes different forms. For the Lagrange multiplier method $\boldsymbol{v} = \boldsymbol{\lambda}, \boldsymbol{R}(\boldsymbol{g}(\boldsymbol{q})) = \boldsymbol{g}(\boldsymbol{q})$. Hence $P_{\mathrm{Lag}}(\boldsymbol{g}(\boldsymbol{q})) = \boldsymbol{g}^T(\boldsymbol{q}) \cdot \boldsymbol{\lambda}$ and the augmented Hamiltonian and Lagrangian correspond to those given in (2.3.7) and (2.3.6) respectively. The equations of motion are then obtained by insertion of H_{aug} and L_{aug} into (2.2.4) and (2.1.2) respectively and supplementation of the resulting systems by the constraint equations. This yields the constrained Hamilton's equations (2.3.8) and the constrained Euler-Lagrange equations (2.3.5).

2.3.2 Penalty method

In optimisation, the main idea of penalty methods is to eliminate the constraints and to add high costs to infeasible points (see e.g. [Bert 95]). In the context of constrained dynamical systems, the intention of penalty methods is to approximate the constrained motion by unconstrained motions in a conservative force field. To this end, a penalty function yields a contribution to the system's potential such that it grows large when the system deviates from the constraint manifold (2.3.3). Thereby, the penalty parameter determines the severity of the violation of the constraints. Generally, as better approximations of the constrained motion are achieved by increasing penalty parameters, the structure of the resulting system becomes more and more unfavourable. There exist so called exact penalty functions that yield the exact solution to the original constrained

problem for a finite value of the penalty parameter, but they introduce the difficulty of not being differentiable (see e.g. [Luen 84]).

For the present investigation of constrained motions of mechanical systems, the question whether or to what extent a sequence of penalty potentials will produce unconstrained motions that converge to a given constrained motion is answered in [Rubi 57] and [Born 96]. The penalty potential can be introduced in terms of the extra function P_{con} to treat the constraints defined in the last Section. Beyond (2.3.12), other conditions on P_{con} to be a penalty function are that

(i) P_{con} must be convex

(ii) P_{con} must be at least quadratic in $\boldsymbol{g}$

$$(2.3.15)$$

The penalty function in use in this work is of the form $P_{\mathrm{P}en}(\boldsymbol{g}(\boldsymbol{q})) = \mu R(\boldsymbol{g}(\boldsymbol{q}))$ with the constant penalty parameter $\mu \in \mathbb{R}^+$ and the function $R : \boldsymbol{g}(Q) \to \mathbb{R}$ such that (2.3.12) and (2.3.15) are fulfilled. A widely-used example of a penalty function is $P_{\mathrm{P}en}(\boldsymbol{g}(\boldsymbol{q})) = \mu \big\|\boldsymbol{g}(\boldsymbol{q})\big\|^2$.

Lagrangian formalism

Using the penalty method in the context of the Lagrangian formalism, the Lagrangian function is augmented by the additional function $P_L(\boldsymbol{q}) = P_{\mathrm{P}en}(\boldsymbol{g}(\boldsymbol{q}))$ according to (2.3.13). Inserting L_{aug} into the Euler-Lagrange equations (2.1.2) yields an n-dimensional system of unconstrained second order differential equations. The accuracy to which the constraints are fulfilled by its solution depends on the magnitude of the penalty parameter. In [Rubi 57], Rubin and Ungar prove the following important theorem. The proof relies on the energy-conservation along solutions of the Euler-Lagrange equations (see Proposition 2.1.2) and the boundedness of the potential energy (see property (iv) in (2.3.14)).

Theorem 2.3.5 *For a sequence of penalty parameters $(\mu_s)_{s \in \mathbb{N}}$ with $\lim_{s \to \infty} \mu_s = \infty$, the limit point $(\boldsymbol{q}(t), \dot{\boldsymbol{q}}(t)) = \lim_{s \to \infty} (\boldsymbol{q}^s(t), \dot{\boldsymbol{q}}^s(t))$ of the sequence of solutions – where $(\boldsymbol{q}^s(t), \dot{\boldsymbol{q}}^s(t))$ solve the Euler-Lagrange equations (2.1.2) corresponding to μ_s – fulfils the constraints. Furthermore there exists a multiplier $\boldsymbol{\lambda}$, such that $(\boldsymbol{q}(t), \dot{\boldsymbol{q}}(t), \boldsymbol{\lambda})$ solve the constrained Euler-Lagrange equations (2.3.5).*

In [Born 96], Bornemann and Schütte carry on with that issue and offer an abstract approach relying on the weak convergence in the sense of distributions. They even give explicitly the sequence converging to the correct Lagrange multiplier.

Hamiltonian formalism

In context of the Hamiltonian formalism, the use of the penalty method to enforce the constraints requires the augmentation of the Hamiltonian by $P_H(\boldsymbol{z}) = P_{\mathrm{P}en}(\boldsymbol{g}(\boldsymbol{q}))$ according to (2.3.13). Then the $2n$-dimensional system of unconstrained Hamilton's equations is obtained by insertion of H_{aug} into (2.2.4). In cases where the Legendre transformation specified in (2.2.1) is invertible (see Remark 2.2.2), Theorem 2.3.5 can be directly transformed to the following equivalent statement.

Theorem 2.3.6 *For a sequence of penalty parameters $(\mu_s)_{s \in \mathbb{N}}$ with $\lim\limits_{s \to \infty} \mu_s = \infty$, the limit point $(\boldsymbol{q}(t), \boldsymbol{p}(t)) = \lim\limits_{s \to \infty} (\boldsymbol{q}^s(t), \boldsymbol{p}^s(t))$ of the sequence of solutions – where $(\boldsymbol{q}^s(t), \boldsymbol{p}^s(t))$ solve the Hamilton's equations (2.2.4) corresponding to μ_s – fulfils the constraints. Furthermore there exists a multiplier $\boldsymbol{\lambda}$, such that $(\boldsymbol{q}(t), \boldsymbol{p}(t), \boldsymbol{\lambda})$ solve the constrained Hamilton's equations (2.3.8).*

In Section (3.2.2) a corresponding result is shown for a certain class of discrete Hamiltonian systems.

Remark 2.3.7 In practice, the penalty method entails a number of drawbacks:

(i)   Moderate penalty parameters do usually allow unacceptable constraint violation.

(ii)   Large penalty parameters lead to stiff systems that may cause unstable numerical solutions.

2.3.3 Augmented Lagrange method

The augmented Lagrange method can be regarded as a combination of a penalty method and a dual method. Dual methods are based on the idea that the Lagrange multipliers are the fundamental unknowns in a constrained problem. They have meaningful interpretations, such as the costs to keep the system on the constraint manifold. A physically insightful interpretation of the augmented Lagrange method in the context of dynamical systems can be found in [Blaj 02] and [Bert 95, Luen 84] offer a general introduction.

The extra function to treat the constraints by the augmented Lagrange method is a combination of those used in the previous methods

$$P_{\mathrm{Aug}}(\boldsymbol{g}(\boldsymbol{q})) \;\; = \;\; \boldsymbol{g}^T(\boldsymbol{q}) \cdot \boldsymbol{\lambda} + \mu R(\boldsymbol{g}(\boldsymbol{q})) \tag{2.3.16}$$

with the difference that $\mu \in \mathbb{R}^+$ needs not to tend to infinity to fulfil the constraints. Instead of that, it may remain of relatively moderate value and the improvement in the constraints is achieved by passing through an extra loop. The multipliers are determined during an iteration process instead of being unknown variables.

Lagrangian formalism

As for the penalty method, the Lagrangian function is augmented by the additional function $P_L(\boldsymbol{q}) = P_{\mathrm{Aug}}(\boldsymbol{g}(\boldsymbol{q}))$ according to (2.3.13). Starting with $\boldsymbol{\lambda}_0 = \boldsymbol{0}$, in each iteration the n-dimensional system of unconstrained Euler-Lagrange equations (2.1.2) with a fixed value $\boldsymbol{\lambda}_k$ is solved for $(\boldsymbol{q}^k, \dot{\boldsymbol{q}}^k)$. Then the multiplier is updated according to the Uzawa-like rule

$$\boldsymbol{\lambda}_{k+1} = \boldsymbol{\lambda}_k + \mu \boldsymbol{g}(\boldsymbol{q}_k) \tag{2.3.17}$$

In each iteration the constraints are less violated and the iterations stop as soon as the constraints are fulfilled satisfactorily.

Hamiltonian formalism

Similarly the Hamiltonian is augmented by $P_H(\boldsymbol{z}) = P_{\text{Aug}}(\boldsymbol{g}(\boldsymbol{q}))$ according to (2.3.13). Starting with $\boldsymbol{\lambda}_0 = \boldsymbol{0}$, in each iteration the $2n$-dimensional system of unconstrained Hamilton's equations (2.2.4) with a fixed value $\boldsymbol{\lambda}_k$ is solved for $(\boldsymbol{q}^k, \boldsymbol{p}^k)$. Then the multiplier is updated according to (2.3.17).

The main drawback of the augmented Lagrange method is that in practice this extra iteration causes high additional computational costs.

Remark 2.3.8 It is known (see e.g. [Bert 95]) that in nonlinear constrained optimisation problems, a sequence $(\boldsymbol{x}_k)_{k \in \mathbb{N}}$ of minimising solutions obtained by augmented Lagrange iterations converges to a value $\boldsymbol{x}$ which, together with the limit $\boldsymbol{\lambda}$ of the corresponding sequence of multipliers $(\boldsymbol{\lambda}_k)_{k \in \mathbb{N}}$, solves the optimisation problem, where the constraints have been enforced by Lagrange multipliers. The existence of both limit points is guaranteed, see [Bert 95]. In Section (3.2.3), a similar result is shown for a certain class of discrete Hamiltonian systems.

2.3.4 Null space method

According to d'Alembert's principle (see e.g. [Arno 78]) the work of the constraint forces on any virtual variation $\delta\boldsymbol{q} \in T_{\boldsymbol{q}}C$ vanishes. According to (2.3.4) for every $\boldsymbol{q} \in C$, the tangent space $T_{\boldsymbol{q}}C$ is an $(n-m)$-dimensional subspace of TQ. Consequently, its basis vectors form the $n \times (n-m)$ matrix $\boldsymbol{P}(\boldsymbol{q})$ with corresponding linear map $\boldsymbol{P}(\boldsymbol{q}) : \mathbb{R}^{n-m} \to T_{\boldsymbol{q}}C$. This matrix is called null space matrix, since

$$\text{range}\,(\boldsymbol{P}(\boldsymbol{q})) = \text{null}\,(\boldsymbol{G}(\boldsymbol{q})) = T_{\boldsymbol{q}}C \tag{2.3.18}$$

Hence admissible virtual variations can be expressed as $\delta\boldsymbol{q} = \boldsymbol{P}(\boldsymbol{q}) \cdot \delta\boldsymbol{u}$ with $\delta\boldsymbol{u} \in \mathbb{R}^{n-m}$. With these preliminaries, d'Alembert's principle reads

$$\delta\boldsymbol{q} \cdot \boldsymbol{G}^T(\boldsymbol{q}) \cdot \boldsymbol{\lambda} = (\boldsymbol{P}(\boldsymbol{q}) \cdot \delta\boldsymbol{u})^T \cdot \boldsymbol{G}^T(\boldsymbol{q}) \cdot \boldsymbol{\lambda} = 0 \quad \text{for all } \delta\boldsymbol{u} \in \mathbb{R}^{n-m} \tag{2.3.19}$$

Lagrangian formalism

According to (2.3.19) a premultiplication of the differential equation $(2.3.5)_1$ of the constrained Euler-Lagrange equations by $\boldsymbol{P}^T(\boldsymbol{q})$ corresponds to a projection of the equations of motion into $T_{\boldsymbol{q}}C$ and eliminates the constraint forces including the Lagrange multipliers from the system. The resulting d'Alembert-type equations of motion read

$$\boldsymbol{P}^T(\boldsymbol{q}) \cdot \left[\frac{d}{dt}\left(\frac{\partial L(\boldsymbol{q}, \dot{\boldsymbol{q}})}{\partial \dot{\boldsymbol{q}}} \right) - \frac{\partial L(\boldsymbol{q}, \dot{\boldsymbol{q}})}{\partial \boldsymbol{q}} \right] = \boldsymbol{0}$$
$$\boldsymbol{g}(\boldsymbol{q}) = \boldsymbol{0} \tag{2.3.20}$$

They constitute an n-dimensional system of second order differential and algebraic equations that is equivalent to the constrained Euler-Lagrange equations (2.3.5). Note that the null space matrix is not unique, necessary and sufficient condition on $\boldsymbol{P}(\boldsymbol{q})$ is (2.3.18). Due to the significant role of the null space matrix for formulation (2.3.20), it is often termed 'null space method' like e.g. in [Benz 05]. In [Bets 05] a deduction of the equations of motion in d'Alembert-type formulation and a short discussion of its different names appearing in the existing literature (e.g. in [Ange 89, Yen 98, Kim 86]) can be found.

Hamiltonian formalism

Likewise, the premultiplication of $(2.3.8)_2$ of the constrained Hamilton's equations by $\boldsymbol{P}^T(\boldsymbol{q})$ eliminates the constraint forces including the Lagrange multipliers from the system. The resulting $2n$-dimensional system of first order differential and algebraic equations

$$
\begin{aligned}
\dot{\boldsymbol{q}} - \frac{\partial H(\boldsymbol{q}, \boldsymbol{p})}{\partial \boldsymbol{p}} &= \boldsymbol{0} \\
\boldsymbol{P}^T(\boldsymbol{q}) \cdot \left[\dot{\boldsymbol{p}} + \frac{\partial H(\boldsymbol{q}, \boldsymbol{p})}{\partial \boldsymbol{q}} \right] &= \boldsymbol{0} \\
\boldsymbol{g}(\boldsymbol{q}) &= \boldsymbol{0}
\end{aligned}
\tag{2.3.21}
$$

is equivalent to (2.3.8).

Construction of a null space matrix

A null space matrix can always be constructed by a decomposition of the $\mathbb{R}^n$ into the tangent space to the constraint manifold $T_{\boldsymbol{q}}C$ and its orthogonal complement $\left(T_{\boldsymbol{q}}C\right)^{\perp}$. From linear algebra (see e.g. [Fisc 97]) it is known that the null space of the constraint Jacobian and the range of its transposed are orthogonal complements in $\mathbb{R}^n$, i.e.

$$
\begin{aligned}
\mathbb{R}^n &= & T_{\boldsymbol{q}}C & \oplus & \left(T_{\boldsymbol{q}}C\right)^{\perp} \\
&= & \text{null}(\boldsymbol{G}(\boldsymbol{q})) & \oplus & \text{range}(\boldsymbol{G}^T(\boldsymbol{q}))
\end{aligned}
\tag{2.3.22}
$$

A QR-decomposition of the $n \times m$ transposed constraint Jacobian matrix yields

$$
\boldsymbol{G}^T = \boldsymbol{Q} \cdot \boldsymbol{R} = [\boldsymbol{Q}_1, \boldsymbol{Q}_2] \cdot \left[\begin{array}{c} \boldsymbol{R}_1 \\ \boldsymbol{0}_{(n-m) \times m} \end{array} \right]
\tag{2.3.23}
$$

with the nonsingular upper triangular matrix $\boldsymbol{R}_1 \in \mathbb{R}^{m \times m}$ and the orthogonal matrix $\boldsymbol{Q} \in O(n)$, which can be partitioned into the orthogonal matrices $\boldsymbol{Q}_1 \in \mathbb{R}^{n \times m}$ and $\boldsymbol{Q}_2 \in \mathbb{R}^{n \times (n-m)}$ with

$$
\begin{aligned}
\text{range}(\boldsymbol{Q}_1(\boldsymbol{q})) &= \text{range}(\boldsymbol{G}^T(\boldsymbol{q})) \\
\text{range}(\boldsymbol{Q}_2(\boldsymbol{q})) &= \text{null}(\boldsymbol{G}(\boldsymbol{q}))
\end{aligned}
\tag{2.3.24}
$$

Then $\boldsymbol{P}(\boldsymbol{q}) = \boldsymbol{Q}_2(\boldsymbol{q})$ serves as null space matrix, which is sometimes called 'natural orthogonal complement' (see [Ange 89]). A null space matrix constructed in the described way is referred to as implicit representation of a null space matrix.

Alternatively, a velocity analysis can be performed, which is closely related to the considerations of d'Alembert's principle (2.3.19). According to (2.3.4) admissible velocities are consistent with the constraints, i.e. they are elements of the $(n-m)$-dimensional tangent space $T_{\boldsymbol{q}}C$ to the constraint manifold. Thus there exist independent generalised velocities $\boldsymbol{\nu} \in \mathbb{R}^{n-m}$ with

$$
\dot{\boldsymbol{q}} = \boldsymbol{P}(\boldsymbol{q}) \cdot \boldsymbol{\nu} \quad \in T_{\boldsymbol{q}}C
\tag{2.3.25}
$$

If the admissible velocities $\dot{\boldsymbol{q}} \in T_{\boldsymbol{q}}C$ can be expressed in terms of $n - m$ independent generalised velocities, the corresponding mapping yields an explicit representation of an appropriate null space matrix.

Remark 2.3.9 (Independent generalised velocities) The independent generalised velocities $\boldsymbol{\nu} \in \mathbb{R}^{n-m}$ may be classified as quasi-velocities because in general, their time integrals need not result in generalised coordinates (see [Gree 88]).

A third possibility, which also yields an explicit representation of a null space matrix is a parametrisation of the constraint manifold C in terms of generalised coordinates, see Remark 2.3.10.

2.3.5 Reparametrisation in generalised coordinates

Another way to deal with holonomic constraints is to formulate the equations of motion directly in the remaining independent coordinates – the unconstrained generalised coordinates. These coordinates are local coordinates in the constraint manifold C (2.3.3). Assume that there is a mapping

$$\boldsymbol{F} : U \subseteq \mathbb{R}^{n-m} \to C \quad \text{i.e.} \quad \boldsymbol{g}(\boldsymbol{q}) = \boldsymbol{g}(\boldsymbol{F}(\boldsymbol{u})) = \boldsymbol{0} \tag{2.3.26}$$

Lagrangian formalism

Reparametrisation of the Lagrangian $\tilde{L}(\boldsymbol{u}, \dot{\boldsymbol{u}}) = L(\boldsymbol{F}(\boldsymbol{u}), D\boldsymbol{F}(\boldsymbol{u}) \cdot \dot{\boldsymbol{u}})$ yields the Lagrange equations of motion of second kind in terms of generalised coordinates

$$\frac{d}{dt}\left(\frac{\partial \tilde{L}(\boldsymbol{u}, \dot{\boldsymbol{u}})}{\partial \dot{\boldsymbol{u}}}\right) - \frac{\partial \tilde{L}(\boldsymbol{u}, \dot{\boldsymbol{u}})}{\partial \boldsymbol{u}} = \boldsymbol{0} \tag{2.3.27}$$

which is also termed the state-space form of the equations of motion. Since the constraints are fulfilled automatically by the reparametrised configuration variable (2.3.26), the system is reduced to $n - m$ second order differential equations. This is the minimal possible dimension for the present mechanical system, which consists of precisely $n - m$ configurational degrees of freedom. For this reason, the concept of generalised coordinates is, e.g. in the context of multibody dynamics, also called 'minimal coordinate approach' (e.g. [Gera 01], [Brem 04]). Besides the dimensional benefits, the Lagrange equations of motion of second kind (2.3.27) comprise the challenge of finding an explicit representation of the reparametrisation $\boldsymbol{F}$ in (2.3.26). Such a reparametrisation is feasible for many practical applications, however there exist examples such as closed loop systems, for which it is hard or even impossible to find.

Remark 2.3.10 If a reparametrisation of the constraint manifold is known, then the Jacobian (see A.4) $D\boldsymbol{F}(\boldsymbol{u})$ of the coordinate transformation plays the role of a null space matrix. Insertion of the coordinate transformation (2.3.26) and its Jacobian into the d'Alembert-type equations of motion reveals that (2.3.20) and (2.3.27) are equivalent.

Hamiltonian formalism

For an introduction of generalised coordinates into the Hamiltonian formalism for constrained mechanical systems, the generalised momenta $y_i = \partial \tilde{L}/\partial \dot{u}_i$, $i = 1, \ldots, n - m$, which are conjugate to the independent generalised coordinates are defined. In analogy to (2.2.1), by Legendre transformation of the reparametrised Lagrangian $\tilde{L}(\boldsymbol{u}, \dot{\boldsymbol{u}})$, a

reparametrised Hamiltonian $\tilde{H}(u^i, y_i) = y_j \dot{u}^j - \tilde{L}(u^i, \dot{u}^i)$ is obtained. The corresponding equations of motion

$$
\begin{aligned}
\dot{\boldsymbol{u}} &= \frac{\partial \tilde{H}}{\partial \boldsymbol{y}} \\
\dot{\boldsymbol{y}} &= -\frac{\partial \tilde{H}}{\partial \boldsymbol{u}}
\end{aligned}
\tag{2.3.28}
$$

constitute $2(n - m)$ first order differential equations of the form (2.2.4).

Remark 2.3.11 (Suitability for temporal discretisation) Theoretically, all evolution equations of constrained motion presented in this section are suited for temporal discretisation. However, the equations of motion emanating from the use of the Lagrange multiplier method, the penalty method or the augmented Lagrange method possess a relatively simple structure – in particular in conjunction with a formulation of the mechanical system involving a constant mass matrix. Thus they are better suited for temporal discretisation in practice than the d'Alembert-type equations or the equations of motion in generalised coordinates, where the configuration-dependent null space matrices cause the temporal discretisation to be very involved. As an illustration of the complexity, the reduced configuration-dependent mass matrix appearing in the equations of motion in generalised coordinates of a double spherical pendulum is given in Appendix D. In [Leim 04], Chapter 7 it is also pointed out that the formulation of constrained equations of motion in generalised coordinates cannot be recommended generally for time integration. However, there exist certain examples (see e.g. [Eich 98], Example 5.2.7) for which a temporal discretisation of the state-space form is preferable.

3 Temporal discrete equations of motion

The equations developed in order to describe the desired evolution of a mechanical system are rarely analytically solvable. Therefore it is necessary to approximate their solutions numerically. Starting with the first numerical approaches by Euler (1768), numerical integration of ordinary differential equations has a long history. Very popular methods are e.g. Runge Kutta and linear multistep methods see e.g. [Butc 87, Hair 93, Hair 96, Hair 04, Leim 04, Deuf 00, Eich 98, Arev 02] and references therein.

3.1 Mechanical integrators

Naturally, one seeks realistic approximations of the solutions of the evolution equations that share the relevant properties of the real process. Mechanical integration schemes aim at carrying over the geometrical properties of the real flow, like the preservation of first integrals or the symplecticity, to the discrete approximation of the solution. Besides the crucial qualitative reliability of numerical solutions possessing such properties, they also improve the error propagation in long-time integrations. The energy-momentum conserving integrator used throughout this work relies on the concept of discrete derivatives introduced by Gonzalez in [Gonz 96c]. It is expatiated in the following Section 3.1.1. This concept can be viewed as a special method within Galerkin-based finite element formulations in time, introduced by Betsch and Steinmann in [Bets 00b, Bets 00a] and described shortly in Section 3.1.2. During the last decades, much work has been done in the field of energy-momentum conserving integrators, e.g. in [Bets 01a, Bets 01b, Bets 02b, Cris 96, Jele 01, Ibra 03, Ibra 00b, Gonz 99, Gonz 00, Hugh 78, LaBu 76a, Noel 04a, Noel 04b, Reic 95, Rome 02b, Simo 91a, Simo 91b, Simo 92a, Simo 94, Simo 95] to mention just a few. Furthermore, energy decaying schemes have been widely investigated, see e.g. [Arme 01a, Arme 01b, Arme 03, Bauc 96, Bott 02a, Hilb 77, Ibra 02a, Rome 02a]. On the other hand there is the class of symplectic-momentum integrators considered e.g. in [Bart 96, Hair 04, Jay 96, Leim 94, Leim 96, Lew 03, Reic 96, Simo 92b, Kane 00, Mars 01, Wend 97].

3.1.1 Discrete derivative

This formalism for the design of conserving time integration schemes for Hamiltonian systems with symmetry is developed by Gonzalez [Gonz 96c]. Many terms and definitions introduced in Section 2.2.2 are transferred to discrete Hamiltonian systems. The concept of discrete derivatives leads to implicit second order one-step schemes which conserve

the Hamiltonian along with at most quadratic integrals arising from symmetries of the underlying continuous system.

Let P be open in a $2n$-dimensional Euclidian space and let (P, ω) be a symplectic space (see A.10) serving as phase space for the Hamiltonian $H : P \to \mathbb{R}$. A discrete approximation of Hamilton's differential equations (2.2.6) is given by

$$\boldsymbol{z}_{n+1} - \boldsymbol{z}_n = h \mathsf{X}_H(\boldsymbol{z}_n, \boldsymbol{z}_{n+1}) \tag{3.1.1}$$

where $h > 0$ denotes the time-step and $\mathsf{X}_H : P \to \mathbb{R}^{2n}$ is the discrete Hamiltonian vector field, defined via the discrete analogue of (2.2.5)

$$\omega^b_{\boldsymbol{z}_{n+\frac{1}{2}}}(\mathsf{X}_H(\boldsymbol{z}_n, \boldsymbol{z}_{n+1})) = \mathsf{D}H(\boldsymbol{z}_n, \boldsymbol{z}_{n+1}) \tag{3.1.2}$$

where the discrete derivative $\mathsf{D}H$ of the Hamiltonian is used on the right hand side. The discrete Hamiltonian vector field X_H can be viewed as an approximation of the exact Hamiltonian vector field X_H at the midpoint $\boldsymbol{z}_{n+\frac{1}{2}} = \frac{1}{2}(\boldsymbol{z}_{n+1} + \boldsymbol{z}_n)$, in particular $\mathsf{X}_H(\boldsymbol{z}_n, \boldsymbol{z}_{n+1}) \approx X_H(\boldsymbol{z}_{n+\frac{1}{2}})$ because of property (ii) in Definition 3.1.1.

Definition 3.1.1 (Discrete derivative) A discrete derivative for a smooth function $f : P \to \mathbb{R}$ is a mapping $\mathsf{D}f : P \times P \to \mathbb{R}^{2n}$ with the following properties:

(i)   Directionality: $\mathsf{D}f(\boldsymbol{x}, \boldsymbol{y}) \cdot (\boldsymbol{y} - \boldsymbol{x}) = f(\boldsymbol{y}) - f(\boldsymbol{x})$ for all $\boldsymbol{x}, \boldsymbol{y} \in P$

(ii)   Consistency: $\mathsf{D}f(\boldsymbol{x}, \boldsymbol{y}) = Df(\boldsymbol{w}) + \mathcal{O}\left(\|\boldsymbol{y} - \boldsymbol{x}\|\right)$ for all $\boldsymbol{x}, \boldsymbol{y} \in P$

with $\|\boldsymbol{y} - \boldsymbol{x}\|$ sufficiently small

Here $\boldsymbol{w} = \frac{1}{2}(\boldsymbol{x} + \boldsymbol{y})$ and $\|\cdot\|$ denotes the standard Euclidian norm in $\mathbb{R}^{2n}$.

Proposition 3.1.2 (Energy conservation) *With this construction, the Hamiltonian H is conserved along a solution sequence $(\boldsymbol{z}_n)_{n \in \mathbb{N}}$ of (3.1.1) in the sense that $H(\boldsymbol{z}_{n+1}) - H(\boldsymbol{z}_n) = 0$ for all $n \in \mathbb{N}$.*

Proof and further details can be found in [Gonz 96c].

Example 3.1.3 (Discrete derivative) A general example of a discrete derivative is given by

$$\mathsf{D}f(\boldsymbol{x}, \boldsymbol{y}) = Df(\boldsymbol{w}) + \frac{f(\boldsymbol{y}) - f(\boldsymbol{x}) - Df(\boldsymbol{w}) \cdot (\boldsymbol{y} - \boldsymbol{x})}{\|\boldsymbol{y} - \boldsymbol{x}\|^2}(\boldsymbol{y} - \boldsymbol{x}) \tag{3.1.3}$$

which is a second-order approximation to the exact derivative at the midpoint.

Recall from Section 2.2.2 that invariance of the Hamiltonian under the action of a Lie group G (see A.17) leads to the conservation of the momentum map $\boldsymbol{J} : T^*Q \to \mathfrak{g}^*$ (see A.21) along the trajectories of the Hamiltonian vector field. In order to transfer this property to the discrete case for a G-invariant function $f : P \to \mathbb{R}$, i.e. $f \circ \phi_g = f$ for all $g \in G$, the discrete derivative is further specified by two more properties, defining the G-equivariant discrete derivative.

Definition 3.1.4 (G-equivariant discrete derivative) A G-equivariant discrete derivative for a smooth G-invariant function $f : P \to \mathbb{R}$ is a mapping $\mathsf{D}^G f : P \times P \to \mathbb{R}^{2n}$ satisfying the requirements of a discrete derivative together with the following properties:

(iii)   Equivariance: $\mathsf{D}^G f(\phi_g(\boldsymbol{x}), \phi_g(\boldsymbol{y})) = [D\phi_g(\boldsymbol{w})]^{-T} \cdot \mathsf{D}^G f(\boldsymbol{x}, \boldsymbol{y})$

$$\text{for all } g \in G \text{ and } \boldsymbol{x}, \boldsymbol{y} \in P$$

(iv)   Orthogonality: $\mathsf{D}^G f(\boldsymbol{x}, \boldsymbol{y}) \cdot \xi_P(\boldsymbol{w}) = 0$ for all $\xi \in \mathfrak{g}$, $\boldsymbol{x}, \boldsymbol{y} \in P$

The G-equivariant discrete derivative $\mathsf{D}^G H(\boldsymbol{z}_n, \boldsymbol{z}_{n+1})$ of a G-invariant Hamiltonian can be inserted in the definition of the discrete Hamiltonian vector field (3.1.2) to define a new system of Hamiltonian difference equations (3.1.1).

Proposition 3.1.5 (Energy-momentum conservation) *If the action ϕ of G possesses a momentum map $\boldsymbol{J} : P \to \mathfrak{g}^*$ that is at most quadratic in $\boldsymbol{z} \in P$, then $\boldsymbol{J}$ is conserved along the solution sequence $(\boldsymbol{z}_n)_{n \in \mathbb{N}}$ of the new discrete system (3.1.1) in the sense that $J(\xi)(\boldsymbol{z}_{n+1}) - J(\xi)(\boldsymbol{z}_n) = 0$ for all $n \in \mathbb{N}$ and $\xi \in \mathfrak{g}$. Furthermore, the Hamiltonian is an integral of the motion.*

Proof and further details can be found in [Gonz 96c].

Example 3.1.6 (G-equivariant discrete derivative) Assume that the regular symplectic action ϕ of G on P has orbits of dimension s. Then a G-invariant function $f : P \to \mathbb{R}$ does not depend on the full $2n$-dimensional space P, but only on the $(2n-s)$-dimensional quotient space P/G. If a maximal set of independent invariants of G can be found, i.e. there exist G-invariant functions $\pi_1, \ldots, \pi_{2n-s} : P \to \mathbb{R}$ with the property that $D\boldsymbol{\pi}(\boldsymbol{z}) \in \mathbb{R}^{(2n-s)\times 2n}$ has rank $2n-s$ at each $\boldsymbol{z} \in P$, then f can be reduced to the function $\tilde{f} : \boldsymbol{\pi}(P) \to \mathbb{R}$, defined by the expression $\tilde{f}(\boldsymbol{\pi}(\boldsymbol{z})) = f(\boldsymbol{z})$ for all $\boldsymbol{z} \in P$. If the invariants $\pi_1, \ldots, \pi_{2n-s} : P \to \mathbb{R}$ are at most of degree two in $\boldsymbol{z}$, then a G-equivariant discrete derivative for f is defined by the relation

$$
\begin{aligned}
\mathsf{D}^G f(\boldsymbol{x}, \boldsymbol{y}) &= \mathsf{D}\tilde{f}(\boldsymbol{\pi}(\boldsymbol{x}), \boldsymbol{\pi}(\boldsymbol{y})) \circ D\boldsymbol{\pi}(\boldsymbol{w}) \\
&= D^T \boldsymbol{\pi}(\boldsymbol{w}) \cdot \mathsf{D}\tilde{f}(\boldsymbol{\pi}(\boldsymbol{x}), \boldsymbol{\pi}(\boldsymbol{y}))
\end{aligned}
\tag{3.1.4}
$$

Where D denotes the discrete derivative given in Example 3.1.3.

Having in mind that P is open in a $2n$-dimensional Euclidian space and represents the phase space of a mechanical system, the following definition introduced in [Gonz 99] is useful.

Definition 3.1.7 (Partial discrete derivative) To a discrete derivative $\mathsf{D}f(\boldsymbol{x}, \boldsymbol{y}) \in \mathbb{R}^{2n}$ one associates partial discrete derivatives $\mathsf{D}_1 f(\boldsymbol{x}, \boldsymbol{y}) \in \mathbb{R}^n$ and $\mathsf{D}_2 f(\boldsymbol{x}, \boldsymbol{y}) \in \mathbb{R}^n$ according to the relation

$$\mathsf{D}f(\boldsymbol{x}, \boldsymbol{y}) \cdot (\boldsymbol{u}_q, \boldsymbol{u}_p) = \mathsf{D}_1 f(\boldsymbol{x}, \boldsymbol{y}) \cdot \boldsymbol{u}_q + \mathsf{D}_2 f(\boldsymbol{x}, \boldsymbol{y}) \cdot \boldsymbol{u}_p \tag{3.1.5}$$

for all $\boldsymbol{u} = (\boldsymbol{u}_q, \boldsymbol{u}_p) \in \mathbb{R}^{2n}$. Furthermore, a discrete derivative operator d on $\mathbb{R}^n$ is induced. Let $h : \mathbb{R}^n \to \mathbb{R}$ and $\bar{h} : P \to \mathbb{R}$ be functions related by

$$\bar{h}(\boldsymbol{x}) = h(\boldsymbol{x}_q) \quad \text{for all } \boldsymbol{x} = (\boldsymbol{x}_q, \boldsymbol{x}_p) \in P \tag{3.1.6}$$

Then d is defined as

$$\mathsf{d}h(\boldsymbol{x}_q, \boldsymbol{y}_q) = \mathsf{D}_1 \bar{h}(\boldsymbol{x}, \boldsymbol{y}) \tag{3.1.7}$$

Remark 3.1.8 For Hamiltonian functions being at most quadratic, the examples of the discrete derivative (3.1.3) and the G-equivariant discrete derivative (3.1.4) coincide. In this case, both formulas reduce to the midpoint rule. Furthermore, the concept of discrete derivatives is equivalent to the assumed distance method in the context of the cG(1)-method for at most quadratic Hamiltonians. This correlation is expatiated in [Grah 02].

Remark 3.1.9 This concept constitutes a special method within the family of time-stepping schemes emanating from finite element approximations in time. The crucial advantage is, that the formulas (3.1.3) and (3.1.4) are given in closed form. Thus the conservation properties do not depend on the numerical solution of arising time integrals. In particular, formula (3.1.3) can be interpreted as a quadrature for the time integral arising in the cG(1)-method in (3.1.13), which fulfils the design criteria for energy conservation (3.1.15) and for angular momentum conservation (3.1.16) respectively.

3.1.2 Galerkin-based finite elements in time

The following introduction to the continuous Galerkin (cG) method in conjunction with Hamilton's equations is based on the work by Betsch and Steinmann in [Bets 00a, Bets 00b]. Its extension to nonlinear elastodynamics and to holonomically constrained mechanical systems is presented in [Bets 01a, Bets 02b] respectively. The discretisation of Hamilton's equations relies on a Petrov-Galerkin finite element formulation in time. The resulting time-stepping scheme is exactly energy conserving, provided that the appearing time integrals are calculated exactly. Since this is rarely feasible, the choice of appropriate quadrature rules plays a crucial role concerning the conservation properties of the resulting algorithm.

Let the time interval $[t_0, t_1]$ be divided into n_e nonoverlapping subintervals. For convenience a typical time interval $[t_n, t_{n+1}]$ is transformed to a master element with local coordinates $\alpha \in [0, 1]$ according to

$$\alpha(t) = \frac{t - t_n}{h_n} \qquad h_n = t_{n+1} - t_n \tag{3.1.8}$$

for $n = 0, \ldots, n_e - 1$.

Hamilton's equations (2.2.6) in conjunction with the special form of the Hamiltonian vector field given in Remark 2.2.1, read in the weak residual form

$$\int_0^1 \left(\delta \boldsymbol{z}^h\right)^T \cdot \mathbb{J} \cdot \left(\frac{d\boldsymbol{z}^h}{d\alpha} - h_n \mathbb{J} \cdot \nabla H(\boldsymbol{z}^h)\right) d\alpha = 0 \tag{3.1.9}$$

Together with the initial condition $\boldsymbol{z}^h(0) = \boldsymbol{z}_{n-1}$, they serve as a vantage point. The goal is to find a continuous piecewise polynomial $\boldsymbol{z}^h \in \mathcal{P}^k(0, 1)^{2n}$ of degree k, satisfying (3.1.9) for all $\delta \boldsymbol{z}^h \in \mathcal{P}^{k-1}(0, 1)^{2n}$. The trial functions are given by

$$\boldsymbol{z}^h(\alpha) = \sum_{i=1}^{k+1} M_i(\alpha) \boldsymbol{z}_i \tag{3.1.10}$$

with the nodal shape functions $M_i(\alpha)$, $i = 1, \ldots, k+1$ being Lagrange polynomials of degree k, such that at the time nodes $\alpha_j \in [0,1]$, $M_i(\alpha_j) = \delta_{ij}$ holds and $\boldsymbol{z}_i = \boldsymbol{z}^h(\alpha_i)$ are the nodal values of $\boldsymbol{z}^h$. Accordingly the global approximation to $\boldsymbol{z} : [t_0, t_1] \to \mathbb{R}^{2n}$ is continuous over the time element boundaries. In contrast to that, the approximation of the test functions

$$\delta \boldsymbol{z}^h(\alpha) = \sum_{i=1}^{k} \tilde{M}_i(\alpha) \delta \boldsymbol{z}_i \tag{3.1.11}$$

with the reduced shape functions $\tilde{M}_i(\alpha)$, $i = 1, \ldots, k$ being Lagrange polynomials of degree $k-1$, allows interelement discontinuities. The reduced shape functions are determined by the relation

$$\frac{d\boldsymbol{z}^h}{d\alpha} = \sum_{i=1}^{k+1} M_i'(\alpha) \boldsymbol{z}_i = \sum_{i=1}^{k} \tilde{M}_i(\alpha) \tilde{\boldsymbol{z}}_i \tag{3.1.12}$$

where the $\tilde{\boldsymbol{z}}_i$, $i = 1, \ldots, k$ consist of linear combinations of the nodal values $\boldsymbol{z}_i$, $i = 1, \ldots, k+1$, see [Bets 01a] for details.

Eventually insertion of (3.1.10) and (3.1.11) into (3.1.9) yields the equations

$$\sum_{j=1}^{k} \int_0^1 \tilde{M}_i \tilde{M}_j \, d\alpha \, \tilde{\boldsymbol{z}}_j - h_n \mathbb{J} \cdot \int_0^1 \tilde{M}_i \nabla H(\boldsymbol{z}^h) \, d\alpha = 0 \tag{3.1.13}$$

for $i = 1, \ldots, k$. An implicit one-step scheme can be obtained by

(i)   selecting the polynomial degree k. Then the integral over a polynomial of degree $2(k-1)$ in the first term in (3.1.13) can be calculated exactly.

(ii) choosing a quadrature formula for the remaining integral in (3.1.13).

It can be shown easily, that the Hamiltonian is conserved along solutions of (3.1.13), provided that the integrals are calculated exactly. If exact integration is not feasible, the choice of the quadrature formula is crucial concerning the conservation properties and the accuracy of the resulting time-stepping scheme. Scalar multiplication of (3.1.13) by $\mathbb{J} \cdot \tilde{\boldsymbol{z}}_i$ and subsequent summation over $i = 1, \ldots, k$ cancels the contributions of the first terms and yields the condition

$$\sum_{i=1}^{k} \int_0^1 \tilde{M}_i \nabla H(\boldsymbol{z}^h) \, d\alpha \cdot \tilde{\boldsymbol{z}}_i = 0 \tag{3.1.14}$$

which is identical with $H_n - H_{n-1} = 0$ for exact integration. Consequently, the energy is exactly conserved along solutions of (3.1.13), if the quadrature rule in use satisfies condition (3.1.14). Assuming that the Hamiltonian is separable and of the form $H(\boldsymbol{z}) = \frac{1}{2} \boldsymbol{p}^T \cdot \boldsymbol{M}^{-1} \cdot \boldsymbol{p} + V(\boldsymbol{q})$ (where $\boldsymbol{M}$ is a symmetric, positive semi-definite, constant mass matrix and V the potential energy), the contribution of the kinetic energy to (3.1.14) is a polynomial of degree $2k - 1$ which can be integrated exactly. Consequently, the quadrature rule applied to the calculation of the remaining integral in (3.1.14) has to fulfil the design criterion

$$\sum_{i=1}^{k} \int_0^1 \tilde{M}_i D_1 H(\boldsymbol{z}^h) \, d\alpha \cdot \tilde{\boldsymbol{q}}_i = V_n - V_{n-1} \tag{3.1.15}$$

to ensure algorithmic energy conservation.

The requirement of algorithmic conservation of momentum maps imposes further restrictions on the evaluation of $\int_0^1 D_1 H(\boldsymbol{z}^h) d\alpha$. E.g. in the case of vanishing external loading, the condition for algorithmic conservation of angular momentum, i.e. $\boldsymbol{L}_n - \boldsymbol{L}_{n-1} = \boldsymbol{0}$, in the context of the cG(1)-method reads

$$\int_0^1 D_1 H(\boldsymbol{z}^h) \, d\alpha \times \boldsymbol{q}^h \left(\frac{1}{2} \right) = \boldsymbol{0} \tag{3.1.16}$$

The attempt to fulfil the design criterion (3.1.15) leads to the consideration of the assumed distance method in [Bets 00a] for N-body problems (which is energy-momentum conserving for at most quadratic Hamiltonians) or the assumed strain method for problems of nonlinear elasticity in [Bets 01a]. In [Gros 04], Groß offers a unified development of higher order energy-momentum conserving time integrators for nonlinear elastodynamics, the so-called enhanced Galerkin (eG) method, see also [Gros 05].

For constrained Hamiltonian systems, where the constraints are enforced using Lagrange multipliers as additional variables, the multipliers as well as their corresponding test functions are approximated by piecewise polynomials of degree $k-1$ allowing discontinuities across the time element boundaries. Thus the trial functions $\boldsymbol{\lambda}^h(\alpha)$ and the test functions $\delta\boldsymbol{\lambda}^h(\alpha)$ are of the form (3.1.11). This leads to the so-called mixed Galerkin (mG) method introduced in [Bets 02b].

As already mentioned in Remark 3.1.8, the cG(1)-method in conjunction with a non-standard quadrature rule fulfilling the design criteria for algorithmic conservation of first integrals is equivalent to the concept of discrete derivatives, see [Grah 02].

3.1.3 Variational integrators

While the time-stepping schemes in the preceding Sections 3.1.1 and 3.1.2 rely on the discretisation of the ordinary differential evolution equations, the concept of variational integrators is based on a direct discretisation of the variational formulation behind the equations of motion. Due to the variational derivation of the time-stepping scheme, its solution is symplectic (i.e. it conserves the same two-form on the phase space as the underlying continuous system) and it also conserves momentum maps arising from symmetries in the true system. Furthermore, the energy error remains bounded along the solution of the discrete system, thus the variational method does not artificially dissipate energy. This is in contrast to the numerical damping pertaining to many standard methods, see e.g. [Arme 01a, Arme 01b, Gros 00]. As a consequence of a theorem proved by Ge and Marsden in [Ge 88], it is not possible to achieve time-stepping schemes for which the solution conserves momentum maps and the symplectic form as well as the energy while using constant time-steps. Therefore, mechanical integrators were divided into two classes, symplectic-momentum and energy-momentum integrators. However, the symplectic-energy-momentum conserving algorithm proposed in [Mars 99] overcomes that shortcoming by using adaptive time-steps. For the application of variational integrators to constrained systems see [Wend 97] and a relation of variational integrators to Newmark algorithms can be found in [Kane 00]. For a detailed introduction to discrete mechanics

and variational integrators see [Mars 01]. In the sequel the basic ideas of the concept of variational integrators are sketched briefly.

Corresponding to a configuration manifold Q, the discrete phase space is defined by $Q \times Q$ which is locally isomorphic to TQ. For a constant time-step $h \in \mathbb{R}$, a path $\boldsymbol{q} : [t_0, t_1] \to Q$ is replaced by a discrete path $\boldsymbol{q}_d : \{t_0, t_0 + h, , \ldots, t_0 + Nh = t_1\} \to Q$, $N \in \mathbb{N}$, where $\boldsymbol{q}_k = \boldsymbol{q}_d(t_0 + kh)$ is viewed as an approximation to $\boldsymbol{q}(t_0 + kh)$. Using the continuous Lagrangian $L : TQ \to \mathbb{R}$ a discrete Lagrangian $L_d : Q \times Q \to \mathbb{R}$ is introduced via

$$L_d(\boldsymbol{q}_k, \boldsymbol{q}_{k+1}) = L\left(\frac{\boldsymbol{q}_{k+1} + \boldsymbol{q}_k}{2}, \frac{\boldsymbol{q}_{k+1} - \boldsymbol{q}_k}{h}\right) \tag{3.1.17}$$

and a discrete action sum $S_d : Q^{N+1} \to \mathbb{R}$ via

$$S_d = \sum_{k=0}^{N-1} L_d(\boldsymbol{q}_k, \boldsymbol{q}_{k+1}) \tag{3.1.18}$$

The discrete variational principle states that the discrete path extremises the action sum for fixed $\boldsymbol{q}_0$ and $\boldsymbol{q}_N$. Similar to the deduction of the continuous Euler-Lagrange equations (2.1.2) from the variational principle of critical action (2.1.1), the requirement $\delta S_d = 0$ yields the discrete Euler-Lagrange equations

$$D_2 L_d(\boldsymbol{q}_{k-1}, \boldsymbol{q}_k) + D_1 L_d(\boldsymbol{q}_k, \boldsymbol{q}_{k+1}) = \boldsymbol{0} \tag{3.1.19}$$

which must hold for $k = 1, \ldots, N-1$. Let $\Phi : Q \times Q \to Q \times Q$, defined implicitly by $\Phi(\boldsymbol{q}_{k-1}, \boldsymbol{q}_k) = (\boldsymbol{q}_k, \boldsymbol{q}_{k+1})$, denote the discrete map which evolves the system forward in time. Furthermore, using the fibre derivative $\mathbb{F}L_d : Q \times Q \to T^*Q$ with

$$\mathbb{F}L_d(\boldsymbol{q}_k, \boldsymbol{q}_{k+1}) = (\boldsymbol{q}_k, D_1 L_d(\boldsymbol{q}_k, \boldsymbol{q}_{k+1})) \tag{3.1.20}$$

a discrete two-form ω_d on $Q \times Q$ is defined by pulling back the canonical two-form ω on T^*Q given in Remark 2.1.1 and reads

$$\omega_d = \mathbb{F}L_d^*(\omega) = \frac{\partial^2 L_d}{\partial q_k^i \partial q_{k+1}^j} dq_k^i \wedge dq_{k+1}^j \tag{3.1.21}$$

Then a tedious but straightforward calculation shows that $\Phi^* \omega_d = \omega_d$, i.e. the discrete evolution map Φ is discretely symplectic, see [Wend 97].

Besides the discrete symplectic structure, Φ preserves discrete momentum maps related to symmetries of the corresponding continuous system. Let $\xi \in \mathfrak{g}$ where $\mathfrak{g}$ denotes the Lie algebra of a Lie group G whose action leaves the continuous Lagrangian invariant. Then the discrete Lagrangian is also invariant under that group action, i.e.

$$L_d(\exp(s\xi)\boldsymbol{q}_k, \exp(s\xi)\boldsymbol{q}_{k+1}) = L_d(\boldsymbol{q}_k, \boldsymbol{q}_{k+1}) \tag{3.1.22}$$

for $s \in \mathbb{R}$. Differentiating this equation and setting $s = 0$ implies

$$D_1 L_d(\boldsymbol{q}_k, \boldsymbol{q}_{k+1}) \cdot \xi_Q(\boldsymbol{q}_k) + D_2 L_d(\boldsymbol{q}_k, \boldsymbol{q}_{k+1}) \cdot \xi_Q(\boldsymbol{q}_{k+1}) = 0 \tag{3.1.23}$$

where ξ_Q is the infinitesimal generator of the action corresponding to ξ. As explained above, $\boldsymbol{q}_{k+1}$ extremises the action sum S_d, so if $\boldsymbol{q}_{k+1}$ is varied over $s \in \mathbb{R}$ by

$\boldsymbol{q}_{k+1}(s) = \exp(s\xi) \cdot \boldsymbol{q}_{k+1}$ then $\boldsymbol{q}_{k+1}(0)$ extremises S_d, what means that $dS_d/ds|_{s=0} = 0$. This implies

$$D_2 L_d(\boldsymbol{q}_k, \boldsymbol{q}_{k+1}) \cdot \xi_Q(\boldsymbol{q}_{k+1}) + D_1 L_d(\boldsymbol{q}_{k+1}, \boldsymbol{q}_{k+2}) \cdot \xi_Q(\boldsymbol{q}_{k+1}) = 0 \qquad (3.1.24)$$

Subtracting equation (3.1.23) from equation (3.1.24) reveals that

$$D_1 L_d(\boldsymbol{q}_{k+1}, \boldsymbol{q}_{k+2}) \cdot \xi_Q(\boldsymbol{q}_{k+1}) - D_1 L_d(\boldsymbol{q}_k, \boldsymbol{q}_{k+1}) \cdot \xi_Q(\boldsymbol{q}_k) = 0 \qquad (3.1.25)$$

This equation shows that a momentum map $J_d : Q \times Q \to \mathfrak{g}^*$ defined analogous to (2.1.8) by

$$\langle J_d(\boldsymbol{q}_k, \boldsymbol{q}_{k+1}), \xi \rangle = \langle D_1 L_d(\boldsymbol{q}_k, \boldsymbol{q}_{k+1}), \xi_Q(\boldsymbol{q}_k) \rangle \qquad (3.1.26)$$

is preserved by the algorithm Φ.

A comparison of the performance of the time-stepping scheme (3.1.1) derived using the concept of discrete derivatives to the time-stepping scheme (3.1.19) based on a discrete variational principle, is documented in [Laue] for a simple constrained mechanical system.

Remark 3.1.10 (Hamiltonian formalism) Just as the standard Legendre transformation (2.2.1) maps the Lagrangian phase space TQ to the Hamiltonian phase space T^*Q, a discrete Legendre transformation can be defined. With its help it can be shown, that a discrete trajectory $\{\boldsymbol{q}_k\}_{k=0}^N$ in Q can be regarded as either a trajectory $\{(\boldsymbol{q}_k, \boldsymbol{q}_{k+1})\}_{k=0}^{N-1}$ in $Q \times Q$ or equivalently as a trajectory $\{(\boldsymbol{q}_k, \boldsymbol{p}_k)\}_{k=0}^N$ in T^*Q, see [Mars 01] for details.

3.2 Mechanical integration of constrained equations of motion

With the different theoretical approaches described in the preceding chapters, a variety of combinations is at disposal to specify time-stepping schemes for constrained mechanical systems. Early work on time integration of constrained dynamical systems has been done e.g. by [Card 89].

Having decided to use the Hamiltonian formalism for the deduction of the continuous equations of motion, the next step is to choose a temporal discretisation technique. The concept of discrete derivatives by Gonzalez [Gonz 96c] described in Section 3.1.1 is used throughout this work. One reason for that is the intention to solve stiff systems (e.g. using high penalty parameters) for which it has been reported that energy-conserving schemes are better suitable, especially for long term simulations, see e.g. [Simo 93]. The concept of discrete derivatives can be interpreted as a formal abstraction of conserving time-stepping schemes, embedding them within the context of discrete dynamical systems. Its technical merits lie in the possibility to prove the conservation of first integrals along the discrete solution sequence by arguments which are in analogy to those used in the continuous setting. In particular, the conservation properties are guaranteed by the design of the concept, see Remark 3.1.9.

In a typical time interval $I_n = [t_n, t_{n+1}] \subseteq [t_0, t_1]$ with corresponding constant time-step $h = t_{n+1} - t_n$ (see Figure 3.1) the configuration and momentum vector are approximated continuously by piecewise linear functions respectively

$$
\begin{aligned}
\boldsymbol{q}(t)|_{I_n} &\approx \boldsymbol{q}_n + \frac{t - t_n}{h}\left(\boldsymbol{q}_{n+1} - \boldsymbol{q}_n\right) \\
\boldsymbol{p}(t)|_{I_n} &\approx \boldsymbol{p}_n + \frac{t - t_n}{h}\left(\boldsymbol{p}_{n+1} - \boldsymbol{p}_n\right)
\end{aligned}
\tag{3.2.1}
$$

PSfrag replacements
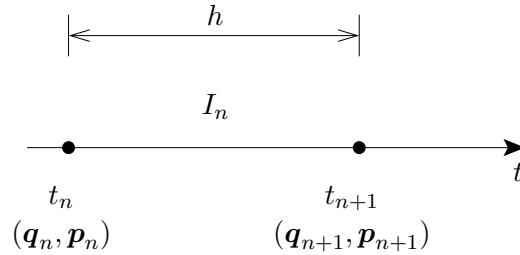
Figure 3.1: Time interval $I_n = [t_n, t_{n+1}] \subseteq [t_0, t_1]$ of length h.

Using the canonical symplectic structure on $2n$-dimensional linear spaces (2.2.8) for the definition of the Hamiltonian vector field (3.1.2) and inserting this in the discrete equations of motion (3.1.1), one arrives at the discrete Hamiltonian system

$$
\begin{aligned}
\boldsymbol{q}_{n+1} - \boldsymbol{q}_n &= h\mathsf{D}_2^G H(\boldsymbol{z}_n, \boldsymbol{z}_{n+1}) \\
\boldsymbol{p}_{n+1} - \boldsymbol{p}_n &= -h\mathsf{D}_1^G H(\boldsymbol{z}_n, \boldsymbol{z}_{n+1})
\end{aligned}
\tag{3.2.2}
$$

which is the discrete counterpart of (2.2.4) involving the partial G-equivariant discrete derivative defined in Section 3.1.1. By design of the G-equivariant discrete derivative, the total energy and at most quadratic momentum maps are conserved along its solution (see Proposition 3.1.5).

Augmentation of the Hamiltonian (2.3.13) according to the method to treat the constraints and insertion of H_{aug} into (3.2.2) along with a possible supplement of the system by the constraint equations eventually yields the desired energy-momentum conserving time-stepping scheme for constrained mechanical systems.

3.2.1 Lagrange multiplier method

As described in Section 2.3.1, the augmentation of the Hamiltonian (2.3.13) according to the Lagrange multiplier method is given by $P_H(\boldsymbol{z}) = P_{\mathrm{Lag}}(\boldsymbol{g}(\boldsymbol{q})) = \boldsymbol{g}^T(\boldsymbol{q}) \cdot \boldsymbol{\lambda}$. The Lagrange multipliers are approximated constantly within one time interval allowing interelement discontinuities. Then the conserving time-stepping scheme for the constrained Hamiltonian system (2.3.8) reads

$$
\begin{aligned}
\boldsymbol{q}_{n+1} - \boldsymbol{q}_n &= h\mathsf{D}_2^G H(\boldsymbol{z}_n, \boldsymbol{z}_{n+1}) \\
\boldsymbol{p}_{n+1} - \boldsymbol{p}_n &= -h\mathsf{D}_1^\mathsf{G} H(\boldsymbol{z}_n, \boldsymbol{z}_{n+1}) - h\mathbf{G}^T(\boldsymbol{q}_n, \boldsymbol{q}_{n+1}) \cdot \boldsymbol{\lambda}_{n+1} \\
\mathbf{0} &= \boldsymbol{g}(\boldsymbol{q}_{n+1})
\end{aligned}
\tag{3.2.3}
$$

where $\mathbf{G}(\boldsymbol{q}_n, \boldsymbol{q}_{n+1}) = \mathsf{d}^G \boldsymbol{g}(\boldsymbol{q}_n, \boldsymbol{q}_{n+1})$ is the the partial G-equivariant discrete derivative (see Definition 3.1.4 and 3.1.7).

A conservative Hamiltonian system with constant symmetric positive semi-definite mass matrix $\boldsymbol{M} \in \mathbb{R}^{n \times n}$ and potential $V : Q \to \mathbb{R}$ building the separable Hamiltonian (2.3.13) satisfying the assumptions in (2.3.14) reads

$$H_{aug}(\boldsymbol{z}) = T_H(\boldsymbol{z}) + V_H(\boldsymbol{z}) + P_H(\boldsymbol{z}) = \frac{1}{2}\boldsymbol{p}^T \cdot \boldsymbol{M}^{-1} \cdot \boldsymbol{p} + V(\boldsymbol{q}) + \boldsymbol{g}^T(\boldsymbol{q}) \cdot \boldsymbol{\lambda} \qquad (3.2.4)$$

Then (3.2.3) can be specified to

$$\begin{aligned}
\boldsymbol{q}_{n+1} - \boldsymbol{q}_n &= \quad h\boldsymbol{M}^{-1} \cdot \boldsymbol{p}_{n+\frac{1}{2}} \\
\boldsymbol{p}_{n+1} - \boldsymbol{p}_n &= \quad -h\mathsf{d}^G V(\boldsymbol{q}_n, \boldsymbol{q}_{n+1}) - h\mathbf{G}^T(\boldsymbol{q}_n, \boldsymbol{q}_{n+1}) \cdot \boldsymbol{\lambda}_{n+1} \\
\boldsymbol{0} &= \quad \boldsymbol{g}(\boldsymbol{q}_{n+1})
\end{aligned} \qquad (3.2.5)$$

Alternatively, the constrained scheme (3.2.5) can be derived from the Galerkin-based mG(1)-method described in Section 3.1.2 as proposed by Betsch and Steinmann [Bets 02b]. By definition of the partial G-equivariant discrete derivative (3.1.7), the resulting scheme (3.2.5) conserves the total energy and at most quadratic momentum maps, related to symmetries of the underlying continuous system, along its solution sequence $(\boldsymbol{z}_n)_{n \in \mathbb{N}}$. According to (3.2.5)$_3$, the constraints are fulfilled exactly at the time nodes. With regard to (3.2.5)$_1$, the directionality property of the discrete derivative implies

$$(\boldsymbol{M}^{-1} \cdot \boldsymbol{p}_{n+\frac{1}{2}})^T \cdot \mathbf{G}^T(\boldsymbol{q}_n, \boldsymbol{q}_{n+1}) \cdot \boldsymbol{\lambda}_{n+1} = 0 \qquad (3.2.6)$$

This can be considered as the discrete counterpart of d'Alembert's requirement that the constraint forces are workless, see (2.3.19). Beyond that, omittance of the Lagrange multiplier in (3.2.6) shows that with regard to (2.3.9) a temporal discrete counterpart of the consistency condition is fulfilled.

For an implementation of the constrained scheme, (3.2.5)$_1$ is solved for $\boldsymbol{p}_{n+1}$ and inserted into (3.2.5)$_2$. This yields the $(n + m)$-dimensional system

$$\begin{aligned}
\frac{2}{h}\boldsymbol{M} \cdot (\boldsymbol{q}_{n+1} - \boldsymbol{q}_n) - 2\boldsymbol{p}_n + h\mathsf{d}^G V(\boldsymbol{q}_n, \boldsymbol{q}_{n+1}) + h\mathbf{G}^T(\boldsymbol{q}_n, \boldsymbol{q}_{n+1}) \cdot \boldsymbol{\lambda}_{n+1} &= \boldsymbol{0} \\
\boldsymbol{g}(\boldsymbol{q}_{n+1}) &= \boldsymbol{0}
\end{aligned} \qquad (3.2.7)$$

to be solved for $\boldsymbol{q}_{n+1}, \boldsymbol{\lambda}_{n+1}$ although there are only $n - m$ independent configurational degrees of freedom. Another drawback of the constrained scheme is that the condition number of the iteration matrix for the solution of the nonlinear system of equations is of the order $\mathcal{O}(h^{-3})$, see [Petz 86] and proof in Appendix C.1. This implies that for decreasing time-steps, the iteration matrix becomes more and more ill-conditioned.

Remark 3.2.1 (Preconditioning) One possibility to remove the conditioning problem is the use of preconditioning techniques which decouple the condition number of the iteration matrix from the time-step. E.g. Bottasso introduces a preconditioning method in [Bott 05] which is very effective and easy to implement. However, preconditioning techniques do not control the magnitude of the condition number.

3.2.2 Penalty method

With the augmentation according to the penalty method by $P_H(\boldsymbol{z}) = P_{\mathrm{Pen}}(\boldsymbol{g}(\boldsymbol{q})) = \mu R(\boldsymbol{g}(\boldsymbol{q}))$ described in Section 2.3.2, a separable Hamiltonian corresponding to (3.2.4) reads

$$H_{aug}(\boldsymbol{z}) = T_H(\boldsymbol{z}) + V_H(\boldsymbol{z}) + P_H(\boldsymbol{z}) = T(\boldsymbol{p}) + V(\boldsymbol{q}) + \mu R(\boldsymbol{g}(\boldsymbol{q})) \tag{3.2.8}$$

with $T(\boldsymbol{p}) = \frac{1}{2}\boldsymbol{p}^T \cdot \boldsymbol{M}^{-1} \cdot \boldsymbol{p}$. Insertion into the discrete Hamiltonian system (3.2.2) yields the energy-momentum conserving penalty time-stepping scheme

$$\begin{aligned} \boldsymbol{q}_{n+1} - \boldsymbol{q}_n &= h\boldsymbol{M}^{-1} \cdot \boldsymbol{p}_{n+\frac{1}{2}} \\ \boldsymbol{p}_{n+1} - \boldsymbol{p}_n &= -h\mathsf{d}^G V(\boldsymbol{q}_n, \boldsymbol{q}_{n+1}) - h\mu\mathsf{d}^G R(\boldsymbol{g}(\boldsymbol{q}_n, \boldsymbol{q}_{n+1})) \end{aligned} \tag{3.2.9}$$

The following proposition may be viewed as the discrete counterpart of Theorem 2.3.5 by Rubin and Ungar [Rubi 57]. It holds for the class of energy conserving time-stepping schemes designed by the use of the discrete derivative given in Example 3.1.3. The statement can also be derived for the subclass of energy-momentum conserving schemes using the G-equivariant discrete derivative, but in the following form it is more general and notationally simpler.

Proposition 3.2.2 *Let $\boldsymbol{z}_n = (\boldsymbol{q}_n, \boldsymbol{p}_n)$ be consistent coordinates at time t_n, $n \in \mathbb{N}$ arbitrary. Let $(\mu_s)_{s\in\mathbb{N}} \subset \mathbb{R}^+$ be an arbitrary sequence with $\lim_{s\to\infty} \mu_s = \infty$ and denote the solution of the system (3.2.9) corresponding to μ_s by $\boldsymbol{z}_{n+1}^s$. Let $\boldsymbol{z}_{n+1} = \lim_{s\to\infty} \boldsymbol{z}_{n+1}^s$ be the limit point of the sequence of solutions. Then there exists a multiplier $\boldsymbol{\lambda}_{n+1}$ such that $(\boldsymbol{z}_{n+1}, \boldsymbol{\lambda}_{n+1})$ solve the constrained scheme (3.2.5).*

Proof: For consistent initial data $\boldsymbol{q}_n \in C$, $\boldsymbol{g}(\boldsymbol{q}_n) = \boldsymbol{0}$, thus the correct energy of the mechanical system $T(\boldsymbol{p}_n) + V(\boldsymbol{q}_n) = H(\boldsymbol{z}_n) = H_0$ is conserved along the solution of (3.2.9). Then for arbitrary $n, s \in \mathbb{N}$

$$T(\boldsymbol{p}_{n+1}^s) + V(\boldsymbol{q}_{n+1}^s) + \mu_s R(\boldsymbol{g}(\boldsymbol{q}_{n+1}^s)) = H_0 \tag{3.2.10}$$

According to the assumptions (2.3.12) and (2.3.14), T and R are non-negative and V is bounded from below. It follows that T, V and R are bounded from above, in particular, there exists $J_{n+1}^s \in \mathbb{R}^+$ with

$$\mu_s R(\boldsymbol{g}(\boldsymbol{q}_{n+1}^s)) \leq J_{n+1}^s \tag{3.2.11}$$

Since the lower bound of V is independent of n and s, there exists $J_{n+1} \in \mathbb{R}^+$ with

$$\lim_{s\to\infty} \mu_s R(\boldsymbol{g}(\boldsymbol{q}_{n+1}^s)) \leq J_{n+1} \tag{3.2.12}$$

With $\lim_{s\to\infty} \mu_s = \infty$ it follows that $\lim_{s\to\infty} R(\boldsymbol{g}(\boldsymbol{q}_{n+1}^s)) = 0$ and then assumption (2.3.12) implies

$$\lim_{s\to\infty} \boldsymbol{g}(\boldsymbol{q}_{n+1}^s) = \boldsymbol{0} \tag{3.2.13}$$

Let $\boldsymbol{z}_{n+1} = (\boldsymbol{q}_{n+1}, \boldsymbol{p}_{n+1}) = \lim\limits_{s\to\infty} \boldsymbol{z}_{n+1}^s$ denote the limit point of the solution sequence $(\boldsymbol{z}_{n+1}^s)_{s\in\mathbb{N}}$ of (3.2.9). Note that the existence of a limit point for the solution sequence follows directly from the corresponding result in the temporal continuous case (see [Rubi 57]). Then it follows by the continuity of the constraint function that

$$\boldsymbol{g}(\boldsymbol{q}_{n+1}) = \boldsymbol{0} \tag{3.2.14}$$

i.e. $(3.2.5)_3$ is fulfilled.

Besides the supplementation of the constrained scheme by the constraint equations, (3.2.5) and (3.2.9) differ in the discrete derivatives

$$\mathsf{d}P_{\mathrm{Lag}}(\boldsymbol{g}(\boldsymbol{q}_n, \boldsymbol{q}_{n+1})) = D^T\boldsymbol{g}(\boldsymbol{q}_{n+\frac{1}{2}})\cdot\boldsymbol{\lambda}_{n+1} + \frac{-D^T\boldsymbol{g}(\boldsymbol{q}_{n+\frac{1}{2}})\cdot\boldsymbol{\lambda}_{n+1}\cdot(\boldsymbol{q}_{n+1}-\boldsymbol{q}_n)}{\left\|\boldsymbol{q}_{n+1}-\boldsymbol{q}_n\right\|^2}(\boldsymbol{q}_{n+1}-\boldsymbol{q}_n) \tag{3.2.15}$$

with $\boldsymbol{q}_{n+\frac{1}{2}} = \frac{1}{2}(\boldsymbol{q}_{n+1}+\boldsymbol{q}_n)$ and

$$\mathsf{d}P_{\mathrm{Pen}}(\boldsymbol{g}(\boldsymbol{q}_n, \boldsymbol{q}_{n+1}^s)) = \mu_s D^T\boldsymbol{g}(\boldsymbol{q}_{n+\frac{1}{2}}^s)\cdot D_g R(\boldsymbol{g}(\boldsymbol{q}_{n+\frac{1}{2}}^s)) +$$

$$\frac{\mu_s R(\boldsymbol{g}(\boldsymbol{q}_{n+1}^s)) - \mu_s D^T\boldsymbol{g}(\boldsymbol{q}_{n+\frac{1}{2}}^s)\cdot D_g R(\boldsymbol{g}(\boldsymbol{q}_{n+\frac{1}{2}}^s))\cdot(\boldsymbol{q}_{n+1}^s-\boldsymbol{q}_n)}{\left\|\boldsymbol{q}_{n+1}^s-\boldsymbol{q}_n\right\|^2}(\boldsymbol{q}_{n+1}^s-\boldsymbol{q}_n) \tag{3.2.16}$$

with $\boldsymbol{q}_{n+\frac{1}{2}}^s = \frac{1}{2}(\boldsymbol{q}_{n+1}^s+\boldsymbol{q}_n)$ and $D_g R(\boldsymbol{g}(\boldsymbol{q}))$ denoting the Jacobian of R with respect to the constraint function $\boldsymbol{g}$.

(3.2.14) implies together with the assumptions (2.3.12) that $P_{\mathrm{Pen}}(\boldsymbol{g}(\boldsymbol{q}_{n+1})) = \lim\limits_{s\to\infty} \mu_s R(\boldsymbol{g}(\boldsymbol{q}_{n+1}^s)) = 0$. In particular, the growth of P_{Pen} is bounded, i.e. the following expression is bounded

$$\begin{aligned} DP_{\mathrm{Pen}}(\boldsymbol{g}(\boldsymbol{q}_{n+\frac{1}{2}})) &= \lim\limits_{s\to\infty} \mu_s D^T\boldsymbol{g}(\boldsymbol{q}_{n+\frac{1}{2}}^s)\cdot D_g R(\boldsymbol{g}(\boldsymbol{q}_{n+\frac{1}{2}}^s)) \\ &= D^T\boldsymbol{g}(\boldsymbol{q}_{n+\frac{1}{2}})\cdot \lim\limits_{s\to\infty} \mu_s D_g R(\boldsymbol{g}(\boldsymbol{z}_{n+\frac{1}{2}}^s)) \end{aligned} \tag{3.2.17}$$

for small enough time-steps. Since $\boldsymbol{0}$ is a regular value of the constraints, $D^T\boldsymbol{g}$ has full rank in $\boldsymbol{q}_n$ and $\boldsymbol{q}_{n+1}$. If the time-step is small enough, it can be assumed that $D^T\boldsymbol{g}(\boldsymbol{q}_{n+\frac{1}{2}})$ has also full rank, particularly it is injective. Hence there exist $(\boldsymbol{\theta}_{n+1}^s)_{s\in\mathbb{N}} \in \mathbb{R}^m$ and $\boldsymbol{\theta}_{n+1} \in \mathbb{R}^m$ with

$$\boldsymbol{\theta}_{n+1} = \lim\limits_{s\to\infty} \boldsymbol{\theta}_{n+1}^s = \lim\limits_{s\to\infty} \mu_s D\boldsymbol{g} R(\tilde{\boldsymbol{g}}(\boldsymbol{q}_{n+\frac{1}{2}}^s)) \tag{3.2.18}$$

and $\left\|\boldsymbol{\theta}_{n+1}\right\| < \infty$. Consequently with $\boldsymbol{q}_{n+\frac{1}{2}} = \frac{1}{2}(\boldsymbol{q}_{n+1}+\boldsymbol{q}_n)$

$$\lim_{s\to\infty} \mathsf{d}P_{\mathrm{Pen}}(\boldsymbol{g}(\boldsymbol{q}_n,\boldsymbol{q}^s_{n+1})) = D^T\boldsymbol{g}(\boldsymbol{q}_{n+\frac{1}{2}})\cdot\boldsymbol{\theta}_{n+1} - \frac{D^T\boldsymbol{g}(\boldsymbol{q}_{n+\frac{1}{2}})\cdot\boldsymbol{\theta}_{n+1}\cdot(\boldsymbol{q}_{n+1}-\boldsymbol{q}_n)}{\left\|\boldsymbol{q}_{n+1}-\boldsymbol{q}_n\right\|^2}(\boldsymbol{q}_{n+1}-\boldsymbol{q}_n)$$

$$(3.2.19)$$

Thus $(\boldsymbol{z}_{n+1},\boldsymbol{\theta}_{n+1})$ solve the constrained scheme (3.2.5). The uniqueness of the solution of (3.2.5) implies $\boldsymbol{\theta}_{n+1} = \boldsymbol{\lambda}_{n+1}$. ∎

Remark 3.2.3 In [Leye 04] a similar result is proved for the slightly more general case, allowing for the dependence of the holonomic constraints on the total phase variable $\boldsymbol{z}$. In [Rubi 57, Born 96], the special penalty function $P_{\mathrm{Pen}}(\boldsymbol{g}(\boldsymbol{q}(t))) = \mu\left\|\boldsymbol{g}(\boldsymbol{q}(t))\right\|^2$ is considered in the continuous (∞-dimensional) case and the weak convergence of $\mu_s\boldsymbol{g}(\boldsymbol{q}^s(t))$ to the correct Lagrange multiplier is discussed. Since the discrete system is finite-dimensional, weak and strong convergence are equivalent for $\boldsymbol{\theta}_{n+1} = \lim_{s\to\infty} \mu_s D_g R(\boldsymbol{g}(\boldsymbol{q}^s_{n+\frac{1}{2}}))$.

For an implementation of the penalty scheme, $(3.2.9)_1$ is solved for $\boldsymbol{p}_{n+1}$ and inserted into $(3.2.9)_2$. This yields the n-dimensional system

$$\frac{2}{h}\boldsymbol{M}\cdot\left(\boldsymbol{q}_{n+1}-\boldsymbol{q}_n\right) - 2\boldsymbol{p}_n + h\mathsf{d}^G V(\boldsymbol{q}_n,\boldsymbol{q}_{n+1}) + h\mu\mathsf{d}^G R(\boldsymbol{g}(\boldsymbol{q}_n,\boldsymbol{q}_{n+1})) \quad = \quad \boldsymbol{0} \quad (3.2.20)$$

to be solved for $\boldsymbol{q}_{n+1}$. The accuracy of the constraint fulfilment of the solution of (3.2.20) depends on the penalty parameter. The condition number of the iteration matrix for the solution of the nonlinear system of equations is of the order $\mathcal{O}(h^2\mu)$, see Appendix C.4 for proof. This implies that for certain well balanced combinations of small time-steps h and large penalty parameters μ, the system is well-conditioned.

3.2.3 Augmented Lagrange method

A separable Hamiltonian corresponding to (3.2.4) comprising the augmentation according to the augmented Lagrange method $P_H(\boldsymbol{z}) = P_{\mathrm{Aug}}(\boldsymbol{g}(\boldsymbol{q})) = \boldsymbol{g}^T(\boldsymbol{q})\cdot\boldsymbol{\lambda} + \mu R(\boldsymbol{g}(\boldsymbol{q}))$ described in Section 2.3.3, reads

$$H_{aug}(\boldsymbol{z}) = T_H(\boldsymbol{z}) + V_H(\boldsymbol{z}) + P_H(\boldsymbol{z}) = T(\boldsymbol{p}) + V(\boldsymbol{q}) + \boldsymbol{g}^T(\boldsymbol{q})\cdot\boldsymbol{\lambda} + \mu R(\boldsymbol{g}(\boldsymbol{q})) \quad (3.2.21)$$

with $T(\boldsymbol{p}) = \frac{1}{2}\boldsymbol{p}^T\cdot\boldsymbol{M}^{-1}\cdot\boldsymbol{p}$. For a fixed value $\boldsymbol{\lambda}^k \in \mathbb{R}^m$, insertion of (3.2.21) into the discrete Hamiltonian system (3.2.2) yields the energy-momentum conserving augmented Lagrange time-stepping scheme

$$\begin{aligned} \boldsymbol{q}^k_{n+1} - \boldsymbol{q}_n &= & h\boldsymbol{M}^{-1}\cdot\boldsymbol{p}^k_{n+\frac{1}{2}} \\ \boldsymbol{p}^k_{n+1} - \boldsymbol{p}_n &= & -h\mathsf{d}^G V(\boldsymbol{q}_n,\boldsymbol{q}^k_{n+1}) - h\mathbf{G}^T(\boldsymbol{q}_n,\boldsymbol{q}^k_{n+1})\cdot\boldsymbol{\lambda}^k_{n+1} - h\mu\mathsf{d}^G R(\boldsymbol{g}(\boldsymbol{q}_n,\boldsymbol{q}^k_{n+1})) \end{aligned}$$

$$(3.2.22)$$

with $\boldsymbol{z}^k_{n+\frac{1}{2}} = \frac{1}{2}(\boldsymbol{z}^k_{n+1} + \boldsymbol{z}_n)$. If the constraints $\boldsymbol{g}(\boldsymbol{q}^k_{n+1})$ are not satisfied satisfactorily by the solution of (3.2.22), the multiplier is updated similar to (2.3.17) according to

$$\boldsymbol{\lambda}^{k+1}_{n+1} = \boldsymbol{\lambda}^k_{n+1} + \mu D_g R(\boldsymbol{g}(\boldsymbol{q}^k_{n+1})) \quad (3.2.23)$$

with $D_g R(\boldsymbol{g}(\boldsymbol{q}))$ denoting the Jacobian of R with respect to the constraint function $\boldsymbol{g}$. Then (3.2.22) is solved again for $\boldsymbol{z}^{k+1}_{n+1}$.

Proposition 3.2.4 *Let $z_n = (q_n, p_n)$ be consistent coordinates at time t_n, $n \in \mathbb{N}$ arbitrary. Let $\mu \in \mathbb{R}^+$ be arbitrary and denote the solution of the system (3.2.22) corresponding to $\boldsymbol{\lambda}_{n+1}^k$ by z_{n+1}^k. Let $z_{n+1} = \lim_{k \to \infty} z_{n+1}^k$ be the limit point of the sequence of solutions. Then the sequence of multipliers $\left(\boldsymbol{\lambda}_{n+1}^k\right)_{k \in \mathbb{N}}$ converges to the correct Lagrange multiplier $\boldsymbol{\lambda}_{n+1}$, such that $(z_{n+1}, \boldsymbol{\lambda}_{n+1})$ solve the constrained scheme (3.2.5).*

Proof: Let $z_{n+1} = \lim_{k \to \infty} z_{n+1}^k$ be the limit point of the solutions of (3.2.22). Note that the existence of a limit point for the solution sequence and for the multiplier sequence follows directly from the corresponding result in the temporal continuous case (see Remark 2.3.8 and [Bert 95]). Denote the limit point of the sequence of multipliers by

$$\bar{\boldsymbol{\lambda}}_{n+1} = \lim_{k \to \infty} \boldsymbol{\lambda}_{n+1}^k = \boldsymbol{\lambda}_{n+1}^0 + \sum_{k=1}^{\infty} \mu D_g R(\boldsymbol{g}(\boldsymbol{q}_{n+1}^k)) \tag{3.2.24}$$

with $\boldsymbol{\lambda}_{n+1}^0 = \bar{\boldsymbol{\lambda}}_n$. Then it follows that

$$\lim_{k \to \infty} D_g R(\boldsymbol{g}(\boldsymbol{q}_{n+1}^k)) = \boldsymbol{0} \tag{3.2.25}$$

This and the convexity of R (see assumption (2.3.12)) imply

$$\boldsymbol{g}(\boldsymbol{q}_{n+1}) = \boldsymbol{0} \tag{3.2.26}$$

i.e. the constraints $(3.2.5)_3$ are fulfilled in the limit point $\boldsymbol{q}_{n+1}$. Besides the supplementation of the constrained scheme by the constraint equations, (3.2.5) and (3.2.22) differ in the discrete derivatives $\mathsf{d}P_{\mathrm{Lag}}(\boldsymbol{g}(\boldsymbol{q}_n, \boldsymbol{q}_{n+1}))$ given in (3.2.15) and

$$\begin{aligned}
\mathsf{d}P_{\mathrm{Aug}}(\boldsymbol{g}(\boldsymbol{q}_n, \boldsymbol{q}_{n+1}^k)) = \quad & D^T \boldsymbol{g}(\boldsymbol{q}_{n+\frac{1}{2}}^k) \cdot \boldsymbol{\lambda}_{n+1}^k + \mu D^T \boldsymbol{g}(\boldsymbol{q}_{n+\frac{1}{2}}^k) \cdot D_g R(\boldsymbol{g}(\boldsymbol{q}_{n+\frac{1}{2}}^k)) + \\[2mm]
& \frac{\boldsymbol{g}^T(\boldsymbol{q}_{n+1}^k) \cdot \boldsymbol{\lambda}_{n+1}^k + \mu R(\boldsymbol{g}(\boldsymbol{q}_{n+1}^k))}{\left\| \boldsymbol{q}_{n+1}^k - \boldsymbol{q}_n \right\|^2}(\boldsymbol{q}_{n+1}^k - \boldsymbol{q}_n) + \\[2mm]
& \frac{-\left(D^T \boldsymbol{g}(\boldsymbol{q}_{n+\frac{1}{2}}^k) \cdot \boldsymbol{\lambda}_{n+1}^k + \mu D^T \boldsymbol{g}(\boldsymbol{q}_{n+\frac{1}{2}}^k) \cdot D_g R(\boldsymbol{g}(\boldsymbol{q}_{n+\frac{1}{2}}^k)) \right) \cdot (\boldsymbol{q}_{n+1}^k - \boldsymbol{q}_n)}{\left\| \boldsymbol{q}_{n+1}^k - \boldsymbol{q}_n \right\|^2}(\boldsymbol{q}_{n+1}^k - \boldsymbol{q}_n)
\end{aligned} \tag{3.2.27}$$

With $\boldsymbol{q}_{n+\frac{1}{2}}^k = \frac{1}{2}(\boldsymbol{q}_{n+1}^k + \boldsymbol{q}_n)$, (3.2.25) and (3.2.26) imply

$$\lim_{k \to \infty} \mathsf{d}P_{\mathrm{Aug}}(\boldsymbol{g}(\boldsymbol{q}_n, \boldsymbol{q}_{n+1}^k)) = D^T \boldsymbol{g}(\boldsymbol{q}_{n+\frac{1}{2}}) \cdot \bar{\boldsymbol{\lambda}}_{n+1} - \frac{D^T \boldsymbol{g}(\boldsymbol{q}_{n+\frac{1}{2}}) \cdot \bar{\boldsymbol{\lambda}}_{n+1} \cdot (\boldsymbol{q}_{n+1} - \boldsymbol{q}_n)}{\left\| \boldsymbol{q}_{n+1} - \boldsymbol{q}_n \right\|^2}(\boldsymbol{q}_{n+1} - \boldsymbol{q}_n) \tag{3.2.28}$$

Thus $(z_{n+1}, \bar{\boldsymbol{\lambda}}_{n+1})$ solve the constrained scheme (3.2.5). The uniqueness of the solution of (3.2.5) implies $\bar{\boldsymbol{\lambda}}_{n+1} = \boldsymbol{\lambda}_{n+1}$. ∎

Remark 3.2.5 In [Leye 04] a similar result is proved for the slightly more general case, allowing for the dependence of the holonomic constraints on the total phase variable $\boldsymbol{z}$. Proposition 3.2.4 holds for the class of energy conserving time-stepping schemes designed by the use of the discrete derivative given in Example 3.1.3. The statement can also be derived for the subclass of energy-momentum conserving schemes using the G-equivariant discrete derivative, but in the given form it is more general and notationally simpler.

For an implementation of the augmented Lagrange time-stepping scheme, $(3.2.22)_1$ is solved for $\boldsymbol{p}_{n+1}^k$ and inserted into $(3.2.22)_2$. This yields the n-dimensional system

$$
\begin{aligned}
\frac{2}{h}\boldsymbol{M}\left(\boldsymbol{q}_{n+1}^k - \boldsymbol{q}_n\right) - 2\boldsymbol{p}_n + h\mathsf{d}^G V(\boldsymbol{q}_n, \boldsymbol{q}_{n+1}^k) + h\mathsf{G}^T(\boldsymbol{q}_n, \boldsymbol{q}_{n+1}^k) \cdot \boldsymbol{\lambda}_{n+1}^k + \\
h\mu \mathsf{d}^G R(\boldsymbol{g}(\boldsymbol{q}_n, \boldsymbol{q}_{n+1}^k)) \;=\; \boldsymbol{0}
\end{aligned}
\tag{3.2.29}
$$

to be solved for $\boldsymbol{q}_{n+1}^k$ using the fixed multiplier $\boldsymbol{\lambda}_{n+1}^k$. Then the multiplier is updated according to (3.2.23) and a more accurate solution is obtained by resolving (3.2.29). This procedure is repeated iteratively until the constraints are fulfilled satisfactorily. The magnitude of the parameter μ influences the accuracy of the first solution in a new time-step and thus determines the number of necessary iterations. It can remain of relatively small magnitude if one allows many iterations. The condition number of the iteration matrix for the solution of the nonlinear system of equations is of the order $\mathcal{O}(h^2\mu)$, see Appendix C.5 for proof. Thus for small time-steps, the system is well-conditioned.

3.2.4 Discrete null space method

In complete analogy to the procedure outlined in Section 2.3.4 for the temporal continuous case, a transition from the constrained scheme (3.2.3) to a discrete d'Alembert-type scheme implicating a size reduction can be accomplished. This transition is introduced by Betsch in [Bets 05] and termed 'discrete null space method'.
A discrete null space matrix $\mathbf{P}(\boldsymbol{q}_n, \boldsymbol{q}_{n+1}) : \mathbb{R}^{n-m} \to \mathbb{R}^n$ whose columns form a basis for the $(n-m)$-dimensional null space of the partial G-equivariant discrete derivative $\mathsf{G}(\boldsymbol{q}_n, \boldsymbol{q}_{n+1}) = \mathsf{d}^G\boldsymbol{g}(\boldsymbol{q}_n, \boldsymbol{q}_{n+1})$ of the constraints, i.e.

$$
\mathrm{range}\left(\mathbf{P}(\boldsymbol{q}_n, \boldsymbol{q}_{n+1})\right) = \mathrm{null}\left(\mathsf{G}(\boldsymbol{q}_n, \boldsymbol{q}_{n+1})\right)
\tag{3.2.30}
$$

must be found. Premultiplying $(3.2.3)_2$ by the transposed of the discrete null space matrix cancels the discrete counterpart of the constraint forces and thus eliminates the Lagrange multipliers from the scheme. The resulting d'Alembert-type time-stepping scheme for the d'Alembert-type Hamiltonian system (2.3.21) reads

$$
\begin{aligned}
\boldsymbol{q}_{n+1} - \boldsymbol{q}_n - h\mathsf{D}_2^G H(\boldsymbol{z}_n, \boldsymbol{z}_{n+1}) &= \boldsymbol{0} \\
\mathbf{P}^T(\boldsymbol{q}_n, \boldsymbol{q}_{n+1}) \cdot \left[\boldsymbol{p}_{n+1} - \boldsymbol{p}_n + h\mathsf{D}_1^G H(\boldsymbol{z}_n, \boldsymbol{z}_{n+1})\right] &= \boldsymbol{0} \\
\boldsymbol{g}(\boldsymbol{q}_{n+1}) &= \boldsymbol{0}
\end{aligned}
\tag{3.2.31}
$$

The following important proposition and proof have been taken from [Bets 05].

Proposition 3.2.6 *The d'Alembert-type time-stepping scheme (3.2.31) is equivalent to the constrained scheme (3.2.3).*

45

Proof: Recapitulating the construction procedure of the d'Alembert-type scheme from the constrained scheme, it is obvious that for given initial values $(\boldsymbol{q}_n, \boldsymbol{p}_n)$, a solution $(\boldsymbol{q}_{n+1}, \boldsymbol{p}_{n+1}, \boldsymbol{\lambda}_{n+1})$ of the constrained scheme (3.2.3) is also a solution of the d'Alembert-type scheme (3.2.31).

Assume that $(\boldsymbol{q}_{n+1}, \boldsymbol{p}_{n+1})$ solve the d'Alembert-type scheme (3.2.31) for given $(\boldsymbol{q}_n, \boldsymbol{p}_n)$. Note that condition (3.2.30) on the discrete null space matrix implies $\text{null}\left(\mathbf{P}^T(\boldsymbol{q}_n, \boldsymbol{q}_{n+1})\right) = \text{range}\left(\mathbf{G}^T(\boldsymbol{q}_n, \boldsymbol{q}_{n+1})\right)$ (see e.g. [Fisc 97]). Together with $(3.2.31)_2$ it follows that

$$\left[\boldsymbol{p}_{n+1} - \boldsymbol{p}_n + h\mathrm{D}_1^G H(\boldsymbol{z}_n, \boldsymbol{z}_{n+1})\right] \in \text{null}\left(\mathbf{P}^T(\boldsymbol{q}_n, \boldsymbol{q}_{n+1})\right) = \text{range}\left(\mathbf{G}^T(\boldsymbol{q}_n, \boldsymbol{q}_{n+1})\right) \quad (3.2.32)$$

Accordingly, there exists a multiplier $\boldsymbol{\lambda}_{n+1} \in \mathbb{R}^m$ such that $(\boldsymbol{q}_{n+1}, \boldsymbol{p}_{n+1}, \boldsymbol{\lambda}_{n+1})$ solve the constrained scheme (3.2.3). $\blacksquare$

Therefore, the d'Alembert-type scheme has the same conservation properties as the constrained scheme. The total energy and at most quadratic momentum maps are conserved along a solution sequence $(\boldsymbol{z}_n)_{n\in\mathbb{N}}$ of (3.2.31) and the constraints are fulfilled exactly at the time nodes.

If the Hamiltonian is separable as given in (3.2.4), $\boldsymbol{p}_{n+1}$ can be extracted from $(3.2.31)_1$ and inserted in $(3.2.31)_2$. This yields the n-dimensional system

$$\mathbf{P}^T(\boldsymbol{q}_n, \boldsymbol{q}_{n+1}) \cdot \left[\frac{2}{h}\boldsymbol{M} \cdot \left(\boldsymbol{q}_{n+1} - \boldsymbol{q}_n\right) - 2\boldsymbol{p}_n + h\mathrm{d}^G V(\boldsymbol{q}_n, \boldsymbol{q}_{n+1})\right] = \boldsymbol{0}$$
$$\boldsymbol{g}(\boldsymbol{q}_{n+1}) = \boldsymbol{0} \quad (3.2.33)$$

to be solved for $\boldsymbol{q}_{n+1}$. Note that this dimension is larger than the number of degrees of freedom $n - m$ of the constrained mechanical system. During the iterative solution procedure for the system of nonlinear algebraic equations (3.2.33), the tangent matrix assumes the form given in (B.2) in Appendix B.

Besides the smaller dimension, the main advantage of the d'Alembert-type scheme over the constrained scheme is that due to the elimination of the Lagrange multipliers from the scheme, the conditioning problem has been removed. The condition number of the iteration matrix for the solution of the d'Alembert-type scheme is independent of the time-step, see Appendix C.3 for proof.

Remark 3.2.7 (Properties of the discrete null space matrix) The discrete null space matrix $\mathbf{P}(\boldsymbol{q}_n, \boldsymbol{q}_{n+1})$ has the following properties:

(i) $\text{rank}\left(\mathbf{P}(\boldsymbol{q}_n, \boldsymbol{q}_{n+1})\right) = n - m$

(ii) $\mathbf{G}(\boldsymbol{q}_n, \boldsymbol{q}_{n+1}) \cdot \mathbf{P}(\boldsymbol{q}_n, \boldsymbol{q}_{n+1}) = \mathbf{0}_{m \times (n-m)}$

(iii) $\lim\limits_{\boldsymbol{q}_{n+1} \to \boldsymbol{q}_n} \mathbf{P}(\boldsymbol{q}_n, \boldsymbol{q}_{n+1}) = \boldsymbol{U}_n$ with $\text{range}\left(\boldsymbol{U}_n\right) = \text{null}\left(\boldsymbol{G}(\boldsymbol{q}_n)\right)$

Properties (i) and (ii) are equivalent to the necessary and sufficient condition (3.2.30) on $\mathbf{P}(\boldsymbol{q}_n, \boldsymbol{q}_{n+1})$ to be a discrete null space matrix. Consistency of the approach is guaranteed by property (iii), which is implied by (i) and (ii) due to the consistency property of the discrete derivative (see Definition 3.1.1). It means that in the limit for vanishing time-steps, the discrete null space matrix coincides with the continuous one.

Remark 3.2.8 (Explicit representation of the discrete null space matrix) For many applications it is possible to infer a viable discrete null space matrix from the corresponding continuous null space matrix by midpoint evaluation. This holds e.g. for the motion of a single rigid body as shown in Section 4.3.4, for the treatment of spatially discretised elastic beams presented in Section 5.4.4 and for lower kinematic pairs without relative translational degrees of freedom described in Sections 6.1.4, 6.1.6, as well as for their generalisations to open kinematic chains (see Example 6.2.3). For other applications, slight modifications of the midpoint evaluation of the continuous null space matrix lead to an appropriate discrete null space matrix. For example for the lower kinematic pairs involving relative translational degrees of freedom treated in Sections 6.1.5, 6.1.7, 6.1.8, these modifications can be detected by a careful inspection of the condition (3.2.30).

If no explicit representation of the discrete null space matrix can be found, nevertheless an implicit representation can be used in any case.

Example 3.2.9 (Implicit representation of the discrete null space matrix) As in the continuous case, the discrete null space matrix is not unique, necessary and sufficient condition on $\mathbf{P}(\boldsymbol{q}_n, \boldsymbol{q}_{n+1})$ is (3.2.30). A general construction procedure for a discrete null space matrix described in [Bets 05] rests on the decomposition of $\mathbb{R}^n$ into an m-dimensional subspace with base vectors $\boldsymbol{b}_1, \ldots, \boldsymbol{b}_m$ and associated matrix $\boldsymbol{W} = [\boldsymbol{b}_1, \ldots, \boldsymbol{b}_m] \in \mathbb{R}^{n \times m}$ and an $(n-m)$-dimensional subspace with base vectors $\boldsymbol{b}_{m+1}, \ldots, \boldsymbol{b}_n$ and associated matrix $\boldsymbol{U} = [\boldsymbol{b}_{m+1}, \ldots, \boldsymbol{b}_n] \in \mathbb{R}^{n \times (n-m)}$. Then every $(\boldsymbol{q}_{n+1} - \boldsymbol{q}_n) \in \mathbb{R}^n$ can be uniquely expressed as

$$\boldsymbol{q}_{n+1} - \boldsymbol{q}_n = \boldsymbol{U} \cdot \boldsymbol{u} + \boldsymbol{W} \cdot \boldsymbol{w} \tag{3.2.34}$$

for some $\boldsymbol{u} \in \mathbb{R}^{n-m}$ and $\boldsymbol{w} \in \mathbb{R}^m$. To transform $\boldsymbol{U}$ to $\mathrm{null}\left(\mathbf{G}(\boldsymbol{q}_n, \boldsymbol{q}_{n+1})\right)$ the directionality property of the discrete derivative

$$\mathbf{G}(\boldsymbol{q}_n, \boldsymbol{q}_{n+1}) \cdot (\boldsymbol{q}_{n+1} - \boldsymbol{q}_n) = \mathbf{0} \tag{3.2.35}$$

(see Definition 3.1.1) is taken into account. Substitution of (3.2.34) into (3.2.35) yields

$$\boldsymbol{w} = -\left(\mathbf{G}(\boldsymbol{q}_n, \boldsymbol{q}_{n+1}) \cdot \boldsymbol{W}\right)^{-1} \cdot \mathbf{G}(\boldsymbol{q}_n, \boldsymbol{q}_{n+1}) \cdot \boldsymbol{U} \cdot \boldsymbol{u} \tag{3.2.36}$$

This representation of $\boldsymbol{w}$ can be inserted into (3.2.34) leading to

$$\boldsymbol{q}_{n+1} - \boldsymbol{q}_n = \mathbf{P}(\boldsymbol{q}_n, \boldsymbol{q}_{n+1}) \cdot \boldsymbol{u} \tag{3.2.37}$$

with the implicit representation of the discrete null space matrix defined by

$$\mathbf{P}(\boldsymbol{q}_n, \boldsymbol{q}_{n+1}) = \left[\boldsymbol{I}_{n \times n} - \boldsymbol{W} \cdot \left(\mathbf{G}(\boldsymbol{q}_n, \boldsymbol{q}_{n+1}) \cdot \boldsymbol{W}\right)^{-1} \cdot \mathbf{G}(\boldsymbol{q}_n, \boldsymbol{q}_{n+1})\right] \cdot \boldsymbol{U} \tag{3.2.38}$$

For this construction procedure it is essential that the linear operator $\mathbf{G}(\boldsymbol{q}_n, \boldsymbol{q}_{n+1}) \cdot \boldsymbol{W} : \mathbb{R}^m \to \mathbb{R}^m$ is invertible. To guarantee the invertibility, $\boldsymbol{W}$ can be constructed as follows. $\mathbb{R}^n$ can be decomposed into

$$\begin{aligned} \mathbb{R}^n &= \mathrm{null}\left(\boldsymbol{G}(\boldsymbol{q}_n)\right) \oplus \mathrm{range}\left(\boldsymbol{G}^T(\boldsymbol{q}_n)\right) \\ &= T_{\boldsymbol{q}_n}C \oplus \left(T_{\boldsymbol{q}_n}C\right)^{\perp} \end{aligned} \tag{3.2.39}$$

Similar to the procedure in the continuous case in (2.3.23), performing a QR-decomposition of the transposed constraint Jacobian at the time node t_n yields

$$\boldsymbol{G}^T(\boldsymbol{q}_n) = \boldsymbol{Q}_n \cdot \boldsymbol{R}_n = [\boldsymbol{W}_n, \boldsymbol{U}_n] \cdot \begin{bmatrix} \bar{\boldsymbol{R}}_n \\ \boldsymbol{0}_{(n-m)\times m} \end{bmatrix} \tag{3.2.40}$$

containing the nonsingular upper triangular matrix $\bar{\boldsymbol{R}}_n \in \mathbb{R}^{m\times m}$ and the orthogonal matrix $\boldsymbol{Q}_n = [\boldsymbol{W}_n, \boldsymbol{U}_n] \in \mathbb{R}^{n\times n}$ that can be partitioned into the $n \times m$ matrix $\boldsymbol{W}_n$ and the $n \times (n-m)$ matrix $\boldsymbol{U}_n$ with

$$\begin{aligned} \text{range}\,(\boldsymbol{W}_n) &= \text{range}\,\big(\boldsymbol{G}^T(\boldsymbol{q}_n)\big) \\ \text{range}\,(\boldsymbol{U}_n) &= \text{null}\,(\boldsymbol{G}(\boldsymbol{q}_n)) \end{aligned} \tag{3.2.41}$$

i.e. the columns of $\boldsymbol{U}_n$ form a basis for the nodal tangent space $T_{\boldsymbol{q}_n}C$. The matrices $\boldsymbol{W}_n, \boldsymbol{U}_n$ or alternatively $\boldsymbol{G}^T(\boldsymbol{q}_n), \boldsymbol{U}_n$ can be used in (3.2.38) to define a discrete null space matrix.

Note that due to consistency property of the discrete derivative (see Definition 3.1.1), the property $\lim_{\boldsymbol{q}_{n+1}\to\boldsymbol{q}_n} \mathsf{G}(\boldsymbol{q}_n, \boldsymbol{q}_{n+1}) = \boldsymbol{G}(\boldsymbol{q}_n)$ holds. Thus presuming that time-steps are small for practical applications, one can assume that the $m \times m$ matrices $\mathsf{G}(\boldsymbol{q}_n, \boldsymbol{q}_{n+1}) \cdot \boldsymbol{W}_n$ or alternatively $\mathsf{G}(\boldsymbol{q}_n, \boldsymbol{q}_{n+1}) \cdot \boldsymbol{G}^T(\boldsymbol{q}_n)$ are invertible.

Remark 3.2.10 (Properties of the discrete null space matrix (3.2.38)) Using $\boldsymbol{W}_n, \boldsymbol{U}_n$ determined by QR-decomposition in (3.2.40), the columns of the discrete null space matrix given in (3.2.38) are pairwise orthonormal, hence $\text{cond}\,\big(\mathsf{P}(\boldsymbol{q}_n, \boldsymbol{q}_{n+1})\big) = 1$. This property is advantageous for the numerical performance of the d'Alembert-type time-stepping scheme (3.2.31) but not necessary for a discrete null space matrix. It states that the condition number of the terms in the brackets in $(3.2.31)_2$ is not deteriorated by the premultiplication of the transposed discrete null space matrix.

Remark 3.2.11 (Computational costs) Instead of the procedure described in Example 3.2.9, a discrete null space matrix could be directly obtained as the least $n - m$ columns in the orthogonal matrix of a QR-factorisation of $\mathsf{G}(\boldsymbol{q}_n, \boldsymbol{q}_{n+1})$. However, this factorisation would be necessary at every iteration during the iterative solution of the system of nonlinear algebraic equations (3.2.31), causing unacceptably high computational costs. An acceptable compromise is the example (3.2.38) of a discrete null space matrix, where the decomposition (3.2.39) has to be carried out at every time-step.

In general, an explicit representation of the discrete null space matrix is desirable for practical applications. Indeed, such an explicit representation is feasible for many applications as presented in the sequel for mass point systems, rigid body motion and multibody systems consisting of rigid and elastic components.

3.2.5 Discrete null space method with nodal reparametrisation

Similar to the continuous case, for many applications a reduction of the system to the minimal possible dimension can be accomplished by a local reparametrisation of the constraint manifold C given in (2.3.3), in the neighbourhood of the discrete configuration

variable $\boldsymbol{q}_n \in C$. At the time nodes $\boldsymbol{q}_{n+1}$ is expressed in terms of the incremental generalised coordinates $\boldsymbol{u} \in U \subseteq \mathbb{R}^{n-m}$, such that the constraints are fulfilled

$$\boldsymbol{F}\boldsymbol{q}_n : U \subseteq \mathbb{R}^{n-m} \to C \quad \text{i.e.} \quad \boldsymbol{g}(\boldsymbol{q}_{n+1}) = \boldsymbol{g}(\boldsymbol{F}\boldsymbol{q}_n(\boldsymbol{u})) = \boldsymbol{0} \tag{3.2.42}$$

Insertion of this nodal reparametrisation into the d'Alembert-type scheme redundantises $(3.2.31)_3$ and leads to the following time-stepping scheme

$$\begin{aligned}
\boldsymbol{F}\boldsymbol{q}_n(\boldsymbol{u}) - \boldsymbol{q}_n - h\mathsf{D}_2^G H(\boldsymbol{z}_n, (\boldsymbol{F}\boldsymbol{q}_n(\boldsymbol{u}), \boldsymbol{p}_{n+1})) &= \boldsymbol{0} \\
\mathbf{P}^T(\boldsymbol{q}_n, \boldsymbol{F}\boldsymbol{q}_n(\boldsymbol{u})) \cdot \left[\boldsymbol{p}_{n+1} - \boldsymbol{p}_n + h\mathsf{D}_1^G H(\boldsymbol{z}_n, (\boldsymbol{F}\boldsymbol{q}_n(\boldsymbol{u}), \boldsymbol{p}_{n+1})) \right] &= \boldsymbol{0}
\end{aligned} \tag{3.2.43}$$

The following important proposition and proof have been taken from [Bets 05].

Proposition 3.2.12 *The d'Alembert-type time-stepping scheme with nodal reparametrisation (3.2.43) is equivalent to the constrained scheme (3.2.3).*

Proof: With regard to the construction procedure of the d'Alembert-type scheme with nodal reparametrisation from the constrained scheme, it is obvious that for given initial values $(\boldsymbol{q}_n, \boldsymbol{p}_n)$, a solution $(\boldsymbol{q}_{n+1}, \boldsymbol{p}_{n+1}, \boldsymbol{\lambda}_{n+1})$ of the constrained scheme (3.2.3) induces the solution $(\boldsymbol{u} = \boldsymbol{F}\boldsymbol{q}_n^{-1}(\boldsymbol{q}_{n+1}), \boldsymbol{p}_{n+1})$ of the d'Alembert-type scheme with nodal reparametrisation (3.2.43).
Along the lines of the second step in proof of Proposition 3.2.6, it follows that for a solution $(\boldsymbol{u}, \boldsymbol{p}_{n+1})$ of the d'Alembert-type scheme with nodal reparametrisation (3.2.43) for given $(\boldsymbol{q}_n, \boldsymbol{p}_n)$ there exists a multiplier $\boldsymbol{\lambda}_{n+1} \in \mathbb{R}^m$ such that $(\boldsymbol{F}\boldsymbol{q}_n(\boldsymbol{u}), \boldsymbol{p}_{n+1}, \boldsymbol{\lambda}_{n+1})$ solve the constrained scheme (3.2.3). ∎

Thus the total energy and at most quadratic momentum maps are conserved along the sequence $(\boldsymbol{z}_n)_{n \in \mathbb{N}} = (\boldsymbol{F}_n(\boldsymbol{u}), \boldsymbol{p}_n)_{n \in \mathbb{N}}$ obtained from system (3.2.43) and the constraints are fulfilled exactly at the time nodes.
If the Hamiltonian is separable as given in (3.2.4), $\boldsymbol{p}_{n+1}$ can be extracted from $(3.2.43)_1$ and inserted in $(3.2.43)_2$. Then one has to solve the $(n-m)$-dimensional system

$$\mathbf{P}^T(\boldsymbol{q}_n, \boldsymbol{F}\boldsymbol{q}_n(\boldsymbol{u})) \cdot \left[\frac{2}{h}\boldsymbol{M} \cdot (\boldsymbol{F}\boldsymbol{q}_n(\boldsymbol{u}) - \boldsymbol{q}_n) - 2\boldsymbol{p}_n + h\mathsf{d}^G V(\boldsymbol{q}_n, \boldsymbol{F}\boldsymbol{q}_n(\boldsymbol{u})) \right] = \boldsymbol{0} \tag{3.2.44}$$

for the discrete generalised coordinate $\boldsymbol{u}$ and obtains the sought configuration $\boldsymbol{q}_{n+1}$ via the transformation (3.2.42).
Furthermore, the d'Alembert-type scheme with nodal reparametrisation retains the independence of the condition number of the iteration matrix on the time-step during the solution procedure from the d'Alembert-type scheme (3.2.31), see Appendix C.2 for proof. Altogether, this scheme features a combination of the required algorithmic conservation properties and the good conditioning quality with a minimal dimension, i.e. the number of equations equals exactly the number of degrees of freedom of the mechanical system.

Remark 3.2.13 (Iterative and incremental unknowns) For the nodal reparametrisation (3.2.42) of $\boldsymbol{q}_{n+1}$ in terms of discrete generalised coordinates $\boldsymbol{u}$ in the context of an iterative solution procedure for the system of nonlinear algebraic equations (3.2.44), one

can distinguish between two types of unknowns. Using iterative unknowns, the configuration variable is updated in each step of the Newton-Raphson iteration according to $\boldsymbol{q}_{n+1}^{l+1} = \boldsymbol{F}\boldsymbol{q}_{n+1}^{l}(\boldsymbol{u})$. On the other hand using incremental unknowns, the total increment of the generalised coordinate in one time-step is determined during the Newton-Raphson iteration and the configuration variable is then obtained from $\boldsymbol{q}_{n+1} = \boldsymbol{F}\boldsymbol{q}_n(\boldsymbol{u})$. The corresponding linearisations of (3.2.44) are given in Appendix B.1. See also [Jele 98, Sans 03] for investigations concerning the interpolation of iterative or incremental rotations.

3.2.6 Summary

Table 3.1 summarises the theoretical aspects of the five different time-stepping schemes resulting from the different methods to treat the constraints. In particular, for the Lagrange multiplier scheme (3.2.7), the penalty scheme (3.2.20), the augmented Lagrange scheme (3.2.29), the d'Alembert-type scheme (3.2.33) and the d'Alembert-type scheme with nodal reparametrisation (3.2.44), the performance in the categories dimension of the system of equations, constraint fulfilment of the solution and dependence of the condition number of the specific iteration matrix on the time-step h and possibly on the penalty parameter μ is compared. Thereby, n is the dimension of the configuration manifold and m denotes the number of holonomic constraints.

Accordingly the constraints are fulfilled exactly for the largest dimensional constrained scheme, as well as for the n-dimensional d'Alembert-type scheme and the smallest dimensional d'Alembert-type scheme with nodal reparametrisation. For the penalty scheme the accuracy of the constraint fulfilment improves for increasing penalty parameters. On the other hand it improves during an extra iteration until a prescribed tolerance is reached for the augmented Lagrange scheme. Thereby, μ remains of constant and moderate magnitude. Besides the dependence of the condition number of the iteration matrix of all schemes on a problem-dependent constant, their behaviour differs significantly. While the constrained scheme becomes more and more ill-conditioned as the time-step decreases, the penalty scheme can be well-conditioned for certain combinations of relatively small time-steps and relatively large penalty parameters. Since the parameter μ remains of moderate magnitude, the augmented Lagrange scheme is generally well-conditioned for small time steps. Both d'Alembert-type schemes possess the convenient independence of the condition number on h and μ. Apparently, the d'Alembert-type scheme with nodal reparametrisation combines the advantageous properties of a small dimensional system whose condition number is independent of the time-step and whose solution fulfils the constraints exactly.

Table 3.1: Comparison of the theoretical aspects of the constrained scheme, penalty scheme, augmented Lagrange scheme, d'Alembert-type scheme and d'Alembert-type scheme with nodal reparametrisation.

	constrained	penalty	augm. Lag.	d'Al.	d'Al. rep.
number of unknowns	$n + m$	n	n	n	$n - m$
constraint fulfilment	exact	dep. on μ	tolerance	exact	exact
condition number	$\mathcal{O}(h^{-3})$	$\mathcal{O}(h^2\mu)$	$\mathcal{O}(h^2\mu)$	$const$	$const$

4 Mass point system and rigid body dynamics

In order to demonstrate the performance and especially the equivalence of the different methods to treat the constraints presented in the preceding chapters illustratively, the constrained dynamics of simple, small dimensional mechanical systems are examined first. In this connection, mass point systems and rigid bodies serve as reliable examples.

4.1 Double spherical pendulum
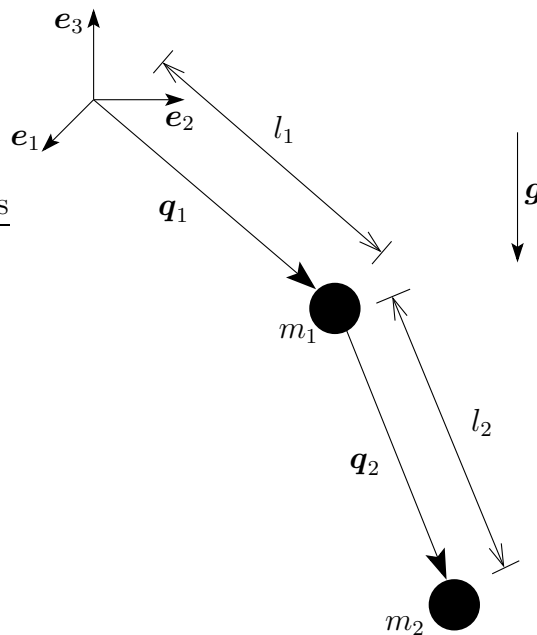
Figure 4.1: Double spherical pendulum.

The double spherical pendulum in Figure 4.1 is suspended at the origin of the inertial frame $\{\boldsymbol{e}_I\}$. Massless rigid rods of lengths l_1 and l_2 connect the masses m_1 and m_2 to each other and to the origin, respectively. The gravitational acceleration with value g points in the negative $\boldsymbol{e}_3$-direction. The kinetic energy T and the potential energy V are given by the following expressions

$$T(\boldsymbol{p}) = \frac{1}{2}\boldsymbol{p}^T \cdot \boldsymbol{M}^{-1} \cdot \boldsymbol{p} \qquad V(\boldsymbol{q}) = -g \begin{bmatrix} \boldsymbol{e}_3 \\ \boldsymbol{0}_{3\times 1} \end{bmatrix}^T \cdot \boldsymbol{M} \cdot \boldsymbol{q} \tag{4.1.1}$$

with

$$\boldsymbol{q}(t) = \begin{bmatrix} \boldsymbol{q}^1(t) \\ \boldsymbol{q}^2(t) \end{bmatrix} \in \mathbb{R}^6 \qquad \boldsymbol{p}(t) = \begin{bmatrix} \boldsymbol{p}^1(t) \\ \boldsymbol{p}^2(t) \end{bmatrix} \in \mathbb{R}^6 \tag{4.1.2}$$

The constant 6×6 mass matrix corresponding to the given phase variable $\boldsymbol{z} = (\boldsymbol{q}, \boldsymbol{p})$ of the double spherical pendulum reads

$$\boldsymbol{M} = \begin{bmatrix} (m_1 + m_2)\boldsymbol{I}_3 & m_2\boldsymbol{I}_3 \\ m_2\boldsymbol{I}_3 & m_2\boldsymbol{I}_3 \end{bmatrix} \tag{4.1.3}$$

Remark 4.1.1 (Generalised coordinates) The parametrisation of the double spherical pendulum's Hamiltonian in terms of generalised coordinates leads to the configuration-dependent mass matrix given in Appendix D. It serves as an example of a configuration-dependent mass matrix causing the temporal discretisation of the equations of motion in generalised coordinates to be very involved.

The constraints are related to the constancy of the lengths of the rigid rods

$$\begin{aligned} g_1(\boldsymbol{q}) &= \frac{1}{2} \left((\boldsymbol{q}^1)^T \cdot \boldsymbol{q}^1 - l_1^2 \right) \\ g_2(\boldsymbol{q}) &= \frac{1}{2} \left((\boldsymbol{q}^2)^T \cdot (\boldsymbol{q}^2) - l_2^2 \right) \end{aligned} \tag{4.1.4}$$

They restrict possible configurations to the constraint manifold $C = S_{l_1}^2 \times S_{l_2}^2$ consisting of two spheres, one about the origin with radius l_1 and one about the first mass with radius l_2.

All time-stepping schemes investigated in the sequel use the G-equivariant discrete derivative (see Definitions 3.1.4 and 3.1.7) given in Example 3.1.6, wherefore the reparametrisation of the Hamiltonian in terms of invariants is necessary. Due to the presence of gravitation, the Hamiltonian $H(\boldsymbol{q}, \boldsymbol{p}) = T(\boldsymbol{p}) + V(\boldsymbol{q})$ consisting of the energies given in (4.1.1) is invariant with respect to rotation of the mass point system about the axis $\boldsymbol{e}_3$. Consequently, the angular momentum's component corresponding to the gravitational direction L_3 is a first integral of the motion of the double spherical pendulum, see Section 2.2.3. The Hamiltonian can be reparametrised in the independent invariants $\boldsymbol{\pi}(\boldsymbol{z})$ comprising

$$\begin{array}{lll} \pi_1(\boldsymbol{z}) = (\boldsymbol{p}^1)^T \cdot \boldsymbol{p}^1 & \pi_2(\boldsymbol{z}) = (\boldsymbol{p}^2)^T \cdot \boldsymbol{p}^2 & \pi_3(\boldsymbol{z}) = (\boldsymbol{p}^1)^T \cdot \boldsymbol{p}^2 \\ \pi_4(\boldsymbol{z}) = (\boldsymbol{e}_3)^T \cdot \boldsymbol{q}^1 & \pi_5(\boldsymbol{z}) = (\boldsymbol{e}_3)^T \cdot \boldsymbol{q}^2 & \pi_6(\boldsymbol{z}) = (\boldsymbol{q}^1)^T \cdot \boldsymbol{q}^1 \\ \pi_7(\boldsymbol{z}) = (\boldsymbol{q}^2)^T \cdot (\boldsymbol{q}^2) & & \end{array} \tag{4.1.5}$$

and reads

$$\tilde{H}(\boldsymbol{\pi}(\boldsymbol{z})) = \frac{1}{2} \left(\frac{\pi_1(\boldsymbol{z})}{m_1} + \frac{(m_1 + m_2)\pi_2(\boldsymbol{z})}{m_1 m_2} - \frac{2\pi_3(\boldsymbol{z})}{m_1} \right) - g \left((m_1 + m_2)\pi_4(\boldsymbol{z}) + m_2\pi_5(\boldsymbol{z}) \right) \tag{4.1.6}$$

The constraints (4.1.4) can be rewritten as

$$\begin{aligned} \tilde{g}_1(\pi_6(\boldsymbol{z})) &= \frac{1}{2} \left(\pi_6(\boldsymbol{z}) - l_1^2 \right) \\ \tilde{g}_2(\pi_7(\boldsymbol{z})) &= \frac{1}{2} \left(\pi_7(\boldsymbol{z}) - l_2^2 \right) \end{aligned} \tag{4.1.7}$$

Since the constraints (4.1.4) are quadratic in the configuration variable, the partial G-equivariant discrete derivative reduces to the midpoint evaluation of the 2×6 constraint Jacobian, i.e.

$$\mathsf{G}(\boldsymbol{q}_n, \boldsymbol{q}_{n+1}) = \begin{bmatrix} (\boldsymbol{q}^1_{n+\frac{1}{2}})^T & \boldsymbol{0} \\ \boldsymbol{0} & (\boldsymbol{q}^2_{n+\frac{1}{2}})^T \end{bmatrix} \tag{4.1.8}$$

4.2 Numerical investigations

4.2.1 Lagrange multiplier method

The energy-momentum conserving constrained time-stepping scheme (3.2.5) for the double spherical pendulum takes the form

$$\begin{aligned} \frac{\boldsymbol{q}_{n+1} - \boldsymbol{q}_n}{h} &= \boldsymbol{M}^{-1} \cdot \boldsymbol{p}_{n+\frac{1}{2}} \\ \frac{\boldsymbol{p}_{n+1} - \boldsymbol{p}_n}{h} &= \boldsymbol{M} \cdot g \begin{bmatrix} \boldsymbol{e}_3 \\ \boldsymbol{0}_{3\times 1} \end{bmatrix} - \begin{bmatrix} \boldsymbol{q}^1_{n+\frac{1}{2}} & \boldsymbol{0} \\ \boldsymbol{0} & \boldsymbol{q}^2_{n+\frac{1}{2}} \end{bmatrix} \cdot \boldsymbol{\lambda}_{n+1} \\ \boldsymbol{0} &= \boldsymbol{g}(\boldsymbol{q}_{n+1}) \end{aligned} \tag{4.2.1}$$

This system is in accordance with the example in [Gonz 99] and the mG(1)-method in [Bets 02b].

Numerical results

In the simulation of the double spherical pendulum's motion, the following parameters have been used. The masses are $m_1 = 10$ and $m_2 = 5$ and the rigid rods have the lengths $l_1 = l_2 = 1$. The gravitational acceleration is given by $g = -9.81$. The initial positions of the point masses are $\boldsymbol{q}^1(0) = \boldsymbol{e}_1$ and $\boldsymbol{q}^2(0) = \boldsymbol{e}_1$ and initial velocities are given by $\dot{\boldsymbol{q}}^1(0) = -2\boldsymbol{e}_2$ and $\dot{\boldsymbol{q}}^2(0) = -3\boldsymbol{e}_2$. Snapshots of the motion of the double spherical pendulum are shown in Figure 4.2 on the left. The diagram on the right confirms the algorithmic conservation of the total energy and the component L_3 of the angular momentum corresponding to the gravitational direction.

It is well known (see e.g. [Bets 02b]) that the constrained scheme is second order accurate in the phase variable and first order accurate in the multiplier. One can see in Figure 4.3 on the left that the calculated solutions converge quadratically to a reference solution as the time-step decreases. The latter has been calculated using $h = 10^{-5}$. The right diagram shows that the relative error in the multipliers drops off linearly for decreasing time-steps.
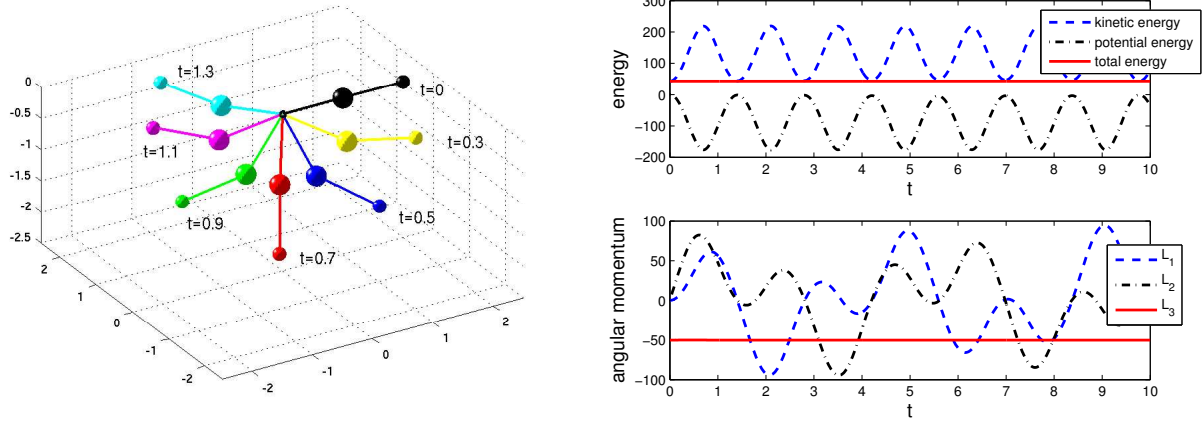
Figure 4.2: Double spherical pendulum: snapshots of the motion at $t \in \{0, 0.3, 0.5, 0.7, 0.9, 1.1, 1.3\}$ and energy and components of angular momentum vector $\boldsymbol{L} = L_i \boldsymbol{e}_i$ ($h = 0.01$).
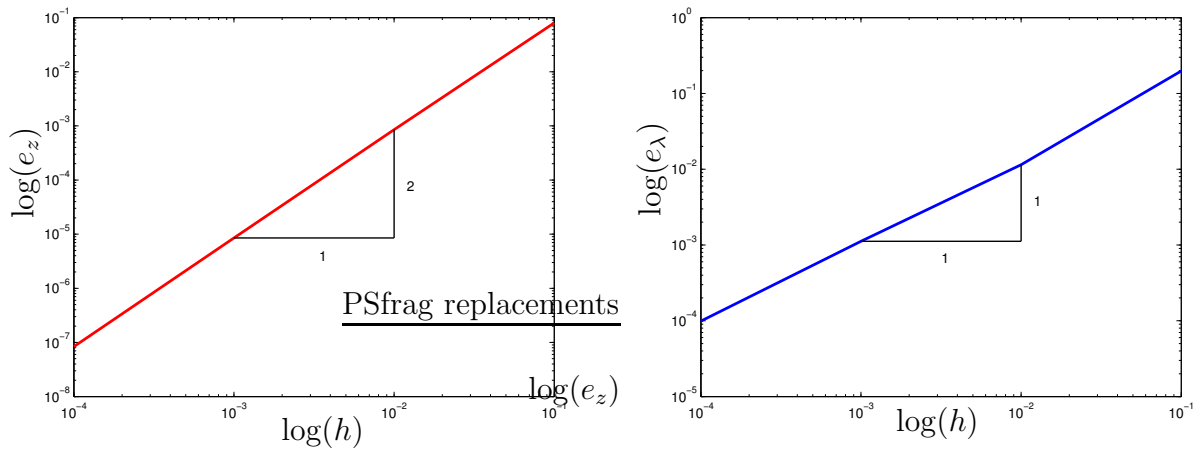
Figure 4.3: Double spherical pendulum: relative error $e_z = \|\boldsymbol{z}_{\mathrm{Lag}} - \boldsymbol{z}_{\mathrm{ref}}\|/\|\boldsymbol{z}_{\mathrm{ref}}\|$ of the phase variable and relative error of the multipliers $e_\lambda = \|\boldsymbol{\lambda}_{\mathrm{Lag}} - \boldsymbol{\lambda}_{\mathrm{ref}}\|/\|\boldsymbol{\lambda}_{\mathrm{ref}}\|$ for the constrained scheme at $t = 1$.

4.2.2 Penalty method

For the double spherical pendulum the penalty method can be interpreted as a replacement of the rods by springs of stiffness μ. The discrete energy-momentum conserving time-stepping scheme (3.2.9) with $P_{Pen}(\boldsymbol{g}(\boldsymbol{q})) = \mu\|\boldsymbol{g}(\boldsymbol{q})\|^2$ is given by

$$
\frac{\boldsymbol{q}_{n+1} - \boldsymbol{q}_n}{h} = \boldsymbol{M}^{-1} \cdot \boldsymbol{p}_{n+\frac{1}{2}}
$$

$$
\frac{\boldsymbol{p}_{n+1} - \boldsymbol{p}_n}{h} = \boldsymbol{M} \cdot g \begin{bmatrix} \boldsymbol{e}_3 \\ \boldsymbol{0}_{3\times 1} \end{bmatrix} - 2\mu \frac{(\tilde{g}_1(\pi_6(\boldsymbol{z}_{n+1})))^2 - (\tilde{g}_1(\pi_6(\boldsymbol{z}_n)))^2}{\pi_6(\boldsymbol{z}_{n+1}) - \pi_6(\boldsymbol{z}_n)} \begin{bmatrix} \boldsymbol{q}^1_{n+\frac{1}{2}} \\ \boldsymbol{0} \end{bmatrix} +
$$

$$
- 2\mu \frac{(\tilde{g}_2(\pi_7(\boldsymbol{z}_{n+1})))^2 - (\tilde{g}_2(\pi_7((\boldsymbol{z}_n)))^2}{\pi_7(\boldsymbol{z}_{n+1}) - \pi_7(\boldsymbol{z}_n)} \begin{bmatrix} \boldsymbol{0} \\ \boldsymbol{q}^2_{n+\frac{1}{2}} \end{bmatrix}
$$

$$(4.2.2)$$

Numerical results

Figure 4.4 shows the statements of Proposition 3.2.2. The fulfilment of the constraints improves and the solution of the penalty scheme (4.2.2) for the double spherical pendulum converges to that of the corresponding constrained scheme (4.2.1) as the penalty parameter increases.
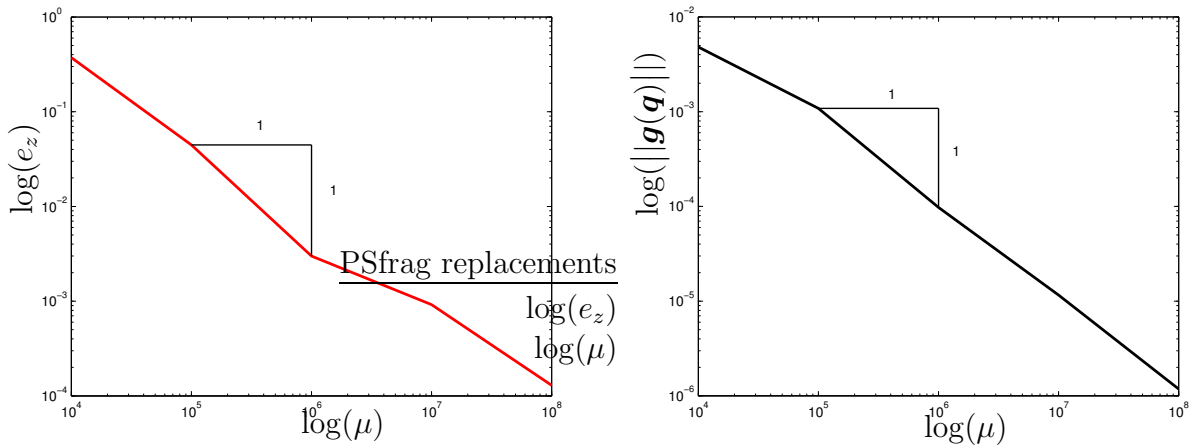
Figure 4.4: Double spherical pendulum: relative error $e_z = \|\boldsymbol{z}_{\mathrm{Pen}} - \boldsymbol{z}_{\mathrm{Lag}}\|/\|\boldsymbol{z}_{\mathrm{Lag}}\|$ of the phase variable and constraint fulfilment for the penalty scheme at $t = 10$ ($h = 0.01$).

4.2.3 Augmented Lagrange method

Enforcing the constraints by means of the augmented Lagrange method and using $P_{Aug}(\boldsymbol{g}(\boldsymbol{q})) = \boldsymbol{g}^T(\boldsymbol{q}) \cdot \boldsymbol{\lambda} + \mu \|\boldsymbol{g}(\boldsymbol{q})\|^2$, the time-stepping scheme (3.2.22) reads for the double spherical pendulum

$$
\begin{aligned}
\frac{\boldsymbol{q}_{n+1}^k - \boldsymbol{q}_n}{h} &= \boldsymbol{M}^{-1} \cdot \boldsymbol{p}_{n+\frac{1}{2}}^k \\
\frac{\boldsymbol{p}_{n+1}^k - \boldsymbol{p}_n}{h} &= \boldsymbol{M} \cdot g \begin{bmatrix} \boldsymbol{e}_3 \\ \boldsymbol{0}_{3\times 1} \end{bmatrix} - \left[\lambda_{n+1}^{k,1} + 2\mu \frac{(\tilde{g}_1(\pi_6(\boldsymbol{z}_{n+1})))^2 - (\tilde{g}_1(\pi_6(\boldsymbol{z}_n)))^2}{\pi_6(\boldsymbol{z}_n) - \pi_6(\boldsymbol{z}_n)}\right] \begin{bmatrix} \boldsymbol{q}_{n+\frac{1}{2}}^{k,1} \\ \boldsymbol{0} \end{bmatrix} + \\
& \qquad - \left[\lambda_{n+1}^{k,2} + 2\mu \frac{(\tilde{g}_2(\pi_7(\boldsymbol{z}_{n+1})))^2 - (\tilde{g}_2(\pi_7((\boldsymbol{z}_n))))^2}{\pi_7(\boldsymbol{z}_{n+1}) - \pi_7(\boldsymbol{z}_n)}\right] \begin{bmatrix} \boldsymbol{0} \\ \boldsymbol{q}_{n+\frac{1}{2}}^{k,2} \end{bmatrix} \\
\boldsymbol{\lambda}_{n+1}^{k+1} &= \boldsymbol{\lambda}_{n+1}^k + 2\mu \boldsymbol{g}(\boldsymbol{q}_{n+1}^k)
\end{aligned}
\tag{4.2.3}
$$

It is solved iteratively until the desired accuracy has been reached for the constraint fulfilment. The greater the parameter μ is, the fewer iterations are required to reach this accuracy, since for high penalty parameters, the constraints are already fulfilled to some degree in the first iteration.

Numerical results

The improvement of the constraint fulfilment and the convergence of the solution of the augmented Lagrange time-stepping scheme (4.2.3) to that of the constrained scheme (4.2.1) during the augmented Lagrange iterations (AL-iterations) is depicted in Figure 4.5. The results corroborate the statements of Proposition 3.2.4.

4.2.4 Discrete null space method with nodal reparametrisation

To derive an explicit representation of the discrete null space matrix pertaining to the double spherical pendulum, the procedure described in Example 3.2.9 is applied with the difference that for the simple discrete constraint Jacobian given in (4.1.8), the QR-decomposition can be performed explicitly (see [Bets 05]). According to (2.3.23), the QR-decomposition of the transposed constraint Jacobian at t_n comprises the matrices

$$
\boldsymbol{W}_n = \begin{bmatrix} \boldsymbol{d}_n^1 & \boldsymbol{0} \\ \boldsymbol{0} & \boldsymbol{d}_n^2 \end{bmatrix} \qquad \boldsymbol{U}_n = \begin{bmatrix} \boldsymbol{r}_n^1 & \boldsymbol{s}_n^1 & \boldsymbol{0} & \boldsymbol{0} \\ \boldsymbol{0} & \boldsymbol{0} & \boldsymbol{r}_n^2 & \boldsymbol{s}_n^2 \end{bmatrix}
\tag{4.2.4}
$$

with the unit vector $\boldsymbol{d}_n^\alpha = \boldsymbol{q}_n^\alpha / l_\alpha \in S^2$, $\alpha = 1, 2$ and the orthonormal basis $\boldsymbol{r}_n^\alpha, \boldsymbol{s}_n^\alpha \in \mathbb{R}^3$ of the tangent plane $T_{\boldsymbol{d}_n^\alpha} S^2$. Thus $\{\boldsymbol{r}_n^\alpha, \boldsymbol{s}_n^\alpha, \boldsymbol{d}_n^\alpha\}$ form an orthonormal triad. For example $\boldsymbol{r}_n^\alpha$ and $\boldsymbol{s}_n^\alpha$ can be calculated via $\boldsymbol{r}_n^\alpha = \boldsymbol{R}_n^\alpha \cdot \boldsymbol{e}_1$ and $\boldsymbol{s}_n^\alpha = \boldsymbol{R}_n^\alpha \cdot \boldsymbol{e}_2$. Thereby, the matrix $\boldsymbol{R}_n^\alpha \in SO(3)$ is given by

$$
\boldsymbol{R}_n^\alpha = (\boldsymbol{e}_3^T \cdot \boldsymbol{d}_n^\alpha)\boldsymbol{I}_{3\times 3} + \widehat{\boldsymbol{e}_3 \times \boldsymbol{d}_n^\alpha} + \frac{(\boldsymbol{e}_3 \times \boldsymbol{d}_n^\alpha) \otimes (\boldsymbol{e}_3 \times \boldsymbol{d}_n^\alpha)}{l^\alpha + \boldsymbol{e}_3^T \cdot \boldsymbol{q}_n^\alpha}
\tag{4.2.5}
$$
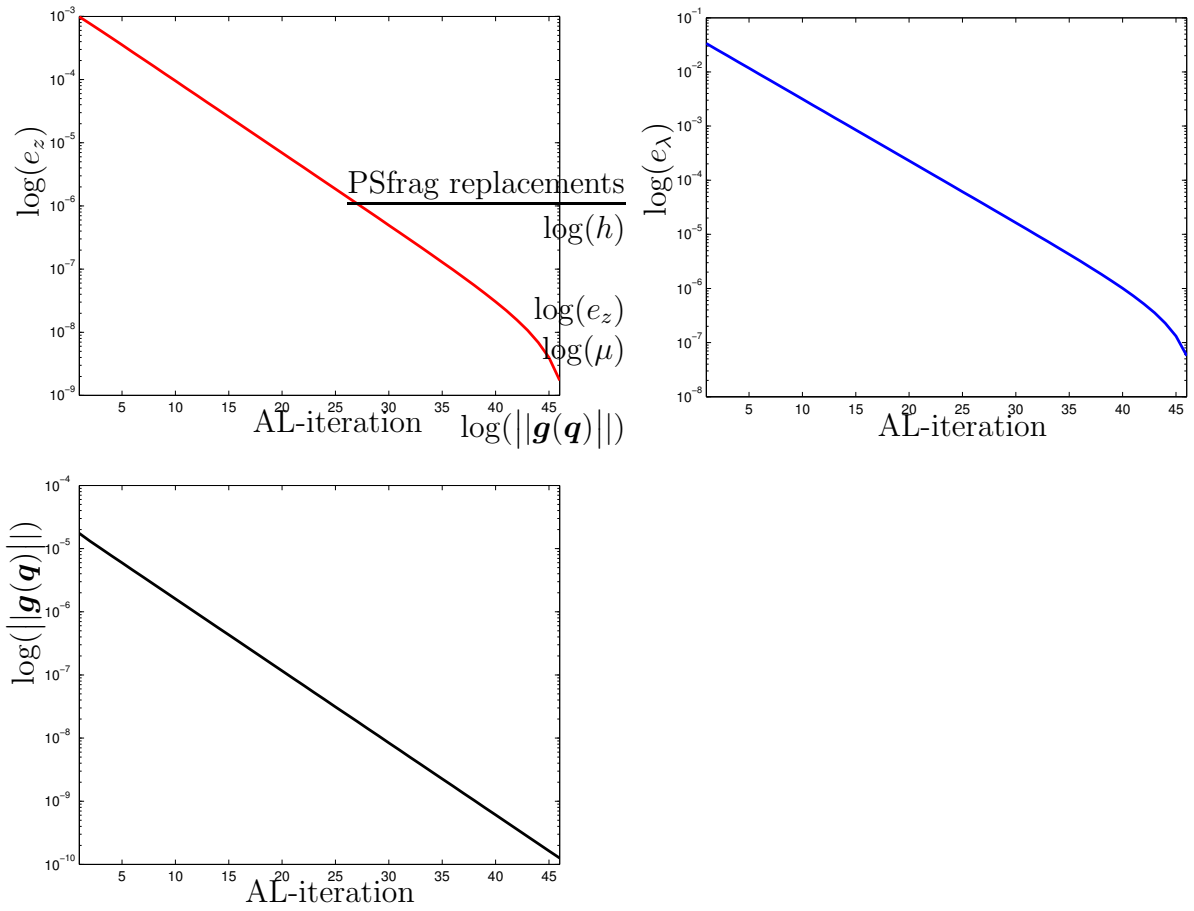
Figure 4.5: Double spherical pendulum: relative error $e_z = \|z_{\mathrm{Aug}} - z_{\mathrm{Lag}}\|/\|z_{\mathrm{Lag}}\|$ of the phase variable and relative error of the multipliers $e_\lambda = \|\lambda_{\mathrm{Aug}} - \lambda_{\mathrm{Lag}}\|/\|\lambda_{\mathrm{Lag}}\|$ and constraint fulfilment for the augmented Lagrange scheme at $t = 10$ ($h = 0.01$, $\mu = 10^5$).

Insertion of $\boldsymbol{W}_n^\alpha$ and $\boldsymbol{U}_n^\alpha$ into (3.2.38) yields the explicit representation of the 6×4 discrete null space matrix for the double spherical pendulum

$$\mathbf{P}(\boldsymbol{q}_n, \boldsymbol{q}_{n+1}) = \begin{bmatrix} \mathbf{P}^1(\boldsymbol{q}_n^1, \boldsymbol{q}_{n+1}^1) & \mathbf{0}_{3\times 2} \\ \mathbf{0}_{3\times 2} & \mathbf{P}^2(\boldsymbol{q}_n^2, \boldsymbol{q}_{n+1}^2) \end{bmatrix} \qquad (4.2.6)$$

with the 3×2 submatrices of the form

$$\mathbf{P}^\alpha(\boldsymbol{q}_n^\alpha, \boldsymbol{q}_{n+1}^\alpha) = \left[\boldsymbol{I}_{3\times 3} - \frac{1}{(\boldsymbol{q}_n^\alpha)^T \cdot \boldsymbol{q}_{n+\frac{1}{2}}^\alpha} \boldsymbol{q}_n^\alpha \otimes \boldsymbol{q}_{n+\frac{1}{2}}^\alpha \right] \cdot \boldsymbol{U}_n^\alpha \qquad (4.2.7)$$

In view of (4.2.4) the 3×2 submatrices $\boldsymbol{U}_n^\alpha$ can be written as $\boldsymbol{U}_n^\alpha = [\boldsymbol{r}_n^\alpha, \boldsymbol{s}_n^\alpha]$.
The nodal reparametrisation $\boldsymbol{F}_{\boldsymbol{q}_n} : U \subseteq \mathbb{R}^4 \to C$ introduced in (3.2.42) is partitioned into

$$\boldsymbol{q}_{n+1}^\alpha = \boldsymbol{F}_{\boldsymbol{q}_n}^\alpha(\boldsymbol{u}^\alpha) = l_\alpha \exp_{\boldsymbol{d}_n^\alpha}(\boldsymbol{U}_n^\alpha \cdot \boldsymbol{u}^\alpha) \in S_{l_\alpha}^2 \qquad (4.2.8)$$

with the incremental unknowns $\boldsymbol{u}^\alpha \in \mathbb{R}^2$ for $\alpha = 1, 2$ and the exponential map $\exp_{\boldsymbol{d}_n^\alpha} : T_{\boldsymbol{d}_n^\alpha} S^2 \to S^2$ given by

$$\exp_{\boldsymbol{d}_n^\alpha}(\boldsymbol{\nu}) = \cos(\|\boldsymbol{\nu}\|)\boldsymbol{d}_n^\alpha + \frac{\sin(\|\boldsymbol{\nu}\|)}{\|\boldsymbol{\nu}\|}\boldsymbol{\nu} \qquad (4.2.9)$$

With these preliminaries, the d'Alembert-type time-stepping scheme with nodal reparametrisation (3.2.43) for the double spherical pendulum reads

$$\begin{aligned} \boldsymbol{F}_{\boldsymbol{q}_n}(\boldsymbol{u}) - \boldsymbol{q}_n - h\boldsymbol{M}^{-1} \cdot \boldsymbol{p}_{n+\frac{1}{2}} &= \mathbf{0} \\ \mathbf{P}^T(\boldsymbol{q}_n, \boldsymbol{q}_{n+1}) \cdot \left[\boldsymbol{p}_{n+1} - \boldsymbol{p}_n - hg\boldsymbol{M} \cdot \begin{bmatrix} \boldsymbol{e}_3 \\ \mathbf{0}_{3\times 1} \end{bmatrix} \right] &= \mathbf{0} \end{aligned} \qquad (4.2.10)$$

Numerical results

Figure 4.6 shows the convergence of the solution of the d'Alembert-type scheme with nodal reparametrisation (4.2.10) to a reference solution calculated with the constrained scheme (4.2.1) using a time-step $h = 10^{-5}$. It confirms the statement of Proposition 3.2.12.

4.2.5 Comparison

Table 4.1 summarises some important aspects of the schemes (4.2.1), (4.2.2), (4.2.3) and (4.2.10). For all schemes, the simple first equation is solved for $\boldsymbol{p}_{n+1}$ and inserted in the second equation. This yields the 8-dimensional constrained scheme, the 6-dimensional system of discrete equations of motion for the penalty and the augmented Lagrange method and the d'Alembert-type scheme with nodal reparametrisation reduces to 4 equations. The CPU-time for each scheme is specified as the ratio between the computation time for 1000 time-steps ($h = 0.01$) by the scheme and that of the d'Alembert-type scheme with nodal reparametrisation.
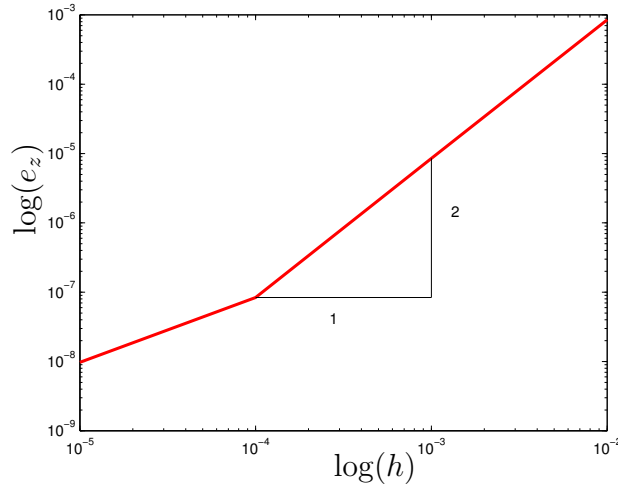
Figure 4.6: Double spherical pendulum: relative error $e_z = \left\|z_{\mathrm{d'}Al} - z_{\mathrm{Lag}}\right\|/\left\|z_{\mathrm{Lag}}\right\|$ of the phase variable for the d'Alembert-type scheme with nodal reparametrisation at $t = 1$.

Although the augmented Lagrange scheme yields acceptable results in the categories constraint fulfilment and condition number, the high computational costs disqualify it in the competition with the other schemes. These costs are caused by the high number of iterations required for the reduction of the constraint violation to the desired tolerance of $\mathrm{tol} = 10^{-10}$, see Figure 4.5.

Since the set up of the discrete null space matrix for the double spherical pendulum is relatively involved (see Section 4.2.4), the calculation of 1000 time-steps by the d'Alembert-type scheme with nodal reparametrisation requires approximately three times more computational time than by the constrained scheme and by the penalty scheme. For larger dimensional problems subject to a higher number of constraints (see Sections 5.5, 6.1.9, 6.2.4, 6.3), this relation is reversed. In the categories constraint fulfilment and condition number, the reduced scheme performs excellently.

The constrained scheme fulfils the constraints equally well as the reduced scheme, but it obviously suffers from increasing conditioning problems for decreasing time-steps.

For the penalty parameter $\mu = 10^5$, the penalty scheme is well conditioned, but the constraint fulfilment in unacceptably inaccurate. In contrast to that, for $\mu = 10^{10}$, the constraint fulfilment is improved, but the condition number deteriorates for $h = 10^{-2}$. Its decrease for $h = 10^{-3}$ and $h = 10^{-4}$ reveals the quadratic dependence of the condition number of the time-step.

Table 4.1: Comparison of constrained scheme, penalty scheme, augmented Lagrange scheme and d'Alembert-type scheme with nodal reparametrisation for the example 'double spherical pendulum'.

	constrained	penalty		augm. Lag.	d'Alembert
number of unknowns $n = 6 \quad m = 2$	8	6		6	4
CPU-time	0.3	0.3		7.2	1
constraint fulfilment	10^{-16}	$\mu = 10^5$ 10^{-3}	$\mu = 10^{10}$ 10^{-8}	10^{-10}	10^{-16}
condition number $h = 10^{-2}$	10^8	1	10^5	1	1
$h = 10^{-3}$	10^{11}	1	10^3	1	1
$h = 10^{-4}$	10^{14}	1	10	1	1
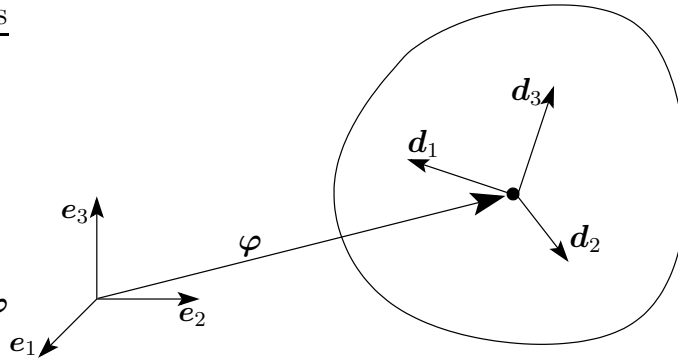
Figure 4.7: Configuration of a rigid body with respect to an orthonormal frame $\{e_I\}$ fixed in space.

4.3 Rigid body dynamics

Rigid body dynamics can be described from different view points. Classically, the evolution of the translational and rotational degrees of freedom under the influence of forces and moments is studied. This leads to the well-known Newton-Euler equations for rigid body dynamics (see e.g. [Schi 86, Kuyp 03, Ange 97]). Based on these equations many conserving integrators have been designed [Krys 05b, Krys 05a, Simo 91b].

On the other hand, a rigid body can be viewed as a constrained continuum, in which all lengths and angles are constrained to be constant. In this approach, the configuration of a rigid body is described in redundant coordinates and the equations of motion assume the form of DAEs described in Section 2.3.1. This formulation bears a number of advantages see e.g. [Leim 04]. It circumvents the difficulties associated with the rotational parameters [Bets 98, Ibra 95, Ibra 97, Bauc 03b] and is well suited for generalisation to the modelling of geometrically exact beams as special Cosserat continuum described in Chapter 5 or to multibody systems as investigated in Chapter 6, in which constraints are naturally present. Concerning the temporal discretisation of the DAE approach, work has been done e.g. by [Reic 96, Anit 04, Bets 01b, Bets 03]. The latter is used as a starting point for the following presentation.

4.3.1 Constrained formulation of rigid body dynamics

The treatment of rigid bodies as structural elements relies on the kinematic assumptions illustrated in Figure 4.7 (see [Antm 95]) that the placement of a material point in the body's configuration $\boldsymbol{X} = X_i \boldsymbol{d}_i \in \mathcal{B} \subset \mathbb{R}^3$ relative to an orthonormal basis $\{\boldsymbol{e}_I\}$ fixed in space can be described as

$$\boldsymbol{x}(\boldsymbol{X}, t) = \boldsymbol{\varphi}(t) + X_i \boldsymbol{d}_i(t) \tag{4.3.1}$$

Here $X_i \in \mathbb{R}$, $i = 1, 2, 3$ represent coordinates in the body-fixed director triad $\{\boldsymbol{d}_I\}$. The time-dependent configuration variable of a rigid body

$$\boldsymbol{q}(t) = \begin{bmatrix} \boldsymbol{\varphi}(t) \\ \boldsymbol{d}_1(t) \\ \boldsymbol{d}_2(t) \\ \boldsymbol{d}_3(t) \end{bmatrix} \in \mathbb{R}^{12} \tag{4.3.2}$$

consists of the placement of the center of mass $\boldsymbol{\varphi} \in \mathbb{R}^3$ and the directors $\boldsymbol{d}_I \in \mathbb{R}^3, I = 1, 2, 3$ which are constrained to stay orthonormal during the motion, representing the rigidity of the body and its orientation. These orthonormality conditions pertaining to the kinematic assumptions of the underlying theory are termed internal constraints. There are $m_{int} = 6$ independent internal constraints for the rigid body with associated constraint functions

$$\boldsymbol{g}_{int}(\boldsymbol{q}) = \begin{bmatrix} \frac{1}{2}[\boldsymbol{d}_1^T \cdot \boldsymbol{d}_1 - 1] \\ \frac{1}{2}[\boldsymbol{d}_2^T \cdot \boldsymbol{d}_2 - 1] \\ \frac{1}{2}[\boldsymbol{d}_3^T \cdot \boldsymbol{d}_3 - 1] \\ \boldsymbol{d}_1^T \cdot \boldsymbol{d}_2 \\ \boldsymbol{d}_1^T \cdot \boldsymbol{d}_3 \\ \boldsymbol{d}_2^T \cdot \boldsymbol{d}_3 \end{bmatrix} \tag{4.3.3}$$

which give rise to the following 6×12 constraint Jacobian

$$\boldsymbol{G}_{int}(\boldsymbol{q}) = \begin{bmatrix} \boldsymbol{0} & \boldsymbol{d}_1^T & \boldsymbol{0} & \boldsymbol{0} \\ \boldsymbol{0} & \boldsymbol{0} & \boldsymbol{d}_2^T & \boldsymbol{0} \\ \boldsymbol{0} & \boldsymbol{0} & \boldsymbol{0} & \boldsymbol{d}_3^T \\ \boldsymbol{0} & \boldsymbol{d}_2^T & \boldsymbol{d}_1^T & \boldsymbol{0} \\ \boldsymbol{0} & \boldsymbol{d}_3^T & \boldsymbol{0} & \boldsymbol{d}_1^T \\ \boldsymbol{0} & \boldsymbol{0} & \boldsymbol{d}_3^T & \boldsymbol{d}_2^T \end{bmatrix} \tag{4.3.4}$$

where $\boldsymbol{0}$ denotes the 1×3 zero vector. For simplicity, it is assumed that the axes of the body frame coincide with the principal axes of inertia of the rigid body. Then the inertia tensor $\boldsymbol{J}$ with respect to the body's center of mass has diagonal form with the principal values

$$J_i = \int_{\mathcal{B}} (X_j^2 + X_k^2) \varrho(\boldsymbol{X}) dV \tag{4.3.5}$$

for even permutations of $i, j, k \in \{1, 2, 3\}$ and with the mass density $\varrho(\boldsymbol{X})$ at $\boldsymbol{X} \in \mathcal{B}$. It can be related to the body's Euler tensor with respect to the center of mass via

$$\boldsymbol{E} = \frac{1}{2}(\mathrm{tr}\boldsymbol{J})\boldsymbol{I} - \boldsymbol{J} \tag{4.3.6}$$

where $\boldsymbol{I}$ denotes the 3×3 identity matrix. Then the principal values of the Euler tensor E_i together with the body's total mass M_φ

$$M_\varphi = \int_{\mathcal{B}} \varrho(\boldsymbol{X}) dV \tag{4.3.7}$$

build the rigid body's constant symmetric positive definite mass matrix

$$\boldsymbol{M} = \begin{bmatrix} M_\varphi \boldsymbol{I} & \boldsymbol{0} & \boldsymbol{0} & \boldsymbol{0} \\ \boldsymbol{0} & E_1 \boldsymbol{I} & \boldsymbol{0} & \boldsymbol{0} \\ \boldsymbol{0} & \boldsymbol{0} & E_2 \boldsymbol{I} & \boldsymbol{0} \\ \boldsymbol{0} & \boldsymbol{0} & \boldsymbol{0} & E_3 \boldsymbol{I} \end{bmatrix} \tag{4.3.8}$$

where $\mathbf{0}$ denotes the 3×3 zero matrix.

Corresponding to the configuration variable given in (4.3.2), the conjugate momenta read

$$
\mathbf{p}(t) = \begin{bmatrix} \mathbf{p}_\varphi(t) \\ \mathbf{p}_1(t) \\ \mathbf{p}_2(t) \\ \mathbf{p}_3(t) \end{bmatrix} \in \mathbb{R}^{12} \tag{4.3.9}
$$

The Hamiltonian for the rigid body takes the separable form

$$
H(\mathbf{q}, \mathbf{p}) = \frac{1}{2} \mathbf{p}^T \cdot \mathbf{M}^{-1} \cdot \mathbf{p} + V(\mathbf{q}) \tag{4.3.10}
$$

As described in (2.3.13), it can be augmented according to the method to treat the constraints leading to the constrained Hamilton's equations (2.3.8) including the Lagrange multipliers or the Hamilton's equations (2.2.4) including the penalty parameter or the Hamilton's equations (2.2.4) in the context of the augmented Lagrange method to enforce the constraints. For the rigid body motion, the constrained Hamilton's equations (2.3.8) read

$$
\begin{aligned}
\dot{\mathbf{q}} &= \mathbf{M}^{-1} \cdot \mathbf{p} \\
\dot{\mathbf{p}} &= -\frac{\partial V(\mathbf{q})}{\partial \mathbf{q}} - \mathbf{G}_{int}^T(\mathbf{q}) \cdot \boldsymbol{\lambda} \\
\mathbf{0} &= \mathbf{g}_{int}(\mathbf{q})
\end{aligned} \tag{4.3.11}
$$

4.3.2 Invariance of the Hamiltonian

The temporal discretisation of the equations of motion for the rigid body makes use of the G-equivariant discrete derivative (see Definitions 3.1.4 and 3.1.7) given in Example 3.1.6, wherefore the reparametrisation of the Hamiltonian in terms of invariants is necessary. Assuming that the gravitational potential takes the form

$$
V(\mathbf{q}) = -g M_\varphi \mathbf{e}_3^T \cdot \boldsymbol{\varphi} \tag{4.3.12}
$$

the Hamiltonian is invariant with respect to rotation of the rigid body around the axis $\mathbf{e}_3$. Consequently, the angular momentum's component corresponding to the gravitational direction L_3 is a first integral of the motion, see Section 2.2.3. The Hamiltonian (4.3.10) and the internal constraints (4.3.3) can be reparametrised in the independent invariants $\boldsymbol{\pi}(\mathbf{z})$ comprising

$$
\begin{aligned}
&\pi_1(\mathbf{z}) = \boldsymbol{\varphi}^T \cdot \mathbf{e}_3 & &\pi_2(\mathbf{z}) = \mathbf{d}_1^T \cdot \mathbf{d}_1 & &\pi_3(\mathbf{z}) = \mathbf{d}_2^T \cdot \mathbf{d}_2 \\
&\pi_4(\mathbf{z}) = \mathbf{d}_3^T \cdot \mathbf{d}_3 & &\pi_5(\mathbf{z}) = \mathbf{d}_1^T \cdot \mathbf{d}_2 & &\pi_6(\mathbf{z}) = \mathbf{d}_3^T \cdot \mathbf{d}_1 \\
&\pi_7(\mathbf{z}) = \mathbf{d}_2^T \cdot \mathbf{d}_3 & &\pi_8(\mathbf{z}) = \mathbf{p}_\varphi^T \cdot \mathbf{p}_\varphi & &\pi_9(\mathbf{z}) = \mathbf{p}_1^T \cdot \mathbf{p}_1 \\
&\pi_{10}(\mathbf{z}) = \mathbf{p}_2^T \cdot \mathbf{p}_2 & &\pi_{11}(\mathbf{z}) = \mathbf{p}_3^T \cdot \mathbf{p}_3
\end{aligned} \tag{4.3.13}
$$

such that

$$
\tilde{H}(\boldsymbol{\pi}(\mathbf{z})) = \frac{1}{2}\left(\frac{\pi_8(\mathbf{z})}{M_\varphi} + \frac{\pi_9(\mathbf{z})}{E_1} + \frac{\pi_{10}(\mathbf{z})}{E_2} + \frac{\pi_{11}(\mathbf{z})}{E_3} \right) - g M_\varphi \pi_1(\mathbf{z}) \tag{4.3.14}
$$

and

$$\tilde{\boldsymbol{g}}_{int}(\boldsymbol{\pi}(\boldsymbol{z})) = \begin{bmatrix} \dfrac{1}{2}[\pi_2(\boldsymbol{z}) - 1] \\[2mm] \dfrac{1}{2}[\pi_3(\boldsymbol{z}) - 1] \\[2mm] \dfrac{1}{2}[\pi_4(\boldsymbol{z}) - 1] \\[2mm] \pi_5(\boldsymbol{z}) \\[2mm] \pi_6(\boldsymbol{z}) \\[2mm] \pi_7(\boldsymbol{z}) \end{bmatrix} \tag{4.3.15}$$

4.3.3 Reduced formulation of rigid body dynamics

To deduce the d'Alembert-type equations of motion in the Hamiltonian formalism (2.3.21), an appropriate null space matrix with property (2.3.18) needs to be found. Remember that due to the consistency condition (2.3.9), $\dot{\boldsymbol{q}} = \boldsymbol{M}^{-1} \cdot \boldsymbol{p}$ is constrained to the null space of the constraint Jacobian. Thus admissible velocities can be expressed in the form

$$\dot{\boldsymbol{q}} = \boldsymbol{P}_{int}(\boldsymbol{q}) \cdot \boldsymbol{\nu} \tag{4.3.16}$$

with the independent generalised velocities $\boldsymbol{\nu} \in \mathbb{R}^{n-m_{int}}$. In case of the rigid body, these independent generalised velocities are called twist (see [Ange 88])

$$\boldsymbol{t} = \begin{bmatrix} \dot{\boldsymbol{\varphi}} \\ \boldsymbol{\omega} \end{bmatrix} \tag{4.3.17}$$

The twist comprises the translational velocity $\dot{\boldsymbol{\varphi}} \in \mathbb{R}^3$ and the angular velocity $\boldsymbol{\omega} \in \mathbb{R}^3$ in terms of which the director velocities can be written as

$$\dot{\boldsymbol{d}}_I = \boldsymbol{\omega} \times \boldsymbol{d}_I = -\widehat{\boldsymbol{d}_I} \cdot \boldsymbol{\omega} \tag{4.3.18}$$

Thus (4.3.16) can be written as $\dot{\boldsymbol{q}} = \boldsymbol{P}_{int}(\boldsymbol{q}) \cdot \boldsymbol{t}$ with the null space matrix for the rigid body

$$\boldsymbol{P}_{int}(\boldsymbol{q}) = \begin{bmatrix} \boldsymbol{I} & \boldsymbol{0} \\ \boldsymbol{0} & -\widehat{\boldsymbol{d}_1} \\ \boldsymbol{0} & -\widehat{\boldsymbol{d}_2} \\ \boldsymbol{0} & -\widehat{\boldsymbol{d}_3} \end{bmatrix} \tag{4.3.19}$$

It can easily be verified that (4.3.19) has full column rank and with regard to (4.3.4) that $\boldsymbol{G}_{int}(\boldsymbol{q}) \cdot \boldsymbol{P}_{int}(\boldsymbol{q}) = \boldsymbol{0}$ is the 6×6 zero matrix.

Thus the d'Alembert-type equations of motion in the Hamiltonian formalism (2.3.21) can be obtained by premultiplication of $(4.3.11)_2$ by the transposed of the null space matrix (4.3.19).

Equivalence to the Euler equations

Having accomplished the just mentioned premultiplication of $(4.3.11)_2$ by the transposed of the null space matrix (4.3.19), $\boldsymbol{p} = \boldsymbol{M} \cdot \boldsymbol{P}_{int}(\boldsymbol{q}) \cdot \boldsymbol{t}$ can be inserted and $(4.3.11)_2$ takes the form

$$\boldsymbol{P}_{int}^T(\boldsymbol{q}) \cdot \boldsymbol{M} \cdot \boldsymbol{P}_{int}(\boldsymbol{q}) \cdot \dot{\boldsymbol{t}} + \boldsymbol{P}_{int}^T(\boldsymbol{q}) \cdot \boldsymbol{M} \cdot \dot{\boldsymbol{P}}_{int}(\boldsymbol{q}) \cdot \boldsymbol{t} + \boldsymbol{P}_{int}^T(\boldsymbol{q}) \cdot \frac{\partial V(\boldsymbol{q})}{\partial \boldsymbol{q}} = \boldsymbol{0} \quad (4.3.20)$$

employing (4.3.8) and the null space matrix (4.3.19) yields

$$\boldsymbol{P}_{int}^T(\boldsymbol{q}) \cdot \boldsymbol{M} \cdot \boldsymbol{P}_{int}(\boldsymbol{q}) = \begin{bmatrix} M_\varphi \boldsymbol{I} & \boldsymbol{0} \\ \boldsymbol{0} & -\sum_{I=1}^{3} E_I (\widehat{\boldsymbol{d}_I})^2 \end{bmatrix} = \begin{bmatrix} M_\varphi \boldsymbol{I} & \boldsymbol{0} \\ \boldsymbol{0} & \boldsymbol{J} \end{bmatrix} \quad (4.3.21)$$

where (4.3.6) and the property $\boldsymbol{d}_I^T \cdot \boldsymbol{d}_I = 1$, $I = 1, 2, 3$ have been taken into account. In order to calculate the term $\boldsymbol{P}_{int}^T(\boldsymbol{q}) \cdot \boldsymbol{M} \cdot \dot{\boldsymbol{P}}_{int}(\boldsymbol{q}) \cdot \boldsymbol{t}$ in (4.3.20), the time derivative of the null space matrix is performed first

$$\dot{\boldsymbol{P}}_{int}(\boldsymbol{q}) = \begin{bmatrix} \boldsymbol{0} & \boldsymbol{0} \\ \boldsymbol{0} & -\widehat{\dot{\boldsymbol{d}}_1} \\ \boldsymbol{0} & -\widehat{\dot{\boldsymbol{d}}_2} \\ \boldsymbol{0} & -\widehat{\dot{\boldsymbol{d}}_3} \end{bmatrix} = \begin{bmatrix} \boldsymbol{0} & \boldsymbol{0} \\ \boldsymbol{0} & \widehat{\boldsymbol{d}_1 \times \boldsymbol{\omega}} \\ \boldsymbol{0} & \widehat{\boldsymbol{d}_2 \times \boldsymbol{\omega}} \\ \boldsymbol{0} & \widehat{\boldsymbol{d}_3 \times \boldsymbol{\omega}} \end{bmatrix} = \begin{bmatrix} \boldsymbol{0} & \boldsymbol{0} \\ \boldsymbol{0} & \boldsymbol{\omega} \otimes \boldsymbol{d}_1 - \boldsymbol{d}_1 \otimes \boldsymbol{\omega} \\ \boldsymbol{0} & \boldsymbol{\omega} \otimes \boldsymbol{d}_2 - \boldsymbol{d}_2 \otimes \boldsymbol{\omega} \\ \boldsymbol{0} & \boldsymbol{\omega} \otimes \boldsymbol{d}_3 - \boldsymbol{d}_3 \otimes \boldsymbol{\omega} \end{bmatrix} \quad (4.3.22)$$

A straightforward calculation then gives the relationship

$$\boldsymbol{P}_{int}^T(\boldsymbol{q}) \cdot \boldsymbol{M} \cdot \dot{\boldsymbol{P}}_{int}(\boldsymbol{q}) \cdot \boldsymbol{t} = \begin{bmatrix} \boldsymbol{0} \\ -\boldsymbol{\omega} \times \left(\sum_{I=1}^{3} E_I \boldsymbol{d}_I \otimes \boldsymbol{d}_I \right) \boldsymbol{\omega} \end{bmatrix} = \begin{bmatrix} \boldsymbol{0} \\ \boldsymbol{\omega} \times \boldsymbol{J}\boldsymbol{\omega} \end{bmatrix} \quad (4.3.23)$$

where use has been made of (4.3.6). Finally, the last term in (4.3.20) yields

$$\boldsymbol{P}_{int}^T(\boldsymbol{q}) \cdot \frac{\partial V(\boldsymbol{q})}{\partial \boldsymbol{q}} = \begin{bmatrix} \dfrac{\partial V(\boldsymbol{q})}{\partial \boldsymbol{\varphi}} \\ \boldsymbol{d}_i \times \dfrac{\partial V(\boldsymbol{q})}{\partial \boldsymbol{d}_i} \end{bmatrix} =: - \begin{bmatrix} \bar{\boldsymbol{f}} \\ \bar{\boldsymbol{m}} \end{bmatrix} \quad (4.3.24)$$

where $\bar{\boldsymbol{f}}$ and $\bar{\boldsymbol{m}}$ are the resultant external force and torque relative to the center of mass of the rigid body, respectively. To summarise, the reduced equations of motion using (4.3.20) can be written in the familiar form

$$\begin{aligned} M_\varphi \ddot{\boldsymbol{\varphi}} &= \bar{\boldsymbol{f}} \\ \boldsymbol{J} \cdot \dot{\boldsymbol{\omega}} + \boldsymbol{\omega} \times \boldsymbol{J} \cdot \boldsymbol{\omega} &= \bar{\boldsymbol{m}} \end{aligned} \quad (4.3.25)$$

which represents the well-known Newton-Euler equations for rigid body motion.

4.3.4 Temporal discrete equations of motion for the rigid body

Lagrange multiplier method

The energy-momentum conserving time-stepping scheme for the constrained Hamiltonian system given in (3.2.5) can be directly applied to the present formulation of rigid body dynamics. In this connection the partial G-equivariant discrete derivative (see Definitions 3.1.4 and 3.1.7) of the constraints needs to be specified. To this end, use is made of the reparametrised constraints (4.3.15) in terms of the invariants (4.3.13). Since the internal constraints are quadratic in $\boldsymbol{q}$, the partial G-equivariant discrete derivative of the constraints coincides with the midpoint evaluation of the constraint Jacobian (4.3.4), i.e.

$$\mathbf{G}_{int}(\boldsymbol{q}_n, \boldsymbol{q}_{n+1}) = \boldsymbol{G}_{int}(\boldsymbol{q}_{n+\frac{1}{2}}) \tag{4.3.26}$$

The implementation of the constrained scheme (3.2.7) for the free rigid body leads to a nonlinear system of algebraic equations in terms of $n + m_{int} = 18$ unknowns. It is worth noting that the present discretisation approach for rigid bodies (i) does not involve any rotational parameters and (ii) yields a second-order accurate energy-momentum method (see also [Bets 01b]).

Penalty and augmented Lagrange method

Similar to the deduction of the penalty time-stepping scheme and the augmented Lagrange time-stepping scheme for the double spherical pendulum in the Sections 4.2.2 and 4.2.3, insertion of the reparametrised Hamiltonian for the rigid body (4.3.14) into the general form of the penalty time-stepping scheme (3.2.9) or into the general augmented Lagrange time-stepping scheme (3.2.22) yields the corresponding energy-momentum conserving time-stepping schemes for the motion of the rigid body.

Discrete null space method with nodal reparametrisation

In order to deduce the discrete d'Alembert-type equations of motion, a temporal discrete null space matrix fulfilling the properties mentioned in Remark 3.2.7 respectively condition (3.2.30) must be found. With regard to the midpoint evaluation of the constraint Jacobian in (4.3.26), it is evident that a midpoint evaluation of (4.3.19) suffices the requirements, i.e.

$$\mathbf{P}_{int}(\boldsymbol{q}_n, \boldsymbol{q}_{n+1}) = \boldsymbol{P}_{int}(\boldsymbol{q}_{n+\frac{1}{2}}) = \begin{bmatrix} \boldsymbol{I} & \boldsymbol{0} \\ \boldsymbol{0} & -(\widehat{\boldsymbol{d}_1})_{n+\frac{1}{2}} \\ \boldsymbol{0} & -(\widehat{\boldsymbol{d}_2})_{n+\frac{1}{2}} \\ \boldsymbol{0} & -(\widehat{\boldsymbol{d}_3})_{n+\frac{1}{2}} \end{bmatrix} \tag{4.3.27}$$

can be inserted into the d'Alembert-type scheme (3.2.31). Due to the six constraints of orthonormality (4.3.3), the configuration space $Q = \mathbb{R}^{12}$ of the free rigid body is reduced to the constraint manifold

$$C = \mathbb{R}^3 \times SO(3) \subset \mathbb{R}^3 \times \mathbb{R}^9 \tag{4.3.28}$$

where $SO(3)$ is the special orthogonal group. A reduction of the number of unknowns can now be achieved by introducing a rotation matrix $\boldsymbol{R}(\boldsymbol{\theta}) \in SO(3)$ parametrised in terms of $\boldsymbol{\theta} \in \mathbb{R}^3$, such that for $I = 1, 2, 3$

$$(\boldsymbol{d}_I)_{n+1} = \boldsymbol{R}(\boldsymbol{\theta}) \cdot (\boldsymbol{d}_I)_n \tag{4.3.29}$$

Thus the three rotational variables $\boldsymbol{\theta} \in \mathbb{R}^3$ play the role of the discrete generalised rotational degrees of freedom (in other words they are incremental rotations) in the time interval $[t_n, t_{n+1}]$ which can be used to express the original nine unknowns associated with the directors $(\boldsymbol{d}_I)_{n+1} \in \mathbb{R}^3$, $I = 1, 2, 3$. Concerning the rotation matrix, use is made of the Rodrigues formula, which may be interpreted as a closed-form expression of the exponential map (see e.g. [Mars 94])

$$\boldsymbol{R}(\boldsymbol{\theta}) = \exp(\widehat{\boldsymbol{\theta}}) = \boldsymbol{I} + \frac{\sin(\|\boldsymbol{\theta}\|)}{\|\boldsymbol{\theta}\|}\widehat{\boldsymbol{\theta}} + \frac{1}{2}\left(\frac{\sin(\|\boldsymbol{\theta}\|/2)}{\|\boldsymbol{\theta}\|/2}\right)^2 (\widehat{\boldsymbol{\theta}})^2 \tag{4.3.30}$$

When the above reparametrisation of unknowns is applied, the new configuration of the free rigid body is specified by six unknowns $\boldsymbol{u} = (\boldsymbol{u}_\varphi, \boldsymbol{\theta}) \in U \subset \mathbb{R}^3 \times \mathbb{R}^3$, characterising the incremental displacement and incremental rotation in $[t_n, t_{n+1}]$, respectively. Accordingly, in the present case the nodal reparametrisation $\boldsymbol{F}_{q_n} : U \to C$ introduced in (3.2.42) assumes the form

$$\boldsymbol{q}_{n+1} = \boldsymbol{F}_{q_n}(\boldsymbol{u}) = \begin{bmatrix} \boldsymbol{\varphi}_n + \boldsymbol{u}_\varphi \\ \exp(\widehat{\boldsymbol{\theta}}) \cdot (\boldsymbol{d}_1)_n \\ \exp(\widehat{\boldsymbol{\theta}}) \cdot (\boldsymbol{d}_2)_n \\ \exp(\widehat{\boldsymbol{\theta}}) \cdot (\boldsymbol{d}_3)_n \end{bmatrix} \tag{4.3.31}$$

Note that the present use of rotation matrix (4.3.30) is restricted to a single time-step such that possible singularities of (4.3.30) are not an issue in practical applications.

Remark 4.3.1 Although the nodal reparametrisation (4.3.31) is written in form of incremental unknowns, one certainly has the choice between an incremental update structure and an iterative update structure during the iterative solution of the nonlinear algebraic equation (3.2.44), see Remark 3.2.13 and Appendix B.

4.3.5 Treatment of boundary conditions and bearings by the null space method

If certain degrees of freedom of the rigid body motion are constantly prescribed by bearings, they are usually eliminated from the system of equations of motion by cancellation of the corresponding equations from the discrete system (3.2.2). This can be accomplished consistently in the framework of the null space method.

Fixing of one point in space

The fixing in space of a rigid body's center of mass gives rise to the external constraints

$$\boldsymbol{g}_{ext}^{(F)}(\boldsymbol{q}) = \boldsymbol{\varphi} - \boldsymbol{c} \tag{4.3.32}$$
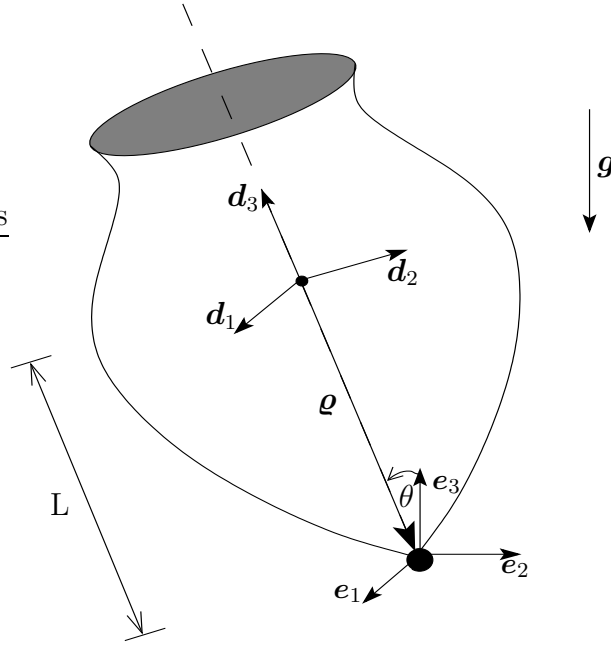
Figure 4.8: Symmetrical top fixed at origin.

where $\boldsymbol{c} \in \mathbb{R}^3$ is constant. For the purely rotational motion, the independent generalised velocities reduce to $\boldsymbol{\nu} = \boldsymbol{\omega}$. Then the rigid body's twist (4.3.17) can be expressed as

$$t = \begin{bmatrix} \mathbf{0} \\ \boldsymbol{I} \end{bmatrix} \cdot \boldsymbol{\omega} = \boldsymbol{P}_{ext}^{(F)}(\boldsymbol{q}) \cdot \boldsymbol{\omega} \tag{4.3.33}$$

with the null space matrix $\boldsymbol{P}_{ext}^{(F)}(\boldsymbol{q})$ pertaining to the external constraints (4.3.32). The admissible velocities in (4.3.16) can be calculated by insertion of $\boldsymbol{P}^{(F)}(\boldsymbol{q}) = \boldsymbol{P}_{int}(\boldsymbol{q}) \cdot \boldsymbol{P}_{ext}^{(F)}(\boldsymbol{q})$ with the internal null space matrix given in (4.3.19).
The discrete null space matrix can be obtained by midpoint evaluation $\mathbf{P}^{(F)}(\boldsymbol{q}_n, \boldsymbol{q}_{n+1}) = \boldsymbol{P}^{(F)}(\boldsymbol{q}_{n+\frac{1}{2}})$. Application of the discrete null space method with nodal reparametrisation leads to the reduced scheme (3.2.44) which is solved for the incremental rotation vector $\boldsymbol{\theta} \in \mathbb{R}^3$. In the present case the reparametrisation (4.3.31) can be used with $\boldsymbol{u}_\varphi = \mathbf{0}$.
The fixing of a point different to the center of mass of a rigid body also reduces its independent generalised velocities to the angular velocity. For the symmetrical top in Figure 4.8, one point on its symmetry axis is fixed at the origin. Assuming that the location of the fixed point is characterised by coordinates ϱ_i with respect to the body frame, i.e. $\boldsymbol{\varrho} = \varrho_i \boldsymbol{d}_i$, the corresponding external constraints read

$$\boldsymbol{g}_{ext}^{(F)}(\boldsymbol{q}) = \boldsymbol{\varphi} + \boldsymbol{\varrho} \tag{4.3.34}$$

Of course the translational velocity of the center of mass of the top is not zero. The twist of the symmetrical top can be calculated from the angular velocity via

$$t = \begin{bmatrix} \widehat{\boldsymbol{\varrho}} \\ \boldsymbol{I} \end{bmatrix} \cdot \boldsymbol{\omega} = \boldsymbol{P}_{ext}^{(F)}(\boldsymbol{q}) \cdot \boldsymbol{\omega} \tag{4.3.35}$$
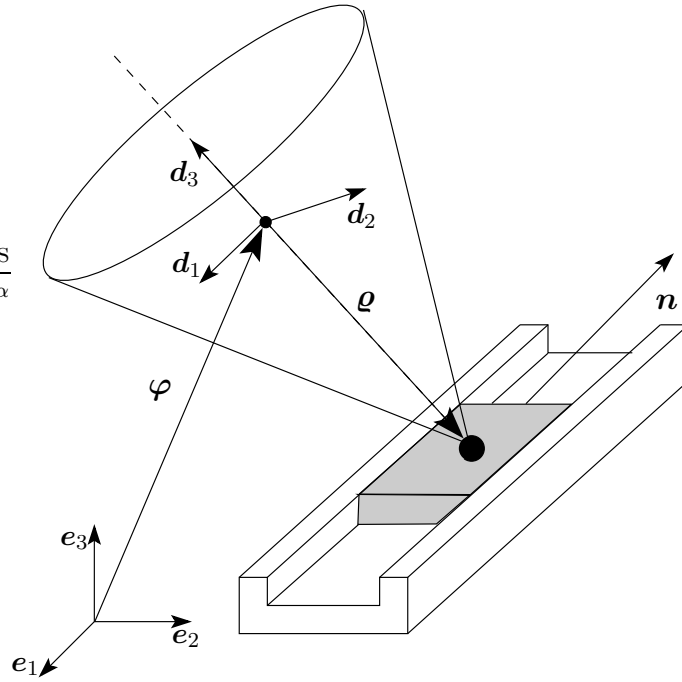
Figure 4.9: Rigid body constrained by sliding bearing.

As explained above, the total null space matrix is given by $\boldsymbol{P}^{(F)}(\boldsymbol{q}) = \boldsymbol{P}_{int}(\boldsymbol{q}) \cdot \boldsymbol{P}_{ext}^{(F)}(\boldsymbol{q})$ and the discrete null space matrix can be inferred by midpoint evaluation. The nodal reparametrisation of the directors takes the form given in $(4.3.31)_{2,3,4}$ and the new placement of the center of mass is given by

$$\boldsymbol{\varphi}_{n+1} = -\exp(\widehat{\boldsymbol{\theta}}) \cdot \boldsymbol{\varrho}_n \tag{4.3.36}$$

Sliding bearing

If a rigid body is fixed in space by a sliding bearing as depicted in Figure 4.9, one point of the rigid body is constrained to slide in the direction of the axis $\boldsymbol{n}$, giving rise to the external constraints

$$\boldsymbol{g}_{ext}^{(F)}(\boldsymbol{q}) = \boldsymbol{\varphi} + \boldsymbol{\varrho} - u\boldsymbol{n} - \boldsymbol{c} \tag{4.3.37}$$

where $u \in \mathbb{R}$ denotes the displacement in the direction of $\boldsymbol{n}$. Thus the sliding bearing reduces the independent generalised velocities of the rigid body to

$$\boldsymbol{\nu} = \begin{bmatrix} \dot{u} \\ \boldsymbol{\omega} \end{bmatrix} \tag{4.3.38}$$

containing the translational velocity $\dot{u}$ besides the angular velocity of the rigid body. Then the twist of the rigid body can be calculated from the independent generalised velocities via

$$\boldsymbol{t} = \begin{bmatrix} \boldsymbol{n} & \widehat{\boldsymbol{\varrho}} \\ \boldsymbol{0} & \boldsymbol{I} \end{bmatrix} \cdot \begin{bmatrix} \dot{u} \\ \boldsymbol{\omega} \end{bmatrix} = \boldsymbol{P}_{ext}^{(B)}(\boldsymbol{q}) \cdot \boldsymbol{\nu} \tag{4.3.39}$$

As explained above, the total null space matrix is given by $\boldsymbol{P}^{(B)}(\boldsymbol{q}) = \boldsymbol{P}_{int}(\boldsymbol{q}) \cdot \boldsymbol{P}_{ext}^{(B)}(\boldsymbol{q})$ and the discrete null space matrix can be inferred by midpoint evaluation. The nodal reparametrisation of the directors takes the form given in $(4.3.31)_{2,3,4}$ and the new placement of the center of mass is given by

$$\boldsymbol{\varphi}_{n+1} = -\exp(\widehat{\boldsymbol{\theta}}) \cdot \boldsymbol{\varrho}_n + \boldsymbol{c} + (u_n + u)\boldsymbol{n}_n \tag{4.3.40}$$

Remark 4.3.2 The treatment of lower kinematic pairs in Section 6.1 reveals that the fixing of one point of a rigid body in space can be modelled as a spherical pair, where the first body is totally fixed in space. Similarly, the sliding bearing coincides with the modelling of a pair, consisting of one totally fixed rigid body, which is connected to the other body by the combination of a spherical joint with a prismatic joint.

4.3.6 Numerical example: symmetrical top

The motion of a symmetrical top with a fixed point on its axis of symmetry (Figure 4.8) is considered as an example. The shape of the top is assumed to be a cone with height $H = 0.1$ and radius $R = 0.05$. The center of mass is located at $L = \frac{3}{4}H$, so that the location of the spherical joint with respect to the body frame is given by

$$\boldsymbol{\varrho} = \varrho_i \boldsymbol{d}_i \qquad [\varrho_i] = [0, 0, -L] \tag{4.3.41}$$

The total mass of the top is $M_\varphi = \frac{1}{3}\varrho\pi R^2 H$, the mass density is assumed to be $\varrho = 2700$ and the principal inertias with respect to the center of mass are

$$J_1 = J_2 = \frac{3M_\varphi}{80}(4R^2 + H^2) \qquad J_3 = \frac{3M_\varphi}{10}R^2 \tag{4.3.42}$$

Then the principal values of the Euler tensor with respect to the center of mass follow from (4.3.6) such that the mass matrix $\boldsymbol{M} \in \mathbb{R}^{12 \times 12}$ in (4.3.8) can be easily set up. Gravity is acting on the top such that the potential energy function is given by (4.3.12) with $g = -9.81$. The initial angle of nutation is chosen to be $\theta = \pi/3$. Accordingly, the initial configuration is characterised by $\boldsymbol{q} \in \mathbb{R}^{12}$ with

$$\boldsymbol{d}_I = \exp(\theta\widehat{\boldsymbol{e}}_1) \cdot \boldsymbol{e}_I \qquad \boldsymbol{\varphi} = -\boldsymbol{\varrho} = L\boldsymbol{d}_3 \tag{4.3.43}$$

In order to provide an illustrative example, the case of precession with no nutation is considered. Let ω_p denote the precession rate and ω_s the spin rate. The condition for steady precession can be written as (see e.g. [Magn 71])

$$\omega_s = \frac{M_\varphi g L}{\tilde{M}_3 \omega_p} + \frac{\tilde{M}_1 - \tilde{M}_3}{\tilde{M}_3}\omega_p \cos(\theta) \tag{4.3.44}$$

Here, $\tilde{M}_I$ are the principal values of the reduced mass matrix (4.3.21). In the present case

$$\widetilde{\boldsymbol{M}} = \left(\boldsymbol{P}^{(F)}(\boldsymbol{q})\right)^T \cdot \boldsymbol{M} \cdot \boldsymbol{P}^{(F)}(\boldsymbol{q}) = \boldsymbol{J} + M_\varphi \left(\|\boldsymbol{\varrho}\|^2 \boldsymbol{I} - \boldsymbol{\varrho} \otimes \boldsymbol{\varrho}\right) \tag{4.3.45}$$

or, in view of (4.3.21)

$$\widetilde{\boldsymbol{M}} = \sum_{I=1}^{3} J_I \boldsymbol{d}_I \otimes \boldsymbol{d}_I + M_\varphi L^2 \left(\boldsymbol{d}_1 \otimes \boldsymbol{d}_1 + \boldsymbol{d}_2 \otimes \boldsymbol{d}_2 \right) \tag{4.3.46}$$

Accordingly, the principal values of the reduced mass matrix to be inserted into (4.3.44) are given by

$$\tilde{M}_1 = J_1 + M_\varphi L^2 \qquad \tilde{M}_3 = J_3 \tag{4.3.47}$$

Note that the reduced mass matrix conforms to the well-known parallel-axis theorem. Consistent initial velocities $\dot{\boldsymbol{q}} \in \mathbb{R}^{12}$ can be calculated by employing the null space matrix in (4.3.35). Accordingly,

$$\dot{\boldsymbol{q}} = \begin{bmatrix} \widehat{\boldsymbol{\varrho}} \\ -\widehat{\boldsymbol{d}_1} \\ -\widehat{\boldsymbol{d}_2} \\ -\widehat{\boldsymbol{d}_3} \end{bmatrix} \cdot \boldsymbol{\omega} = \boldsymbol{P}^{(F)}(\boldsymbol{q}) \cdot \boldsymbol{\omega} \tag{4.3.48}$$

with the initial angular velocity vector given by

$$\boldsymbol{\omega} = \omega_p \boldsymbol{e}_3 + \omega_s \boldsymbol{d}_3 \tag{4.3.49}$$

and the precession rate $\omega_p = 10$.

Lagrange multiplier method

The energy-momentum conserving constrained time-stepping scheme for the motion of the heavy symmetrical top follows from (3.2.5).

The motion of the center of mass $\boldsymbol{\varphi}(t) = x_1(t)\boldsymbol{e}_1 + x_2(t)\boldsymbol{e}_2 + x_3(t)\boldsymbol{e}_3$ is depicted in Figure 4.10 on the left hand side. For the time-step $h = 0.001$, a constant evolution of the x_3-coordinate can be observed, corresponding to the steady precession of the top. The diagram on the right hand side shows the evolution of the energies and the components of the angular momentum. Apparently, the algorithmic conservation of the total energy and the angular momentum's component corresponding to the gravitational direction is confirmed. Furthermore, corresponding to the steady precession of the top, the evolution of the kinetic and potential energies are also constant.

Penalty method

The discrete energy-momentum conserving penalty time-stepping scheme (3.2.9) with $P_{Pen}(\boldsymbol{g}(\boldsymbol{q})) = \mu \|\boldsymbol{g}(\boldsymbol{q})\|^2$ is used.

Figure 4.11 shows the statements of Proposition 3.2.2. The fulfilment of the constraints improves and the solution of the penalty scheme for the heavy symmetrical top converges to that of the corresponding constrained scheme as the penalty parameter increases.
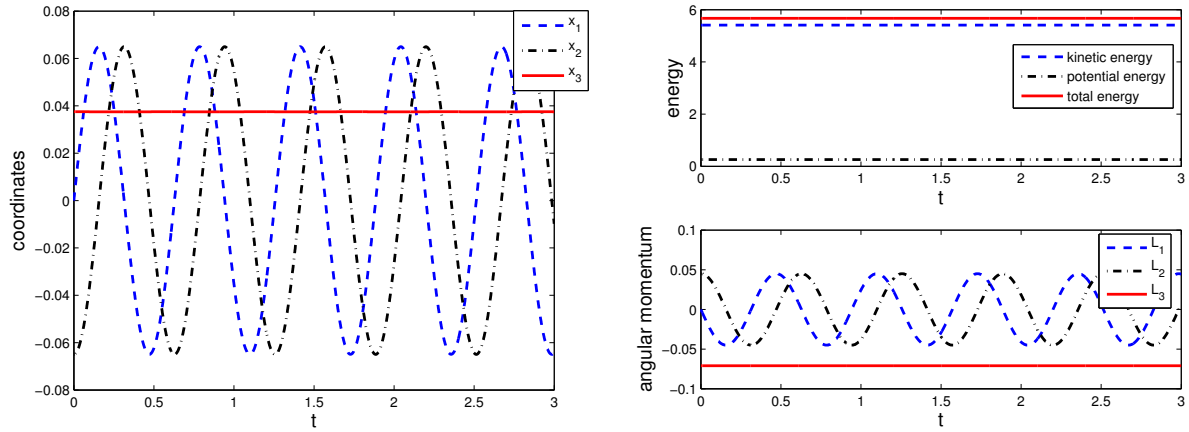
Figure 4.10: Heavy symmetrical top: motion of the center of mass and energy and components of angular momentum vector $\boldsymbol{L} = L_i \boldsymbol{e}_i$ ($h = 0.001$).
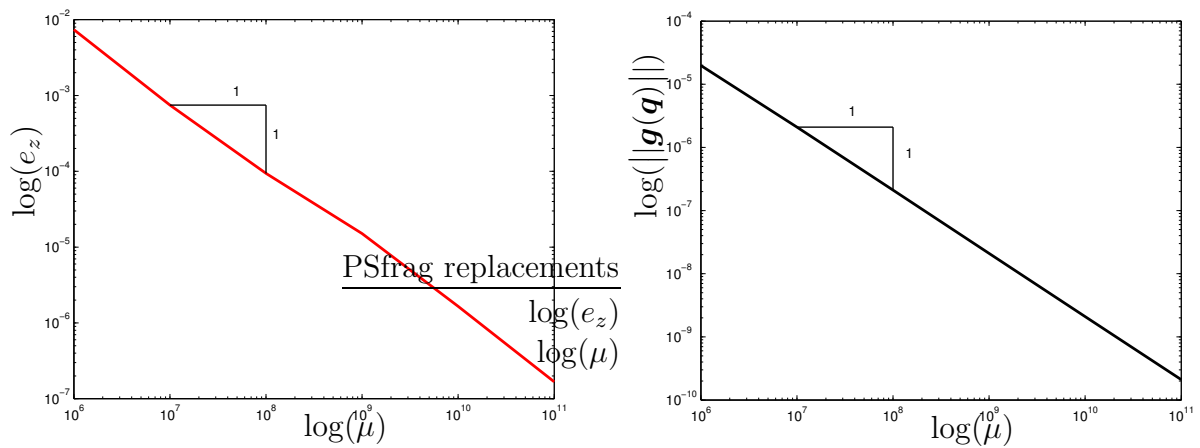
Figure 4.11: Heavy symmetrical top: relative error $e_z = \left\| \boldsymbol{z}_{\mathrm{Pen}} - \boldsymbol{z}_{\mathrm{Lag}} \right\| / \left\| \boldsymbol{z}_{\mathrm{Lag}} \right\|$ of the phase variable and constraint fulfilment for the penalty scheme at $t = 3$ ($h = 0.01$).

Augmented Lagrange method

Enforcing the constraints by means of the augmented Lagrange method, the time-stepping scheme (3.2.22) is solved using $P_{Aug}(\boldsymbol{g}(\boldsymbol{q})) = \boldsymbol{g}^T(\boldsymbol{q}) \cdot \boldsymbol{\lambda} + \mu \|\boldsymbol{g}(\boldsymbol{q})\|^2$ with $\mu = 10^5$.

The improvement of the constraint fulfilment and the convergence of the solution of the augmented Lagrange time stepping scheme to that of the constrained scheme during the augmented Lagrange iteration (AL-iteration) is depicted in Figure 4.12. The results corroborate the statements of Proposition 3.2.4.
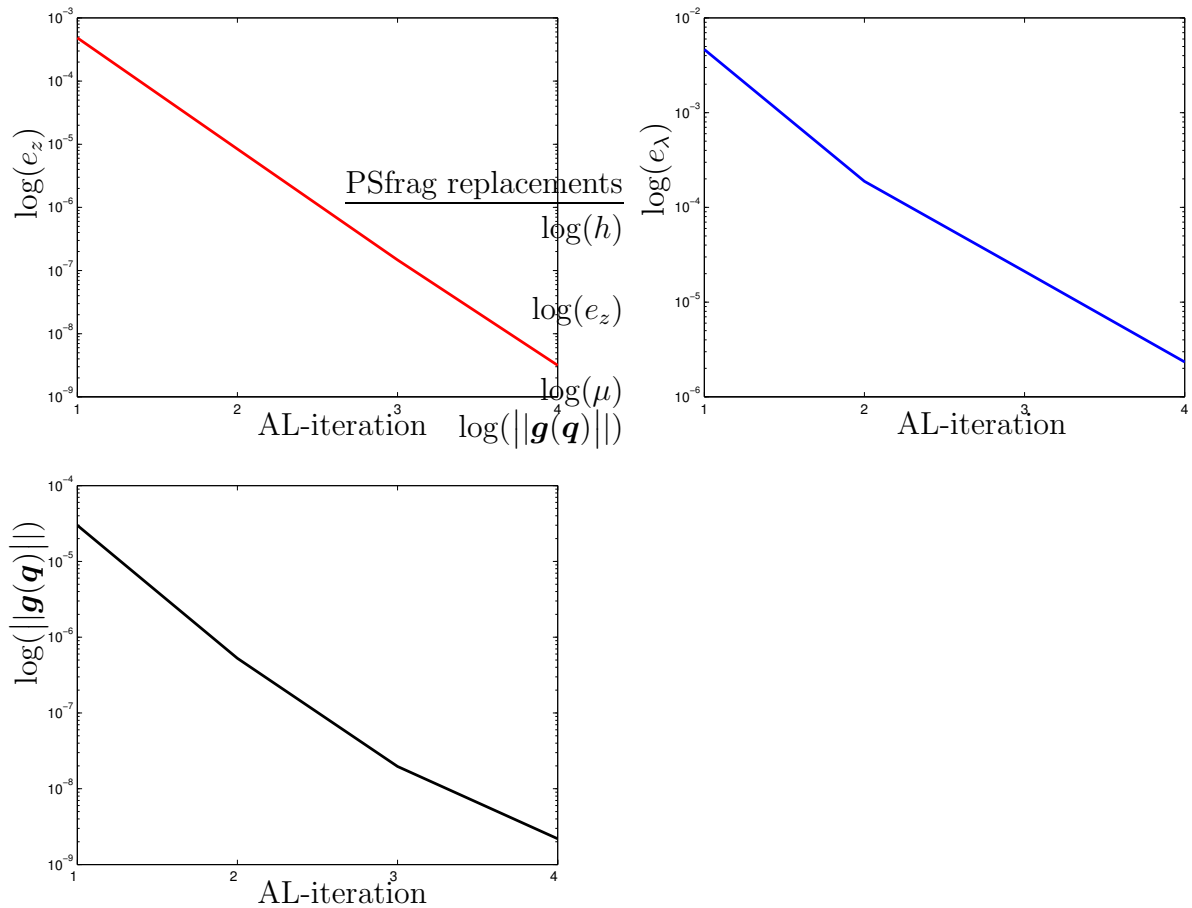
Figure 4.12: Heavy symmetrical top: relative error $e_z = \|\boldsymbol{z}_{\mathrm{Aug}} - \boldsymbol{z}_{\mathrm{Lag}}\|/\|\boldsymbol{z}_{\mathrm{Lag}}\|$ of the phase variable and relative error of the multipliers $e_\lambda = \|\boldsymbol{\lambda}_{\mathrm{Aug}} - \boldsymbol{\lambda}_{\mathrm{Lag}}\|/\|\boldsymbol{\lambda}_{\mathrm{Lag}}\|$ and constraint fulfilment for the augmented Lagrange scheme at $t = 3$ ($h = 0.01$, $\mu = 10^5$).

Discrete null space method with nodal reparametrisation

Similar to (4.3.27), an explicit representation of the discrete counterpart of the null space matrix for the heavy symmetrical top with a point on the symmetry axis fixed used in (4.3.48), reads

$$
\mathbf{P}^{(F)}(\boldsymbol{q}_n, \boldsymbol{q}_{n+1}) =
\begin{bmatrix}
\widehat{\boldsymbol{\varrho}}_{n+\frac{1}{2}} \\
-(\widehat{\boldsymbol{d}_1})_{n+\frac{1}{2}} \\
-(\widehat{\boldsymbol{d}_2})_{n+\frac{1}{2}} \\
-(\widehat{\boldsymbol{d}_3})_{n+\frac{1}{2}}
\end{bmatrix}
\tag{4.3.50}
$$

Insertion of (4.3.50) and the reparametrisation of the directors $(4.3.31)_{2,3,4}$ and that of the placement of the center of mass given in (4.3.36) into (3.2.43) yields the d'Alembert-type time-stepping scheme with nodal reparametrisation. Figure 4.13 shows the convergence of the solution of the d'Alembert-type scheme with nodal reparametrisation to a reference solution calculated with the constrained scheme, using the time-step $h = 10^{-6}$. It confirms the statement of Proposition 3.2.12.

PSfrag replacements
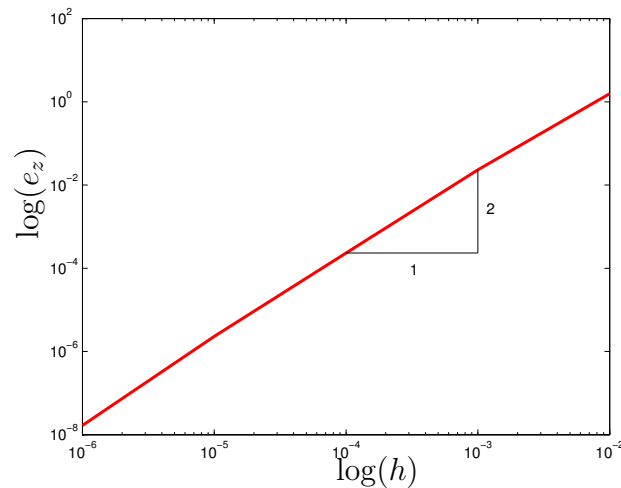
Figure 4.13: Heavy symmetrical top: relative error $e_z = \left\| \boldsymbol{z}_{\mathrm{d'Al}} - \boldsymbol{z}_{\mathrm{Lag}} \right\| / \left\| \boldsymbol{z}_{\mathrm{Lag}} \right\|$ of the phase variable for the d'Alembert-type scheme with nodal reparametrisation at $t = 0.1$.

Comparison

The summary of the computational aspects of the different schemes in Table 4.2 shows that the calculation of 1000 time-steps using the 3-dimensional d'Alembert-type scheme with nodal reparametrisation takes the least computational time. The fulfilment of the constraints can be considered as numerically exact, since the constraint violation is smaller than the tolerance $\mathrm{tol} = 10^{-10}$ used in the Newton-Raphson iteration. In combination with the well-conditionedness for all time-steps, these properties distinguish the d'Alembert-type scheme with nodal reparametrisation to be the most favourable time-stepping scheme for the rigid body motion.

The CPU-time for each scheme is specified as the ratio between the computation time for 1000 time-steps ($h = 0.01$) by the scheme and that of the d'Alembert-type scheme

with nodal reparametrisation. Although the constrained scheme yields a 21-dimensional system of equations, the calculation of 1000 time-steps is substantially quicker than using the 12-dimensional penalty or augmented Lagrange scheme, where the set up of the G-equivariant discrete derivative of the extra function for the treatment of the constraints is quite involved. As expected, the constraints are fulfilled numerically exactly by the constrained scheme and the condition number of the iteration matrix deteriorates for decreasing time-steps.

For decreasing time-steps, the condition numbers of the penalty scheme and the augmented Lagrange scheme are decreasing, which is in accordance with it's theoretically computed quadratic dependence on the time-step.

Although the constraint fulfilment by the augmented Lagrange scheme is acceptable, its high computational costs disqualify it in the competition with the other schemes. Just so, the bad constraint fulfilment using $\mu = 10^5$ and the high condition numbers for $\mu = 10^{10}$ do not recommend the use of the penalty scheme for the simulation of the rigid body motion.

Apparantly the d'Alembert-type scheme with nodal reparametrisation surpasses the other schemes by provdiding quickly a highly accurate solution without suffering from conditioning problems.

Table 4.2: Comparison of constrained scheme, penalty scheme, augmented Lagrange scheme and d'Alembert-type scheme with nodal reparametrisation for the example 'heavy symmetrical top'.

	constrained	penalty		augm. Lag.	d'Alembert
number of unknowns $n = 12 \quad m = 9$	21	12		12	3
CPU-time	1.4	2.7		7.2	1
constraint fulfilment	10^{-16}	$\mu = 10^5$ 10^{-4}	$\mu = 10^{10}$ 10^{-9}	10^{-9}	10^{-14}
condition number $h = 10^{-2}$ $h = 10^{-3}$ $h = 10^{-4}$	10^6 10^9 10^{12}	10^4 10^3 10^3	10^9 10^7 10^5	10^4 10^3 10^3	1 1 1

5 Objective formulation of geometrically exact beam dynamics

Modelling geometrically exact beams as a special Cosserat continuum (see e.g. [Antm 95]) has been the basis for many finite element formulations starting with the work of Simo [Simo 85]. The formulation of the beam dynamics as Hamiltonian system subject to internal constraints, which are associated with the kinematic assumptions of the underlying continuous theory, has the advantages that external constraints representing the connection to other components of a multibody system can be easily incorporated.

Many current semi-discrete beam formulations avoid the introduction of internal constraints by using rotational degrees of freedom, see e.g. [Jele 98], [Ibra 98]. However, it has been shown by Chrisfield & Jelenic [Cris 99], that the interpolation of non-commutative finite rotations bears the risk of destroying the objectivity of the strain measures in the semi-discrete model. This can be circumvented by the introduction of the director triad, which is constrained to be orthonormal in each node of the central line of the beam. The main advantage is that the directors belong to a linear space. The spatial interpolation of the director triad in (5.3.1) leads to objective strain measures in the spatially discretised configuration. This idea is independently developed in [Rome 02b] and [Bets 02d]. [Rome 04] offers an overview on the effects of different interpolation techniques concerning frame invariance and the appearance of singularities. Furthermore, this subject is elaborated in [Bets 98, Ibra 95, Ibra 97, Ibra 02b, Jele 99, Jele 02, Bott 02b].

While the authors in [Bets 02d] restrict themselves to the specification of the weak form of balance equations for the beam in the static case, in [Bets 03] the equations of motion are given as Hamiltonian system subject to holonomic constraints, which are realised by the Lagrange multiplier method. As expatiated in Section 2.3, the Hamiltonian formalism provides the possibility to use different methods for the constraint enforcement. In Section 3.2 (see also [Leye 04]) various methods are compared and the results are illustrated with the examples of mass point systems and rigid bodies in Chapter 4. The same methods are used here for the realisation of the internal constraints of the beam.

The major difference between the beam formulation in [Bets 03] and that presented in the sequel (see [Leye 06]) is the reparametrisation of the Hamiltonian. Since objectivity of the strain measures is a main goal of the formulation, it suggests itself to parametrise the rotationally invariant Hamiltonian directly in the invariants of the Lie group $SO(3)$. Consequently the strain measures are approximated objectively. This is an ideal basis for a temporal discretisation using the concept of G-equivariant discrete derivatives by Gonzalez [Gonz 96c] presented in Section 3.1.1, which leads to energy-momentum conserving time-integration of the equations of motion. Thus a time-stepping scheme is obtained which is objective and by construction energy-momentum preserving.

5.1 Kinematics

PSfrag replacements
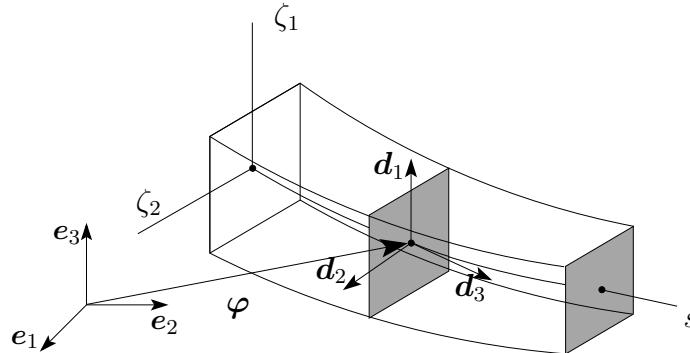
Figure 5.1: Configuration of a beam with respect to an orthonormal frame $\{e_I\}$ fixed in space.

In [Bets 02d], Betsch and Steinmann introduce frame-indifferent finite elements for the geometrically exact beam theory, in the sense that they inherit the objectivity of the underlying continuous beam strains. The concept is a generalisation of the description of the rigid body as a 'one-node structure' in Section 4.3.1. It relies on the kinematic assumption illustrated in Figure 5.1 (see [Antm 95]) that the placement of a material point in the inertial frame $\{e_I\}$, which is identified by its position vector $\boldsymbol{X}(\zeta^i) \in \mathcal{B}_0 \subset \mathbb{R}^3$ in the reference configuration $\mathcal{B}_0$, can be described by

$$\boldsymbol{x}(\zeta^\kappa, s, t) = \boldsymbol{\varphi}(s, t) + \zeta^\kappa \boldsymbol{d}_\kappa(s, t) \tag{5.1.1}$$

Here $(\zeta^1, \zeta^2, \zeta^3 = s) \in \mathbb{R}^3$ is a triple of curvilinear coordinates with $s \in [0, L] \subset \mathbb{R}$ being the arc-length of the line of centroids $\boldsymbol{\varphi}(s, 0) \in \mathbb{R}^3$ in the reference configuration. $\{\boldsymbol{d}_I\}$ represent an orthonormal triad. The directors $\boldsymbol{d}_\kappa(s, t), \kappa = 1, 2$ span a principal basis of the cross-section at s and time t which is accordingly assumed to stay plane. In the reference configuration, $\boldsymbol{d}_3$ is tangent to the central line $\boldsymbol{\varphi}(s, 0)$ but this is not necessary in a deformed configuration. This allowance of transverse shear deformation corresponds to the Timoshenko beam theory (see [Warb 76]). In contrast to kinematic assumption for the placement of a material point in a rigid body (4.3.1), the sum over the repeated index in (5.1.1) comprises $\kappa = 1, 2$ and the spatial extension of the beam in the longitudinal direction is accounted for by the parametrisation in s.

Remark 5.1.1 Setting up the Lagrangian $L : TQ \to \mathbb{R}$, $L = L(\boldsymbol{x}, \dot{\boldsymbol{x}})$ where $\boldsymbol{x}$ is specified in (5.1.1) and $\dot{\boldsymbol{x}}$ denotes its temporal derivative, one comes across the fact that the kinetic energy is independent of $\dot{\boldsymbol{d}}_3$. Due to that property, the Lagrangian is degenerate and it follows that $\boldsymbol{p}_3 = \partial L / \partial \dot{\boldsymbol{d}}_3 = \boldsymbol{0}$. One can still pass to the Hamiltonian formulation using Dirac's theory (see [Bets 03, Dira 50] and references therein). Thereby, the relevant momenta are denoted by $\bar{\boldsymbol{p}}$ and the corresponding configurational quantities by $\bar{\boldsymbol{q}}$. The

Hamiltonian depends on the reduced phase space variable $\boldsymbol{z} = \boldsymbol{z}(s,t)$ with

$$
\boldsymbol{z}(s,t) = \left[\begin{array}{c} \boldsymbol{q}(s,t) \\ \bar{\boldsymbol{p}}(s,t) \end{array} \right] = \left[\begin{array}{c} \bar{\boldsymbol{q}}(s,t) \\ \boldsymbol{d}_3(s,t) \\ \bar{\boldsymbol{p}}(s,t) \end{array} \right] \in \mathbb{R}^{21}
$$

$$
\bar{\boldsymbol{q}}(s,t) = \left[\begin{array}{c} \boldsymbol{\varphi}(s,t) \\ \boldsymbol{q}_1(s,t) \\ \boldsymbol{q}_2(s,t) \end{array} \right] \in \mathbb{R}^9 \qquad \bar{\boldsymbol{p}}(s,t) = \left[\begin{array}{c} \boldsymbol{p}_\varphi(s,t) \\ \boldsymbol{p}_1(s,t) \\ \boldsymbol{p}_2(s,t) \end{array} \right] \in \mathbb{R}^9
$$

(5.1.2)

5.2 Dynamics of the beam as Hamiltonian system subject to internal constraints

The beam's kinetic energy can be written in the form

$$
T(\boldsymbol{p}(t)) = \frac{1}{2} \int_0^L \bar{\boldsymbol{p}}^T \cdot \bar{\boldsymbol{M}}^{-1} \cdot \bar{\boldsymbol{p}} \, ds \tag{5.2.1}
$$

with the non-singular reduced mass matrix (see Remark 5.1.1)

$$
\bar{\boldsymbol{M}} = \left[\begin{array}{ccc} A_\rho \boldsymbol{I} & \boldsymbol{0} & \boldsymbol{0} \\ \boldsymbol{0} & M_\rho^1 \boldsymbol{I} & \boldsymbol{0} \\ \boldsymbol{0} & \boldsymbol{0} & M_\rho^2 \boldsymbol{I} \end{array} \right] \tag{5.2.2}
$$

where $\boldsymbol{I}$ and $\boldsymbol{0}$ denote the 3×3 identity and zero matrices respectively, A_ρ is the mass density per reference length and M_ρ^1, M_ρ^2 can be interpreted as principal mass-moments of inertia of the cross-section.

In the present case the potential energy function is assumed to be the sum of stored and external energy

$$
V(\boldsymbol{q}(t)) = V_{int}(\boldsymbol{q}(t)) + V_{ext}(\boldsymbol{q}(t)) = \int_0^L W_{int}(\boldsymbol{\Gamma}(\boldsymbol{q}), \boldsymbol{K}(\boldsymbol{q})) \, ds + \int_0^L W_{ext}(\boldsymbol{q}) \, ds \tag{5.2.3}
$$

W_{ext} is the density of the conservative external loads and W_{int} is a strain energy density function expressed in terms of the objective strain measures

$$
\begin{aligned}
\boldsymbol{\Gamma}(\boldsymbol{q}) &= \Gamma_i \boldsymbol{e}_i & \Gamma_i &= \boldsymbol{d}_i^T \cdot \boldsymbol{\varphi}_{,s} - \delta_{i3} \\
\boldsymbol{K}(\boldsymbol{q}) &= K_i \boldsymbol{e}_i & K_i &= \tfrac{1}{2} \epsilon_{ijk} \left(\boldsymbol{d}_k^T \cdot \boldsymbol{d}_{j,s} - (\boldsymbol{d}_k^T \cdot \boldsymbol{d}_{j,s})|_{t=0} \right)
\end{aligned} \tag{5.2.4}
$$

where δ_{ij} is the Kronecker delta and ϵ_{ijk} the alternating symbol. An interpretation of these strain measures can be found in [Antm 95], whereupon Γ_1 and Γ_2 measure shear strains, Γ_3 elongation, K_1 and K_2 quantify flexure and K_3 torsion. The constitutive equations

$$
\boldsymbol{n} = \frac{\partial W_{int}}{\partial \boldsymbol{\Gamma}} \qquad \boldsymbol{m} = \frac{\partial W_{int}}{\partial \boldsymbol{K}} \tag{5.2.5}
$$

define the resulting shear forces n_1, n_2 and axial force n_3 and the resulting bending momenta m_1, m_2 and torsional moment m_3 respectively.

The assumption of orthonormality of the director triad gives rise to six independent holonomic internal constraints of the form (4.3.3) at each point of the central line of the beam. Independent of the method in use, the treatment of the configuration constraints is represented by the extra function $P_{con} : \boldsymbol{g}_{int}(Q) \to \mathbb{R}$ introduced in (2.3.12). For the geometrically exact beam, the contribution of the unfulfilled constraints to the Hamiltonian can be calculated as

$$P_H(\boldsymbol{z}(t)) = \int_0^L \boldsymbol{v}(s,t)\boldsymbol{R}(\boldsymbol{g}_{int}(\boldsymbol{q}(s,t)))\,ds \tag{5.2.6}$$

As mentioned in Remark 5.1.1, Dirac's theory must be used to derive the equations of motion for the geometrically exact beam in the Hamiltonian formalism. The transition form the Lagrangian formulation (with a degenerate Lagrangian) to the Hamiltonian formulation is performed in detail in [Bets 03]. Along the lines described there, but neglecting the secondary constraints (see Remark 2.3.3) and using the augmented Hamiltonian introduced in (2.3.13), one arrives at the following infinite dimensional equations of motion for the geometrically exact beam

$$
\begin{aligned}
\dot{\bar{\boldsymbol{q}}}(s,t) &= \delta_{\bar{\boldsymbol{p}}}H(\boldsymbol{z}(s,t)) \\
\dot{\bar{\boldsymbol{p}}}(s,t) &= -\delta_{\bar{\boldsymbol{q}}}H(\boldsymbol{z}(s,t)) \\
\boldsymbol{0} &= -\delta_{\boldsymbol{d}_3}H(\boldsymbol{z}(s,t))
\end{aligned} \tag{5.2.7}
$$

where δ denotes the functional derivative (see A.5).

Remark 5.2.1 If the Lagrange multiplier method is used to enforce the constraints, the system (5.2.7) is supplemented by the constraint equations $\boldsymbol{g}_{int}(\boldsymbol{q}(s,t)) = \boldsymbol{0}$ of the form (4.3.3).

5.3 Hamiltonian formulation of the semi-discrete beam

PSfrag replacements
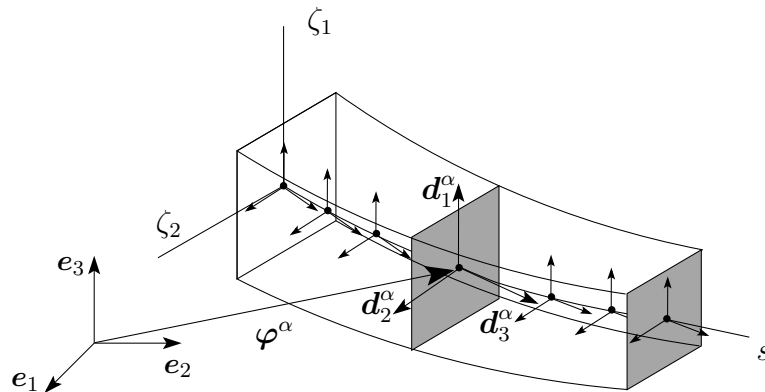
Figure 5.2: Configuration of a spatially discretised beam with respect to an orthonormal frame $\{\boldsymbol{e}_I\}$ fixed in space.

To perform a discretisation in space, n_{node} nodes subdivide the central line of the beam into finite elements, see Figure 5.2. Isoparametric finite element interpolations are introduced,

using Lagrange-type nodal shape functions $N_\alpha(s)$ and Dirac deltas $M_\alpha(s) = \delta(s - s_\alpha)$ associated with the nodal points $s^\alpha \in [0, L]$, $\alpha = 1, \ldots, n_{node}$

$$
\boldsymbol{\varphi}^h(s,t) = \sum_{\alpha=1}^{n_{node}} N_\alpha(s)\boldsymbol{\varphi}^\alpha(t) \qquad \boldsymbol{d}_I^h(s,t) = \sum_{\alpha=1}^{n_{node}} N_\alpha(s)\boldsymbol{d}_I^\alpha(t) \quad I = 1, 2, 3
$$

$$
\boldsymbol{p}_\varphi^h(s,t) = \sum_{\alpha=1}^{n_{node}} N_\alpha(s)\boldsymbol{p}_\varphi^\alpha(t) \qquad \boldsymbol{p}_I^h(s,t) = \sum_{\alpha=1}^{n_{node}} N_\alpha(s)\boldsymbol{p}_I^\alpha(t) \quad I = 1, 2 \qquad (5.3.1)
$$

$$
\boldsymbol{z}^h(s,t) = \sum_{\alpha=1}^{n_{node}} N_\alpha(s)\boldsymbol{z}^\alpha(t) \qquad \boldsymbol{v}^h(s,t) = \sum_{\alpha=1}^{n_{node}} M_\alpha(s)\boldsymbol{v}^\alpha(t)
$$

Thus the semi-discrete mechanical system is characterised by the phase vector

$$
\boldsymbol{z}(t) = \begin{bmatrix} \boldsymbol{z}^1(t) \\ \vdots \\ \boldsymbol{z}^{n_{node}}(t) \end{bmatrix} \in \mathbb{R}^{21 n_{node}} \qquad \boldsymbol{z}^\alpha(t) = \begin{bmatrix} \boldsymbol{q}^\alpha(t) \\ \bar{\boldsymbol{p}}^\alpha(t) \end{bmatrix} \in \mathbb{R}^{21}
$$

$$
\boldsymbol{q}(t) = \begin{bmatrix} \boldsymbol{q}^1(t) \\ \vdots \\ \boldsymbol{q}^{n_{node}}(t) \end{bmatrix} \in \mathbb{R}^{12 n_{node}} \qquad \boldsymbol{q}^\alpha(t) = \begin{bmatrix} \boldsymbol{\varphi}^\alpha(t) \\ \boldsymbol{d}_1^\alpha(t) \\ \boldsymbol{d}_2^\alpha(t) \\ \boldsymbol{d}_3^\alpha(t) \end{bmatrix} \in \mathbb{R}^{12} \qquad (5.3.2)
$$

$$
\bar{\boldsymbol{p}}(t) = \begin{bmatrix} \bar{\boldsymbol{p}}^1(t) \\ \vdots \\ \bar{\boldsymbol{p}}^{n_{node}}(t) \end{bmatrix} \in \mathbb{R}^{9 n_{node}} \qquad \bar{\boldsymbol{p}}^\alpha(t) = \begin{bmatrix} \boldsymbol{p}_\varphi^\alpha(t) \\ \boldsymbol{p}_1^\alpha(t) \\ \boldsymbol{p}_2^\alpha(t) \end{bmatrix} \in \mathbb{R}^9
$$

Insertion of (5.3.1) and (5.3.2) into the kinetic energy (5.2.1) yields

$$
T^h(\bar{\boldsymbol{p}}(t)) = \frac{1}{2} \sum_{\alpha,\beta=1}^{n_{node}} (\bar{\boldsymbol{p}}^\alpha)^T \cdot \left(\bar{\boldsymbol{M}}_{\alpha\beta}^h\right)^{-1} \cdot \bar{\boldsymbol{p}}^\beta = \frac{1}{2}\bar{\boldsymbol{p}}^T \cdot \left(\bar{\boldsymbol{M}}^h\right)^{-1} \cdot \bar{\boldsymbol{p}} \qquad (5.3.3)
$$

with the consistent $9n_{node} \times 9n_{node}$ mass matrix $\bar{\boldsymbol{M}}^h$ consisting of the submatrices

$$
\bar{\boldsymbol{M}}_{\alpha\beta}^h = \begin{bmatrix} M_{\alpha\beta}\boldsymbol{I} & \boldsymbol{0} & \boldsymbol{0} \\ \boldsymbol{0} & M_{\alpha\beta}^1\boldsymbol{I} & \boldsymbol{0} \\ \boldsymbol{0} & \boldsymbol{0} & M_{\alpha\beta}^2\boldsymbol{I} \end{bmatrix}
$$

$$(5.3.4)$$

$$
M_{\alpha\beta} = \int_0^L A_\rho N_\alpha(s)N_\beta(s)\, ds \quad M_{\alpha\beta}^\kappa = \int_0^L M_\rho^\kappa N_\alpha(s)N_\beta(s)\, ds \quad \kappa = 1, 2
$$

Remark 5.3.1 Provided that the nodes are numbered appropriately, for a k-node beam element, the compact support of the shape functions N_α, $\alpha = 1, \ldots, k$ causes $M_{\alpha\beta} = M_{\alpha\beta}^1 = M_{\alpha\beta}^2 = 0$ for $|\alpha - \beta| \geq k$. Thus the symmetric, global mass matrix $\bar{\boldsymbol{M}}^h$ is banded with nonzero elements on the diagonal and on $k - 1$ subdiagonals.

Insertion of $\boldsymbol{v}^h(s,t)$ from (5.3.1) into (5.2.6) yields

$$
P_H^h(\boldsymbol{z}(t)) = \sum_{\alpha=1}^{n_{node}} \boldsymbol{v}^\alpha(t)\boldsymbol{R}(\boldsymbol{g}_{int}^\alpha(\boldsymbol{q}^\alpha(t))) \qquad (5.3.5)
$$

i.e. the constraint fulfilment is enforced at the nodes. The nodal internal constraint functions $\boldsymbol{g}_{int}^{\alpha}(\boldsymbol{q}^{\alpha}) \in \mathbb{R}^6$ of the form (4.3.3) can be combined to

$$\boldsymbol{g}_{int}(\boldsymbol{q}(t)) = \begin{bmatrix} \boldsymbol{g}_{int}^{1}(\boldsymbol{q}^{1}(t)) \\ \vdots \\ \boldsymbol{g}_{int}^{n_{node}}(\boldsymbol{q}^{n_{node}}(t)) \end{bmatrix} \in \mathbb{R}^{m_{int}} \tag{5.3.6}$$

with $m_{int} = 6n_{node}$. Similarly, the $6n_{node} \times 12n_{node}$ Jacobian of the internal constraints takes the form

$$\boldsymbol{G}_{int}(\boldsymbol{q}(t)) = \begin{bmatrix} \boldsymbol{G}_{int}^{1}(\boldsymbol{q}^{1}(t)) & \boldsymbol{0} & \cdots & \boldsymbol{0} \\ \boldsymbol{0} & \boldsymbol{G}_{int}^{2}(\boldsymbol{q}^{2}(t)) & \cdots & \boldsymbol{0} \\ \vdots & \vdots & \ddots & \vdots \\ \boldsymbol{0} & \boldsymbol{0} & \cdots & \boldsymbol{G}_{int}^{n_{node}}(\boldsymbol{q}^{n_{node}}(t)) \end{bmatrix} \tag{5.3.7}$$

with $\boldsymbol{G}_{int}^{\alpha}(\boldsymbol{q}^{\alpha})$ given in (4.3.4) for $\alpha = 1, \ldots, n_{node}$.

After the spatial discretisation (5.3.1), (5.3.2) has been inserted, the potential energy (5.2.3) reads

$$V^{h}(\boldsymbol{q}(t)) = \int_{0}^{L} W_{int}(\boldsymbol{\Gamma}(\boldsymbol{q}^{h}(s,t)), \boldsymbol{K}(\boldsymbol{q}^{h}(s,t))) \, ds + \int_{0}^{L} W_{ext}(\boldsymbol{q}^{h}(s,t)) \, ds \tag{5.3.8}$$

The special form of (5.3.8) depends on the behaviour of the material under consideration and on the external potential.

Example 5.3.2 (Gravitation) Let the external conservative load be the gravitation in the negative $\boldsymbol{e}_3$-direction with gravitational acceleration g and define $\bar{\boldsymbol{g}} = [0, 0, g, 0, 0, 0, 0, 0, 0]^{T}$.

$$\begin{aligned} V_{ext}^{h}(\boldsymbol{q}(t)) &= \int_{0}^{L} W_{ext}(\boldsymbol{q}^{h}(s,t)) \, ds = \int_{0}^{L} -\bar{\boldsymbol{g}}^{T} \cdot \bar{\boldsymbol{M}} \cdot \bar{\boldsymbol{q}}^{h}(s,t) \, ds \\ &= \sum_{\alpha=1}^{n_{node}} -\bar{\boldsymbol{g}}^{T} \cdot \bar{\boldsymbol{M}} \cdot \bar{\boldsymbol{q}}^{\alpha}(t) \int_{0}^{L} N_{\alpha}(s) \, ds = \sum_{\alpha=1}^{n_{node}} W_{ext}^{\alpha}(\boldsymbol{q}^{\alpha}(t)) \end{aligned} \tag{5.3.9}$$

Example 5.3.3 (Hyperelastic material) Assume that the hyperelastic material behaviour of the beam is governed by the stored-energy function

$$W_{int}(\boldsymbol{\Gamma}, \boldsymbol{K}) = \frac{1}{2}\boldsymbol{\Gamma}^{T} \cdot \boldsymbol{D}^{\Gamma} \cdot \boldsymbol{\Gamma} + \frac{1}{2}\boldsymbol{K}^{T} \cdot \boldsymbol{D}^{K} \cdot \boldsymbol{K} \tag{5.3.10}$$

with

$$\boldsymbol{D}^{\Gamma} = \begin{bmatrix} GA_1 & 0 & 0 \\ 0 & GA_2 & 0 \\ 0 & 0 & EA \end{bmatrix} \qquad \boldsymbol{D}^{K} = \begin{bmatrix} EI_1 & 0 & 0 \\ 0 & EI_2 & 0 \\ 0 & 0 & GJ \end{bmatrix} \tag{5.3.11}$$

Insertion into (5.3.8) yields

$$
\begin{aligned}
V_{int}^h(\boldsymbol{q}(t)) &= \frac{1}{2}\sum_{i=1}^{3} D_{ii}^\Gamma \underbrace{\int_0^L \left(\Gamma_i(\boldsymbol{q}^h(s,t))\right)^2 ds}_{:=} + D_{ii}^K \underbrace{\int_0^L \left(K_i(\boldsymbol{q}^h(s,t))\right)^2 ds}_{:=} \\
&= \frac{1}{2}\sum_{i=1}^{3} D_{ii}^\Gamma \qquad \Gamma_i^h(\boldsymbol{q}(t)) \qquad + D_{ii}^K \qquad K_i^h(\boldsymbol{q}(t)) \\
&= \sum_{i=1}^{3} W_{int}^i(\boldsymbol{\Gamma}^h(\boldsymbol{q}(t)),\boldsymbol{K}^h(\boldsymbol{q}(t)))
\end{aligned}
\tag{5.3.12}
$$

where

$$
W_{int}^i(\boldsymbol{\Gamma}^h(\boldsymbol{q}(t)),\boldsymbol{K}^h(\boldsymbol{q}(t))) = \frac{1}{2}\left[D_{ii}^\Gamma \Gamma_i^h(\boldsymbol{q}(t)) + D_{ii}^K K_i^h(\boldsymbol{q}(t))\right] \quad i = 1,2,3 \tag{5.3.13}
$$

The composition of (5.3.3), (5.3.5) and (5.3.8) yields the Hamiltonian for the semi-discrete beam $H^h(\boldsymbol{z}(t)) = T^h(\boldsymbol{p}(t)) + V^h(\boldsymbol{q}(t)) + P_H^h(\boldsymbol{z}(t))$ and the semi-discrete Hamiltonian system of equations, which has to be solved for $\boldsymbol{z}^\alpha(t)$, $\alpha = 1,\ldots,n_{node}$

$$
\begin{aligned}
\dot{\boldsymbol{q}}^\alpha(t) &= D_{\bar{\boldsymbol{p}}^\alpha} H^h(\boldsymbol{z}(t)) \\
\dot{\boldsymbol{p}}^\alpha(t) &= -D_{\bar{\boldsymbol{q}}^\alpha} H^h(\boldsymbol{z}(t)) \\
\boldsymbol{0} &= -D_{\boldsymbol{d}_3^\alpha} H^h(\boldsymbol{z}(t))
\end{aligned}
\tag{5.3.14}
$$

Remark 5.3.4 If the Lagrange multiplier method is used to enforce the constraints, the system (5.3.14) is supplemented by the constraint equations $\boldsymbol{g}_{int}(\boldsymbol{q}(t)) = \boldsymbol{0}$ introduced in (5.3.6), resulting in the constrained Hamilton's equations of the form (2.3.8).

5.3.1 Discrete strain measures – objectivity

Insertion of the interpolation (5.3.1) for $\boldsymbol{q}^h$ in (5.2.4) yields the discrete strain measures $\boldsymbol{\Gamma}(\boldsymbol{q}^h),\boldsymbol{K}(\boldsymbol{q}^h)$, which inherit the objectivity of the underlying geometrically exact beam theory. Consider superposed rigid body motion of the discrete beam configuration

$$
(\boldsymbol{\varphi}^\alpha)^\sharp = \boldsymbol{c} + \boldsymbol{Q}\cdot\boldsymbol{\varphi}^\alpha \qquad (\boldsymbol{d}_I^\alpha)^\sharp = \boldsymbol{Q}\cdot\boldsymbol{d}_I^\alpha \quad I = 1,2,3 \tag{5.3.15}
$$

with $\boldsymbol{c}(t) \in \mathbb{R}^3$ and $\boldsymbol{Q}(t) \in SO(3)$. Then for all $s \in [0,L]$ and $i = 1,2,3$ one gets

$$
\begin{aligned}
\Gamma_i((\boldsymbol{q}^h)^\sharp) &= \left((\boldsymbol{d}_i^h)^\sharp\right)^T\cdot(\boldsymbol{\varphi}_{,s}^h)^\sharp - \delta_{i3} \\
&= \sum_{\alpha,\beta=1}^{n_{node}} N_\alpha N_{\beta,s}(\boldsymbol{Q}\cdot\boldsymbol{d}_i^\alpha)^T\cdot(\boldsymbol{c} + \boldsymbol{Q}\cdot\boldsymbol{\varphi}^\beta) - \delta_{i3} \\
&= \sum_{\alpha,\beta=1}^{n_{node}} N_\alpha N_{\beta,s}\left(\boldsymbol{d}_i^\alpha\right)^T\cdot\boldsymbol{\varphi}^\beta - \delta_{i3}
\end{aligned}
\tag{5.3.16}
$$

due to the completeness of the Lagrangian shape functions $\displaystyle\sum_{\alpha=1}^{n_{node}} N_\alpha = 1$ implying $\displaystyle\sum_{\alpha=1}^{n_{node}} N_{\alpha,s}\boldsymbol{c} = 0$. Accordingly,

$$
\Gamma_i((\boldsymbol{q}^h)^\sharp) = \Gamma_i(\boldsymbol{q}^h) \qquad K_i((\boldsymbol{q}^h)^\sharp) = K_i(\boldsymbol{q}^h) \tag{5.3.17}
$$

and the discrete strain measures corresponding to the interpolation (5.3.1) are invariant with respect to superposed rigid body motion. This is in contrast to beam elements based on the interpolation of rotational degrees of freedom, see [Cris 99].

Further details on the only sketched proof of the objectivity of the discrete strain measures can be found in [Bets 02d].

5.4 Objective energy-momentum conserving time-stepping scheme

The objectivity of the strain measures relies on the fact that $\Gamma_i, K_i, i = 1, 2, 3$ are scalar-valued isotropic functions of the vector argument $\boldsymbol{q}$. Thus they do not depend on the full configuration vector $\boldsymbol{q}$, but on the scalar products of the vectors $\{\boldsymbol{\varphi}^\alpha, \boldsymbol{d}_1^\alpha, \boldsymbol{d}_2^\alpha, \boldsymbol{d}_3^\alpha, \boldsymbol{\varphi}^\beta, \boldsymbol{d}_1^\beta, \boldsymbol{d}_2^\beta, \boldsymbol{d}_3^\beta \,|\, \alpha, \beta = 1, \ldots, n_{node}\}$, which are invariant with respect to superposed rigid body motion. Consequently, V_{int} is an isotropic function. Detailed inspection of the kinetic energy of the discrete beam (5.3.3) and the extra function to enforce the constraints (5.3.5) shows that these parts of the Hamiltonian are rotationally invariant as well.

Remark 5.4.1 From (5.3.9), it can be seen that in Example 5.3.2 V_{ext}^h is invariant with respect to rotations about the gravitational axis only, whereas T^h, P^h and V_{int}^h are invariant under the action of the full Lie group $SO(3)$. For simplicity but without loss of generality, it is assumed from now on that V_{ext}^h is invariant under the action of all elements of $SO(3)$ as well, thus the composition $H^h(\boldsymbol{z}(t)) = T^h(\boldsymbol{p}(t)) + V^h(\boldsymbol{q}(t)) + P^h(\boldsymbol{z}(t))$ is also invariant under the action of $SO(3)$. Therewith Example 5.3.2 is excluded in the theoretical considerations.

These considerations suggest parametrising the entire isotropic Hamiltonian in the invariants of the Lie group $SO(3)$.

5.4.1 Invariance of the Hamiltonian

Assume that the semi-discrete Hamiltonian H^h is invariant under the action of the Lie group $SO(3)$, i.e.

$$H^h(\boldsymbol{z}) = H^h(\boldsymbol{Q} \circ \boldsymbol{z}) \quad \text{for all } \boldsymbol{Q} \in SO(3) \text{ and } \boldsymbol{z} \in \mathbb{R}^{21 n_{node}} \tag{5.4.1}$$

where $\boldsymbol{Q} \circ \boldsymbol{z}$ denotes the multiplication of each three-dimensional vector component of $\boldsymbol{z}$ by $\boldsymbol{Q}$, i.e.

$$\boldsymbol{Q} \circ \boldsymbol{z} = \begin{bmatrix} \boldsymbol{Q} \cdot \boldsymbol{\varphi}^1 \\ \vdots \\ \boldsymbol{Q} \cdot \boldsymbol{p}_2^{n_{node}} \end{bmatrix} \tag{5.4.2}$$

Then H^h is an isotropic, scalar valued function with vector arguments, hence by Cauchy's Representation Theorem (see e.g. [Antm 95]) H^h can be expressed in terms of the invariants

$$S(\boldsymbol{z}^1, \ldots, \boldsymbol{z}^{n_{node}}) = \left\{ (\boldsymbol{y}^\alpha)^T \cdot \boldsymbol{y}^\beta | 1 \leq \alpha \leq \beta \leq n_{node}, \boldsymbol{y}^\alpha \in \{\boldsymbol{\varphi}^\alpha, \boldsymbol{d}_1^\alpha, \boldsymbol{d}_2^\alpha, \boldsymbol{d}_3^\alpha, \boldsymbol{p}_\varphi^\alpha, \boldsymbol{p}_1^\alpha, \boldsymbol{p}_2^\alpha\} \right\} \tag{5.4.3}$$

S is the set of all possible scalar products of the three-dimensional vectors composing the phase vector $\boldsymbol{z}$ in (5.3.2) and contains $\frac{1}{2}(7n_{node} + 1)7n_{node}$ elements.

Remark 5.4.2 The elements of S are functionally dependent in the sense of Olver [Olve 86]. The Lie group $SO(3)$ operates semi-regularly on the $n = 21n_{node}$-dimensional phase space P with orbits of dimension $s = 3$. According to Theorem 2.17 in [Olve 86] there exist precisely $d = n - s = 21n_{node} - 3$ independent invariants $\pi_i : P \to \mathbb{R}$ composing the maximal set $\boldsymbol{\pi} = [\pi_1, \ldots, \pi_d]^T$. The invariants $\pi_1(\boldsymbol{z}), \ldots, \pi_d(\boldsymbol{z})$ are functionally independent if and only if the Jacobian $D\boldsymbol{\pi}(\boldsymbol{z}) \in \mathbb{R}^{d \times n}$ is of rank d for each $\boldsymbol{z} \in P$. Any other invariant $\pi_e, e > d$ of the group action does depend on the quotient space $P/SO(3) \cong \boldsymbol{\pi}(P)$, i.e. it is of the form $\pi_e(\boldsymbol{z}) = \pi_e(\pi_1(\boldsymbol{z}), \ldots, \pi_d(\boldsymbol{z}))$.

If a maximal set $\boldsymbol{\pi}$ of independent invariants can be found, then the Hamiltonian can be reduced to

$$\tilde{H}^h : \boldsymbol{\pi}(P) \to \mathbb{R} \quad \text{with} \quad \tilde{H}^h(\boldsymbol{\pi}(\boldsymbol{z})) = H^h(\boldsymbol{z}) \tag{5.4.4}$$

According to Proposition 2.2.9, the invariance of the Hamiltonian under the action of a Lie group G with Lie algebra $\mathfrak{g}$ leads to the temporal conservation of a momentum map $\boldsymbol{J} : P \to \mathfrak{g}^*$ along the solution of Hamilton's equations. Along the solution of the semi-discrete Hamiltonian system (5.3.14), a momentum map is conserved in the sense that $\sum_{\alpha=1}^{n_{node}} \boldsymbol{J}(\boldsymbol{z}^\alpha(t)) = \boldsymbol{c}$ for all $t \in [t_0, t_1]$ where $\boldsymbol{c} \in \mathbb{R}^3$ is constant. For $G = SO(3)$, the momentum map is the sum of the angular momentum at each node $\boldsymbol{J}(\boldsymbol{z}^\alpha) = \boldsymbol{q}^\alpha \times \boldsymbol{p}^\alpha$. The set of invariants S in (5.4.3) comprises the elements

$$
\begin{aligned}
&\pi_1^{\alpha\beta}(\boldsymbol{z}) = (\boldsymbol{\varphi}^\alpha)^T \cdot \boldsymbol{\varphi}^\beta && \pi_2^{\alpha\beta}(\boldsymbol{z}) = (\boldsymbol{d}_1^\alpha)^T \cdot \boldsymbol{d}_1^\beta && \pi_3^{\alpha\beta}(\boldsymbol{z}) = (\boldsymbol{d}_2^\alpha)^T \cdot \boldsymbol{d}_2^\beta \\
&\pi_4^{\alpha\beta}(\boldsymbol{z}) = (\boldsymbol{d}_3^\alpha)^T \cdot \boldsymbol{d}_3^\beta && \pi_5^{\alpha\beta}(\boldsymbol{z}) = (\boldsymbol{p}_\varphi^\alpha)^T \cdot \boldsymbol{p}_\varphi^\beta && \pi_6^{\alpha\beta}(\boldsymbol{z}) = (\boldsymbol{p}_1^\alpha)^T \cdot \boldsymbol{p}_1^\beta \\
&\pi_7^{\alpha\beta}(\boldsymbol{z}) = (\boldsymbol{p}_2^\alpha)^T \cdot \boldsymbol{p}_2^\beta && \pi_8^{\alpha\beta}(\boldsymbol{z}) = (\boldsymbol{\varphi}^\alpha)^T \cdot \boldsymbol{d}_1^\beta && \pi_9^{\alpha\beta}(\boldsymbol{z}) = (\boldsymbol{\varphi}^\alpha)^T \cdot \boldsymbol{d}_2^\beta \\
&\pi_{10}^{\alpha\beta}(\boldsymbol{z}) = (\boldsymbol{\varphi}^\alpha)^T \cdot \boldsymbol{d}_3^\beta && \pi_{11}^{\alpha\beta}(\boldsymbol{z}) = (\boldsymbol{d}_1^\alpha)^T \cdot \boldsymbol{d}_2^\beta && \pi_{12}^{\alpha\beta}(\boldsymbol{z}) = (\boldsymbol{d}_3^\alpha)^T \cdot \boldsymbol{d}_1^\beta \\
&\pi_{13}^{\alpha\beta}(\boldsymbol{z}) = (\boldsymbol{d}_2^\alpha)^T \cdot \boldsymbol{d}_3^\beta && \pi_{14}^{\alpha\beta}(\boldsymbol{z}) = (\boldsymbol{p}_\varphi^\alpha)^T \cdot \boldsymbol{p}_1^\beta && \pi_{15}^{\alpha\beta}(\boldsymbol{z}) = (\boldsymbol{p}_\varphi^\alpha)^T \cdot \boldsymbol{p}_2^\beta \\
&\pi_{16}^{\alpha\beta}(\boldsymbol{z}) = (\boldsymbol{p}_1^\alpha)^T \cdot \boldsymbol{p}_2^\beta && \pi_{17}^{\alpha\beta}(\boldsymbol{z}) = (\boldsymbol{\varphi}^\alpha)^T \cdot \boldsymbol{p}_\varphi^\beta && \pi_{18}^{\alpha\beta}(\boldsymbol{z}) = (\boldsymbol{\varphi}^\alpha)^T \cdot \boldsymbol{p}_1^\beta \\
&\pi_{19}^{\alpha\beta}(\boldsymbol{z}) = (\boldsymbol{\varphi}^\alpha)^T \cdot \boldsymbol{p}_2^\beta && \pi_{20}^{\alpha\beta}(\boldsymbol{z}) = (\boldsymbol{d}_1^\alpha)^T \cdot \boldsymbol{p}_\varphi^\beta && \pi_{21}^{\alpha\beta}(\boldsymbol{z}) = (\boldsymbol{d}_1^\alpha)^T \cdot \boldsymbol{p}_1^\beta \\
&\pi_{22}^{\alpha\beta}(\boldsymbol{z}) = (\boldsymbol{d}_1^\alpha)^T \cdot \boldsymbol{p}_2^\beta && \pi_{23}^{\alpha\beta}(\boldsymbol{z}) = (\boldsymbol{d}_2^\alpha)^T \cdot \boldsymbol{p}_\varphi^\beta && \pi_{24}^{\alpha\beta}(\boldsymbol{z}) = (\boldsymbol{d}_2^\alpha)^T \cdot \boldsymbol{p}_1^\beta \\
&\pi_{25}^{\alpha\beta}(\boldsymbol{z}) = (\boldsymbol{d}_2^\alpha)^T \cdot \boldsymbol{p}_2^\beta && \pi_{26}^{\alpha\beta}(\boldsymbol{z}) = (\boldsymbol{d}_3^\alpha)^T \cdot \boldsymbol{p}_\varphi^\beta && \pi_{27}^{\alpha\beta}(\boldsymbol{z}) = (\boldsymbol{d}_3^\alpha)^T \cdot \boldsymbol{p}_1^\beta \\
&\pi_{28}^{\alpha\beta}(\boldsymbol{z}) = (\boldsymbol{d}_3^\alpha)^T \cdot \boldsymbol{p}_2^\beta
\end{aligned}
\tag{5.4.5}
$$

$\alpha, \beta = 1, \ldots, n_{node}$. According to Theorem 2.17 in [Olve 86] (see Remark 5.4.2), one can choose $d = 21n_{node} - 3$ functionally independent invariants of those given in (5.4.5), generating the maximal set $\boldsymbol{\pi}$ in which the Hamiltonian can be parametrised.

5.4.2 Fully-discrete Hamiltonian system for the beam in terms of invariants

According to the spatial finite element discretisation (5.3.1), the phase space variable (5.3.2) at time t_n is given by

$$z_n^h(s) = z^h(s, t_n) = \sum_{\alpha=1}^{n_{node}} N_\alpha(s) z_n^\alpha \quad \in \mathbb{R}^{21} \quad n \in \mathbb{N} \tag{5.4.6}$$

with $z_n^\alpha = z^\alpha(t_n)$, $\alpha = 1 \ldots, n_{node}$.

Using (5.3.3), (5.4.5) and $\mathsf{t}_1 = 5, \mathsf{t}_2 = 6, \mathsf{t}_3 = 7$, the kinetic energy at time t_n can be written in the form

$$
\begin{aligned}
\tilde{T}^h(\boldsymbol{\pi}(z_n)) &= \sum_{i=1}^{3} \sum_{\alpha,\beta=1}^{n_{node}} \tilde{T}_i^h(\pi_{\mathsf{t}_i}^{\alpha\beta}(z_n)) \\
&= \frac{1}{2} \sum_{\alpha,\beta=1}^{n_{node}} (M_{\alpha\beta})^{-1} \pi_5^{\alpha\beta}(z_n) + (M_{\alpha\beta}^1)^{-1} \pi_6^{\alpha\beta}(z_n) + (M_{\alpha\beta}^2)^{-1} \pi_7^{\alpha\beta}(z_n)
\end{aligned}
\tag{5.4.7}
$$

where $M_{\alpha\beta}, M_{\alpha\beta}^1, M_{\alpha\beta}^2$ are the entries of the consistent mass matrix (5.3.4), see Remark 5.3.1.

Inspection of the internal constraints (4.3.3) obviously shows on which invariants in (5.4.5) the constraints at the node α do depend on. With $\mathsf{p}_1 = 2, \mathsf{p}_2 = 3, \mathsf{p}_3 = 4, \mathsf{p}_4 = 11$, $\mathsf{p}_5 = 12, \mathsf{p}_6 = 13$ the function to treat the constraints (5.3.5) at time t_n can be written as

$$\tilde{P}_H^h(\boldsymbol{\pi}(z_n)) = \sum_{\alpha=1}^{n_{node}} v^\alpha(t_n) \boldsymbol{R} \left((\tilde{g}_{int}^\alpha)_1 (\pi_{\mathsf{p}_1}^{\alpha\alpha}(z_n)), \ldots, (\tilde{g}_{int}^\alpha)_6 (\pi_{\mathsf{p}_6}^{\alpha\alpha}(z_n)) \right) \tag{5.4.8}$$

With $\gamma_1 = 8, \gamma_2 = 9, \gamma_3 = 10, \mathsf{k}_1 = 13, \mathsf{k}_2 = 12, \mathsf{k}_3 = 11$ the objective strain measures $\boldsymbol{\Gamma}(q^h), \boldsymbol{K}(q^h)$ at time t_n take the form

$$
\begin{aligned}
\tilde{\Gamma}_i(\boldsymbol{\pi}(z_n^h)) &= \sum_{\alpha,\beta=1}^{n_{node}} N_\alpha(s) N_\beta'(s) \pi_{\Gamma_i}^{\alpha\beta}(z_n) - \delta_{i3} && i = 1,2,3 \\
\tilde{K}_i(\boldsymbol{\pi}(z_n^h)) &= \sum_{\alpha,\beta=1}^{n_{node}} N_\alpha(s) N_\beta'(s) \left[\pi_{\mathsf{k}_i}^{\alpha\beta}(z_n) - \pi_{\mathsf{k}_i}^{\alpha\beta}(z_0) \right] && i = 1,2,3
\end{aligned}
\tag{5.4.9}
$$

Assuming that also the external energy density function is invariant under the action of $SO(3)$ (see Remark 5.4.1), i.e. $W_{ext}(z_n^h) = \tilde{W}_{ext}(\boldsymbol{\pi}(z_n^h))$, the potential energy (5.3.8) at time t_n reads

$$\tilde{V}^h(\boldsymbol{\pi}(z_n)) = \int_0^L W_{int}(\tilde{\boldsymbol{\Gamma}}(\boldsymbol{\pi}(z_n^h)), \tilde{\boldsymbol{K}}(\boldsymbol{\pi}(z_n^h))) \, ds + \int_0^L \tilde{W}_{ext}(\boldsymbol{\pi}(z_n^h)) \, ds \tag{5.4.10}$$

Of course, the integrals transform to sums over the nodes due to the spatial discretisation (5.4.6).

Summarising, the $SO(3)$-invariant Hamiltonian of the beam at time t_n is of the form

$$H^h(z_n) = \tilde{H}^h(\boldsymbol{\pi}(z_n)) = \tilde{T}^h(\boldsymbol{\pi}(z_n)) + \tilde{V}^h(\boldsymbol{\pi}(z_n)) + \tilde{P}_H^h(\boldsymbol{\pi}(z_n)) \tag{5.4.11}$$

Using the partial G-equivariant discrete derivative (see Definitions 3.1.4 and 3.1.7) of the Hamiltonian in (5.4.11), one arrives at the fully-discrete constrained Hamiltonian equations (3.2.2) for the dynamics of the geometrically exact beam, which have to be solved for $\boldsymbol{z}_{n+1}^\alpha = [\boldsymbol{q}_{n+1}^\alpha, \bar{\boldsymbol{p}}_{n+1}^\alpha], \alpha = 1, \ldots, n_{node}$

$$
\begin{aligned}
\bar{\boldsymbol{q}}_{n+1}^\alpha - \bar{\boldsymbol{q}}_n^\alpha &= h\,\mathsf{D}_{\bar{\boldsymbol{p}}^\alpha}^G H^h(\boldsymbol{z}_n, \boldsymbol{z}_{n+1}) \\
\bar{\boldsymbol{p}}_{n+1}^\alpha - \bar{\boldsymbol{p}}_n^\alpha &= -h\mathsf{D}_{\bar{\boldsymbol{q}}^\alpha}^G H^h(\boldsymbol{z}_n, \boldsymbol{z}_{n+1}) \\
\boldsymbol{0} &= -h\mathsf{D}_{\boldsymbol{d}_3^\alpha}^G H^h(\boldsymbol{z}_n, \boldsymbol{z}_{n+1})
\end{aligned}
\tag{5.4.12}
$$

Remark 5.4.3 If the Lagrange multiplier method is used to enforce the constraints, the $21 n_{node}$-dimensional system (5.4.12) is supplemented by the constraint equations $\boldsymbol{g}_{int}(\boldsymbol{q}(t)) = \boldsymbol{0}$ introduced in (5.3.6), resulting in the $27 n_{node}$-dimensional constrained Hamilton's equations of the form (3.2.3).

5.4.3 Overview

Table 5.1 gives an overview over the phase vector, the Hamiltonian and Hamilton's equations corresponding to the continuous, the semi-discrete and the fully-discrete case respectively.

Table 5.1: Overview over the phase vector, the Hamiltonian and Hamilton's equations corresponding to the continuous, the semi-discrete and the fully-discrete case respectively.

	phase vector	Hamiltonian	H. e.
continuous	$\boldsymbol{z}(s,t) = [\boldsymbol{q}(s,t), \bar{\boldsymbol{p}}(s,t)] \in \mathbb{R}^{21} (5.1.2)$	$\begin{aligned} H(\boldsymbol{z}) &= \\ T(\boldsymbol{p}) &+ V(\boldsymbol{q}) + P_H(\boldsymbol{z}) \\ (5.2.1) & \quad (5.2.3) \quad (5.2.6) \end{aligned}$	(5.2.7)
semi-discrete	$\boldsymbol{z}^h(s,t) = \sum_{\alpha=1}^{n_{node}} N_\alpha(s)\boldsymbol{z}^\alpha(t) \in \mathbb{R}^{21} (5.3.1)$ $\boldsymbol{z}^\alpha(t) = [\boldsymbol{q}^\alpha(t), \bar{\boldsymbol{p}}^\alpha(t)] \in \mathbb{R}^{21}$ $\boldsymbol{z}(t) = [\boldsymbol{z}^1(t), \dots, \boldsymbol{z}^{n_{node}}(t)] \in \mathbb{R}^{21 n_{node}}$	$\begin{aligned} H(\boldsymbol{z}^h) &= H^h(\boldsymbol{z}) = \\ T^h(\boldsymbol{p}) &+ V^h(\boldsymbol{q}) + P_H^h(\boldsymbol{z}) \\ (5.3.3) & \quad (5.3.8) \quad (5.3.5) \end{aligned}$	(5.3.14)
fully-discrete	$\boldsymbol{z}_n^h(s) = \sum_{\alpha=1}^{n_{node}} N_\alpha(s)\boldsymbol{z}_n^\alpha \in \mathbb{R}^{21} (5.4.6)$ $\boldsymbol{z}_n^\alpha = [\boldsymbol{q}_n^\alpha, \bar{\boldsymbol{p}}_n^\alpha] \in \mathbb{R}^{21}$ $\boldsymbol{z}_n = [\boldsymbol{z}_n^1, \dots, \boldsymbol{z}_n^{n_{node}}] \in \mathbb{R}^{21 n_{node}}$	$\begin{aligned} H(\boldsymbol{z}_n^h) &= \tilde{H}^h(\boldsymbol{\pi}(\boldsymbol{z}_n)) = \\ \tilde{T}^h(\boldsymbol{\pi}(\boldsymbol{z}_n)) &+ \tilde{V}^h(\boldsymbol{\pi}(\boldsymbol{z}_n)) + \\ (5.4.7) & \quad (5.4.10) \\ \tilde{P}_H^h(\boldsymbol{\pi}(\boldsymbol{z}_n)) & \\ (5.4.8) & \end{aligned}$	(5.4.12)

5.4.4 Time-stepping schemes for the beam dynamics

In the sequel, the actual fully-discrete Hamiltonian equations for the dynamics of the geometrically exact beam are deduced for the different methods to enforce the constraints. They constitute nonlinear, objective, energy-momentum conserving one-step schemes. According to (5.4.12), the partial G-equivariant discrete derivatives of T, V and P have to be calculated. Therefore formulas (3.1.3) and (3.1.4), given in Example 3.1.6, are applied. For the kinetic energy (5.4.7) one obtains

$$\mathsf{D}_{\tilde{\boldsymbol{p}}^A}^G T^h(\boldsymbol{z}_n, \boldsymbol{z}_{n+1}) = \sum_{i=1}^{3} \sum_{\alpha,\beta=1}^{n_{node}} \mathsf{D}\tilde{T}_i^h(\pi_{\mathsf{t}_i}^{\alpha\beta}(\boldsymbol{z}_n), \pi_{\mathsf{t}_i}^{\alpha\beta}(\boldsymbol{z}_{n+1})) \circ D\pi_{\mathsf{t}_i}^{\alpha\beta}(\boldsymbol{z}_{n+\frac{1}{2}}) \tag{5.4.13}$$

Since $\tilde{T}_i^h : \mathbb{R}_+ \to \mathbb{R}$, using (3.1.3) yields

$$\mathsf{D}\tilde{T}_i^h(\pi_{\mathsf{t}_i}^{\alpha\beta}(\boldsymbol{z}_n), \pi_{\mathsf{t}_i}^{\alpha\beta}(\boldsymbol{z}_{n+1})) = \frac{\tilde{T}_i^h\left(\pi_{\mathsf{t}_i}^{\alpha\beta}(\boldsymbol{z}_{n+1})\right) - \tilde{T}_i^h\left(\pi_{\mathsf{t}_i}^{\alpha\beta}(\boldsymbol{z}_n)\right)}{\pi_{\mathsf{t}_i}^{\alpha\beta}(\boldsymbol{z}_{n+1}) - \pi_{\mathsf{t}_i}^{\alpha\beta}(\boldsymbol{z}_n)} =: S_{\tilde{T}_i}^{\alpha\beta} \tag{5.4.14}$$

for $i = 1, 2, 3$. Then it follows from (5.4.7) that

$$S_{\tilde{T}_1}^{\alpha\beta} = \frac{1}{2} M_{\alpha\beta}^{-1} \qquad S_{\tilde{T}_2}^{\alpha\beta} = \frac{1}{2}(M_{\alpha\beta}^1)^{-1} \qquad S_{\tilde{T}_3}^{\alpha\beta} = \frac{1}{2}(M_{\alpha\beta}^2)^{-1} \tag{5.4.15}$$

Because of the parametrisation of the Hamiltonian and particularly the stored energy in the quadratic invariants and the special strain measures (5.2.4) of the beam theory in use, an energy-momentum conserving time-stepping scheme is obtained by application of the G-equivariant discrete derivative in Example 3.1.6 to the stored energy with $f = W_{int} \circ (\tilde{\boldsymbol{\varGamma}}, \tilde{\boldsymbol{K}})$ and $\boldsymbol{\pi}$ from (5.4.5). This is equivalent to the application of the G-equivariant discrete derivative to the stored energy with $f = W_{int}$ and $\tilde{\boldsymbol{\pi}} = (\tilde{\boldsymbol{\varGamma}}, \tilde{\boldsymbol{K}}) \circ \boldsymbol{\pi}$, see Appendix E.

Remark 5.4.4 A special modification in the temporal discretisation of the stored energy terms to obtain an energy-conserving integrator (e.g. cG(1)-method in connection with the assumed strain modification in [Bets 01a, Simo 86a] or interpolation of the strains at different times instead of evaluation of the strains at the temporally interpolated configuration in the case of nonlinear elasticity in [Simo 92a, Gonz 00]) is unnecessary here.

For many methods to treat the constraints (e.g. Lagrange multiplier method, penalty method, augmented Lagrange method), (5.4.8) can be transformed to

$$\tilde{P}_H^h(\boldsymbol{\pi}(\boldsymbol{z}_n)) = \sum_{i=1}^{6} \sum_{\alpha=1}^{n_{node}} \tilde{P}_i^h(\pi_{\mathsf{p}_i}^{\alpha\alpha}(\boldsymbol{z}_n)) \tag{5.4.16}$$

and the G-equivariant discrete derivative can be calculated along the lines of (5.4.13), (5.4.14). For the three methods mentioned, the scalars $S_{\tilde{P}_i}^\alpha, i = 1, \dots, 6$ will be specified in the following subsections accordingly.

Lagrange multiplier method

Using the Lagrange multiplier method, the function representing the treatment of the constraints takes the form $P_H(\boldsymbol{z}) = P_{\mathsf{Lag}}(\boldsymbol{g}_{int}(\boldsymbol{q})) = \boldsymbol{g}_{int}^T(\boldsymbol{q}) \cdot \boldsymbol{\lambda}$ with the Lagrange multiplier $\boldsymbol{\lambda} \in \mathbb{R}^6$. Thus the contribution of the constraints to the Hamiltonian in (5.2.6) can be calculated as

$$\boldsymbol{v}(s,t) = \boldsymbol{\lambda}(s,t) \qquad \boldsymbol{R}(\boldsymbol{g}_{int}(\boldsymbol{q}(s,t))) = \boldsymbol{g}_{int}(\boldsymbol{q}(s,t)) \tag{5.4.17}$$

and insertion of the interpolation (5.3.1) yields corresponding to (5.3.5)

$$P_{\mathsf{Lag}}^h(\boldsymbol{g}_{int}(\boldsymbol{q}(t))) = \sum_{\alpha=1}^{n_{node}} (\boldsymbol{g}_{int}^\alpha)^T (\boldsymbol{q}^\alpha(t)) \cdot \boldsymbol{\lambda}^\alpha(t) \tag{5.4.18}$$

with the nodal Lagrange multipliers $\boldsymbol{\lambda}^\alpha \in \mathbb{R}^6$. (5.4.18) can be written in terms of the invariants at time t_n as follows

$$\tilde{P}_{\mathsf{Lag}}^h(\boldsymbol{\pi}(\boldsymbol{z}_n)) = \sum_{i=1}^{6} \sum_{\alpha=1}^{n_{node}} \lambda_i^\alpha(t_n) (\tilde{g}_{int}^\alpha)_i (\pi_{\mathsf{p}_i}^{\alpha\alpha}(\boldsymbol{z}_n)) \tag{5.4.19}$$

In the G-equivariant discrete derivative $\mathsf{D}^G P_{\mathsf{Lag}}^h$, the scalars corresponding to (5.4.14) take the values

$$S_{\tilde{P}_{\mathsf{Lag}_i}}^\alpha = \frac{1}{2}\lambda_i^\alpha \quad i = 1, 2, 3 \quad \alpha = 1, \ldots, n_{node}$$

$$\tag{5.4.20}$$

$$S_{\tilde{P}_{\mathsf{Lag}_i}}^\alpha = \lambda_i^\alpha \quad i = 4, 5, 6 \quad \alpha = 1, \ldots, n_{node}$$

Corresponding to the treatment of the internal constraints for a rigid body in Section 4.3, the gradients of the invariants $\pi_{\mathsf{p}_i}^{\alpha\alpha}$ at the nodes coincide with rows of the midpoint evaluation $\boldsymbol{G}_{int}^\alpha(\boldsymbol{q}_{n+\frac{1}{2}}^\alpha)$ of the constraint Jacobian for the rigid body in (4.3.4).

Remark 5.4.5 The use of Dirac deltas as shape functions for $\boldsymbol{v} = \boldsymbol{\lambda}$ in (5.3.1) relates the multipliers directly to the spatial nodes. As explained in Section 3.2.1, the multipliers are discontinuous across time elements, particularly the multipliers are constant at each spatial node during the time interval $[t_n, t_{n+1})$ and jump at the time nodes. For this reason all multipliers appearing in the time-stepping scheme are evaluated at the time node t_{n+1} and their time dependence is not indicated in (5.4.20).

Penalty method

The penalty potential being in use here is composed by a spatially and temporally constant penalty parameter $\mu \in \mathbb{R}$ and the squared norm of the constraints

$$v(s,t) = \mu \qquad R(\boldsymbol{g}_{int}(\boldsymbol{q}(s,t))) = \left\| \boldsymbol{g}_{int}(\boldsymbol{q}(s,t)) \right\|^2 \tag{5.4.21}$$

The same steps as in the previous paragraph for the Lagrange multiplier method lead to

$$P_{\mathsf{Pen}}^h(\boldsymbol{g}_{int}(\boldsymbol{q}(t))) = \sum_{\alpha=1}^{n_{node}} \mu \left\| \boldsymbol{g}_{int}^\alpha(\boldsymbol{q}^\alpha(t)) \right\|^2 \tag{5.4.22}$$

and finally

$$\tilde{P}^h_{\mathsf{Pen}}(\boldsymbol{\pi}(\boldsymbol{z}_n)) = \sum_{i=1}^{6} \sum_{\alpha=1}^{n_{node}} \mu\left((\tilde{g}^\alpha_{int})_i\left(\pi^{\alpha\alpha}_{\mathsf{p}_i}(\boldsymbol{z}_n)\right)\right)^2 \tag{5.4.23}$$

The scalars (corresponding to (5.4.14)) arising in $\mathsf{D}^G P^h_{\mathsf{Pen}}$ result in

$$S^\alpha_{\tilde{P}_{\mathsf{Pen}_i}} = \frac{\mu}{4}\left[\pi^{\alpha\alpha}_{\mathsf{p}_i}(\boldsymbol{z}_{n+1}) + \pi^{\alpha\alpha}_{\mathsf{p}_i}(\boldsymbol{z}_n) - 2\right] \quad i = 1,2,3 \quad \alpha = 1,\ldots,n_{node}$$

$$S^\alpha_{\tilde{P}_{\mathsf{Pen}_i}} = \mu\left[\pi^{\alpha\alpha}_{\mathsf{p}_i}(\boldsymbol{z}_{n+1}) + \pi^{\alpha\alpha}_{\mathsf{p}_i}(\boldsymbol{z}_n)\right] \qquad i = 4,5,6 \quad \alpha = 1,\ldots,n_{node} \tag{5.4.24}$$

Augmented Lagrange method

In the augmented Lagrange method the function to treat the constraints is the sum of those just described

$$\boldsymbol{v}(s,t) = \left[\begin{array}{c} \boldsymbol{\lambda}^k(s,t) \\ \mu \end{array}\right] \qquad \boldsymbol{R}(\boldsymbol{g}_{int}(\boldsymbol{q}^k(s,t))) = \left[\begin{array}{c} \boldsymbol{g}_{int}(\boldsymbol{q}^k(s,t)) \\ \left\|\boldsymbol{g}_{int}(\boldsymbol{q}^k(s,t))\right\|^2 \end{array}\right] \tag{5.4.25}$$

Therewith, it ensues

$$P^h_{\mathsf{Aug}}(\boldsymbol{g}_{int}(\boldsymbol{q}^k(t))) = \sum_{\alpha=1}^{n_{node}} (\boldsymbol{g}^\alpha_{int})^T \left(\boldsymbol{q}^{\alpha,k}(t)\right) \cdot \boldsymbol{\lambda}^{\alpha,k}(t) + \mu\left\|\boldsymbol{g}^\alpha_{int}(\boldsymbol{q}^{\alpha,k}(t))\right\|^2 \tag{5.4.26}$$

and finally

$$\tilde{P}^h_{\mathsf{Aug}}(\boldsymbol{\pi}(\boldsymbol{z}^k_n)) = \sum_{i=1}^{6} \sum_{\alpha=1}^{n_{node}} \lambda^{\alpha,k}_i(t_n)\left(\tilde{g}^\alpha_{int}\right)_i\left(\pi^{\alpha\alpha}_{\mathsf{p}_i}(\boldsymbol{z}^k_n)\right) + \mu\left((\tilde{g}^\alpha_{int})_i\left(\pi^{\alpha\alpha}_{\mathsf{p}_i}(\boldsymbol{z}_n)\right)\right)^2$$

$$\boldsymbol{\lambda}^{\alpha,0}(t_0) = \boldsymbol{0} \qquad \boldsymbol{\lambda}^{\alpha,0}(t_n) = \boldsymbol{\lambda}^{\alpha,k_{max}}(t_{n-1}) \tag{5.4.27}$$

$$\boldsymbol{\lambda}^{\alpha,k+1}(t_n) = \boldsymbol{\lambda}^{\alpha,k}(t_n) + \mu\tilde{\boldsymbol{g}}^\alpha_{int}(\pi^{\alpha\alpha}_{\mathsf{p}_1}(\boldsymbol{z}^k_n),\ldots,\pi^{\alpha\alpha}_{\mathsf{p}_6}(\boldsymbol{z}^k_n)) \quad \alpha = 1,\ldots,n_{node}$$

Accordingly, the scalars corresponding to (5.4.14) in $\mathsf{D}^G P^h_{\mathsf{Aug}}$ are composed by

$$S^{\alpha,k}_{\tilde{P}_{\mathsf{Aug}_i}} = \frac{1}{2}\lambda^{\alpha,k}_i + \frac{\mu}{4}\left[\pi^{\alpha\alpha}_{\mathsf{p}_i}(\boldsymbol{z}^k_{n+1}) + \pi^{\alpha\alpha}_{\mathsf{p}_i}(\boldsymbol{z}_n) - 2\right] \quad i = 1,2,3 \quad \alpha = 1,\ldots,n_{node}$$

$$S^{\alpha,k}_{\tilde{P}_{\mathsf{Aug}_i}} = \lambda^{\alpha,k}_i + \mu\left[\pi^{\alpha\alpha}_{\mathsf{p}_i}(\boldsymbol{z}^k_{n+1}) + \pi^{\alpha\alpha}_{\mathsf{p}_i}(\boldsymbol{z}_n)\right] \qquad i = 4,5,6 \quad \alpha = 1,\ldots,n_{node} \tag{5.4.28}$$

Discrete null space method with nodal reparametrisation

The description of the spatially discretised beam in terms of the phase vector given in (5.3.2) is a generalisation of that of rigid bodies in (4.3.2) and (4.3.9), which can be considered as a 'one-node structure'. The independent generalised velocities of the semi-discrete beam are given by its twist

$$\boldsymbol{t} = \left[\begin{array}{c} \boldsymbol{t}^1 \\ \vdots \\ \boldsymbol{t}^{n_{node}} \end{array}\right] \in \mathbb{R}^{6n_{node}} \tag{5.4.29}$$

where, analogous to (4.3.17), the twist of the α-th node $\boldsymbol{t}^\alpha \in \mathbb{R}^6$ reads

$$\boldsymbol{t}^\alpha = \left[\begin{array}{c} \dot{\boldsymbol{\varphi}}^\alpha \\ \boldsymbol{\omega}^\alpha \end{array} \right] \tag{5.4.30}$$

comprising the nodal translational velocity $\dot{\boldsymbol{\varphi}}^\alpha \in \mathbb{R}^3$ and the nodal angular velocity $\boldsymbol{\omega}^\alpha \in \mathbb{R}^3$. Now the redundant velocities $\dot{\boldsymbol{q}} \in \mathbb{R}^{12n_{node}}$ of the semi-discrete beam may be expressed as $\dot{\boldsymbol{q}} = \boldsymbol{P}_{int}(\boldsymbol{q}) \cdot \boldsymbol{t}$ where the $12n_{node} \times 6n_{node}$ internal null space matrix $\boldsymbol{P}_{int}(\boldsymbol{q})$ is given by

$$\boldsymbol{P}_{int}(\boldsymbol{q}) = \left[\begin{array}{cccc} \boldsymbol{P}_{int}^1(\boldsymbol{q}^1) & \boldsymbol{0} & \cdots & \boldsymbol{0} \\ \boldsymbol{0} & \boldsymbol{P}_{int}^2(\boldsymbol{q}^2) & \cdots & \boldsymbol{0} \\ \vdots & \vdots & \ddots & \vdots \\ \boldsymbol{0} & \boldsymbol{0} & \cdots & \boldsymbol{P}_{int}^{n_{node}}(\boldsymbol{q}^{n_{node}}) \end{array} \right] \tag{5.4.31}$$

and $\boldsymbol{P}_{int}^\alpha(\boldsymbol{q}^\alpha)$ is the null space matrix associated with the α-th node, which with regard to (4.3.19) reads

$$\boldsymbol{P}_{int}^\alpha(\boldsymbol{q}^\alpha) = \left[\begin{array}{cc} \boldsymbol{I} & \boldsymbol{0} \\ \boldsymbol{0} & -\widehat{\boldsymbol{d}_1^\alpha} \\ \boldsymbol{0} & -\widehat{\boldsymbol{d}_2^\alpha} \\ \boldsymbol{0} & -\widehat{\boldsymbol{d}_3^\alpha} \end{array} \right] \tag{5.4.32}$$

Remark 5.4.6 (Relation to kinematic chains) From the treatment of simple kinematic chains in Section 6.2.1 it will become clear, that a spatially discretised beam can be interpreted as a chain of rigid bodies for which the interconnections are prescribed by the connectivity of the spatial finite element method, see e.g. [Hugh 00].

In analogy to the treatment of rigid bodies by the discrete null space method in Section 4.3.4, assembly of the nodal discrete null space matrices $\mathbf{P}_{int}^\alpha(\boldsymbol{q}_n^\alpha, \boldsymbol{q}_{n+1}^\alpha) = \boldsymbol{P}_{int}^\alpha(\boldsymbol{q}_{n+\frac{1}{2}}^\alpha)$ given by the midpoint evaluation of (5.4.32), yields in a straightforward way the discrete null space matrix $\mathbf{P}_{int}(\boldsymbol{q}_n, \boldsymbol{q}_{n+1}) = \boldsymbol{P}_{int}(\boldsymbol{q}_{n+\frac{1}{2}})$ for the semi-discrete beam. Premultiplication of $(5.4.12)_{2,3}$ by its transposed and insertion of $\bar{\boldsymbol{p}}_{n+1}$ from $(5.4.12)_1$ into $(5.4.12)_{2,3}$ reduces its dimension to $6n_{node}$.

Analogous to the reparametrisation of the free rigid body's new configuration at time t_{n+1} in (4.3.31), the configuration of the semi-discrete beam can be expressed in terms of the incremental unknowns

$$\boldsymbol{u} = \left[\begin{array}{c} \boldsymbol{u}^1 \\ \vdots \\ \boldsymbol{u}^{n_{node}} \end{array} \right] \in \mathbb{R}^{6n_{node}} \qquad \boldsymbol{u}^\alpha = (\boldsymbol{u}_\varphi^\alpha, \boldsymbol{\theta}^\alpha) \in U^\alpha \subset \mathbb{R}^3 \times \mathbb{R}^3 \tag{5.4.33}$$

characterising the nodal incremental displacement $\boldsymbol{u}_\varphi^\alpha$ and nodal incremental rotation $\boldsymbol{\theta}^\alpha$ in $[t_n, t_{n+1}]$, respectively. Accordingly, in the present case the nodal reparametrisation introduced in (3.2.42) assumes the form

$$\boldsymbol{q}_{n+1} = \boldsymbol{F}_{q_n}(\boldsymbol{u}) \in Q = \mathbb{R}^{3n_{node}} \times (SO(3))^{n_{node}} \subset \mathbb{R}^{3n_{node}} \times \mathbb{R}^{9n_{node}} \tag{5.4.34}$$

with

$$\boldsymbol{q}_{n+1}^{\alpha} = \boldsymbol{F}_{q_n^{\alpha}}^{\alpha}(\boldsymbol{u}^{\alpha}) = \begin{bmatrix} \boldsymbol{\varphi}_n^{\alpha} + \boldsymbol{u}_{\varphi}^{\alpha} \\ \exp(\widehat{\boldsymbol{\theta}^{\alpha}}) \cdot (\boldsymbol{d}_1^{\alpha})_n \\ \exp(\widehat{\boldsymbol{\theta}^{\alpha}}) \cdot (\boldsymbol{d}_2^{\alpha})_n \\ \exp(\widehat{\boldsymbol{\theta}^{\alpha}}) \cdot (\boldsymbol{d}_3^{\alpha})_n \end{bmatrix} \qquad \alpha = 1, \ldots, n_{node} \qquad (5.4.35)$$

5.5 Numerical example: beam with concentrated masses
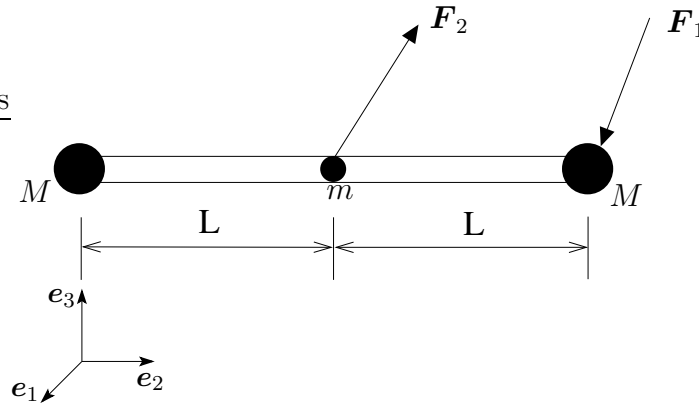
Figure 5.3: Initial configuration of the beam with concentrated masses.

The following example represents a three-dimensional extension of the plane version previously dealt with in [Bott 02a, Bets 03]. The results documented in these works could be recalculated using the present formulation. However, a three-dimensional loading is chosen here to demonstrate the performance of the present formulation in a general setting. The initial configuration of a beam with concentrated masses can be seen in Figure 5.3. For this problem the following parameters have been used: half-length $L = 1$, concentrated masses $M = 10$ and $m = 1$, mass density per reference length $A_\rho = 0.27$, mass moment of inertia of the cross-section $M_\rho = 9 \cdot 10^{-8}$, beam stiffness parameters $EI = 0.16$, $EA = 4.8 \cdot 10^5$, $GJ = 0.1230769$ and $GA = 1.84615 \cdot 10^5$. The hyperelastic material behaviour of the beams is specified in Example 5.3.3. The temporally bounded external loading has the form

$$\boldsymbol{F}_\kappa(t) = f(t)\boldsymbol{P}_\kappa \qquad \begin{array}{rcl} \boldsymbol{P}_1 & = & 1.3\boldsymbol{e}_1 + 1.0\boldsymbol{e}_2 + 0.8\boldsymbol{e}_3 \\ \boldsymbol{P}_2 & = & -1.2\boldsymbol{e}_1 - 1.6\boldsymbol{e}_2 + 1.0\boldsymbol{e}_3 \end{array} \qquad (5.5.1)$$

with the function

$$f(t) = \begin{cases} (1 - \cos(2\pi t/T))/2 & \text{for} \quad t \leq T \\ 0 & \text{for} \quad t > T \end{cases} \qquad (5.5.2)$$

and $T = 0.5$.

No other external loads are present in this example. The numerical results are based on a constant time-step $h = 0.01$ and an equidistant spatial discretisation of the central line of the beam by 22 linear beam elements.

5.5.1 Lagrange multiplier method

An impression of the motion and deformation of the spatially discretised beam with concentrated masses is given in Figure 5.5 by snapshots of consecutive configurations. Thereby, the small concentrated mass at the midnode is hidden by the cuboids representing the orientation of the spatial elements. The edge directions of a cuboid are specified by the director triad at the left element node. The conjugate stress resultants $\boldsymbol{n}_e, \boldsymbol{m}_e$ of the e-th element are obtained as pointwise evaluation of the resultants in the Gauß-points. The cuboids are coloured by a linear interpolation of the weighted sum of the norms of the stress resultants $\|\boldsymbol{n}_e\| + 10\|\boldsymbol{m}_e\| \in [0, 2]$ in the elements. Thereby, blue represents zero, while red represents two. The evolution of the conjugate stress resultants in the 11-th spatial element is depicted in Figure 5.4 on the right hand side. The conservation properties of the algorithm can be checked in Figure 5.4 in the left diagram. After the vanishing of the external loads at $t = 0.5$, the total energy and all components of the angular momentum are conserved.
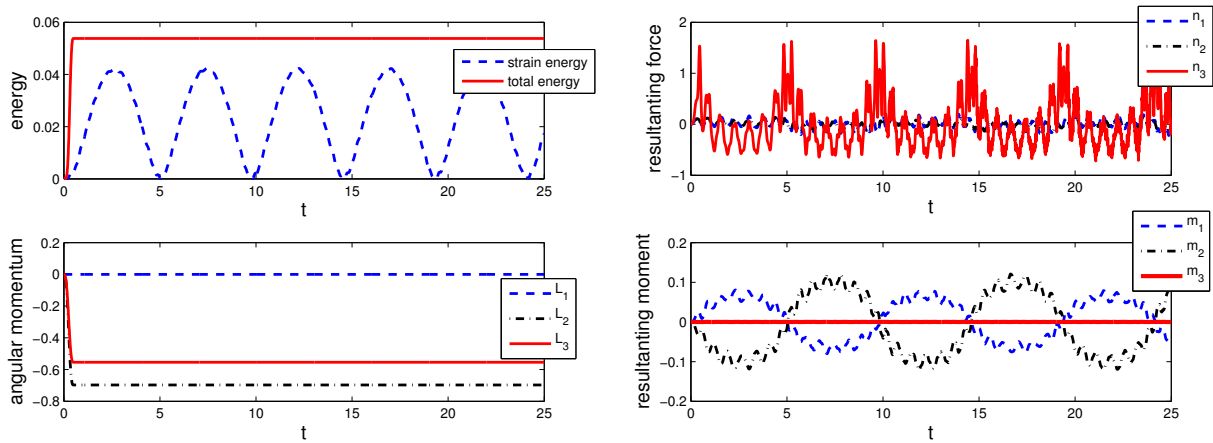
Figure 5.4: Beam with concentrated masses: energy and components of angular momentum vector $\boldsymbol{L} = L_i \boldsymbol{e}_i$ and stress resultants in 11-th element ($h = 0.01$).

$t = 2.5$

$t = 7.5$

$t = 12.5$

$t = 17.5$

$t = 22.5$

$t = 25$
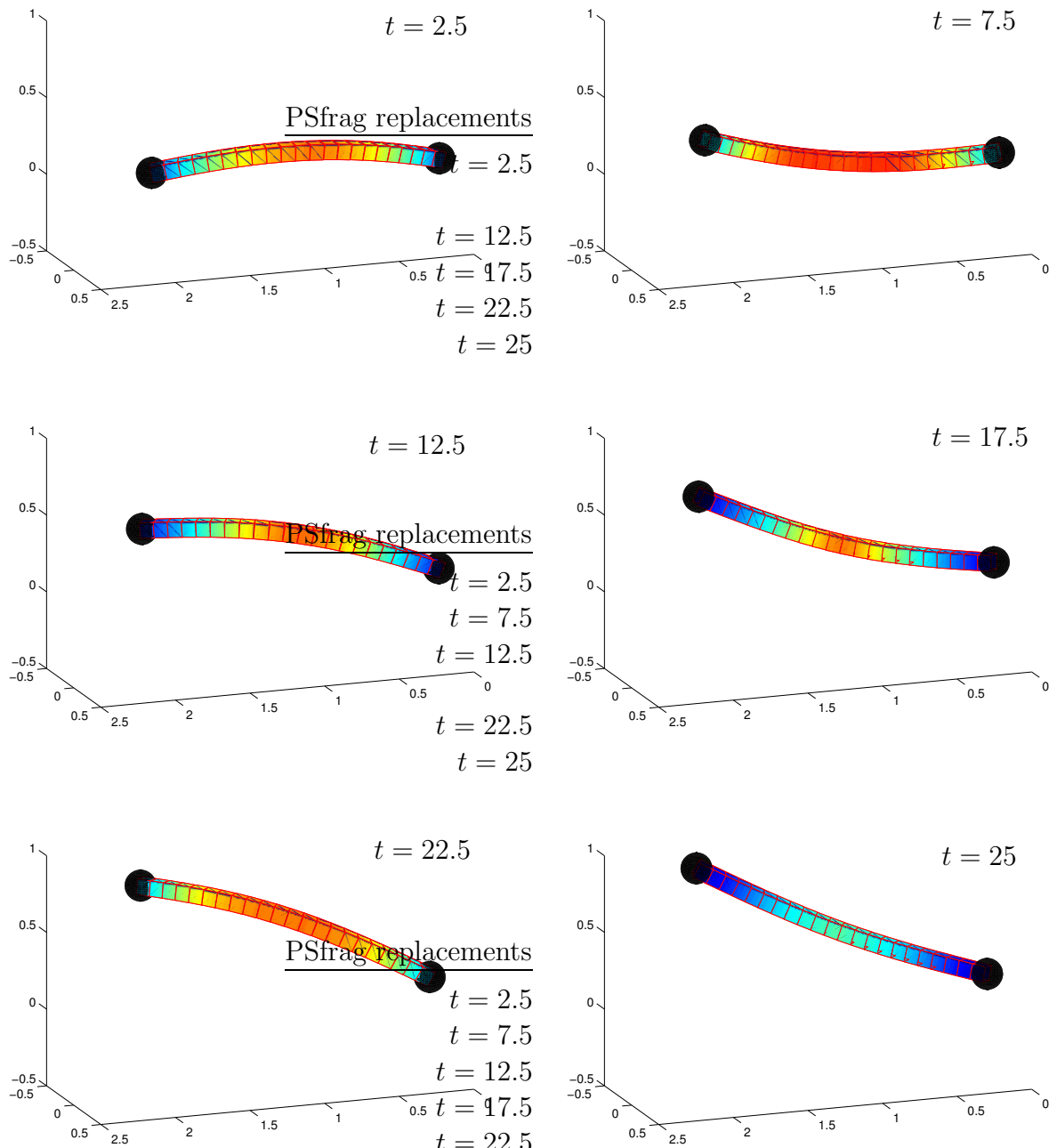
Figure 5.5: Beam with concentrated masses: snapshots of the motion and deformation at $t \in \{2.5, 7.5, 12.5, 17.5, 22.5, 25\}$.

5.5.2 Penalty method

The penalty function P_{Pen}^h given in (5.4.22) is used. The linear decrease of the constraint violation for increasing penalty parameters can be seen in Figure 5.6 on the right hand side. This verifies the first statement of Proposition 3.2.2. The second statement, that the solution of (5.4.12) using the Penalty method converges to that using the Lagrange multiplier method is visualised in the left diagram in Figure 5.6.
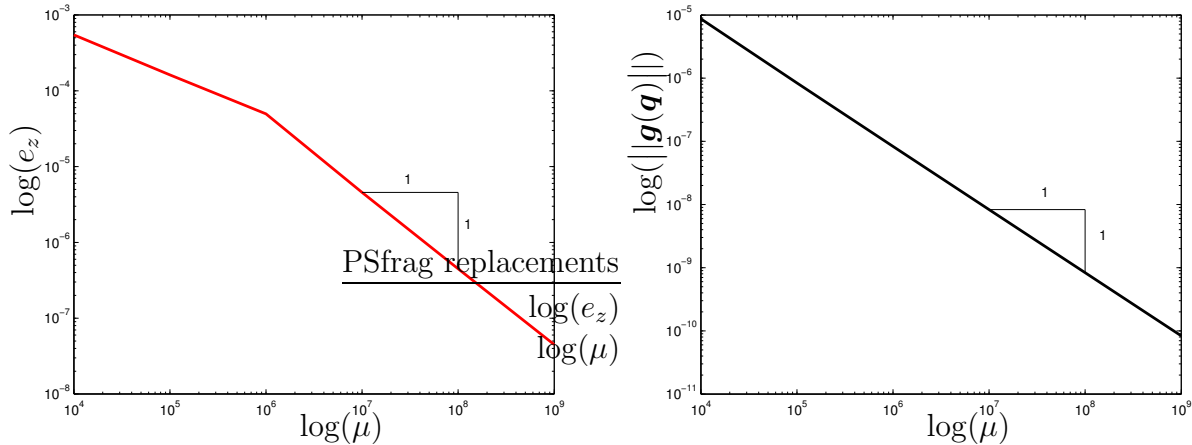
Figure 5.6: Beam with concentrated masses: relative error $e_z = \|z_{\mathrm{Pen}} - z_{\mathrm{Lag}}\|/\|z_{\mathrm{Lag}}\|$ of the phase variable and constraint fulfilment for the penalty scheme at $t = 1$ ($h = 0.01$).

5.5.3 Augmented Lagrange method

The same beam deformation problem is calculated using the augmented Lagrange method with the function P_{Aug}^h given in (5.4.26) and $\mu = 10^5$. All statements of Proposition 3.2.4 are verified by the three diagrams in Figure 5.7. The convergence of the configuration calculated by solving (5.4.12) using the augmented Lagrange method to that using the Lagrange multiplier method can be observed. Similarly the multipliers approach the true Lagrange multipliers during the augmented Lagrange iteration (AL-iteration). Furthermore, the decrease in the constraint violation is demonstrated.

5.5.4 Discrete null space method with nodal reparametrisation

Figure 5.8 shows the convergence of the solution of the d'Alembert-type scheme with nodal reparametrisation to a reference solution calculated by the constrained scheme using a time-step $h = 10^{-5}$. It confirms the statement of Proposition 3.2.12.
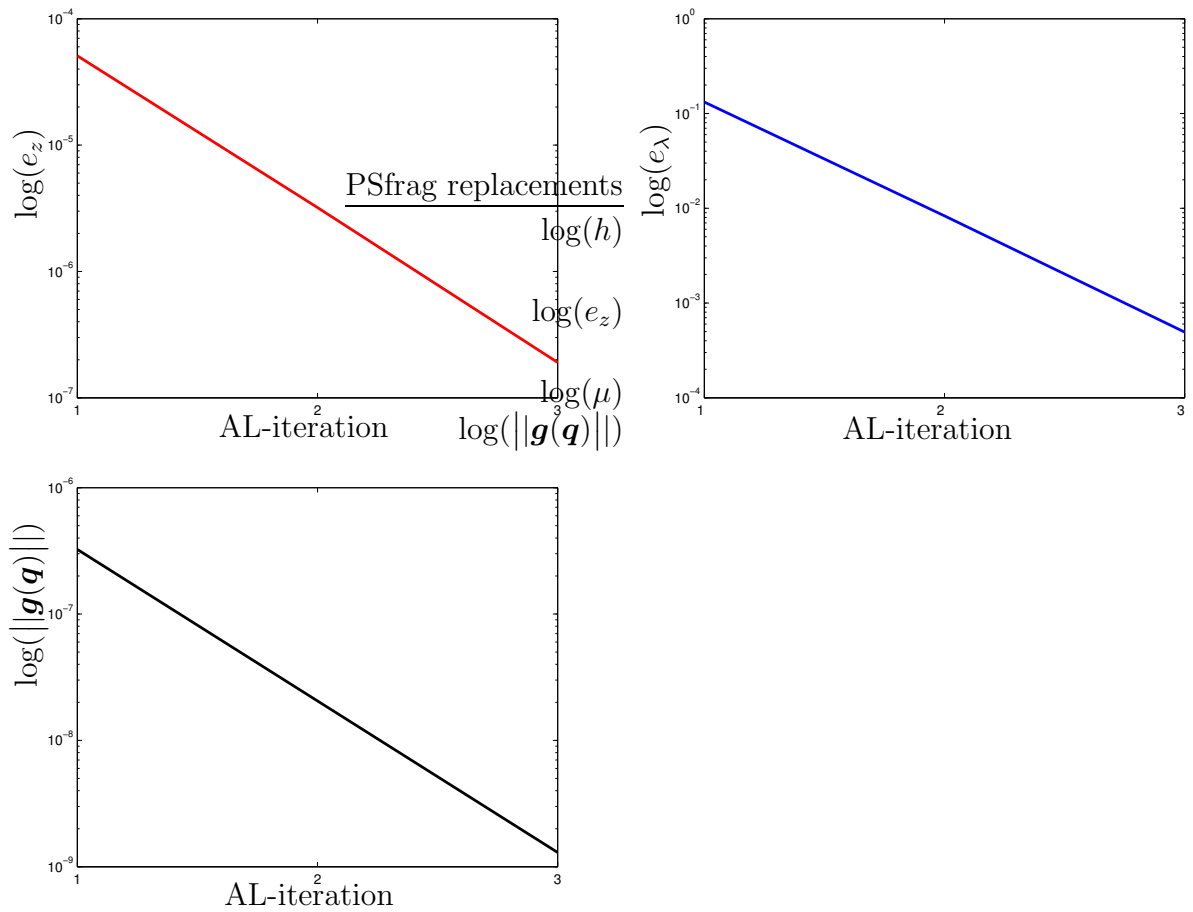
Figure 5.7: Beam with concentrated masses: relative error $e_z = \|z_{\mathrm{Aug}} - z_{\mathrm{Lag}}\| / \|z_{\mathrm{Lag}}\|$ of the phase variable and relative error of the multipliers $e_\lambda = \|\lambda_{\mathrm{Aug}} - \lambda_{\mathrm{Lag}}\| // \|\lambda_{\mathrm{Lag}}\|$ and constraint fulfilment for the augmented Lagrange scheme at $t = 0.58$ ($h = 0.01$, $\mu = 10^5$).
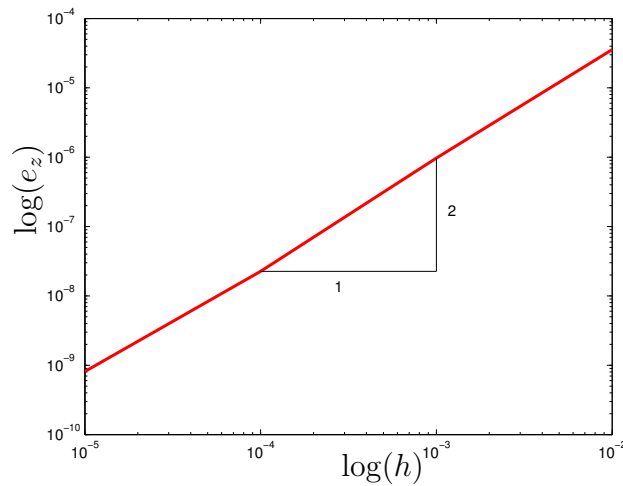
Figure 5.8: Beam with concentrated masses: relative error $e_z = \|z_{\mathrm{d'Al}} - z_{\mathrm{Lag}}\| / \|z_{\mathrm{Lag}}\|$ of the phase variable for the d'Alembert-type scheme with nodal reparametrisation at $t = 0.05$.

5.5.5 Comparison

Table 5.2 summarises the computational performance of the four schemes under consideration for the simulation of motion and deformation of the beam with concentrated masses. For this problem involving spatial finite beam elements in the context of geometrically nonlinear elastic deformation, the condition number is relatively high. Its deterioration for decreasing time-steps cannot be observed until the time-steps drops under the value of $h = 10^{-5}$ for the Lagrange multiplier method. For the other schemes, almost no influence of the time-step or the penalty parameter on the condition number is observable, it stays nearly constant at a relatively high value.

The 'coupling' of the director triads by the connectivity assumptions of the spatial finite element method improves the constraint fulfilment for the penalty method in general and for the augmented Lagrange method in the first iteration. Thus only a small number of iterations is required to reduce the constraint fulfilment under the desired tolerance. However, neither the penalty method nor the augmented Lagrange method can compete with the numerical exact constraint fulfilment of the constrained scheme and the discrete null space method.

The high numerical effort caused by the assembly of the internal forces $\mathsf{D}\boldsymbol{q}_\alpha V_{int}^h$ for all nodes $\alpha = 1, \ldots, n_{node}$ in (5.4.12) assimilates the computational time by the different schemes despite the large differences in the system's dimensions. Nevertheless, the augmented Lagrange schemes requires the highest computational time to calculate 100 time-steps due to the extra iterations in each time-step. The costs for the assembly of the null space matrix in (5.4.32) and the more involved update structure preponderates the benefits of the small dimensional system. The penalty method requires less computational time, although twice the number of equations are solved in each time-step, whereas the assembly and solution of the three times larger dimensional system in the Lagrange multiplier method is only slightly more expensive.

Nevertheless, the d'Alembert-type scheme with nodal reparametrisation performs superior to the other schemes, since it combines numerically exact constraint fulfilment with the lowest possible condition numbers.

Table 5.2: Comparison of constrained scheme, penalty scheme, augmented Lagrange scheme and d'Alembert-type scheme with nodal reparametrisation for the example 'beam with concentrated masses'.

	constrained	penalty		augm. Lag.	d'Alembert
number of unknowns $n = 276 \quad m = 138$	414	276		276	138
CPU-time	1.1	0.8		1.6	1
constraint fulfilment	10^{-16}	$\mu = 10^5$ 10^{-7}	$\mu = 10^{10}$ 10^{-10}	10^{-10}	10^{-16}
condition number $h = 10^{-5}$	10^{11}	10^9	10^9	10^9	10^9
$h = 10^{-6}$	10^{13}	10^9	10^9	10^9	10^9
$h = 10^{-7}$	10^{15}	10^{10}	10^9	10^{10}	10^9

6 Multibody system dynamics

The description of rigid body dynamics in terms of redundant coordinates presented in Section 4.3 as well as that of geometrically exact beams as special Cosserat continuum in Chapter 5, can be generalised to multibody systems consisting of rigid and elastic components in a systematic way. The internal constraints pertaining to the underlying kinematic assumptions of the components of the multibody system are retained and the interconnecting joints between the components of multibody systems constitute the so-called external constraints. Thus the constrained formulations of the equations of motion for rigid body motion or beam dynamics provide a uniform framework to include both types of constraints.

6.1 Lower kinematic pairs

The coupling of rigid bodies by means of configurational constraints constitutes so-called kinematic chains, see [Ange 88, Ange 97]. In this context, the rigid bodies are often termed links. The links are coupled pairwise, hence two neighbouring links, whose relative motion is constrained, form a kinematic pair. These can be divided into two classes, namely upper and lower kinematic pairs. An upper kinematic pair arises when the contact between two bodies takes place along a line or a point. Examples are a cylinder or a sphere rolling on a plane. The appearing constraints may be any kind of holonomic or nonholonomic constraint. Often they can be replaced by a combination of lower pairs, see [Gera 01]. Opposite to that in a lower kinematic pair, contact takes place along a surface common to both bodies.

In the sequel, a detailed description of the external constraints caused by joints connecting lower kinematic pairs and their treatment by the the constrained formulations of the equations of motion, as well as the d'Alembert-type formulation, is presented (see [Bets 06]). The penalty method and the augmented Lagrange method are set aside from now on, since the theoretical considerations at the end of Section 3.2 and the examples up to now (see Chapters 4 and 5) revealed that the performance of the constrained scheme and the d'Alembert-type scheme with nodal reparametrisation is substantially superior, especially concerning the computational costs and the accuracy of the constraint fulfilment.

With regard to Section 4.3, the configuration of the α-th rigid link in a kinematic chain can be characterised by redundant coordinates $\boldsymbol{q}^\alpha \in \mathbb{R}^{12}$. Thus the configuration of two rigid links, denoted by 1 and 2, can be characterised by redundant coordinates which may be arranged in the configuration vector

$$\boldsymbol{q}(t) = \left[\begin{array}{c} \boldsymbol{q}^1(t) \\ \boldsymbol{q}^2(t) \end{array} \right] \in \mathbb{R}^{24} \tag{6.1.1}$$

6.1.1 Constrained formulation

The constrained formulation of each rigid body leads to constraint functions $\boldsymbol{g}_{int}^{\alpha} \in \mathbb{R}^6$ of the form (4.3.3) along with constraint Jacobians $\boldsymbol{G}_{int}^{\alpha}$ of the form (4.3.4). For the 2-body system at hand this yields

$$\boldsymbol{g}_{int}(\boldsymbol{q}) = \left[\begin{array}{c} \boldsymbol{g}_{int}^1(\boldsymbol{q}^1) \\ \boldsymbol{g}_{int}^2(\boldsymbol{q}^2) \end{array} \right] \tag{6.1.2}$$

together with

$$\boldsymbol{G}_{int}(\boldsymbol{q}) = \left[\begin{array}{cc} \boldsymbol{G}_{int}^1(\boldsymbol{q}^1) & \boldsymbol{0} \\ \boldsymbol{0} & \boldsymbol{G}_{int}^2(\boldsymbol{q}^2) \end{array} \right] \tag{6.1.3}$$

Accordingly, the 2-body system under consideration leads to $m_{int} = 12$ internal constraints with associated constraint Jacobian $\boldsymbol{G}_{int}(\boldsymbol{q}) \in \mathbb{R}^{12 \times 24}$. The coupling of the two bodies by means of a specific joint leads to further constraints termed external constraints. Table 6.1 gives an overview over lower kinematic pairs $J \in \{R, P, C, S, E\}$, that will be investigated in the following. Depending on the number of external constraints $m_{ext}^{(J)}$ they give rise to, the degrees of freedom of the relative motion of one body with respect to the other is decreased from 6 to $r^{(J)} = 6 - m_{ext}^{(J)}$.

Table 6.1: Different types of lower kinematic pairs with corresponding number of external constraints $m_{ext}^{(J)}$ and number or relative degrees of freedom $r^{(J)}$.

	revolute (R)	prismatic (P)	cylindrical (C)	spherical (S)	planar (E)
$m_{ext}^{(J)}$	5	5	4	3	3
$r^{(J)}$	1	1	2	3	3

Remark 6.1.1 (Elementary pairs) From the six types of lower kinematic pairs, those five giving rise to maximal quadratic configurational constraints are investigated. The C, S, and E pair can be obtained as compositions of the R and P pair, which are termed elementary pairs. See e.g. [Ange 88] for further background on the classification of kinematic pairs.

Each kinematic pair is characterised by altogether $m^{(J)} = m_{int} + m_{ext}^{(J)}$ constraints. The systematic approach to constrained dynamical systems presented in Section 2.3 allows the arrangement of the corresponding constraint functions in the vector valued function $\boldsymbol{g}^{(J)} : Q = \mathbb{R}^{24} \to \mathbb{R}^{m^{(J)}}$, which may be written in partitioned form

$$\boldsymbol{g}^{(J)}(\boldsymbol{q}) = \left[\begin{array}{c} \boldsymbol{g}_{int}(\boldsymbol{q}) \\ \boldsymbol{g}_{ext}^{(J)}(\boldsymbol{q}) \end{array} \right] \tag{6.1.4}$$

Similarly, the constraint Jacobian $\boldsymbol{G}^{(J)} \in \mathbb{R}^{m^{(J)} \times 24}$ pertaining to a specific kinematic pair can be written as

$$\boldsymbol{G}^{(J)}(\boldsymbol{q}) = \left[\begin{array}{c} \boldsymbol{G}_{int}(\boldsymbol{q}) \\ \boldsymbol{G}_{ext}^{(J)}(\boldsymbol{q}) \end{array} \right] \tag{6.1.5}$$

The Hamiltonian for the kinematic pair takes the separable form given in (3.2.4) with the constant mass matrix

$$
\boldsymbol{M} = \left[\begin{array}{cc} \boldsymbol{M}^1 & \boldsymbol{0} \\ \boldsymbol{0} & \boldsymbol{M}^2 \end{array} \right]
\tag{6.1.6}
$$

where each submatrix $\boldsymbol{M}^\alpha \in \mathbb{R}^{12 \times 12}$ coincides with (4.3.8). As described in (2.3.13), the Hamiltonian can be augmented according to the method to treat the constraints, leading to the constrained Hamilton's equations (2.3.8) including the Lagrange multipliers or the Hamilton's equations (2.2.4) including the penalty parameter or the Hamilton's equations (2.2.4) in the context of the augmented Lagrange method to enforce the constraints. Temporal discretisation using the concept of G-equivariant discrete derivatives described in Section 3.1.1 leads to the discrete system (3.2.2), which in the special case of the Lagrange multiplier method takes the form (3.2.5).

6.1.2 Reduced formulation

In this section the construction of continuous null space matrices for the kinematic pairs under consideration is outlined. Similar to the case of a single rigid body treated in Section 4.3.3, the twist of a pair of two free rigid bodies reads

$$
\boldsymbol{t} = \left[\begin{array}{c} \boldsymbol{t}^1 \\ \boldsymbol{t}^2 \end{array} \right]
\tag{6.1.7}
$$

where, analogous to (4.3.17), the twist of the α-th body $\boldsymbol{t}^\alpha \in \mathbb{R}^6$, is given by

$$
\boldsymbol{t}^\alpha = \left[\begin{array}{c} \dot{\boldsymbol{\varphi}}^\alpha \\ \boldsymbol{\omega}^\alpha \end{array} \right]
\tag{6.1.8}
$$

Now the redundant velocities $\dot{\boldsymbol{q}} \in \mathbb{R}^{24}$ of the kinematic pair may be expressed as $\dot{\boldsymbol{q}} = \boldsymbol{P}_{int}(\boldsymbol{q}) \cdot \boldsymbol{t}$ where the 24×12 matrix $\boldsymbol{P}_{int}(\boldsymbol{q})$ is given by

$$
\boldsymbol{P}_{int}(\boldsymbol{q}) = \left[\begin{array}{cc} \boldsymbol{P}_{int}^1(\boldsymbol{q}^1) & \boldsymbol{0} \\ \boldsymbol{0} & \boldsymbol{P}_{int}^2(\boldsymbol{q}^2) \end{array} \right]
\tag{6.1.9}
$$

and $\boldsymbol{P}_{int}^\alpha(\boldsymbol{q}^\alpha)$ is the null space matrix associated with the α-th free body, which with regard to (4.3.19) reads

$$
\boldsymbol{P}_{int}^\alpha(\boldsymbol{q}^\alpha) = \left[\begin{array}{cc} \boldsymbol{I} & \boldsymbol{0} \\ \boldsymbol{0} & -\widehat{\boldsymbol{d}_1^\alpha} \\ \boldsymbol{0} & -\widehat{\boldsymbol{d}_2^\alpha} \\ \boldsymbol{0} & -\widehat{\boldsymbol{d}_3^\alpha} \end{array} \right]
\tag{6.1.10}
$$

Note that by design $\boldsymbol{G}_{int}(\boldsymbol{q}) \cdot \boldsymbol{P}_{int}(\boldsymbol{q}) = \boldsymbol{0}$, the 12×12 zero matrix.

In a kinematic pair $J \in \{R, P, C, S, E\}$, the interconnection of the two rigid bodies by means of a specific joint restricts the relative motion of the second body with respect to the first body (see Table 6.1). The relative motion can be accounted for by introducing

$r^{(J)}$ joint velocities $\boldsymbol{\tau}^{(J)}$. Thus the motion of the kinematic pair can be characterised by the independent generalised velocities $\boldsymbol{\nu}^{(J)} \in \mathbb{R}^{6+r^{(J)}}$ with

$$\boldsymbol{\nu}^{(J)} = \begin{bmatrix} \boldsymbol{t}^1 \\ \boldsymbol{\tau}^{(J)} \end{bmatrix} \qquad (6.1.11)$$

In particular, introducing the $6 \times (6+r^{(J)})$ matrix $\boldsymbol{P}_{ext}^{2,(J)}(\boldsymbol{q})$, the twist of the second body $\boldsymbol{t}^2 \in \mathbb{R}^6$ can be expressed as

$$\boldsymbol{t}^{2,(J)} = \boldsymbol{P}_{ext}^{2,(J)}(\boldsymbol{q}) \cdot \boldsymbol{\nu}^{(J)} \qquad (6.1.12)$$

Accordingly, the twist of the kinematic pair $J \in \{R, P, C, S, E\}$ can be written in the form

$$\boldsymbol{t}^{(J)} = \boldsymbol{P}_{ext}^{(J)}(\boldsymbol{q}) \cdot \boldsymbol{\nu}^{(J)} \qquad (6.1.13)$$

with the $12 \times (6+r^{(J)})$ matrix $\boldsymbol{P}_{ext}^{(J)}(\boldsymbol{q})$, which may be partitioned according to

$$\boldsymbol{P}_{ext}^{(J)}(\boldsymbol{q}) = \begin{bmatrix} \boldsymbol{I}_{6\times 6} & \boldsymbol{0}_{6\times r^{(J)}} \\ \boldsymbol{P}_{ext}^{2,(J)}(\boldsymbol{q}) \end{bmatrix} \qquad (6.1.14)$$

Once $\boldsymbol{P}_{ext}^{(J)}(\boldsymbol{q})$ has been established, the total null space matrix pertaining the kinematic pair under consideration can be calculated from

$$\boldsymbol{P}^{(J)}(\boldsymbol{q}) = \boldsymbol{P}_{int}(\boldsymbol{q}) \cdot \boldsymbol{P}_{ext}^{(J)}(\boldsymbol{q}) = \begin{bmatrix} \boldsymbol{P}_{int}^1(\boldsymbol{q}^1) & \boldsymbol{0}_{12\times r^{(J)}} \\ \boldsymbol{P}_{int}^2(\boldsymbol{q}^2) \cdot \boldsymbol{P}_{ext}^{2,(J)}(\boldsymbol{q}) \end{bmatrix} \qquad (6.1.15)$$

Finally, the 24-dimensional redundant velocity vector of the kinematic pair can be expressed in terms of the independent generalised velocities $\boldsymbol{\nu}^{(J)} \in \mathbb{R}^{6+r^{(J)}}$ via

$$\dot{\boldsymbol{q}} = \boldsymbol{P}^{(J)}(\boldsymbol{q}) \cdot \boldsymbol{\nu}^{(J)} \qquad (6.1.16)$$

Provided that $\boldsymbol{P}_{ext}^{2,(J)}(\boldsymbol{q})$ has been properly deduced from (6.1.12),

$$\dot{\boldsymbol{q}} \in \text{null}\left(\boldsymbol{G}^{(J)}(\boldsymbol{q})\right) \qquad (6.1.17)$$

and the above procedure warrants the design of viable null space matrices which automatically satisfy the relationship

$$\boldsymbol{G}^{(J)}(\boldsymbol{q}) \cdot \boldsymbol{P}^{(J)}(\boldsymbol{q}) = \boldsymbol{0} \qquad (6.1.18)$$

To summarise, in order to construct a null space matrix pertaining to a specific kinematic pair, essentially relationship (6.1.12) is applied to deduce the matrix $\boldsymbol{P}_{ext}^{2,(J)}(\boldsymbol{q})$. Once $\boldsymbol{P}_{ext}^{2,(J)}(\boldsymbol{q})$ has been determined, the complete null space matrix pertaining to a specific pair follows directly from (6.1.15).

Remark 6.1.2 Similar to the procedure for the design of appropriate null space matrices outlined above, the relationship between rigid body twists and joint velocities is used in [Ange 89] to deduce the 'natural orthogonal complement' in the context of simple kinematic chains comprised of elementary kinematic pairs.

6.1.3 Discrete null space method with nodal reparametrisation

To deduce the discrete equations of motion (3.2.5) for the kinematic pair in the Hamiltonian formalism using the concept of G-equivariant discrete derivatives, the partial G-equivariant discrete derivative (see Definition 3.1.4 and 3.1.7) of the constraints needs be specified. It is obvious from the above treatment of the single rigid body, that the discrete counterparts of $\boldsymbol{G}_{int}(\boldsymbol{q})$ and $\boldsymbol{P}_{int}(\boldsymbol{q})$ are given by

$$
\begin{array}{rcl}
\mathbf{G}_{int}(\boldsymbol{q}_n, \boldsymbol{q}_{n+1}) & = & \boldsymbol{G}_{int}(\boldsymbol{q}_{n+\frac{1}{2}}) \\
\mathbf{P}_{int}(\boldsymbol{q}_n, \boldsymbol{q}_{n+1}) & = & \boldsymbol{P}_{int}(\boldsymbol{q}_{n+\frac{1}{2}})
\end{array}
\tag{6.1.19}
$$

and it can be easily checked that

$$
\boldsymbol{G}_{int}(\boldsymbol{q}_{n+\frac{1}{2}}) \cdot \boldsymbol{P}_{int}(\boldsymbol{q}_{n+\frac{1}{2}}) = \mathbf{0}
\tag{6.1.20}
$$

In Sections 6.1.4 to 6.1.8 it is shown that all external constraint functions associated with the kinematic pairs under consideration are at most quadratic in the redundant coordinates. Consequently, due to the properties of the partial G-equivariant discrete derivative, the discrete constraint Jacobians are given by

$$
\mathbf{G}_{ext}^{(J)}(\boldsymbol{q}_n, \boldsymbol{q}_{n+1}) = \boldsymbol{G}_{ext}^{(J)}(\boldsymbol{q}_{n+\frac{1}{2}})
\tag{6.1.21}
$$

for $J \in \{R, P, C, S, E\}$.

It thus remains to provide a discrete version of $\boldsymbol{P}_{ext}^{2,(J)}(\boldsymbol{q})$. Then the discrete version of the null space matrix pertaining to the external constraints (6.1.14) reads

$$
\mathbf{P}_{ext}^{(J)}(\boldsymbol{q}_n, \boldsymbol{q}_{n+1}) = \left[\begin{array}{cc} \boldsymbol{I}_{6\times 6} & \mathbf{0}_{6\times r^{(J)}} \\ \mathbf{P}_{ext}^{2,(J)}(\boldsymbol{q}_n, \boldsymbol{q}_{n+1}) & \end{array} \right]
\tag{6.1.22}
$$

and the total discrete null space matrix pertaining the kinematic pair under consideration is given by

$$
\mathbf{P}^{(J)}(\boldsymbol{q}_n, \boldsymbol{q}_{n+1}) = \boldsymbol{P}_{int}(\boldsymbol{q}_{n+\frac{1}{2}}) \cdot \mathbf{P}_{ext}^{(J)}(\boldsymbol{q}_n, \boldsymbol{q}_{n+1}) = \left[\begin{array}{cc} \boldsymbol{P}_{int}^1(\boldsymbol{q}_{n+\frac{1}{2}}^1) & \mathbf{0}_{12\times r^{(J)}} \\ \boldsymbol{P}_{int}^2(\boldsymbol{q}_{n+\frac{1}{2}}^2) \cdot \mathbf{P}_{ext}^{2,(J)}(\boldsymbol{q}_n, \boldsymbol{q}_{n+1}) & \end{array} \right]
\tag{6.1.23}
$$

where (6.1.19) has been taken into account.

To this end, the fulfilment of condition (3.2.30) respectively, the properties mentioned in Remark 3.2.7 are required. Since in the present case (6.1.20) is already fulfilled, the following condition remains as a design criterion for the $\mathbf{P}_{ext}^{(J)}(\boldsymbol{q}_n, \boldsymbol{q}_{n+1})$

$$
\boldsymbol{G}_{ext}^{(J)}(\boldsymbol{q}_{n+\frac{1}{2}}) \cdot \boldsymbol{P}_{int}(\boldsymbol{q}_{n+\frac{1}{2}}) \cdot \mathbf{P}_{ext}^{(J)}(\boldsymbol{q}_n, \boldsymbol{q}_{n+1}) = \mathbf{0}
\tag{6.1.24}
$$

where $\mathbf{0}$ is the $m_{ext}^{(J)} \times (6 + r^{(J)})$ zero matrix.

Remark 6.1.3 The discrete null space matrices designed so far for internal constraints in (4.3.27) and (6.1.19) suggest the midpoint evaluation of $\boldsymbol{P}_{ext}^{(J)}(\boldsymbol{q})$ as well. Indeed, for the examples of kinematic pairs given in Sections 6.1.4 and 6.1.6, $\boldsymbol{P}_{ext}^{(J)}(\boldsymbol{q}_{n+\frac{1}{2}})$ yields viable discrete null space matrices. However, this circumstance is closely related to the facts that

first of all, the appearing constraints are at most quadratic in the configuration variable, secondly, that there exists a reparametrisation of the constraint manifold in the temporal continuous setting (2.3.26), which is likewise maximal quadratic in the generalised coordinates and thirdly, that no relative translational degrees of freedom are present. It will become evident for the kinematic pairs in Sections 6.1.5, 6.1.7, 6.1.8 and in the context of closed loop systems described in Section 6.2.3 that the midpoint evaluation of $\boldsymbol{P}_{ext}^{(J)}(\boldsymbol{q})$ does not yield viable discrete null space matrices in general. While a slight modification of the midpoint evaluation yields an explicit representations of a discrete null space matrix in the case of kinematic pairs with translational degrees of freedom, one has to revert to the implicit representation for the closed loop system.

Corresponding to the independent generalised velocities $\boldsymbol{\nu}^{(J)} \in \mathbb{R}^{6+r^{(J)}}$ introduced in (6.1.16), the redundant coordinates $\boldsymbol{q} \in \mathbb{R}^{24}$ of each kinematic pair $J \in \{R, P, C, S, E\}$ may be expressed in terms of $6 + r^{(J)}$ independent generalised coordinates. Concerning the reparametrisation of unknowns in the discrete null space method, relationships of the form

$$\boldsymbol{q}_{n+1} = \boldsymbol{F}_{q_n}^{(J)}(\boldsymbol{\mu}^{(J)}) \tag{6.1.25}$$

are required, where

$$\boldsymbol{\mu}^{(J)} = (\boldsymbol{u}_{\varphi}^1, \boldsymbol{\theta}^1, \boldsymbol{\vartheta}^{(J)}) \in \mathbb{R}^{6+r^{(J)}} \tag{6.1.26}$$

consists of a minimal number of incremental unknowns in $[t_n, t_{n+1}]$ for a specific kinematic pair. In (6.1.26), $(\boldsymbol{u}_{\varphi}^1, \boldsymbol{\theta}^1) \in \mathbb{R}^3 \times \mathbb{R}^3$ are incremental displacements and rotations, respectively, associated with the first body (see Section 4.3.4). Furthermore, $\boldsymbol{\vartheta}^{(J)} \in \mathbb{R}^{r^{(J)}}$ denote incremental unknowns which characterise the configuration of the second body relative to the first one. In view of (6.1.1), the mapping in (6.1.25) may be partitioned according to

$$\begin{aligned} \boldsymbol{q}_{n+1}^1 &= \boldsymbol{F}_{q_n^1}^1(\boldsymbol{u}_{\varphi}^1, \boldsymbol{\theta}^1) \\ \boldsymbol{q}_{n+1}^2 &= \boldsymbol{F}_{q_n}^{2,(J)}(\boldsymbol{\mu}^{(J)}) \end{aligned} \tag{6.1.27}$$

Here, $\boldsymbol{F}_{q_n^1}^1(\boldsymbol{u}_{\varphi}^1, \boldsymbol{\theta}^1)$ is given by (4.3.31). It thus remains to specify the mapping $\boldsymbol{F}_{q_n}^{2,(J)}(\boldsymbol{\mu}^{(J)})$ for each kinematic pair under consideration. Of course, the mapping $\boldsymbol{F}_{q_n}^{(J)}$ is required to satisfy the constraints specified by (6.1.4), i.e. $\boldsymbol{g}^{(J)}(\boldsymbol{F}_{q_n}^{(J)}(\boldsymbol{\mu}^{(J)})) = \boldsymbol{0}$, for arbitrary $\boldsymbol{\mu}^{(J)}$.

Remark 6.1.4 As mentioned in Remarks 3.2.13 and 4.3.1, either incremental or iterative unknowns can be used during the iterative solution of the nonlinear algebraic equation (3.2.44). Details concerning the linearisation for both cases can be found in Appendix B.

In the following Sections 6.1.4 to 6.1.8 details of the treatment of specific kinematic pairs $J \in \{R, P, C, S, E\}$ are provided. In essence, the present approach requires the specification of (i) the external constraint function $\boldsymbol{g}_{ext}^{(J)}(\boldsymbol{q})$, along with the corresponding constraint Jacobian $\boldsymbol{G}_{ext}^{(J)}(\boldsymbol{q})$, and (ii) the null space matrix $\boldsymbol{P}_{ext}^{2,(J)}(\boldsymbol{q})$, which is needed to set up the complete null space matrix (6.1.14). Then (iii) the corresponding discrete null space matrix is deduced according to the design criterion (6.1.24) (see Remark 6.1.3). Finally, (iv) the mapping $\boldsymbol{F}_{q_n}^{2,(J)}(\boldsymbol{\mu}^{(J)})$ is specified, which is needed to perform the reparametrisation

of unknowns according to (6.1.25), and allows the reduction of the discrete system of equations of motion to the minimal possible dimension.

In the sequel the location of a specific joint on the α-th body is supposed to be characterised by coordinates ϱ_i^α with respect to the body frame $\{d_I^\alpha\}$ for $\alpha = 1, 2$

$$\boldsymbol{\varrho}^\alpha = \varrho_i^\alpha \boldsymbol{d}_i^\alpha \tag{6.1.28}$$

6.1.4 Spherical pair
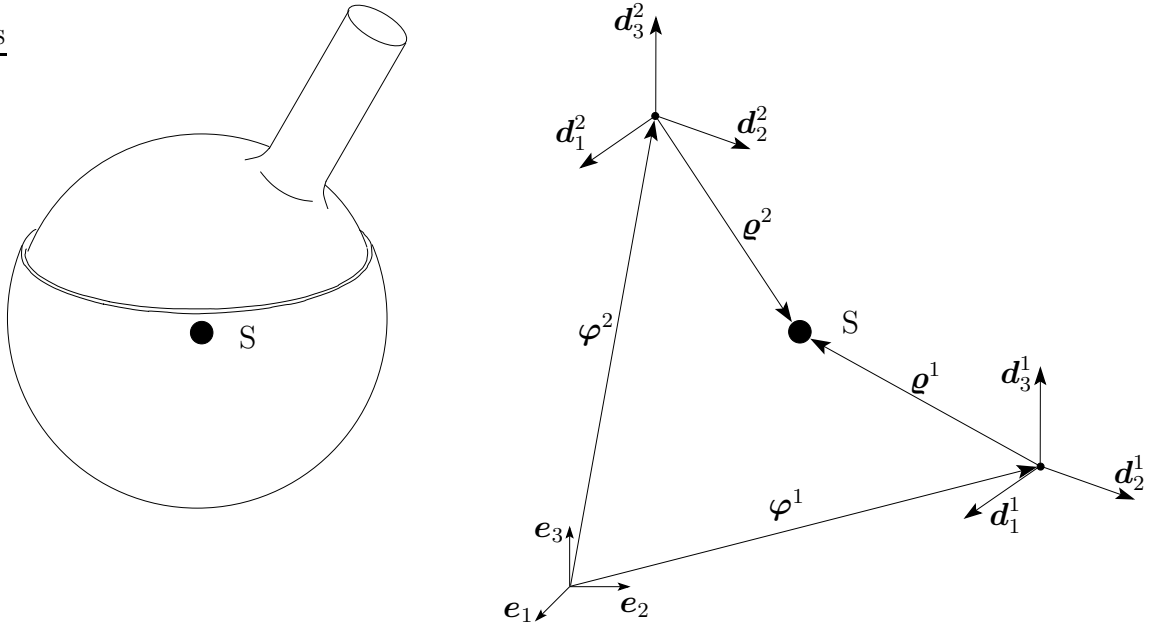
Figure 6.1: Spherical pair.

Constraints and constraint Jacobian

The S pair (Figure 6.1) prevents all relative translation between the two bodies, thus it entails three external constraints of the form

$$\boldsymbol{g}_{ext}^{(S)}(\boldsymbol{q}) = \boldsymbol{\varphi}^2 - \boldsymbol{\varphi}^1 + \boldsymbol{\varrho}^2 - \boldsymbol{\varrho}^1 = \boldsymbol{0} \tag{6.1.29}$$

The corresponding constraint Jacobian is given by the constant 3×24 matrix

$$\boldsymbol{G}_{ext}^{(S)}(\boldsymbol{q}) = \left[\begin{array}{cccccccc} -\boldsymbol{I} & -\varrho_1^1\boldsymbol{I} & -\varrho_2^1\boldsymbol{I} & -\varrho_3^1\boldsymbol{I} & \boldsymbol{I} & \varrho_1^2\boldsymbol{I} & \varrho_2^2\boldsymbol{I} & \varrho_3^2\boldsymbol{I} \end{array} \right] \tag{6.1.30}$$

Continuous form of the null space matrix

The motion of body 2 relative to body 1 is characterised by $r^{(S)} = 3$ degrees of freedom. Specifically, with regard to (6.1.11) $\boldsymbol{\tau}^{(S)} = \boldsymbol{\omega}^2$, the angular velocity of the second body. Accordingly, in the present case, the vector of independent generalised velocities reads

$$\boldsymbol{\nu}^{(S)} = \left[\begin{array}{c} \boldsymbol{t}^1 \\ \boldsymbol{\omega}^2 \end{array} \right] \tag{6.1.31}$$

Recall that the twist of the first rigid body given in (6.1.8) consists of its translational velocity $\dot{\boldsymbol{\varphi}}^1$ and its angular velocity $\boldsymbol{\omega}^1$. Taking the time derivative of the external constraints (6.1.29) and expressing the redundant velocities in terms of the independent generalised velocities (6.1.31) yields

$$\dot{\boldsymbol{\varphi}}^2 = \dot{\boldsymbol{\varphi}}^1 + \boldsymbol{\omega}^1 \times \boldsymbol{\varrho}^1 - \boldsymbol{\omega}^2 \times \boldsymbol{\varrho}^2 \tag{6.1.32}$$

Now it can be easily deduced from the relationship $\boldsymbol{t}^{2,(S)} = \boldsymbol{P}_{ext}^{2,(S)}(\boldsymbol{q}) \cdot \boldsymbol{\nu}^{(S)}$, that

$$\boldsymbol{P}_{ext}^{2,(S)}(\boldsymbol{q}) = \begin{bmatrix} \boldsymbol{I} & -\widehat{\boldsymbol{\varrho}^1} & \widehat{\boldsymbol{\varrho}^2} \\ \boldsymbol{0} & \boldsymbol{0} & \boldsymbol{I} \end{bmatrix} \tag{6.1.33}$$

so that (6.1.14) yields

$$\boldsymbol{P}_{ext}^{(S)}(\boldsymbol{q}) = \begin{bmatrix} \boldsymbol{I}_{6\times 6} & \boldsymbol{0}_{6\times 3} \\ \boldsymbol{P}_{ext}^{2,(S)}(\boldsymbol{q}) \end{bmatrix} \tag{6.1.34}$$

Furthermore, the null space matrix for the S pair follows directly from (6.1.15). It is given by

$$\boldsymbol{P}^{(S)}(\boldsymbol{q}) = \boldsymbol{P}_{int}(\boldsymbol{q}) \cdot \boldsymbol{P}_{ext}^{(S)}(\boldsymbol{q}) = \begin{bmatrix} \boldsymbol{P}_{int}^1(\boldsymbol{q}^1) & \boldsymbol{0}_{6\times 3} \\ \boldsymbol{P}_{int}^2(\boldsymbol{q}^2) \cdot \boldsymbol{P}_{ext}^{2,(S)}(\boldsymbol{q}) \end{bmatrix} \tag{6.1.35}$$

with

$$\boldsymbol{P}_{int}^2(\boldsymbol{q}^2) \cdot \boldsymbol{P}_{ext}^{2,(S)}(\boldsymbol{q}) = \begin{bmatrix} \boldsymbol{I} & -\widehat{\boldsymbol{\varrho}^1} & \widehat{\boldsymbol{\varrho}^2} \\ \boldsymbol{0} & \boldsymbol{0} & -\widehat{\boldsymbol{d}_1^2} \\ \boldsymbol{0} & \boldsymbol{0} & -\widehat{\boldsymbol{d}_2^2} \\ \boldsymbol{0} & \boldsymbol{0} & -\widehat{\boldsymbol{d}_3^2} \end{bmatrix} \tag{6.1.36}$$

Obviously with regard to (6.1.30) the present design procedure for $\boldsymbol{P}_{ext}^{2,(S)}(\boldsymbol{q})$ guarantees that

$$\boldsymbol{G}_{ext}^{(S)}(\boldsymbol{q}) \cdot \boldsymbol{P}^{(S)}(\boldsymbol{q}) = \boldsymbol{0} \tag{6.1.37}$$

Discrete version of the null space matrix

As stated in (6.1.21) the partial G-equivariant discrete derivative of the constraints of the spherical joint is given by

$$\mathbf{G}_{ext}^{(S)}(\boldsymbol{q}_n, \boldsymbol{q}_{n+1}) = \boldsymbol{G}_{ext}^{(S)}(\boldsymbol{q}_{n+\frac{1}{2}}) \tag{6.1.38}$$

With regard to (6.1.30) the discrete counterpart of (6.1.33) is chosen as

$$\mathbf{P}_{ext}^{2,(S)}(\boldsymbol{q}_n, \boldsymbol{q}_{n+1}) = \boldsymbol{P}_{ext}^{2,(S)}(\boldsymbol{q}_{n+\frac{1}{2}}) \tag{6.1.39}$$

It can be easily verified that this choice fulfils the design conditions (6.1.24). In particular,

$$\boldsymbol{G}_{ext}^{(S)}(\boldsymbol{q}_{n+\frac{1}{2}}) \cdot \boldsymbol{P}_{int}(\boldsymbol{q}_{n+\frac{1}{2}}) \cdot \boldsymbol{P}_{ext}^{(S)}(\boldsymbol{q}_{n+\frac{1}{2}}) = \boldsymbol{0} \tag{6.1.40}$$

Accordingly,

$$\mathbf{P}^{(S)}(\boldsymbol{q}_n, \boldsymbol{q}_{n+1}) = \boldsymbol{P}^{(S)}(\boldsymbol{q}_{n+\frac{1}{2}}) \tag{6.1.41}$$

is a viable discrete null space matrix for the S pair.

Reparametrisation of unknowns

To specify the reduced set of incremental unknowns (6.1.26) for the S pair, (6.1.31) induces $\boldsymbol{\vartheta}^{(S)} = \boldsymbol{\theta}^2 \in \mathbb{R}^3$, the incremental rotation vector pertaining to the second body. Then the rotational update of the body frame associated with the second body can be performed according to

$$(\boldsymbol{d}_I^2)_{n+1} = \exp(\widehat{\boldsymbol{\theta}^2}) \cdot (\boldsymbol{d}_I^2)_n \tag{6.1.42}$$

Enforcing the external constraints (6.1.29) at the end of the time-step implies

$$\boldsymbol{\varphi}_{n+1}^2 = \boldsymbol{\varphi}_{n+1}^1 + \boldsymbol{\varrho}_{n+1}^1 - \boldsymbol{\varrho}_{n+1}^2 \tag{6.1.43}$$

Eventually, the last two equations can be used to determine the mapping

$$\boldsymbol{q}_{n+1}^2 = \boldsymbol{F}_{q_n}^{2,(S)}(\boldsymbol{\mu}^{(S)}) = \begin{bmatrix} \boldsymbol{\varphi}_n^1 + \boldsymbol{u}_\varphi^1 + \exp(\widehat{\boldsymbol{\theta}^1}) \cdot \boldsymbol{\varrho}_n^1 - \exp(\widehat{\boldsymbol{\theta}^2}) \cdot \boldsymbol{\varrho}_n^2 \\ \exp(\widehat{\boldsymbol{\theta}^2}) \cdot (\boldsymbol{d}_1^2)_n \\ \exp(\widehat{\boldsymbol{\theta}^2}) \cdot (\boldsymbol{d}_2^2)_n \\ \exp(\widehat{\boldsymbol{\theta}^2}) \cdot (\boldsymbol{d}_3^2)_n \end{bmatrix} \tag{6.1.44}$$

6.1.5 Cylindrical pair
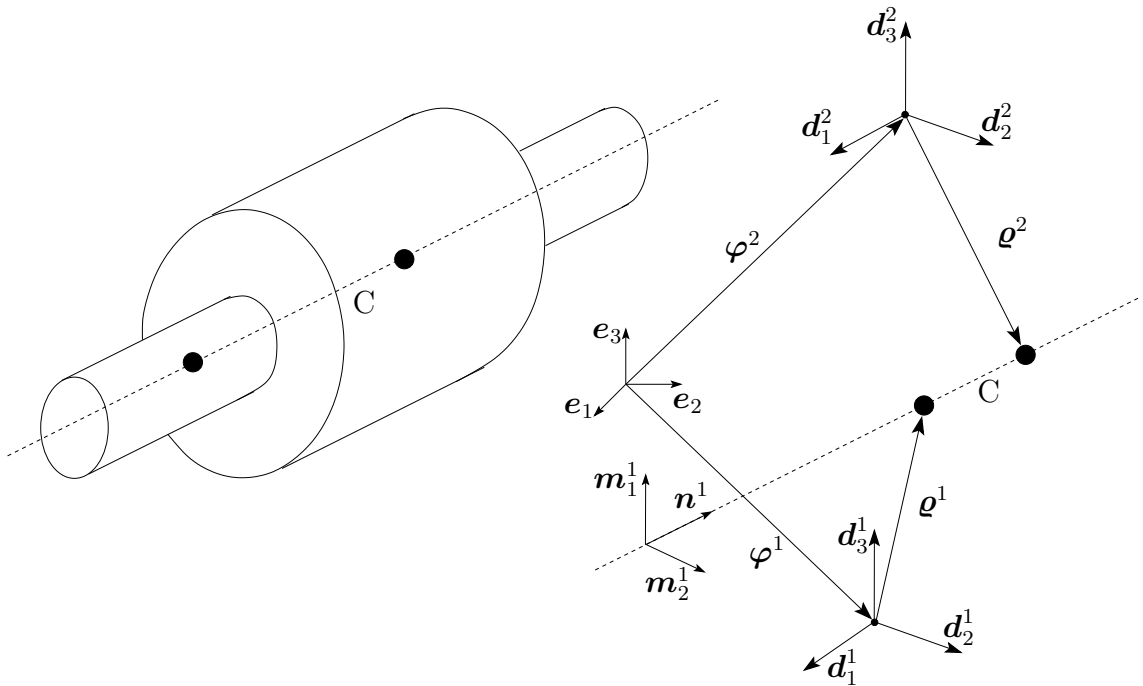
Figure 6.2: Cylindrical pair.

For the C pair (Figure 6.2) a unit vector $\boldsymbol{n}^1$ is introduced which is fixed in the first body and specified by constant components n_i^1 with respect to the body frame $\{\boldsymbol{d}_I^1\}$

$$\boldsymbol{n}^1 = n_i^1 \boldsymbol{d}_i^1 \tag{6.1.45}$$

In addition to that for $\kappa = 1, 2$, two vectors

$$\boldsymbol{m}_\kappa^1 = (m_\kappa^1)_i \boldsymbol{d}_i^1 \tag{6.1.46}$$

are introduced such that $\{\boldsymbol{m}_1^1, \boldsymbol{m}_2^1, \boldsymbol{n}^1\}$ constitute a right-handed orthonormal frame. The motion of the second body relative to the first one can be described by $r^{(C)} = 2$ degrees of freedom: Translation along $\boldsymbol{n}^1$ and rotation about $\boldsymbol{n}^1$. The translational motion along $\boldsymbol{n}^1$ may be characterised by the displacement $u^2 \in \mathbb{R}$, such that (see Figure 6.2)

$$\boldsymbol{\varphi}^1 + \boldsymbol{\varrho}^1 + u^2 \boldsymbol{n}^1 = \boldsymbol{\varphi}^2 + \boldsymbol{\varrho}^2 \tag{6.1.47}$$

For the subsequent treatment it proves convenient to introduce the vectors

$$\boldsymbol{p}^\alpha = \boldsymbol{\varphi}^\alpha + \boldsymbol{\varrho}^\alpha \tag{6.1.48}$$

for $\alpha = 1, 2$.

Constraints and constraint Jacobian

The C pair entails $m_{ext}^{(C)} = 4$ external constraint functions that may be written in the form

$$\boldsymbol{g}_{ext}^{(C)}(\boldsymbol{q}) = \begin{bmatrix} (\boldsymbol{m}_1^1)^T \cdot (\boldsymbol{p}^2 - \boldsymbol{p}^1) \\ (\boldsymbol{m}_2^1)^T \cdot (\boldsymbol{p}^2 - \boldsymbol{p}^1) \\ (\boldsymbol{n}^1)^T \cdot \boldsymbol{d}_1^2 - \eta_1 \\ (\boldsymbol{n}^1)^T \cdot \boldsymbol{d}_2^2 - \eta_2 \end{bmatrix} \tag{6.1.49}$$

where η_1, η_2 are constant and need be consistent with the initial conditions. The first two components of (6.1.49) conform with (6.1.47) and thus confine the translational motion of the second body relative to the first one. Similarly, the last two components of (6.1.49) restrict the relative rotational motion. The constraint Jacobian associated with (6.1.49) is given by the 4×24 matrix

$$\boldsymbol{G}_{ext}^{(C)}(\boldsymbol{q}) = \begin{bmatrix} -(\boldsymbol{m}_1^1)^T & \boldsymbol{G}_{11}^T & \boldsymbol{G}_{12}^T & \boldsymbol{G}_{13}^T & (\boldsymbol{m}_1^1)^T & \varrho_1^2(\boldsymbol{m}_1^1)^T & \varrho_2^2(\boldsymbol{m}_1^1)^T & \varrho_3^2(\boldsymbol{m}_1^1)^T \\ -(\boldsymbol{m}_2^1)^T & \boldsymbol{G}_{21}^T & \boldsymbol{G}_{22}^T & \boldsymbol{G}_{23}^T & (\boldsymbol{m}_2^1)^T & \varrho_1^2(\boldsymbol{m}_2^1)^T & \varrho_2^2(\boldsymbol{m}_2^1)^T & \varrho_3^2(\boldsymbol{m}_2^1)^T \\ \boldsymbol{0}^T & n_1^1(\boldsymbol{d}_1^2)^T & n_2^1(\boldsymbol{d}_1^2)^T & n_3^1(\boldsymbol{d}_1^2)^T & \boldsymbol{0}^T & (\boldsymbol{n}^1)^T & \boldsymbol{0}^T & \boldsymbol{0}^T \\ \boldsymbol{0}^T & n_1^1(\boldsymbol{d}_2^2)^T & n_2^1(\boldsymbol{d}_2^2)^T & n_3^1(\boldsymbol{d}_2^2)^T & \boldsymbol{0}^T & \boldsymbol{0}^T & (\boldsymbol{n}^1)^T & \boldsymbol{0}^T \end{bmatrix} \tag{6.1.50}$$

with

$$\boldsymbol{G}_{\kappa i} = (m_\kappa^1)_i (\boldsymbol{p}^2 - \boldsymbol{p}^1) - \varrho_i^1 \boldsymbol{m}_\kappa^1 \tag{6.1.51}$$

for $\kappa = 1, 2$ and $i = 1, 2, 3$.

Remark 6.1.5 (Singularities in the constrained formulation) For certain applications, e.g. in cases where the joints are located in each body's center of mass, i.e. $\boldsymbol{\varrho}^\alpha = \boldsymbol{0}$, $\alpha = 1, 2$, the constraint Jacobian (6.1.50) is singular, whenever the rotation axis $\boldsymbol{n}^1$ is colinear with either of the directors $\boldsymbol{d}_1^2$ or $\boldsymbol{d}_2^2$ used to check the fulfilment of the constraints (6.1.49). In this case either the sixth or the seventh column in (6.1.50) can be expressed as a linear combination of the second, third and fourth column.

Continuous form of the null space matrix

Corresponding to the $r^{(C)} = 2$ degrees of freedom characterising the motion of the second body relative to the first one, the independent generalised velocities of the relative motion read

$$\boldsymbol{\tau}^{(C)} = \left[\begin{array}{c} \dot{u}^2 \\ \dot{\theta}^2 \end{array} \right] \tag{6.1.52}$$

where, in addition to u^2 already introduced in (6.1.47), $\dot{\theta}^2$ accounts for the angular velocity of the second body relative to the first one. Specifically, one gets

$$\boldsymbol{\omega}^2 = \boldsymbol{\omega}^1 + \dot{\theta}^2 \boldsymbol{n}^1 \tag{6.1.53}$$

The vector of independent generalised velocities pertaining to the C pair is now given by

$$\boldsymbol{\nu}^{(C)} = \left[\begin{array}{c} \boldsymbol{t}^1 \\ \dot{u}^2 \\ \dot{\theta}^2 \end{array} \right] \tag{6.1.54}$$

Differentiating (6.1.47) with respect to time and taking into account (6.1.53) and (6.1.47), a straightforward calculation yields

$$\dot{\boldsymbol{\varphi}}^2 = \dot{\boldsymbol{\varphi}}^1 + \boldsymbol{\omega}^1 \times (\boldsymbol{\varphi}^2 - \boldsymbol{\varphi}^1) + \dot{u}^2 \boldsymbol{n}^1 + \dot{\theta}^2 \boldsymbol{\varrho}^2 \times \boldsymbol{n}^1 \tag{6.1.55}$$

Now the twist of the second body can be expressed in terms of the independent generalised velocities via $\boldsymbol{t}^{2,(C)} = \boldsymbol{P}_{ext}^{2,(C)}(\boldsymbol{q}) \cdot \boldsymbol{\nu}^{(C)}$, with the 6×8 matrix

$$\boldsymbol{P}_{ext}^{2,(C)}(\boldsymbol{q}) = \left[\begin{array}{cccc} \boldsymbol{I} & \widehat{\boldsymbol{\varphi}^1 - \boldsymbol{\varphi}^2} & \boldsymbol{n}^1 & \boldsymbol{\varrho}^2 \times \boldsymbol{n}^1 \\ \boldsymbol{0} & \boldsymbol{I} & \boldsymbol{0} & \boldsymbol{n}^1 \end{array} \right] \tag{6.1.56}$$

Then (6.1.14) yields

$$\boldsymbol{P}_{ext}^{(C)}(\boldsymbol{q}) = \left[\begin{array}{cc} \boldsymbol{I}_{6\times6} & \boldsymbol{0}_{6\times2} \\ \boldsymbol{P}_{ext}^{2,(C)}(\boldsymbol{q}) \end{array} \right] \tag{6.1.57}$$

Finally, with regard to (6.1.15), the null space matrix for the C pair is given by

$$\boldsymbol{P}^{(C)}(\boldsymbol{q}) = \left[\begin{array}{cc} \boldsymbol{P}_{int}^1(\boldsymbol{q}^1) & \boldsymbol{0}_{6\times2} \\ \boldsymbol{P}_{int}^2(\boldsymbol{q}^2) \cdot \boldsymbol{P}_{ext}^{2,(C)}(\boldsymbol{q}) \end{array} \right] \tag{6.1.58}$$

with

$$\boldsymbol{P}_{int}^2(\boldsymbol{q}^2) \cdot \boldsymbol{P}_{ext}^{2,(C)}(\boldsymbol{q}) = \left[\begin{array}{cccc} \boldsymbol{I} & \widehat{\boldsymbol{\varphi}^1 - \boldsymbol{\varphi}^2} & \boldsymbol{n}^1 & \boldsymbol{\varrho}^2 \times \boldsymbol{n}^1 \\ \boldsymbol{0} & -\widehat{\boldsymbol{d}_1^2} & \boldsymbol{0} & \boldsymbol{n}^1 \times \boldsymbol{d}_1^2 \\ \boldsymbol{0} & -\widehat{\boldsymbol{d}_2^2} & \boldsymbol{0} & \boldsymbol{n}^1 \times \boldsymbol{d}_2^2 \\ \boldsymbol{0} & -\widehat{\boldsymbol{d}_3^2} & \boldsymbol{0} & \boldsymbol{n}^1 \times \boldsymbol{d}_3^2 \end{array} \right] \tag{6.1.59}$$

It can be easily checked by a straightforward calculation that the present design procedure for $\boldsymbol{P}_{ext}^{2,(C)}(\boldsymbol{q})$ ensures that

$$\boldsymbol{G}_{ext}^{(C)}(\boldsymbol{q}) \cdot \boldsymbol{P}_{int}(\boldsymbol{q}) \cdot \boldsymbol{P}_{ext}^{(C)}(\boldsymbol{q}) = \boldsymbol{0} \tag{6.1.60}$$

Discrete version of the null space matrix

In the present case the discrete null space matrix does not coincide with $\boldsymbol{P}^{(C)}(\boldsymbol{q}_{n+\frac{1}{2}})$. Instead, with regard to the midpoint evaluation of the constraint Jacobian in (6.1.50), the discrete counterpart of (6.1.56) is chosen as

$$\mathbf{P}_{ext}^{2,(C)}(\boldsymbol{q}_n, \boldsymbol{q}_{n+1}) = \begin{bmatrix} \boldsymbol{I} & \widehat{\boldsymbol{\varphi}^1_{n+\frac{1}{2}} - \boldsymbol{\varphi}^2_{n+\frac{1}{2}}} & (\boldsymbol{m}_1^1)_{n+\frac{1}{2}} \times (\boldsymbol{m}_2^1)_{n+\frac{1}{2}} & \boldsymbol{\varrho}^2_{n+\frac{1}{2}} \times \boldsymbol{n}^1_{n+\frac{1}{2}} \\ \boldsymbol{0} & \boldsymbol{I} & \boldsymbol{0} & \boldsymbol{n}^1_{n+\frac{1}{2}} \end{bmatrix} \quad (6.1.61)$$

Remark 6.1.6 In general $(\boldsymbol{m}_1^1)_{n+\frac{1}{2}} \times (\boldsymbol{m}_2^1)_{n+\frac{1}{2}}$ does not coincide with $\boldsymbol{n}^1_{n+\frac{1}{2}}$, although $\boldsymbol{m}_1^1 \times \boldsymbol{m}_2^1 = \boldsymbol{n}^1_1$ in the continuous case. This is due to the fact that in the discrete setting the internal constraints of orthonormality of the director frame $\{\boldsymbol{d}_I^1\}$ are only enforced at the time nodes.

In any case it can be easily verified that (6.1.61) fulfils the design conditions (6.1.24). Finally, in view of (6.1.23), the discrete null space matrix for the C pair assumes the form

$$\mathbf{P}^{(C)}(\boldsymbol{q}_n, \boldsymbol{q}_{n+1}) = \begin{bmatrix} \boldsymbol{P}_{int}^1(\boldsymbol{q}^1_{n+\frac{1}{2}}) & \boldsymbol{0}_{6\times 2} \\ \boldsymbol{P}_{int}^2(\boldsymbol{q}^2_{n+\frac{1}{2}}) \cdot \mathbf{P}_{ext}^{2,(C)}(\boldsymbol{q}_n, \boldsymbol{q}_{n+1}) \end{bmatrix} \quad (6.1.62)$$

where

$$\boldsymbol{P}_{int}^2(\boldsymbol{q}^2_{n+\frac{1}{2}}) \cdot \mathbf{P}_{ext}^{2,(C)}(\boldsymbol{q}_n, \boldsymbol{q}_{n+1}) = \begin{bmatrix} \boldsymbol{I} & \widehat{\boldsymbol{\varphi}^1_{n+\frac{1}{2}} - \boldsymbol{\varphi}^2_{n+\frac{1}{2}}} & (\boldsymbol{m}_1^1)_{n+\frac{1}{2}} \times (\boldsymbol{m}_2^1)_{n+\frac{1}{2}} & \boldsymbol{\varrho}^2_{n+\frac{1}{2}} \times \boldsymbol{n}^1_{n+\frac{1}{2}} \\ \boldsymbol{0} & -\widehat{(\boldsymbol{d}_1^2)}_{n+\frac{1}{2}} & \boldsymbol{0} & \boldsymbol{n}^1_{n+\frac{1}{2}} \times (\boldsymbol{d}_1^2)_{n+\frac{1}{2}} \\ \boldsymbol{0} & -\widehat{(\boldsymbol{d}_2^2)}_{n+\frac{1}{2}} & \boldsymbol{0} & \boldsymbol{n}^1_{n+\frac{1}{2}} \times (\boldsymbol{d}_2^2)_{n+\frac{1}{2}} \\ \boldsymbol{0} & -\widehat{(\boldsymbol{d}_3^2)}_{n+\frac{1}{2}} & \boldsymbol{0} & \boldsymbol{n}^1_{n+\frac{1}{2}} \times (\boldsymbol{d}_3^2)_{n+\frac{1}{2}} \end{bmatrix} \quad (6.1.63)$$

Reparametrisation of unknowns

For the C pair the configuration of the second body with respect to the first one can be characterised by $\boldsymbol{\vartheta}^{(C)} = (u^2, \theta^2) \in \mathbb{R}^2$. Here θ^2 accounts for the incremental relative rotation which may be expressed via the product of exponentials formula

$$(\boldsymbol{d}_I^2)_{n+1} = \exp(\widehat{\boldsymbol{\theta}^1}) \cdot \exp\left(\theta^2(\widehat{\boldsymbol{n}^1})_n\right) \cdot (\boldsymbol{d}_I^2)_n \quad (6.1.64)$$

Enforcing the external constraints (6.1.47) at the end of the time-step implies

$$\boldsymbol{\varphi}^2_{n+1} = \boldsymbol{\varphi}^1_{n+1} + \boldsymbol{\varrho}^1_{n+1} - \boldsymbol{\varrho}^2_{n+1} + (u_n^2 + u^2)\boldsymbol{n}^1_{n+1} \quad (6.1.65)$$

Accordingly, the mapping $\boldsymbol{F}_{q_n}^{2,(C)}(\boldsymbol{\mu}^{(C)})$ can be written in the form

$$\boldsymbol{q}^2_{n+1} = \boldsymbol{F}_{q_n}^{2,(C)}(\boldsymbol{\mu}^{(C)}) = \begin{bmatrix} \boldsymbol{\varphi}^1_n + \boldsymbol{u}^1_\varphi + \exp(\widehat{\boldsymbol{\theta}^1}) \cdot [\boldsymbol{\varrho}^1_n - \exp\left(\theta^2(\widehat{\boldsymbol{n}^1})_n\right) \cdot \boldsymbol{\varrho}^2_n + (u_n^2 + u^2)\boldsymbol{n}^1_n] \\ \exp(\widehat{\boldsymbol{\theta}^1}) \cdot \exp\left(\theta^2(\widehat{\boldsymbol{n}^1})_n\right) \cdot (\boldsymbol{d}_1^2)_n \\ \exp(\widehat{\boldsymbol{\theta}^1}) \cdot \exp\left(\theta^2(\widehat{\boldsymbol{n}^1})_n\right) \cdot (\boldsymbol{d}_2^2)_n \\ \exp(\widehat{\boldsymbol{\theta}^1}) \cdot \exp\left(\theta^2(\widehat{\boldsymbol{n}^1})_n\right) \cdot (\boldsymbol{d}_3^2)_n \end{bmatrix}$$

$$(6.1.66)$$

6.1.6 Revolute pair
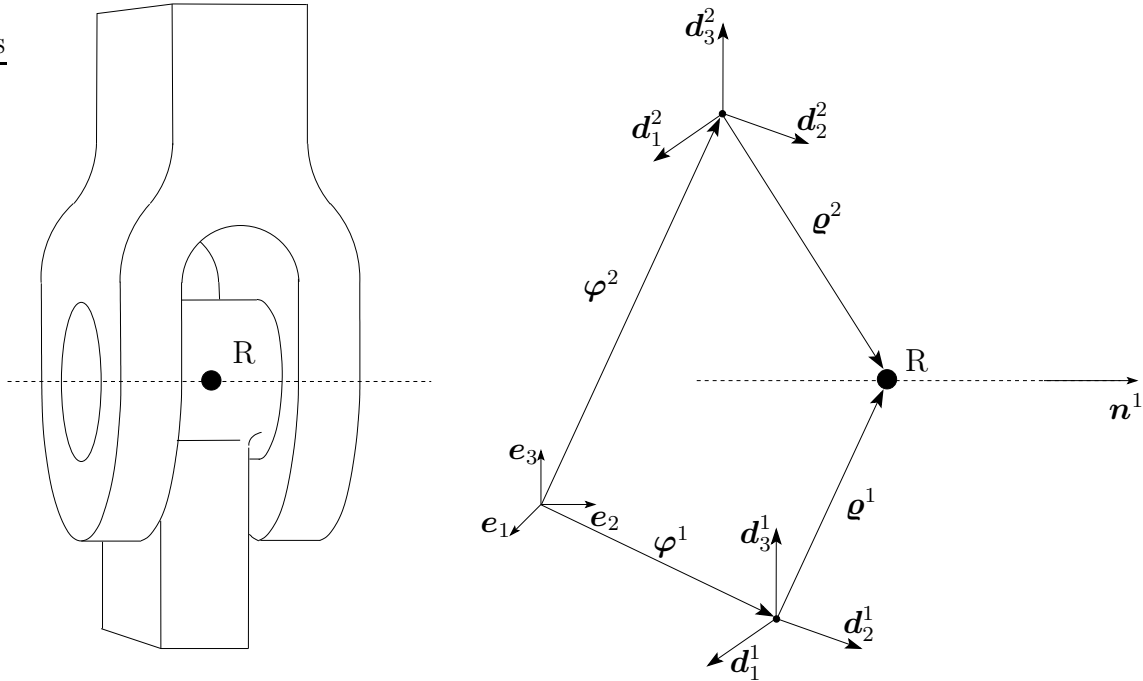
Figure 6.3: Revolute pair.

As for the cylindrical pair use is made of the unit vector $\boldsymbol{n}^1$ given by (6.1.45), which specifies the axis of rotation of the second body relative to the first one.

Constraints and constraint Jacobian

The R pair (Figure 6.3) entails $m_{ext}^{(R)} = 5$ external constraint functions which may be written in the form

$$\boldsymbol{g}_{ext}^{(R)}(\boldsymbol{q}) = \begin{bmatrix} \boldsymbol{\varphi}^2 - \boldsymbol{\varphi}^1 + \boldsymbol{\varrho}^2 - \boldsymbol{\varrho}^1 \\ (\boldsymbol{n}^1)^T \cdot \boldsymbol{d}_1^2 - \eta_1 \\ (\boldsymbol{n}^1)^T \cdot \boldsymbol{d}_2^2 - \eta_2 \end{bmatrix} \tag{6.1.67}$$

Analogous to the cylindrical pair η_1, η_2 are constant and need be consistent with the initial conditions. The corresponding constraint Jacobian is given by the 5×24 matrix

$$\boldsymbol{G}_{ext}^{(R)}(\boldsymbol{q}) = \begin{bmatrix} -\boldsymbol{I} & -\varrho_1^1\boldsymbol{I} & -\varrho_2^1\boldsymbol{I} & -\varrho_3^1\boldsymbol{I} & \boldsymbol{I} & \varrho_1^2\boldsymbol{I} & \varrho_2^2\boldsymbol{I} & \varrho_3^2\boldsymbol{I} \\ \boldsymbol{0}^T & n_1^1(\boldsymbol{d}_1^2)^T & n_2^1(\boldsymbol{d}_1^2)^T & n_3^1(\boldsymbol{d}_1^2)^T & \boldsymbol{0}^T & (\boldsymbol{n}^1)^T & \boldsymbol{0}^T & \boldsymbol{0}^T \\ \boldsymbol{0}^T & n_1^1(\boldsymbol{d}_2^2)^T & n_2^1(\boldsymbol{d}_2^2)^T & n_3^1(\boldsymbol{d}_2^2)^T & \boldsymbol{0}^T & \boldsymbol{0}^T & (\boldsymbol{n}^1)^T & \boldsymbol{0}^T \end{bmatrix} \tag{6.1.68}$$

Remark 6.1.7 (Singularities in the constrained formulation) For certain applications, e.g. in cases where the joints are located in each bodies center of mass, i.e. $\boldsymbol{\varrho}^\alpha = \boldsymbol{0}$, $\alpha = 1, 2$, the constraint Jacobian (6.1.68) is singular, whenever the rotation axis $\boldsymbol{n}^1$ is colinear with either of the directors $\boldsymbol{d}_1^2$ or $\boldsymbol{d}_2^2$ used to check the fulfilment of the constraints (6.1.67).

Continuous and discrete form of the null space matrix

Both the continuous and the discrete null space matrix for the R pair can directly be inferred from the previous treatment of the cylindrical pair. Since the R pair does not allow translational motion of the second body relative to the first one, the corresponding column in the null space matrix (associated with $\dot{u}^2$) of the C pair has to be eliminated. This is consistent with the fact that the R pair has only one ($r^{(R)} = 1$) degree of freedom which characterises the rotational motion of the second body relative to the first one. In particular, relationship (6.1.53) applies again. Note that, similar to (6.1.55), the translational velocity of the second body can be expressed as

$$\dot{\boldsymbol{\varphi}}^2 = \dot{\boldsymbol{\varphi}}^1 + \boldsymbol{\omega}^1 \times (\boldsymbol{\varrho}^1 - \boldsymbol{\varrho}^2) + \dot{\theta}^2 \boldsymbol{\varrho}^2 \times \boldsymbol{n}^1 \tag{6.1.69}$$

which follows from differentiating the first three constraint equations resulting from (6.1.67) with respect to time and taking into account (6.1.53). Now, similar to (6.1.56), (6.1.69) gives rise to

$$\boldsymbol{P}_{ext}^{2,(R)}(\boldsymbol{q}) = \begin{bmatrix} \boldsymbol{I} & \widehat{\boldsymbol{\varrho}^2 - \boldsymbol{\varrho}^1} & \boldsymbol{\varrho}^2 \times \boldsymbol{n}^1 \\ \boldsymbol{0} & \boldsymbol{I} & \boldsymbol{n}^1 \end{bmatrix} \tag{6.1.70}$$

In this connection note that the first three constraints resulting from (6.1.67) imply that $\boldsymbol{\varrho}^2 - \boldsymbol{\varrho}^1 = \boldsymbol{\varphi}^1 - \boldsymbol{\varphi}^2$. Proceeding along the lines of the previous treatment of the C pair one now gets

$$\boldsymbol{P}^{(R)}(\boldsymbol{q}) = \begin{bmatrix} \boldsymbol{P}_{int}^1(\boldsymbol{q}) & \boldsymbol{0}_{6\times 1} \\ \boldsymbol{P}_{int}^2(\boldsymbol{q}) \cdot \boldsymbol{P}_{ext}^{2,(R)}(\boldsymbol{q}) \end{bmatrix} \tag{6.1.71}$$

with

$$\boldsymbol{P}_{int}^2(\boldsymbol{q}) \cdot \boldsymbol{P}_{ext}^{2,(R)}(\boldsymbol{q}) = \begin{bmatrix} \boldsymbol{I} & \widehat{\boldsymbol{\varrho}^2 - \boldsymbol{\varrho}^1} & \boldsymbol{\varrho}^2 \times \boldsymbol{n}^1 \\ \boldsymbol{0} & -\widehat{\boldsymbol{d}_1^2} & \boldsymbol{n}^1 \times \boldsymbol{d}_1^2 \\ \boldsymbol{0} & -\widehat{\boldsymbol{d}_2^2} & \boldsymbol{n}^1 \times \boldsymbol{d}_2^2 \\ \boldsymbol{0} & -\widehat{\boldsymbol{d}_3^2} & \boldsymbol{n}^1 \times \boldsymbol{d}_3^2 \end{bmatrix} \tag{6.1.72}$$

In addition to that, the discrete null space matrix for the R pair follows from the mid-point evaluation of (6.1.71), that is,

$$\mathbf{P}^{(R)}(\boldsymbol{q}_n, \boldsymbol{q}_{n+1}) = \boldsymbol{P}^{(R)}(\boldsymbol{q}_{n+\frac{1}{2}}) \tag{6.1.73}$$

Reparametrisation of unknowns

For the R pair the mapping $\boldsymbol{F}_{q_n}^{2,(R)}(\boldsymbol{\mu}^{(R)})$ can be directly obtained from that of the C pair by fixing $u^2 = 0$. Then the incremental rotational motion of the second body relative to the first one is specified by $\vartheta^{(R)} = \theta^2 \in \mathbb{R}$. With regard to (6.1.66) one thus gets

$$\boldsymbol{q}_{n+1}^2 = \boldsymbol{F}_{q_n}^{2,(R)}(\boldsymbol{\mu}^{(R)}) = \begin{bmatrix} \boldsymbol{\varphi}_n^1 + \boldsymbol{u}_\varphi^1 + \exp(\widehat{\boldsymbol{\theta}^1}) \cdot [\boldsymbol{\varrho}_n^1 - \exp\left(\theta^2 (\widehat{\boldsymbol{n}^1})_n\right) \cdot \boldsymbol{\varrho}_n^2] \\ \exp(\widehat{\boldsymbol{\theta}^1}) \cdot \exp\left(\theta^2 (\widehat{\boldsymbol{n}^1})_n\right) \cdot (\boldsymbol{d}_1^2)_n \\ \exp(\widehat{\boldsymbol{\theta}^1}) \cdot \exp\left(\theta^2 (\widehat{\boldsymbol{n}^1})_n\right) \cdot (\boldsymbol{d}_2^2)_n \\ \exp(\widehat{\boldsymbol{\theta}^1}) \cdot \exp\left(\theta^2 (\widehat{\boldsymbol{n}^1})_n\right) \cdot (\boldsymbol{d}_3^2)_n \end{bmatrix} \tag{6.1.74}$$

6.1.7 **Prismatic pair**
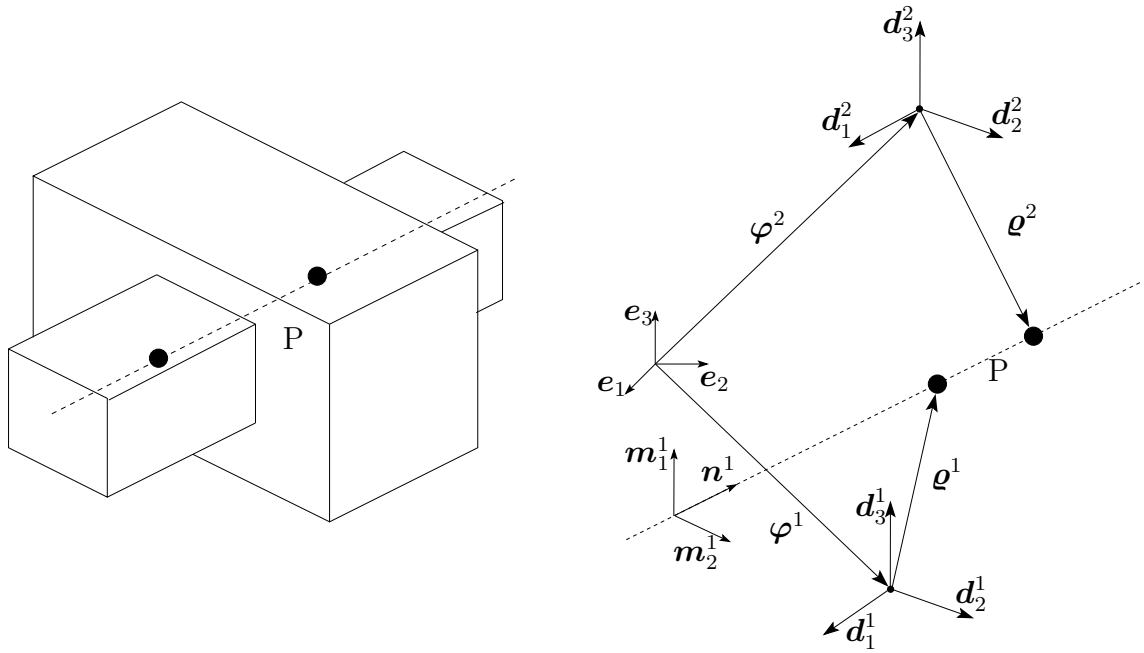
Figure 6.4: Prismatic pair.

In the case of the P pair (Figure 6.4) translational motion of the second body relative to the first one may occur along the axis specified by the unit vector $\boldsymbol{n}^1$, which as before is specified by (6.1.45). Analogous to (6.1.47) one gets the kinematic relationship

$$\boldsymbol{\varphi}^1 + \boldsymbol{\varrho}^1 + u^2 \boldsymbol{n}^1 = \boldsymbol{\varphi}^2 + \boldsymbol{\varrho}^2 \tag{6.1.75}$$

Furthermore, the kinematic constraint

$$\boldsymbol{\omega}^2 = \boldsymbol{\omega}^1 \tag{6.1.76}$$

applies to the P pair.

Constraints and constraint Jacobian

The P pair entails $m_{ext}^{(P)} = 5$ external constraint functions that may be written in the form

$$\boldsymbol{g}_{ext}^{(P)}(\boldsymbol{q}) = \begin{bmatrix} (\boldsymbol{m}_1^1)^T \cdot (\boldsymbol{p}^2 - \boldsymbol{p}^1) \\ (\boldsymbol{m}_2^1)^T \cdot (\boldsymbol{p}^2 - \boldsymbol{p}^1) \\ (\boldsymbol{d}_1^1)^T \cdot \boldsymbol{d}_2^2 - \eta_1 \\ (\boldsymbol{d}_2^1)^T \cdot \boldsymbol{d}_3^2 - \eta_2 \\ (\boldsymbol{d}_3^1)^T \cdot \boldsymbol{d}_1^2 - \eta_3 \end{bmatrix} \tag{6.1.77}$$

where η_i, $i = 1, 2, 3$ are constant and need be consistent with the initial conditions. Again, $\boldsymbol{m}_\kappa^1 \in \mathbb{R}^3$ and $\boldsymbol{p}^\alpha \in \mathbb{R}^3$ are given by (6.1.46) and (6.1.48), respectively. Note that the constraints resulting from the last three components of (6.1.77) conform with (6.1.76).

The constraint Jacobian emanating from (6.1.77) is given by the 5×24 matrix

$$
\boldsymbol{G}_{ext}^{(P)}(\boldsymbol{q}) = \begin{bmatrix}
-(\boldsymbol{m}_1^1)^T & \boldsymbol{G}_{11}^T & \boldsymbol{G}_{12}^T & \boldsymbol{G}_{13}^T & (\boldsymbol{m}_1^1)^T & \varrho_1^2(\boldsymbol{m}_1^1)^T & \varrho_2^2(\boldsymbol{m}_1^1)^T & \varrho_3^2(\boldsymbol{m}_1^1)^T \\
-(\boldsymbol{m}_2^1)^T & \boldsymbol{G}_{21}^T & \boldsymbol{G}_{22}^T & \boldsymbol{G}_{23}^T & (\boldsymbol{m}_2^1)^T & \varrho_1^2(\boldsymbol{m}_2^1)^T & \varrho_2^2(\boldsymbol{m}_2^1)^T & \varrho_3^2(\boldsymbol{m}_2^1)^T \\
\boldsymbol{0}^T & (\boldsymbol{d}_2^2)^T & \boldsymbol{0}^T & \boldsymbol{0}^T & \boldsymbol{0}^T & \boldsymbol{0}^T & (\boldsymbol{d}_1^1)^T & \boldsymbol{0}^T \\
\boldsymbol{0}^T & \boldsymbol{0}^T & (\boldsymbol{d}_3^2)^T & \boldsymbol{0}^T & \boldsymbol{0}^T & \boldsymbol{0}^T & \boldsymbol{0}^T & (\boldsymbol{d}_2^1)^T \\
\boldsymbol{0}^T & \boldsymbol{0}^T & \boldsymbol{0}^T & (\boldsymbol{d}_1^2)^T & \boldsymbol{0}^T & (\boldsymbol{d}_3^1)^T & \boldsymbol{0}^T & \boldsymbol{0}^T
\end{bmatrix} \tag{6.1.78}
$$

where the $\boldsymbol{G}_{\kappa i}$'s are again given by (6.1.51).

Discrete null space matrix

To get proper representations of both the continuous and the discrete null space matrices for the P pair, the previous treatment of the C pair requires slight modification. To this end one essentially has to remove $\dot{\theta}^2$ so that only $\dot{u}^2$ remains to characterise the motion of the second body relative to the first one ($r^{(P)} = 1$). Then (6.1.55) yields

$$
\dot{\boldsymbol{\varphi}}^2 = \dot{\boldsymbol{\varphi}}^1 + \boldsymbol{\omega}^1 \times (\boldsymbol{\varphi}^2 - \boldsymbol{\varphi}^1) + \dot{u}^2 \boldsymbol{n}^1 \tag{6.1.79}
$$

such that

$$
\boldsymbol{P}_{ext}^{2,(P)}(\boldsymbol{q}) = \begin{bmatrix} \boldsymbol{I} & \widehat{\boldsymbol{\varphi}^1 - \boldsymbol{\varphi}^2} & \boldsymbol{n}^1 \\ \boldsymbol{0} & \boldsymbol{I} & \boldsymbol{0} \end{bmatrix} \tag{6.1.80}
$$

Analogous to (6.1.61), the discrete version of (6.1.80) is given by

$$
\mathbf{P}_{ext}^{2,(P)}(\boldsymbol{q}_n, \boldsymbol{q}_{n+1}) = \begin{bmatrix} \boldsymbol{I} & \widehat{\boldsymbol{\varphi}_{n+\frac{1}{2}}^1 - \boldsymbol{\varphi}_{n+\frac{1}{2}}^2} & (\boldsymbol{m}_1^1)_{n+\frac{1}{2}} \times (\boldsymbol{m}_2^1)_{n+\frac{1}{2}} \\ \boldsymbol{0} & \boldsymbol{I} & \boldsymbol{0} \end{bmatrix} \tag{6.1.81}
$$

such that the discrete null space matrix for the P pair can be written as

$$
\mathbf{P}^{(P)}(\boldsymbol{q}_n, \boldsymbol{q}_{n+1}) = \begin{bmatrix} \boldsymbol{P}_{int}^1(\boldsymbol{q}_{n+\frac{1}{2}}^1) & \boldsymbol{0}_{6 \times 1} \\ \boldsymbol{P}_{int}^2(\boldsymbol{q}_{n+\frac{1}{2}}^2) \cdot \mathbf{P}_{ext}^{2,(P)}(\boldsymbol{q}_n, \boldsymbol{q}_{n+1}) \end{bmatrix} \tag{6.1.82}
$$

where

$$
\boldsymbol{P}_{int}^2(\boldsymbol{q}_{n+\frac{1}{2}}^2) \cdot \mathbf{P}_{ext}^{2,(P)}(\boldsymbol{q}_n, \boldsymbol{q}_{n+1}) = \begin{bmatrix} \boldsymbol{I} & \widehat{\boldsymbol{\varphi}_{n+\frac{1}{2}}^1 - \boldsymbol{\varphi}_{n+\frac{1}{2}}^2} & (\boldsymbol{m}_1^1)_{n+\frac{1}{2}} \times (\boldsymbol{m}_2^1)_{n+\frac{1}{2}} \\ \boldsymbol{0} & -(\widehat{\boldsymbol{d}_1^2})_{n+\frac{1}{2}} & \boldsymbol{0} \\ \boldsymbol{0} & -(\widehat{\boldsymbol{d}_2^2})_{n+\frac{1}{2}} & \boldsymbol{0} \\ \boldsymbol{0} & -(\widehat{\boldsymbol{d}_3^2})_{n+\frac{1}{2}} & \boldsymbol{0} \end{bmatrix} \tag{6.1.83}
$$

Reparametrisation of unknowns

The mapping $\boldsymbol{F}_{q_n}^{2,(P)}(\boldsymbol{\mu}^{(P)})$ can be inferred from the corresponding one for the C pair, equation (6.1.66), by setting $\theta^2 = 0$. Accordingly,

$$\boldsymbol{q}_{n+1}^2 = \boldsymbol{F}_{q_n}^{2,(P)}(\boldsymbol{\mu}^{(P)}) = \begin{bmatrix} \boldsymbol{\varphi}_n^1 + \boldsymbol{u}_\varphi^1 + \exp(\widehat{\boldsymbol{\theta}^1}) \cdot [\boldsymbol{\varrho}_n^1 - \boldsymbol{\varrho}_n^2 + (u_n^2 + u^2)\boldsymbol{n}_n^1] \\ \exp(\widehat{\boldsymbol{\theta}^1}) \cdot (\boldsymbol{d}_1^2)_n \\ \exp(\widehat{\boldsymbol{\theta}^1}) \cdot (\boldsymbol{d}_2^2)_n \\ \exp(\widehat{\boldsymbol{\theta}^1}) \cdot (\boldsymbol{d}_3^2)_n \end{bmatrix} \qquad (6.1.84)$$

with incremental unknowns $\boldsymbol{\mu}^{(P)} = (\boldsymbol{u}_\varphi^1, \boldsymbol{\theta}^1, u^2) \in \mathbb{R}^3 \times \mathbb{R}^3 \times \mathbb{R}$.

6.1.8 Planar pair
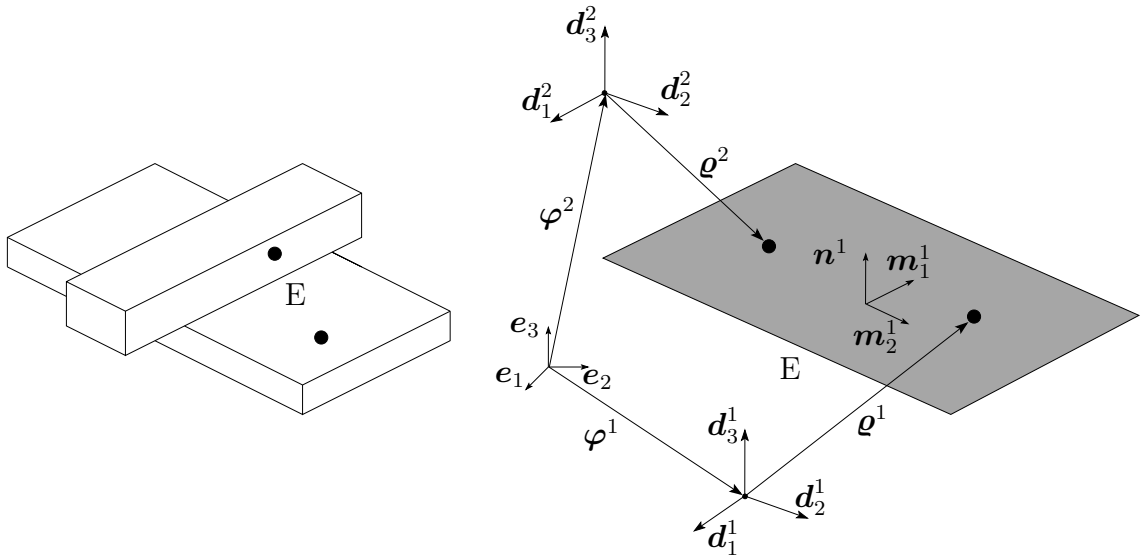
Figure 6.5: Planar pair.

As before in the context of the cylindrical pair, for the E pair (Figure 6.5) use is made of the orthonormal frame $\{\boldsymbol{m}_1^1, \boldsymbol{m}_2^1, \boldsymbol{n}^1\}$, with $\boldsymbol{n}^1 = n_i^1 \boldsymbol{d}_i^1$ and $\boldsymbol{m}_\kappa^1 = (m_\kappa^1)_i \boldsymbol{d}_i^1$. In the present case the motion of the second body relative to the first one can be characterised by $r^{(E)} = 3$ degrees of freedom. Specifically, the second body may rotate about the axis specified by $\boldsymbol{n}^1$ and translate in the plane spanned by $\boldsymbol{m}_1^1$ and $\boldsymbol{m}_2^1$. Correspondingly, the rotational motion can be described by the kinematical relationship

$$\boldsymbol{\omega}^2 = \boldsymbol{\omega}^1 + \dot{\theta}^2 \boldsymbol{n}^1 \qquad (6.1.85)$$

whereas the relative translational motion may be accounted for by two coordinates $(u_1^2, u_2^2) \in \mathbb{R}^2$, such that

$$\boldsymbol{p}^2 = \boldsymbol{p}^1 + u_\kappa^2 \boldsymbol{m}_\kappa^1 \qquad (6.1.86)$$

As before, $\boldsymbol{p}^\alpha = \boldsymbol{\varphi}^\alpha + \boldsymbol{\varrho}^\alpha$ for $\alpha = 1, 2$.

Constraints and constraint Jacobian

The E pair gives rise to $m_{ext}^{(E)} = 3$ external constraint functions that may be written in the form

$$g_{ext}^{(E)}(q) = \begin{bmatrix} (n^1)^T \cdot (p^2 - p^1) \\ (n^1)^T \cdot d_1^2 - \eta_1 \\ (n^1)^T \cdot d_2^2 - \eta_2 \end{bmatrix} \tag{6.1.87}$$

where η_1, η_2 are constant and need be consistent with the initial conditions. Note that the first component of (6.1.87) conforms with (6.1.86), whereas the last two components of (6.1.87) conform with (6.1.85). The constraint Jacobian emanating from (6.1.87) is given by the 3×24 matrix

$$G_{ext}^{(E)}(q) = \begin{bmatrix} -(n^1)^T & G_1^T & G_2^T & G_3^T & (n^1)^T & \varrho_1^2(n^1)^T & \varrho_2^2(n^1)^T & \varrho_3^2(n^1)^T \\ 0^T & n_1^1(d_1^2)^T & n_2^1(d_1^2)^T & n_3^1(d_1^2)^T & 0^T & (n^1)^T & 0^T & 0^T \\ 0^T & n_1^1(d_2^2)^T & n_2^1(d_2^2)^T & n_3^1(d_2^2)^T & 0^T & 0^T & (n^1)^T & 0^T \end{bmatrix} \tag{6.1.88}$$

with

$$G_i = n_i^1(p^2 - p^1) - \varrho_i^1 n^1 \tag{6.1.89}$$

for $i = 1, 2, 3$.

Continuous form of the null space matrix

Differentiating (6.1.86) with respect to time and taking into account (6.1.85) yields

$$\dot{\varphi}^2 = \dot{\varphi}^1 + \omega^1 \times (\varphi^2 - \varphi^1) + \dot{u}_\kappa^2 m_\kappa^1 + \dot{\theta}^2 \varrho^2 \times n^1 \tag{6.1.90}$$

The last equation in conjunction with (6.1.85) indicates that the twist of the second body can be expressed in terms of the independent velocities $\nu^{(E)} = [t^1, \dot{u}_1^2, \dot{u}_2^2, \dot{\theta}^2]^T$, such that $t^{2,(E)} = P_{ext}^{2,(E)} \cdot \nu^{(E)}$. Here the 6×9 matrix $P_{ext}^{2,(E)}$ is given by

$$P_{ext}^{2,(E)}(q) = \begin{bmatrix} I & \widehat{\varphi^1 - \varphi^2} & m_1^1 & m_2^1 & \varrho^2 \times n^1 \\ 0 & I & 0 & 0 & n^1 \end{bmatrix} \tag{6.1.91}$$

Then (6.1.14) yields

$$P_{ext}^{(E)}(q) = \begin{bmatrix} I_{6\times6} & 0_{6\times3} \\ P_{ext}^{2,(E)}(q) \end{bmatrix} \tag{6.1.92}$$

Finally, with regard to (6.1.15), the null space matrix for the E pair is given by

$$P^{(E)}(q) = \begin{bmatrix} P_{int}^1(q) & 0_{6\times2} \\ P_{int}^2(q) \cdot P_{ext}^{2,(E)}(q) \end{bmatrix} \tag{6.1.93}$$

with

$$
\boldsymbol{P}_{int}^2(\boldsymbol{q}) \cdot \boldsymbol{P}_{ext}^{2,(E)}(\boldsymbol{q}) =
\begin{bmatrix}
\boldsymbol{I} & \widehat{\boldsymbol{\varphi}^1 - \boldsymbol{\varphi}^2} & \boldsymbol{m}_1^1 & \boldsymbol{m}_2^1 & \boldsymbol{\varrho}^2 \times \boldsymbol{n}^1 \\
\boldsymbol{0} & -\widehat{\boldsymbol{d}_1^2} & \boldsymbol{0} & \boldsymbol{0} & \boldsymbol{n}^1 \times \boldsymbol{d}_1^2 \\
\boldsymbol{0} & -\widehat{\boldsymbol{d}_2^2} & \boldsymbol{0} & \boldsymbol{0} & \boldsymbol{n}^1 \times \boldsymbol{d}_2^2 \\
\boldsymbol{0} & -\widehat{\boldsymbol{d}_3^2} & \boldsymbol{0} & \boldsymbol{0} & \boldsymbol{n}^1 \times \boldsymbol{d}_3^2
\end{bmatrix}
\tag{6.1.94}
$$

It can be easily checked by a straightforward calculation that the present design procedure for $\boldsymbol{P}_{ext}^{2,(E)}(\boldsymbol{q})$ ensures that

$$
\boldsymbol{G}_{ext}^{(E)}(\boldsymbol{q}) \cdot \boldsymbol{P}_{int}(\boldsymbol{q}) \cdot \boldsymbol{P}_{ext}^{(E)}(\boldsymbol{q}) = \boldsymbol{0}
\tag{6.1.95}
$$

Discrete version of the null space matrix

In the present case the discrete null space matrix does not coincide with $\boldsymbol{P}^{(E)}(\boldsymbol{q}_{n+\frac{1}{2}})$. Instead, it can be easily verified that the choice

$$
\mathsf{P}_{ext}^{2,(E)}(\boldsymbol{q}_n, \boldsymbol{q}_{n+1}) =
$$
$$
\begin{bmatrix}
\boldsymbol{I} & (\widehat{\boldsymbol{\varphi}^1 - \boldsymbol{\varphi}^2})_{n+\frac{1}{2}} & (\boldsymbol{m}_2^1)_{n+\frac{1}{2}} \times (\boldsymbol{n}^1)_{n+\frac{1}{2}} & (\boldsymbol{n}^1)_{n+\frac{1}{2}} \times (\boldsymbol{m}_1^1)_{n+\frac{1}{2}} & \boldsymbol{\varrho}_{n+\frac{1}{2}}^2 \times \boldsymbol{n}_{n+\frac{1}{2}}^1 \\
\boldsymbol{0} & \boldsymbol{I} & \boldsymbol{0} & \boldsymbol{0} & \boldsymbol{n}_{n+\frac{1}{2}}^1
\end{bmatrix}
\tag{6.1.96}
$$

satisfies the design conditions (6.1.24). Finally, in view of (6.1.23), the discrete null space matrix for the E pair assumes the form

$$
\mathsf{P}^{(E)}(\boldsymbol{q}_n, \boldsymbol{q}_{n+1}) =
\begin{bmatrix}
\boldsymbol{P}_{int}^1(\boldsymbol{q}_{n+\frac{1}{2}}^1) & \boldsymbol{0}_{6\times3} \\
\boldsymbol{P}_{int}^2(\boldsymbol{q}_{n+\frac{1}{2}}^2) \cdot \mathsf{P}_{ext}^{2,(E)}(\boldsymbol{q}_n, \boldsymbol{q}_{n+1})
\end{bmatrix}
\tag{6.1.97}
$$

where

$$
\boldsymbol{P}_{int}^2(\boldsymbol{q}_{n+\frac{1}{2}}^2) \cdot \mathsf{P}_{ext}^{2,(E)}(\boldsymbol{q}_n, \boldsymbol{q}_{n+1}) =
$$
$$
\begin{bmatrix}
\boldsymbol{I} & (\widehat{\boldsymbol{\varphi}^1 - \boldsymbol{\varphi}^2})_{n+\frac{1}{2}} & (\boldsymbol{m}_2^1)_{n+\frac{1}{2}} \times (\boldsymbol{n}^1)_{n+\frac{1}{2}} & (\boldsymbol{n}^1)_{n+\frac{1}{2}} \times (\boldsymbol{m}_1^1)_{n+\frac{1}{2}} & \boldsymbol{\varrho}_{n+\frac{1}{2}}^2 \times \boldsymbol{n}_{n+\frac{1}{2}}^1 \\
\boldsymbol{0} & -(\widehat{\boldsymbol{d}_1^2})_{n+\frac{1}{2}} & \boldsymbol{0} & \boldsymbol{0} & \boldsymbol{n}_{n+\frac{1}{2}}^1 \times (\boldsymbol{d}_1^2)_{n+\frac{1}{2}} \\
\boldsymbol{0} & -(\widehat{\boldsymbol{d}_2^2})_{n+\frac{1}{2}} & \boldsymbol{0} & \boldsymbol{0} & \boldsymbol{n}_{n+\frac{1}{2}}^1 \times (\boldsymbol{d}_2^2)_{n+\frac{1}{2}} \\
\boldsymbol{0} & -(\widehat{\boldsymbol{d}_3^2})_{n+\frac{1}{2}} & \boldsymbol{0} & \boldsymbol{0} & \boldsymbol{n}_{n+\frac{1}{2}}^1 \times (\boldsymbol{d}_3^2)_{n+\frac{1}{2}}
\end{bmatrix}
\tag{6.1.98}
$$

Reparametrisation of unknowns

In the present case the configuration of the second body with respect to the first one can be characterised by the incremental variables $\boldsymbol{\vartheta}^{(E)} = (u_1^2, u_2^2, \theta^2) \in \mathbb{R}^3$. Here θ^2 accounts for the incremental relative rotation which may be expressed via the product of exponentials formula

$$
(\boldsymbol{d}_I^2)_{n+1} = \exp(\widehat{\boldsymbol{\theta}^1}) \cdot \exp\left(\theta^2 (\widehat{\boldsymbol{n}^1})_n\right) \cdot (\boldsymbol{d}_I^2)_n
\tag{6.1.99}
$$

Enforcing the external constraints (6.1.86) at the end of the time-step implies

$$\boldsymbol{\varphi}_{n+1}^2 = \boldsymbol{\varphi}_{n+1}^1 + \boldsymbol{\varrho}_{n+1}^1 - \boldsymbol{\varrho}_{n+1}^2 + ((u_\kappa^2)_n + u_\kappa^2)(\boldsymbol{m}_\kappa^1)_{n+1} \tag{6.1.100}$$

Accordingly, the mapping $\boldsymbol{F}_{q_n}^{2,(E)}(\boldsymbol{\mu}^{(E)})$ can be written in the form

$$\boldsymbol{q}_{n+1}^2 = \boldsymbol{F}_{q_n}^{2,(E)}(\boldsymbol{\mu}^{(E)}) = \begin{bmatrix} \boldsymbol{\varphi}_n^1 + \boldsymbol{u}_\varphi^1 + \exp(\widehat{\boldsymbol{\theta}^1}) \cdot [\boldsymbol{\varrho}_n^1 - \exp\left(\theta^2(\widehat{\boldsymbol{n}^1})_n\right) \cdot \boldsymbol{\varrho}_n^2 + ((u_\kappa^2)_n + u_\kappa^2)(\boldsymbol{m}_\kappa^1)_n] \\ \exp(\widehat{\boldsymbol{\theta}^1}) \cdot \exp\left(\theta^2(\widehat{\boldsymbol{n}^1})_n\right) \cdot (\boldsymbol{d}_1^2)_n \\ \exp(\widehat{\boldsymbol{\theta}^1}) \cdot \exp\left(\theta^2(\widehat{\boldsymbol{n}^1})_n\right) \cdot (\boldsymbol{d}_2^2)_n \\ \exp(\widehat{\boldsymbol{\theta}^1}) \cdot \exp\left(\theta^2(\widehat{\boldsymbol{n}^1})_n\right) \cdot (\boldsymbol{d}_3^2)_n \end{bmatrix} \tag{6.1.101}$$

6.1.9 Numerical examples

Revolute pair
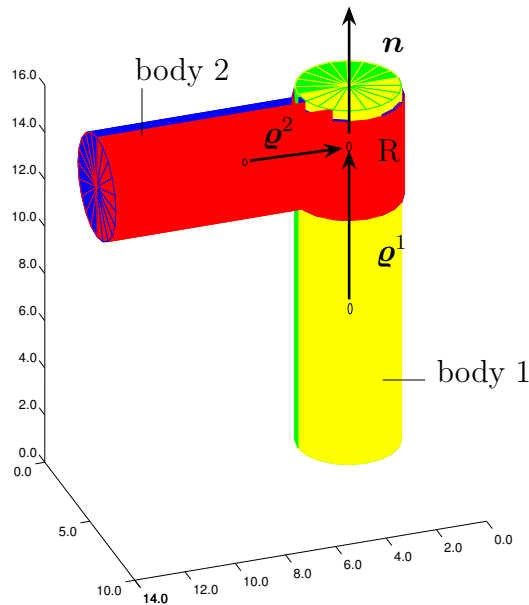
Figure 6.6: Initial configuration of the revolute pair.

First of all, the free flight of a revolute pair (Figure 6.6, see also Figure 6.3) is investigated. The first body consists of a cylinder of length $l^1 = 15$, radius $r^1 = 2$ and mass $M_\varphi^1 = 100$. The second body consists of two parts, a hollow cylinder of length $l^2 = 4.2$, outer radius $r_o^2 = 2.1$, inner radius $r_i^2 = 2$ and mass $M_\varphi^{21} = 1$. The hollow cylinder is slipped over the first body and connected to a solid cylinder of length $l^3 = 10$ and radius $r^3 = 2.1$ and mass $M_\varphi^{22} = 1$. Consequently, the total mass of the second body is given by $M_\varphi^2 = 2$ and the principal values of the inertia tensor with respect to the center of mass are given by

$$[J_i^1] = [1975, 1975, 200] \tag{6.1.102}$$

and

$$[J_i^2] = [12.64083, 32.3717, 26.14083] \tag{6.1.103}$$

respectively. Relative to the respective body frame the location of the revolute joint is characterised by

$$[\varrho_i^1] = [0, 0, 5] \qquad [\varrho_i^2] = [-2.5, 0, 0] \tag{6.1.104}$$

Furthermore, the unit vector (6.1.45) is specified by

$$[n_i^1] = [0, 0, 1] \tag{6.1.105}$$

The initial configuration of the revolute pair is characterised by $\boldsymbol{\varphi}^\alpha = \varphi_i^\alpha \boldsymbol{e}_i$ with

$$[\varphi_i^1] = [3, 3, 8] \qquad [\varphi_i^2] = [5.5, 3, 13] \tag{6.1.106}$$

along with

$$\boldsymbol{d}_I^1 = \boldsymbol{e}_I \qquad \boldsymbol{d}_I^2 = \boldsymbol{e}_I \tag{6.1.107}$$

for $I = 1, 2, 3$. The corresponding consistent initial relative rotation is $\theta^2 = 0$. Consistent initial velocities can be computed by using the null space matrix (6.1.71), such that

$$\dot{\boldsymbol{q}} = \boldsymbol{P}^{(R)}(\boldsymbol{q}) \cdot \boldsymbol{\nu}^{(R)} \tag{6.1.108}$$

where the independent generalised velocities are specified by

$$\boldsymbol{\nu}^{(R)} = \begin{bmatrix} \dot{\boldsymbol{\varphi}}^1 \\ \boldsymbol{\omega}^1 \\ \dot{\theta}^2 \end{bmatrix} = \begin{bmatrix} \boldsymbol{0} \\ 10 \\ -20 \\ -20 \\ -15 \end{bmatrix} \tag{6.1.109}$$

No external forces are acting on the R pair such that the total energy and the vector of angular momentum are first integrals of the motion, see Figure 6.8. To illustrate the motion of the R pair, Figure 6.7 shows some snapshots at $t \in \{0.06, 0.08, 0.11, 0.15, 0.17, 0.18\}$. Furthermore, the evolution of the relative rotation $\theta^2(t)$ is depicted in Figure 6.9.

Table 6.2 reveals that the implementation of the constrained scheme (3.2.7) leads to 41 unknowns, whereas the discrete null space method with nodal reparametrisation (3.2.44) yields a reduction to 7 unknowns. Furthermore, from Table 6.2 the condition number of the iteration matrix for the constrained scheme and the reduced scheme can be compared. Accordingly, the condition number of the reduced scheme is of constant and moderate value, whereas the iteration matrix of the constrained scheme becomes more and more ill-conditioned for decreasing time-steps.

The second-order accuracy of the d'Alembert-type scheme with nodal reparametrisation (3.2.44) can be observed in Figure 6.10. The relative error in the phase variable $e_z = \|\boldsymbol{z} - \boldsymbol{z}_{ref}\| / \|\boldsymbol{z}_{ref}\|$ at $t = 2$ drops off quadratically as the time-step decreases. The diagram on the left hand side shows the convergence to a reference solution calculated with the d'Alembert-type scheme with nodal reparametrisation using a time-step $h = 10^{-5}$, thus it represents the consistency of the scheme. The diagram on the right hand side shows the convergence to a reference solution calculated with the constrained scheme (3.2.7) using a time-step $h = 10^{-5}$. It confirms the statement of Proposition 3.2.12.
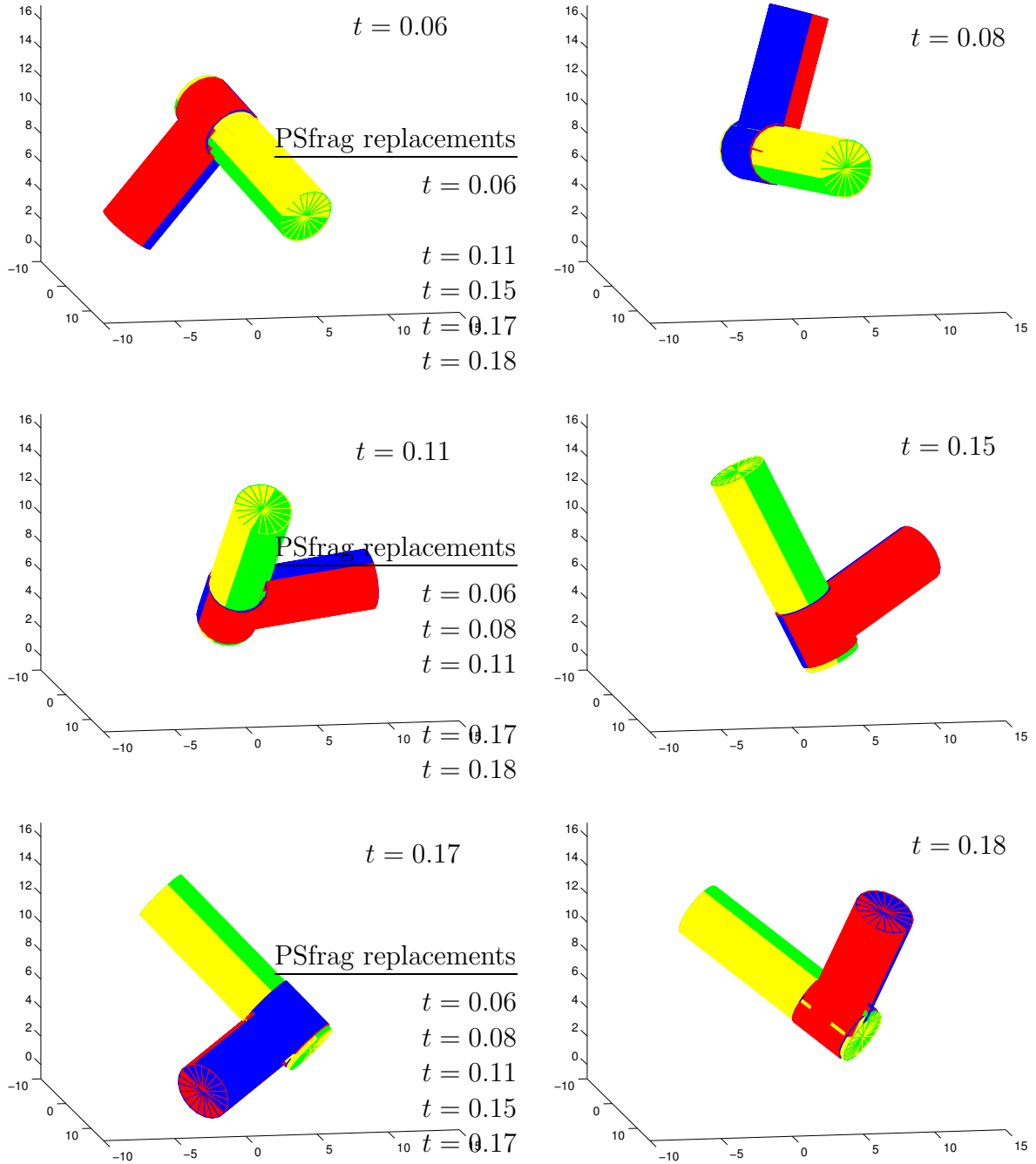
Figure 6.7: Revolute pair: snapshots of the motion at $t \in \{0.06, 0.08, 0.11, 0.15, 0.17, 0.18\}$.
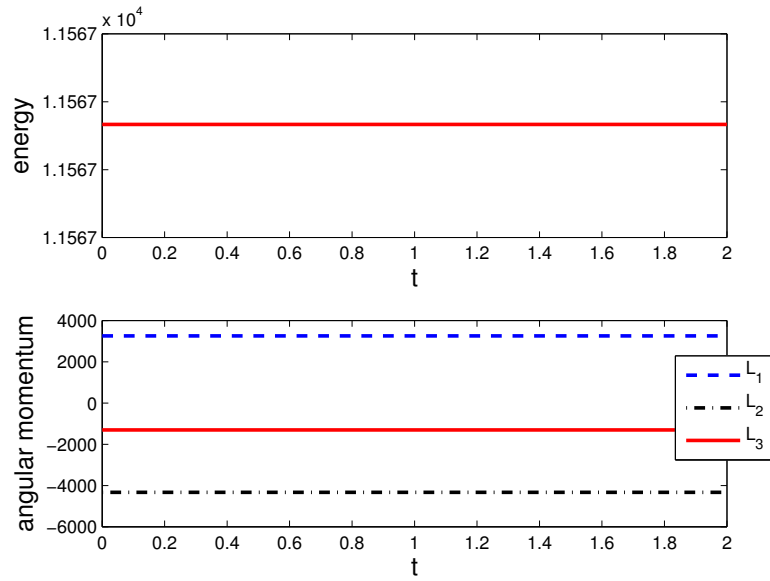
Figure 6.8: Revolute pair: energy and components of angular momentum vector $\boldsymbol{L} = L_i \boldsymbol{e}_i$ ($h = 0.01$).

PSfrag replacements
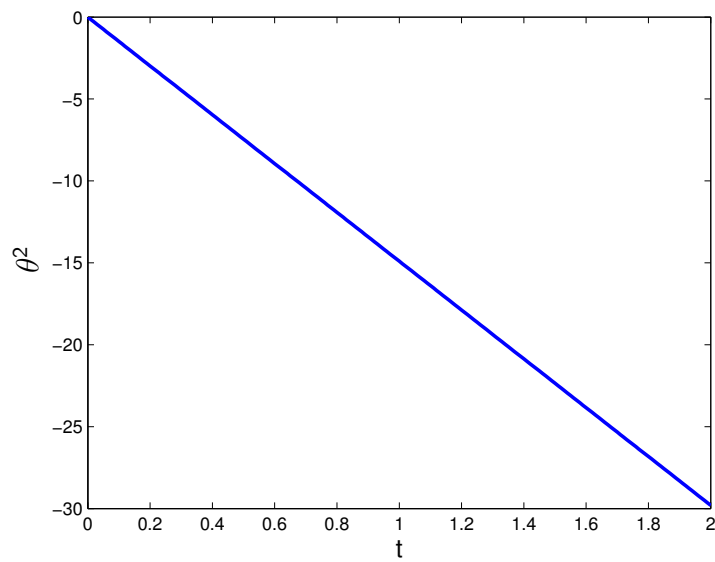
Figure 6.9: Revolute pair: relative coordinate $\theta^2(t)$ ($h = 0.01$).
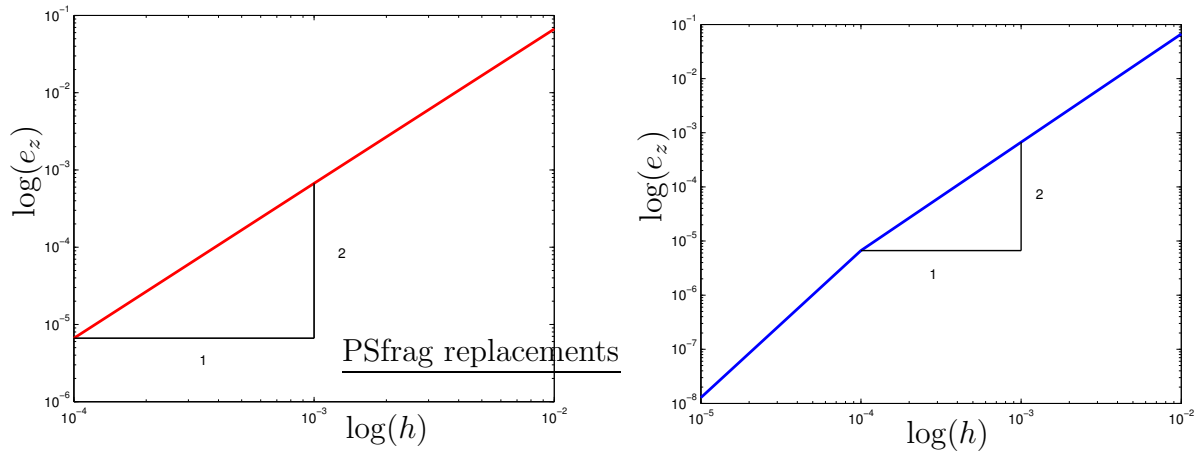
Figure 6.10: Revolute pair: relative error of phase variable with respect to a reference solution ($h = 10^{-5}$) calculated with the d'Alembert-type scheme with nodal reparametrisation (left) and with the constrained scheme (right).

Table 6.2: Comparison of constrained scheme to d'Alembert-type scheme with nodal reparametrisation for the example 'revolute pair'.

	constrained	d'Alembert
number of unknowns $n = 24 \quad m = 17$	41	7
CPU-time	5.8	1
condition number $h = 10^{-2}$ $h = 10^{-3}$ $h = 10^{-4}$	10^{13} 10^{16} 10^{19}	10^{2} 10^{2} 10^{2}

Cylindrical pair

PSfrag replacements
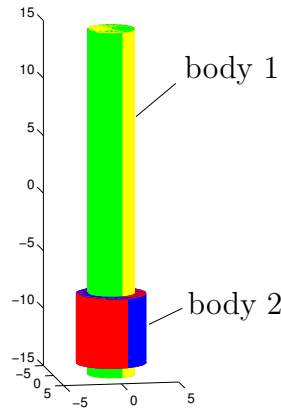
Figure 6.11: Initial configuration of the cylindrical pair.

The free flight of a cylindrical pair (Figure 6.11, see also Figure 6.2) is investigated next. The first body consists of a cylinder of length $l^1 = 30$, radius $r^1 = 2$ and mass $M^1_\varphi = 4$. The second body is modelled as a hollow cylinder of length $l^2 = 6$, outer radius $r^2_o = 3$, inner radius $r^2_i = 2$ and mass $M^2_\varphi = 3$. The principal values of the inertia tensor with respect to the center of mass are given by

$$[J^1_i] = [304, 304, 8] \tag{6.1.110}$$

and

$$[J^2_i] = [18.75, 18.75, 19.5] \tag{6.1.111}$$

respectively. The cylindrical joints are located in the center of mass of each body. Consequently, relative to the respective body frame the location is characterised by

$$[\varrho^1_i] = [0, 0, 0] \qquad [\varrho^2_i] = [0, 0, 0] \tag{6.1.112}$$

Furthermore, the unit vector (6.1.45) is specified by

$$[n^1_i] = [0, 0, 1] \tag{6.1.113}$$

The initial configuration of the cylindrical pair is characterised by $\boldsymbol{\varphi}^\alpha = \varphi^\alpha_i \boldsymbol{e}_i$ with

$$[\varphi^1_i] = [0, 0, 0] \qquad [\varphi^2_i] = [0, 0, -11] \tag{6.1.114}$$

along with

$$\boldsymbol{d}^1_I = \boldsymbol{e}_I \qquad \boldsymbol{d}^2_I = \boldsymbol{e}_I \tag{6.1.115}$$

for $I = 1, 2, 3$. Note that corresponding consistent initial relative coordinates are $u^2 = -11$ and $\theta^2 = 0$. Consistent initial velocities can be computed by using the null space matrix (6.1.58), such that

$$\dot{\boldsymbol{q}} = \boldsymbol{P}^{(C)}(\boldsymbol{q}) \cdot \boldsymbol{\nu}^{(C)} \tag{6.1.116}$$

where the independent generalised velocities are specified by

$$
\boldsymbol{\nu}^{(C)} = \begin{bmatrix} \dot{\boldsymbol{\varphi}}^1 \\ \boldsymbol{\omega}^1 \\ \dot{u}^2 \\ \dot{\theta}^2 \end{bmatrix} = \begin{bmatrix} 0 \\ 50 \\ 0 \\ -1 \\ -1.5 \\ 0 \\ 35.5 \\ 100 \end{bmatrix} \tag{6.1.117}
$$

No external forces are acting on the C pair such that the total energy and the vector of angular momentum are first integrals of the motion, see Figure 6.13. To illustrate the motion of the C pair, Figure 6.12 shows some snapshots at $t \in \{0.1, 0.3, 0.7\}$. Furthermore, the evolution of the relative degrees of freedom $u^2(t)$ and $\theta^2(t)$ is depicted in Figure 6.14. From Table 6.3, the condition number of the iteration matrix for the constrained scheme and the reduced scheme can be compared. Accordingly, the reduced scheme is well conditioned for all time-steps, whereas the condition number of the constrained scheme increases heavily for decreasing time-steps. Note that the implementation of the constrained scheme (3.2.7) leads to 40 unknowns, whereas the discrete null space method with nodal reparametrisation (3.2.44) yields a reduction to 8 unknowns.
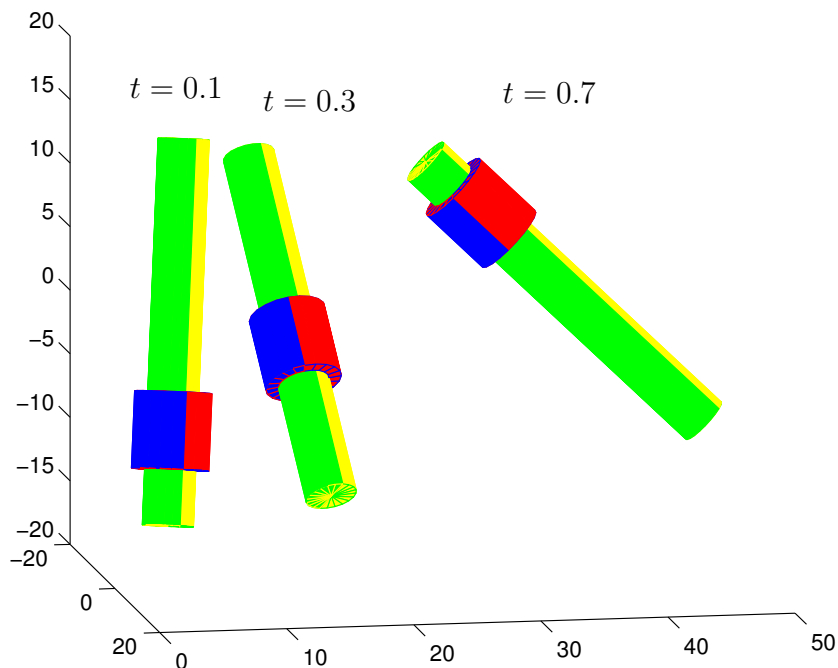
Figure 6.12: Cylindrical pair: snapshots of the motion at $t = 0.1$, $t = 0.3$, $t = 0.7$.
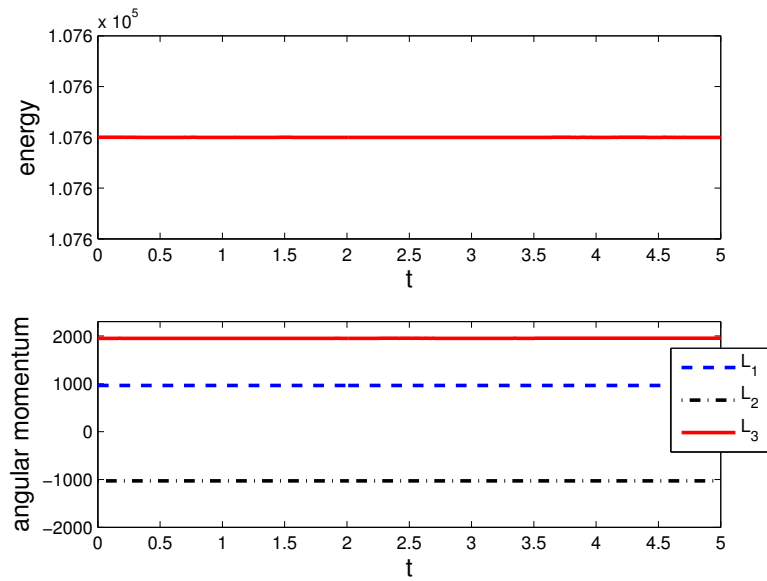
Figure 6.13: Cylindrical pair: energy and components of angular momentum vector $\boldsymbol{L} = L_i \boldsymbol{e}_i$ ($h = 0.01$).

PSfrag replacements
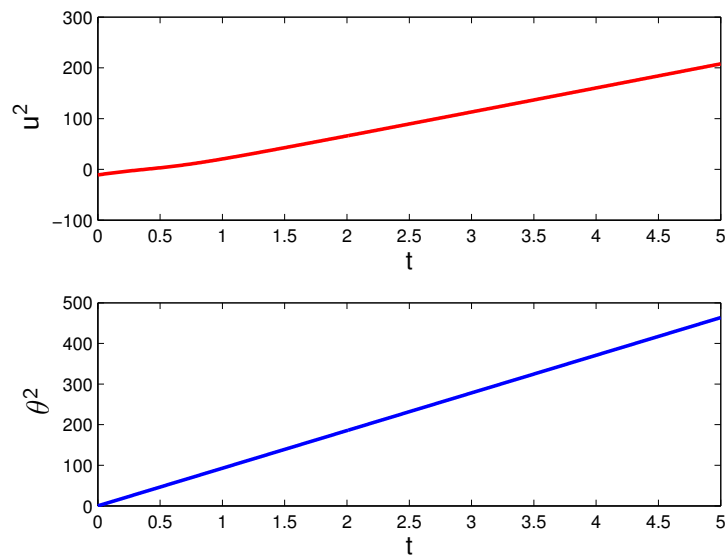
Figure 6.14: Cylindrical pair: relative coordinates $u^2(t)$ and $\theta^2(t)$ ($h = 0.01$).

Table 6.3: Comparison of constrained scheme to d'Alembert-type scheme with nodal reparametrisation for the example 'cylindrical pair'.

	constrained	d'Alembert
number of unknowns $n = 24 \quad m = 16$	40	8
CPU-time	1.2	1
condition number $h = 10^{-2}$ $h = 10^{-3}$ $h = 10^{-4}$	10^{11} 10^{14} 10^{17}	10^2 10^2 10^2

Planar pair

PSfrag replacements
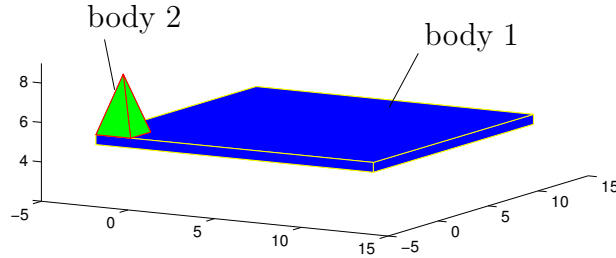
Figure 6.15: Initial configuration of the planar pair.

Now the free flight of a planar pair (Figure 6.15, see also Figure 6.5) is investigated. The E pair consists of a parallelepiped of mass $M_\varphi^1 = 5$ and side lengths $l_x^1 = l_y^1 = 16$, $l_z^1 = 0.5$, such that the principal values of the inertia tensor with respect to the center of mass are given by

$$[J_i^1] = \left[\frac{5125}{48}, \frac{5125}{48}, \frac{640}{3} \right] \tag{6.1.118}$$

The second body is modelled as a pyramid with mass $M_\varphi^2 = 2$, side length of the square base $l_x^2 = l_y^2 = 2$ and height $l_z^2 = 3$, leading to the principal values of the inertia tensor with respect to the center of mass

$$[J_i^2] = \left[\frac{43}{40}, \frac{43}{40}, \frac{4}{5} \right] \tag{6.1.119}$$

The location of the planar joint relative to the respective body frame is characterised by

$$[\varrho_i^1] = [0, 0, 0.25] \qquad [\varrho_i^2] = [0, 0, -1] \tag{6.1.120}$$

Furthermore, the orthonormal frame needed for the description of the relative motion is specified by

$$[n_i^1] = [0, 0, 1] \qquad [(m_1^1)_i] = [1, 0, 0] \qquad [(m_2^1)_i] = [0, 1, 0] \tag{6.1.121}$$

such that the pyramid is constrained to slide on the top surface of the parallelepiped. The initial configuration of the planar pair is characterised by $\varphi^\alpha = \varphi_i^\alpha e_i$ with

$$[\varphi_i^1] = [5, 5, 5] \qquad [\varphi_i^2] = [-2, -2, 6.25] \tag{6.1.122}$$

along with

$$d_I^1 = e_I \qquad d_I^2 = e_I \tag{6.1.123}$$

for $I = 1, 2, 3$. Correspondingly, consistent initial values for the relative coordinates are given by

$$u_1^2 = -7 \qquad u_2^2 = -7 \qquad \theta^2 = 0 \tag{6.1.124}$$

Consistent initial velocities are specified by using the null space matrix (6.1.93), so that

$$\dot{\boldsymbol{q}} = \boldsymbol{P}^{(E)}(\boldsymbol{q}) \cdot \boldsymbol{\nu}^{(E)} \tag{6.1.125}$$

with independent generalised velocities

$$\boldsymbol{\nu}^{(E)} = \begin{bmatrix} \dot{\boldsymbol{\varphi}}^1 \\ \boldsymbol{\omega}^1 \\ \dot{u}_1^2 \\ \dot{u}_2^2 \\ \dot{\theta}^2 \end{bmatrix} = \begin{bmatrix} \mathbf{0} \\ 20 \\ 20 \\ -10 \\ 150 \\ -120 \\ -60 \end{bmatrix} \tag{6.1.126}$$

Note that, for clearness of exposition, the initial velocity of the mass center of the first body has been set to zero ($\dot{\boldsymbol{\varphi}}^1 = \mathbf{0}$). Snapshots of the planar pair at consecutive instants illustrate the simulated motion in Figure 6.16. Since no external forces are acting on the planar pair, both the energy and the vector of angular momentum are conserved quantities. The corresponding algorithmic conservation properties are confirmed in Figure 6.17. Furthermore, Figure 6.18 depicts the evolution of the relative coordinates specifying the configuration of the second body relative to the first one.

Table 6.4 again verifies that the condition number of the iteration matrix can be significantly improved by applying the discrete null space method. In this connection, recall that the implementation of the constrained scheme (3.2.7) is based on $n + m^{(E)} = 24 + 15 = 39$ unknowns, whereas the application of the discrete null space method with nodal reparametrisation (3.2.44) yields a reduction to $n - m^{(E)} = 9$ unknowns. This has an impact on the computational costs, which are about five times higher for the constrained scheme.
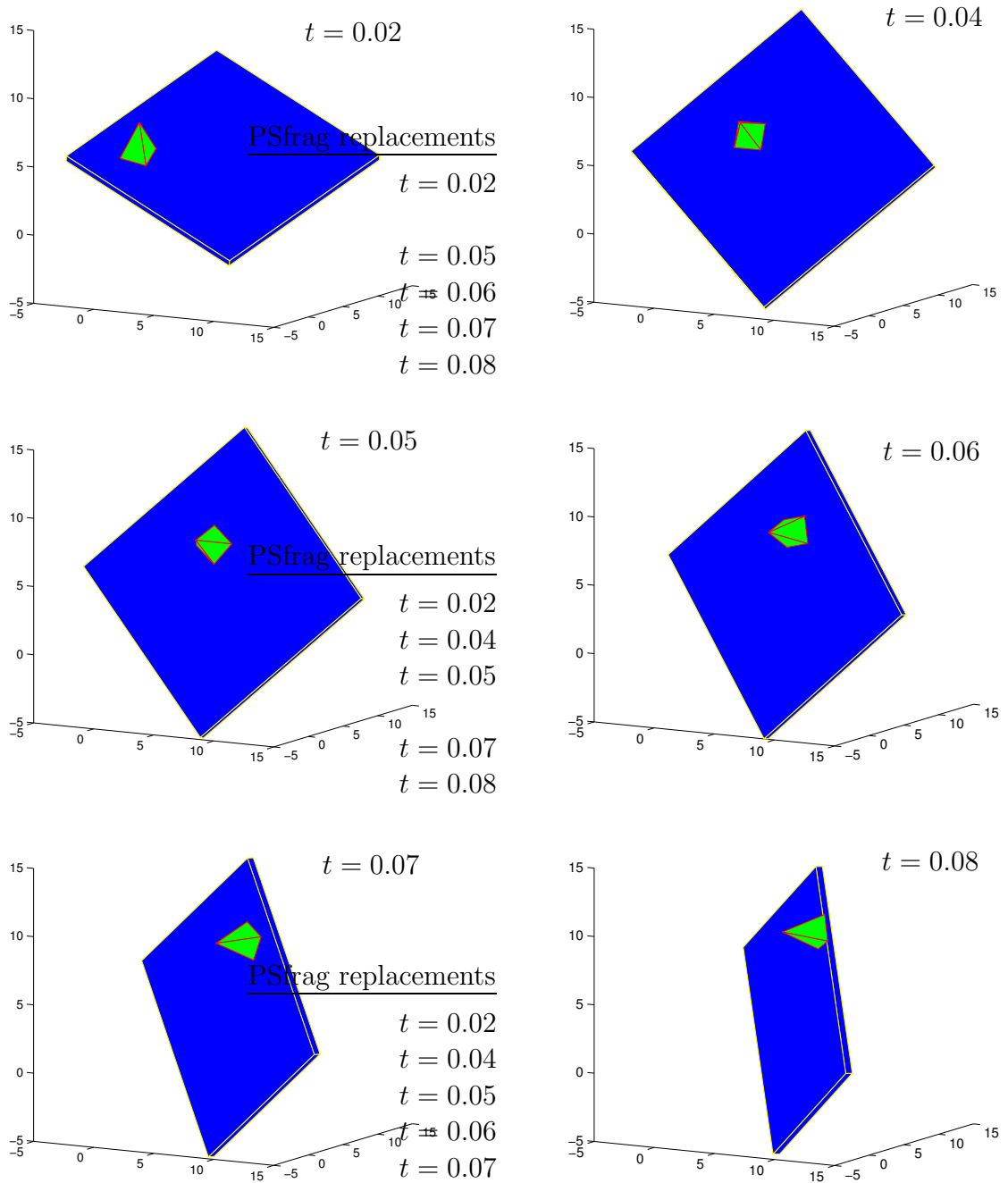
Figure 6.16: Planar pair: snapshots of the motion at $t \in \{0.02, 0.04, 0.05, 0.06, 0.07, 0.08\}$.
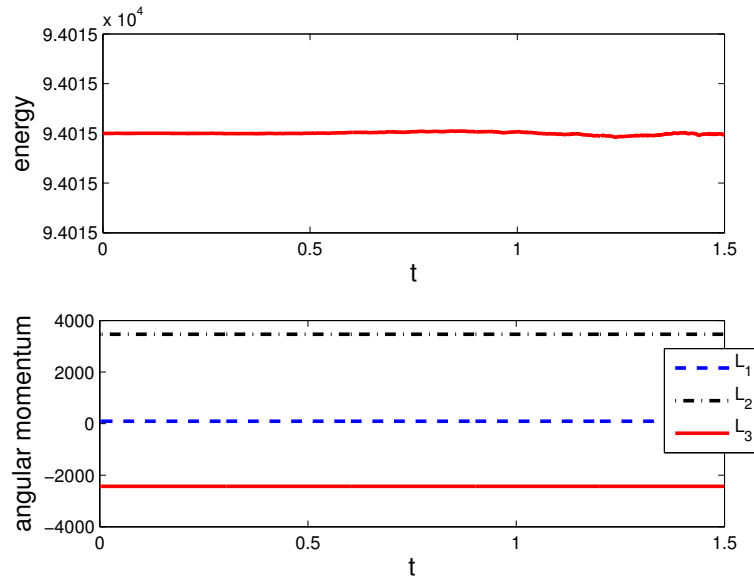
Figure 6.17: Planar pair: energy and components of angular momentum vector $\boldsymbol{L} = L_i \boldsymbol{e}_i$ ($h = 0.001$).
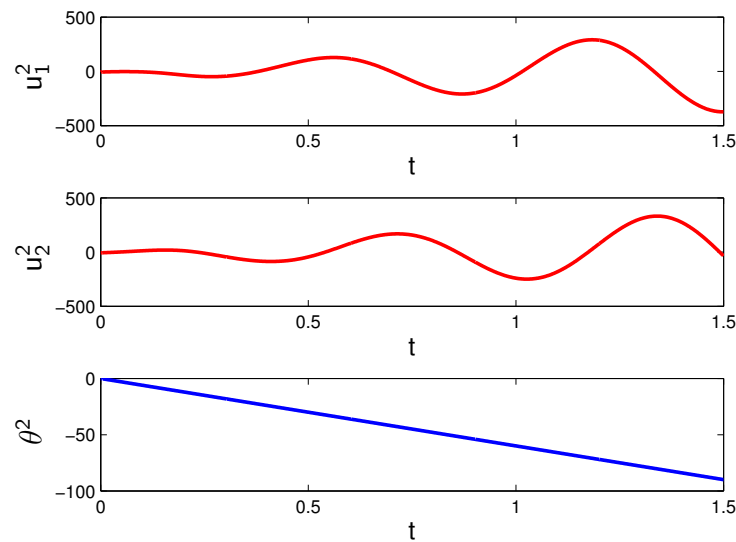
Figure 6.18: Planar pair: relative coordinates $u_1^2(t)$, $u_2^2(t)$ and $\theta^2(t)$ ($h = 0.001$).

Table 6.4: Comparison of constrained scheme to d'Alembert-type scheme with nodal reparametrisation for the example 'planar pair'.

	constrained	d'Alembert
number of unknowns $n = 24 \quad m = 15$	39	9
CPU-time	4.9	1
condition number $h = 10^{-2}$	10^{10}	10^2
$h = 10^{-3}$	10^{13}	10^2
$h = 10^{-4}$	10^{16}	10^2
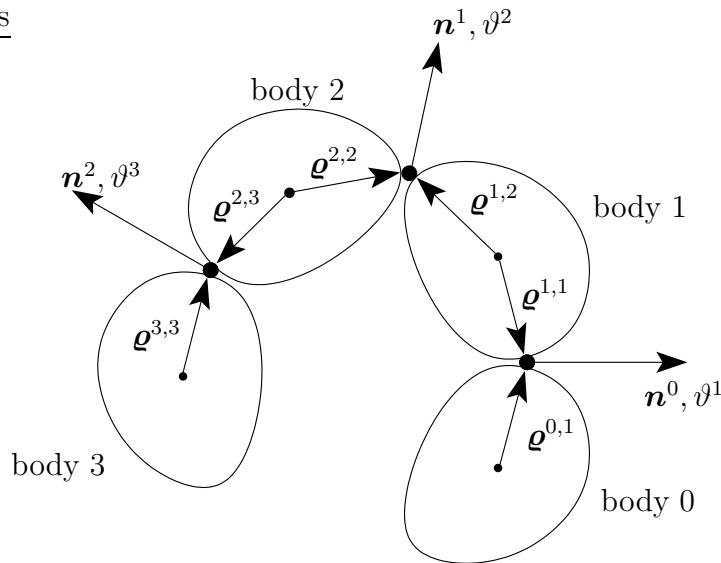
Figure 6.19: Schematic illustration of a simple open kinematic chain.

6.2 Simple kinematic chains

Combinations of kinematic pairs constitute kinematic chains. Only simple kinematic chains, where each link is coupled to maximal two other links are considered in this work. If every link is coupled to exactly two other links, the resulting closed chain is also called linkage. An open kinematic chain, where precisely two links, the end links, are coupled to only one other link is also termed manipulator. From the rich robotics terminology, only the notation relevant for the following investigations are introduced, further discussion on the subject can be found e.g. in [Ange 88, Ange 97, Gera 01, Schi 86, Eich 98]. The Denavit-Hartenberg nomenclature described in the second and third reference is a powerful notation to describe the architecture of simple kinematic chains consisting of elementary kinematic pairs, i.e. of revolute and prismatic pairs. Its variable applicability exceeds the frame of the following investigations in kinematic chains, thus only parts of the notation are introduced.

6.2.1 Open kinematic chains

Simple open kinematic chains, that can be described as an extension of the previous treatment of lower kinematic pairs, are considered in this section. In particular, only chains consisting of the elementary R and P pair are considered, since all other kinematic couplings can be described as a combination of those.

Let a serial manipulator, as depicted schematically in Figure 6.19, consist of $N + 1$ rigid bodies numbered by $\alpha = 0, \ldots, N$ and N axes $\boldsymbol{n}^0, \ldots \boldsymbol{n}^{N-1}$, where corresponding to (6.1.45), $\boldsymbol{n}^\alpha$ is specified in the α-th body frame by

$$\boldsymbol{n}^\alpha = n_i^\alpha \boldsymbol{d}_i^\alpha \tag{6.2.1}$$

The N joints connecting the bodies in the simple open kinematic chain are numbered by $\alpha = 1, \ldots, N$ and corresponding to (6.1.28) the location of the α-th joint in the $(\alpha - 1)$-st
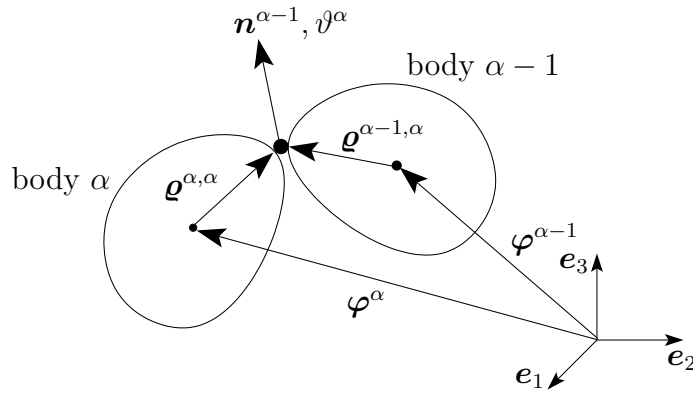
Figure 6.20: Pair in a simple open kinematic chain.

and α-th body is characterised by

$$\boldsymbol{\varrho}^{\alpha-1,\alpha} = \varrho_i^{\alpha-1}\boldsymbol{d}_i^{\alpha-1} \qquad \boldsymbol{\varrho}^{\alpha,\alpha} = \varrho_i^{\alpha}\boldsymbol{d}_i^{\alpha} \tag{6.2.2}$$

Assuming that none of the links are fixed in space, the manipulator can be described in terms of $n = 12(N+1)$ redundant coordinates

$$\boldsymbol{q}(t) = \begin{bmatrix} \boldsymbol{q}^0(t) \\ \vdots \\ \boldsymbol{q}^N(t) \end{bmatrix} \in \mathbb{R}^n \tag{6.2.3}$$

generalising (6.1.1). The rigidity of each link gives rise to six internal constraints $\boldsymbol{g}_{int}^{\alpha}(\boldsymbol{q}^{\alpha}) \in \mathbb{R}^6$ of the form (4.3.3) along with constraint Jacobians $\boldsymbol{G}_{int}^{\alpha}(\boldsymbol{q}^{\alpha}) \in \mathbb{R}^{6\times 12}$ of the form (4.3.4) for $\alpha = 0, \ldots, N$. Similar to (6.1.2) and (6.1.3) they can be combined to the $m_{int} = 6(N+1)$-dimensional vector of internal constraints $\boldsymbol{g}_{int}(\boldsymbol{q})$ and the $m_{int} \times n$ internal constraint Jacobian matrix $\boldsymbol{G}_{int}(\boldsymbol{q})$.

The coupling of two neighbouring links in Figure 6.20 by a revolute or prismatic joint yields five external constraints $\boldsymbol{g}_{ext}^{\alpha}([\boldsymbol{q}^{\alpha-1}, \boldsymbol{q}^{\alpha}]^T) \in \mathbb{R}^5$ with constraint Jacobians $\boldsymbol{G}_{ext}^{\alpha}([\boldsymbol{q}^{\alpha-1}, \boldsymbol{q}^{\alpha}]^T) \in \mathbb{R}^{5\times 24}$ given in (6.1.67) and (6.1.68) for the R pair and in (6.1.77) and (6.1.78) for the P pair respectively. Similar to (6.1.4) and (6.1.5) all $m^o = m_{int} + m_{ext}^o = 6(N+1) + 5N$ constraints pertaining to the open loop system and the corresponding constraint Jacobians can be combined to

$$\boldsymbol{g}^o(\boldsymbol{q}) = \begin{bmatrix} \boldsymbol{g}_{int}(\boldsymbol{q}) \\ \boldsymbol{g}_{ext}^o(\boldsymbol{q}) \end{bmatrix} \in \mathbb{R}^{m^o} \qquad \boldsymbol{G}^o(\boldsymbol{q}) = \begin{bmatrix} \boldsymbol{G}_{int}(\boldsymbol{q}) \\ \boldsymbol{G}_{ext}^o(\boldsymbol{q}) \end{bmatrix} \in \mathbb{R}^{m^o \times n} \tag{6.2.4}$$

The Hamiltonian for the open kinematic chain takes the separable form given in (3.2.4) with the constant mass matrix

$$\boldsymbol{M} = \begin{bmatrix} \boldsymbol{M}^0 & \boldsymbol{0} & \cdots & \boldsymbol{0} \\ \boldsymbol{0} & \boldsymbol{M}^1 & \cdots & \boldsymbol{0} \\ \vdots & \vdots & \ddots & \vdots \\ \boldsymbol{0} & \boldsymbol{0} & \cdots & \boldsymbol{M}^N \end{bmatrix} \tag{6.2.5}$$

where each submatrix $\boldsymbol{M}^{\alpha} \in \mathbb{R}^{12\times 12}$ coincides with (4.3.8).

Accordingly, the continuous constrained Hamiltonian equations can be inferred directly from the procedure presented in Section 2.3 and corresponding time-stepping schemes can be chosen from Section 3.2. Note that using the Lagrange multiplier method, the time-stepping scheme (3.2.5) is $n + m^o = (23N + 18)$-dimensional. Opposite to that, the simple open kinematic chain has $n - m^o = N + 6$ degrees of freedom.

6.2.2 Null space method

The first step in the reduction procedure according to the null space method for lower kinematic pairs presented in Section 6.1.2 is the introduction of the α-th bodies twist $\boldsymbol{t}^\alpha \in \mathbb{R}^6$ given in (6.1.8). Then the redundant velocities of $N + 1$ free rigid bodies can be expressed in terms of the twist $\boldsymbol{t} \in \mathbb{R}^{6(N+1)}$ according to $\dot{\boldsymbol{q}} = \boldsymbol{P}_{int}(\boldsymbol{q}) \cdot \boldsymbol{t}$ where the $12(N + 1) \times 6(N + 1)$ internal null space matrix

$$\boldsymbol{P}_{int}(\boldsymbol{q}) = \begin{bmatrix} \boldsymbol{P}_{int}^0(\boldsymbol{q}^0) & \boldsymbol{0} & \cdots & \boldsymbol{0} \\ \boldsymbol{0} & \boldsymbol{P}_{int}^1(\boldsymbol{q}^1) & \cdots & \boldsymbol{0} \\ \vdots & \vdots & \ddots & \vdots \\ \boldsymbol{0} & \boldsymbol{0} & \cdots & \boldsymbol{P}_{int}^N(\boldsymbol{q}^N) \end{bmatrix} \tag{6.2.6}$$

consists of submatrices $\boldsymbol{P}_{int}^\alpha(\boldsymbol{q}^\alpha)$ of the form (6.1.10).

The treatment of the revolute pair in Section 6.1.6 and of the prismatic pair in Section 6.1.7 can be easily generalised to the kinematic chain at hand. Let the α-th pair in the chain be a revolute pair. Then using $\boldsymbol{P}_{ext}^{\alpha,(R)}(\boldsymbol{q})$ of the form (6.1.70), the relationship between the α-th and $(\alpha - 1)$-st body's twist can be written as

$$\boldsymbol{t}^\alpha = \boldsymbol{P}_{ext}^{\alpha,(R)}(\boldsymbol{q}) \cdot \begin{bmatrix} \boldsymbol{t}^{\alpha-1} \\ \dot{\theta}^\alpha \end{bmatrix} \tag{6.2.7}$$

Partitioning $\boldsymbol{P}_{ext}^{\alpha,(R)}(\boldsymbol{q}) = [\boldsymbol{P}_{ext}^{\alpha,(R),a}(\boldsymbol{q}), \boldsymbol{P}_{ext}^{\alpha,(R),b}(\boldsymbol{q})]$, with $\boldsymbol{P}_{ext}^{\alpha,(R),a}(\boldsymbol{q}) \in \mathbb{R}^{6\times6}$ and $\boldsymbol{P}_{ext}^{\alpha,(R),b}(\boldsymbol{q}) \in \mathbb{R}^{6\times1}$, equation (6.2.7) may be rewritten as

$$\boldsymbol{t}^\alpha = \boldsymbol{P}_{ext}^{\alpha,(R),a}(\boldsymbol{q}) \cdot \boldsymbol{t}^{\alpha-1} + \boldsymbol{P}_{ext}^{\alpha,(R),b}(\boldsymbol{q}) \cdot \dot{\theta}^\alpha \tag{6.2.8}$$

where

$$\boldsymbol{P}_{ext}^{\alpha,(R),a}(\boldsymbol{q}) = \begin{bmatrix} \boldsymbol{I} & \widehat{\boldsymbol{\varrho}^{\alpha,\alpha} - \boldsymbol{\varrho}^{\alpha-1,\alpha}} \\ \boldsymbol{0} & \boldsymbol{I} \end{bmatrix} \qquad \boldsymbol{P}_{ext}^{\alpha,(R),b}(\boldsymbol{q}) = \begin{bmatrix} \boldsymbol{\varrho}^{\alpha,\alpha} \times \boldsymbol{n}^{\alpha-1} \\ \boldsymbol{n}^{\alpha-1} \end{bmatrix} \tag{6.2.9}$$

Similarly for the α-th pair being prismatic, using $\boldsymbol{P}_{ext}^{\alpha,(P)}(\boldsymbol{q})$ of the form (6.1.80) yields

$$\boldsymbol{t}^\alpha = \boldsymbol{P}_{ext}^{\alpha,(P)}(\boldsymbol{q}) \cdot \begin{bmatrix} \boldsymbol{t}^{\alpha-1} \\ \dot{u}^\alpha \end{bmatrix} \tag{6.2.10}$$

or in partitioned form

$$\boldsymbol{t}^\alpha = \boldsymbol{P}_{ext}^{\alpha,(P),a}(\boldsymbol{q}) \cdot \boldsymbol{t}^{\alpha-1} + \boldsymbol{P}_{ext}^{\alpha,(P),b}(\boldsymbol{q}) \cdot \dot{u}^\alpha \tag{6.2.11}$$

with

$$\boldsymbol{P}_{ext}^{\alpha,(P),a}(\boldsymbol{q}) = \begin{bmatrix} \boldsymbol{I} & \widehat{\boldsymbol{\varphi}^{\alpha-1} - \boldsymbol{\varphi}^{\alpha}} \\ \boldsymbol{0} & \boldsymbol{I} \end{bmatrix} \qquad \boldsymbol{P}_{ext}^{\alpha,(P),b}(\boldsymbol{q}) = \begin{bmatrix} \boldsymbol{n}^{\alpha-1} \\ \boldsymbol{0} \end{bmatrix} \tag{6.2.12}$$

As already stated, any kinematic chain can be decomposed into combinations of R and P pairs. Therefore using the scalar generalised velocity ν^k, $k = 1, \ldots, N$ (with $\nu^k = \dot{\theta}^k$ if the k-th joint is a revolute joint and $\nu^k = \dot{u}^k$ if the k-th pair is a P pair), the twist of the α-th link in a general series manipulator can be obtained from recursive application of formula (6.2.8) and (6.2.11):

$$\boldsymbol{t}^{\alpha} = \boldsymbol{P}_{ext}^{\alpha,0}(\boldsymbol{q}) \cdot \boldsymbol{t}^0 + \sum_{k=1}^{\alpha} \boldsymbol{P}_{ext}^{\alpha,k}(\boldsymbol{q})\nu^k \tag{6.2.13}$$

with $\boldsymbol{P}_{ext}^{0,(J),0}(\boldsymbol{q}) = \boldsymbol{I}_{6\times 6}$ and for $\alpha = 1, \ldots, N$

$$\boldsymbol{P}_{ext}^{\alpha,0}(\boldsymbol{q}) = \prod_{l=\alpha}^{1} \boldsymbol{P}_{ext}^{l,(J),a}(\boldsymbol{q}) \tag{6.2.14}$$

and $k = 1, \ldots, N$

$$\boldsymbol{P}_{ext}^{\alpha,k}(\boldsymbol{q}) = \begin{cases} \left(\prod_{l=\alpha}^{k+1} \boldsymbol{P}_{ext}^{l,(J),a}(\boldsymbol{q})\right) \cdot \boldsymbol{P}_{ext}^{k,(J),b}(\boldsymbol{q}) & \alpha > k \\ \boldsymbol{P}_{ext}^{k,(J),b}(\boldsymbol{q}) & \alpha = k \\ \boldsymbol{0} & \alpha < k \end{cases} \tag{6.2.15}$$

where the matrices $\boldsymbol{P}_{ext}^{\alpha,(J),a}(\boldsymbol{q})$ and $\boldsymbol{P}_{ext}^{\alpha,(J),b}(\boldsymbol{q})$, $J \in \{R, P\}$ are either of the form (6.2.9) or (6.2.12) depending on whether the α-th pair is a R or P pair.

Example 6.2.1 (Pure R chain, null space matrix) For a kinematic chain consisting purely of R pairs, calculating the matrix products in (6.2.14) and (6.2.15) leads to the following more explicit expressions

$$\boldsymbol{P}_{ext}^{\alpha,0}(\boldsymbol{q}) = \begin{bmatrix} \boldsymbol{I}_{3\times 3} & \sum_{l=1}^{\alpha} \widehat{\boldsymbol{\varrho}^{l,l} - \boldsymbol{\varrho}^{l-1,l}} \\ \boldsymbol{0}_{3\times 3} & \boldsymbol{I}_{3\times 3} \end{bmatrix} \tag{6.2.16}$$

and

$$\boldsymbol{P}_{ext}^{\alpha,k}(\boldsymbol{q}) = \begin{cases} \begin{bmatrix} \boldsymbol{g}^{\alpha,k} \times \boldsymbol{n}^{k-1} \\ \boldsymbol{n}^{k-1} \end{bmatrix} & \alpha > k \\ \begin{bmatrix} \boldsymbol{\varrho}^{k,k} \times \boldsymbol{n}^{k-1} \\ \boldsymbol{n}^{k-1} \end{bmatrix} & \alpha = k \\ \boldsymbol{0} & \alpha < k \end{cases} \tag{6.2.17}$$

with

$$\boldsymbol{g}^{\alpha,k} = \boldsymbol{\varrho}^{\alpha,\alpha} + \sum_{l=k}^{\alpha-1} \left(\boldsymbol{\varrho}^{l,l} - \boldsymbol{\varrho}^{l-1,l}\right) \tag{6.2.18}$$

Example 6.2.2 (Pure P chain, null space matrix) For kinematic chains consisting purely of P pairs, the matrix products in (6.2.14) and (6.2.15) are given more explicitly by

$$
\boldsymbol{P}_{ext}^{\alpha,0}(\boldsymbol{q}) = \begin{bmatrix} \boldsymbol{I}_{3\times3} & \widehat{\boldsymbol{\varphi}^0 - \boldsymbol{\varphi}^\alpha} \\ \boldsymbol{0}_{3\times3} & \boldsymbol{I}_{3\times3} \end{bmatrix} \tag{6.2.19}
$$

and

$$
\boldsymbol{P}_{ext}^{\alpha,k}(\boldsymbol{q}) = \begin{bmatrix} \boldsymbol{n}^{k-1} \\ \boldsymbol{0} \end{bmatrix} \quad \alpha \geq k \tag{6.2.20}
$$

Accordingly the $6(N+1)$-dimensional twist of the simple open kinematic chain under consideration can be written in terms of the independent generalised velocities $\boldsymbol{\nu}^o \in \mathbb{R}^{N+6}$ of the simple open kinematic chain as

$$
\boldsymbol{t} = \boldsymbol{P}_{ext}^o(\boldsymbol{q}) \cdot \boldsymbol{\nu}^o \tag{6.2.21}
$$

or more explicitly using the submatrices given in (6.2.14) and (6.2.15)

$$
\begin{bmatrix} \boldsymbol{t}^0 \\ \boldsymbol{t}^1 \\ \vdots \\ \boldsymbol{t}^N \end{bmatrix} = \begin{bmatrix} \boldsymbol{I}_{6\times6} & \boldsymbol{0} & \cdots & \boldsymbol{0} \\ \boldsymbol{P}_{ext}^{1,0} & \boldsymbol{P}_{ext}^{1,1} & \cdots & \boldsymbol{0} \\ \vdots & \vdots & \ddots & \vdots \\ \boldsymbol{P}_{ext}^{N,0} & \boldsymbol{P}_{ext}^{N,1} & \cdots & \boldsymbol{P}_{ext}^{N,N} \end{bmatrix} \cdot \begin{bmatrix} \boldsymbol{t}^0 \\ \nu^1 \\ \vdots \\ \nu^N \end{bmatrix} \tag{6.2.22}
$$

where for clearness of exposition the dependence on $\boldsymbol{q}$ is not indicated in the matrix representation of $\boldsymbol{P}_{ext}^o(\boldsymbol{q})$.

Eventually, in analogy to formula (6.1.15) for the total null space matrix pertaining to a kinematic pair, the redundant $12(N+1)$-dimensional velocity vector of the open chain can be expressed as $\dot{\boldsymbol{q}} = \boldsymbol{P}^o(\boldsymbol{q}) \cdot \boldsymbol{\nu}^o$ with the total $n \times (n - m^o)$ null space matrix pertaining to the open chain

$$
\boldsymbol{P}^o(\boldsymbol{q}) = \boldsymbol{P}_{int}(\boldsymbol{q}) \cdot \boldsymbol{P}_{ext}^o(\boldsymbol{q}) \tag{6.2.23}
$$

where $\boldsymbol{P}_{int}(\boldsymbol{q})$ is given in (6.2.6).

Discrete null space method with nodal reparametrisation

From the treatment of kinematic pairs in Section 6.1.2 it is obvious, that the discrete null space matrix pertaining to the internal constraints equals the midpoint evaluation of the continuous one, i.e.

$$
\mathbf{P}_{int}(\boldsymbol{q}_n, \boldsymbol{q}_{n+1}) = \boldsymbol{P}_{int}(\boldsymbol{q}_{n+\frac{1}{2}}) \tag{6.2.24}
$$

Similar to the midpoint evaluation of the total null space matrix pertaining to the R pair in (6.1.73), the discrete versions of (6.2.9) are given by

$$
\mathbf{P}_{ext}^{\alpha,(R),a}(\boldsymbol{q}_n, \boldsymbol{q}_{n+1}) = \boldsymbol{P}_{ext}^{\alpha,(R),a}(\boldsymbol{q}_{n+\frac{1}{2}}) \qquad \mathbf{P}_{ext}^{\alpha,(R),b}(\boldsymbol{q}_n, \boldsymbol{q}_{n+1}) = \boldsymbol{P}_{ext}^{\alpha,(R),b}(\boldsymbol{q}_{n+\frac{1}{2}}) \tag{6.2.25}
$$

For the P pair, the discrete null space matrix pertaining to the external constraints is not equal to the midpoint evaluation of the continuous one. With regard to (6.1.81), for the α-th pair being prismatic, the discrete counterparts of the matrices in (6.2.12) are given by

$$
\begin{aligned}
\mathbf{P}_{ext}^{\alpha,(P),a}(\boldsymbol{q}_n, \boldsymbol{q}_{n+1}) &= \begin{bmatrix} \boldsymbol{I} & \widehat{\boldsymbol{\varphi}_{n+\frac{1}{2}}^{\alpha-1} - \boldsymbol{\varphi}_{n+\frac{1}{2}}^{\alpha}} \\ \boldsymbol{0} & \boldsymbol{I} \end{bmatrix} \\
\mathbf{P}_{ext}^{\alpha,(P),b}(\boldsymbol{q}_n, \boldsymbol{q}_{n+1}) &= \begin{bmatrix} (\boldsymbol{m}_1^{\alpha-1})_{n+\frac{1}{2}} \times (\boldsymbol{m}_2^{\alpha-1})_{n+\frac{1}{2}} \\ \boldsymbol{0} \end{bmatrix}
\end{aligned}
\tag{6.2.26}
$$

Then the discrete counterpart $\mathbf{P}_{ext}^{o}(\boldsymbol{q}_n, \boldsymbol{q}_{n+1})$ of the null space matrix pertaining to the external constraints of the open kinematic chain consists of the discrete submatrices for $\alpha, k = 1, \ldots, N$ denoted by $\mathbf{P}^{\alpha,0}(\boldsymbol{q}_n, \boldsymbol{q}_{n+1})$ and $\mathbf{P}^{\alpha,k}(\boldsymbol{q}_n, \boldsymbol{q}_{n+1})$, which can be calculated by insertion of the discrete null space matrices pertaining to the specific α-th pair given in (6.2.25) and (6.2.26), into formulas (6.2.14) and (6.2.15). Eventually, in accordance with (6.1.23) for kinematic pairs, the total discrete null space matrix for the simple open kinematic chain is given explicitly by

$$
\mathbf{P}^{o}(\boldsymbol{q}_n, \boldsymbol{q}_{n+1}) = \boldsymbol{P}_{int}(\boldsymbol{q}_{n+\frac{1}{2}}) \cdot \mathbf{P}_{ext}^{o}(\boldsymbol{q}_n, \boldsymbol{q}_{n+1})
\tag{6.2.27}
$$

Example 6.2.3 (Pure R chain, discrete null space matrix) For a simple open kinematic chain consisting purely of R pairs, the discrete null space matrix coincides with the midpoint evaluation of the continuous one, i.e. $\mathbf{P}^{o}(\boldsymbol{q}_n, \boldsymbol{q}_{n+1}) = \boldsymbol{P}_{int}(\boldsymbol{q}_{n+\frac{1}{2}}) \cdot \boldsymbol{P}_{ext}^{o}(\boldsymbol{q}_{n+\frac{1}{2}})$.

The reparametrisation $\boldsymbol{q}_{n+1} = \boldsymbol{F}_{\boldsymbol{q}_n}(\boldsymbol{\mu}^o) \in C$ of the configuration vector in terms of the independent incremental unknowns $\boldsymbol{\mu}^o = (\boldsymbol{u}_\varphi^0, \boldsymbol{\theta}^0, \vartheta^1, \ldots, \vartheta^N) \in \mathbb{R}^{N+6}$ can be accomplished successively for the N kinematic pairs in the chain. Depending on whether the α-th pair is a R or P pair, $\vartheta^\alpha = \theta^\alpha$ or $\vartheta^\alpha = u^\alpha$ and the reparametrisation given for the R pair in (6.1.74) or for the P pair in (6.1.84) is applied. As for kinematic pairs or for the motion of a single rigid body, for the reparametrisation of the first body in the open chain, body 0, formula (4.3.31) is used.

Example 6.2.4 (Pure R chain, nodal reparametrisation) For a simple open kinematic chain consisting purely of R pairs, the reparametrisation of $\boldsymbol{q}_{n+1}^\alpha \in \mathbb{R}^{12}$, $\alpha = 1, \ldots, N$ is based on a product of exponentials formula (4.3.30), which characterisess the incremental rotational motion in terms of the incremental joint angles $\theta^1, \ldots, \theta^N$. Accordingly, the director frame of the α-th body at the end of a time-step is given by

$$
(\boldsymbol{d}_I^\alpha)_{n+1} = \prod_{k=1}^{\alpha} \exp(\widehat{\boldsymbol{\theta}^0}) \cdot \exp(\theta^k \widehat{(\boldsymbol{n}^{k-1})}_n) \cdot (\boldsymbol{d}_I^\alpha)_n
\tag{6.2.28}
$$

In addition to that, the placement of the center of mass of the α-th body with respect to the inertial frame $\{\boldsymbol{e}_I\}$ is given by

$$
\boldsymbol{\varphi}_{n+1}^\alpha = \boldsymbol{\varphi}_{n+1}^0 + \sum_{k=1}^{\alpha} \left((\boldsymbol{\varrho}^{k-1,k})_{n+1} - (\boldsymbol{\varrho}^{k,k})_{n+1} \right)
\tag{6.2.29}
$$
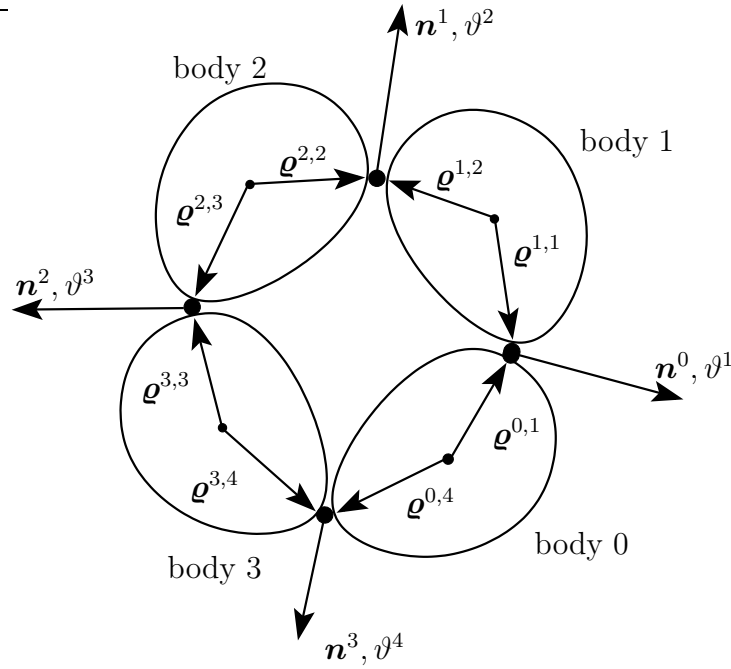
Figure 6.21: Schematic illustration of closed kinematic chain.

Example 6.2.5 (Pure P chain, nodal reparametrisation) For a simple open kinematic chain consisting purely of P pairs, the reparametrisation of the director frames is trivial, all director frames are updated according to the rotational increment of the first body, i.e.

$$(\boldsymbol{d}_I^\alpha)_{n+1} = \exp(\widehat{\boldsymbol{\theta}^0}) \cdot (\boldsymbol{d}_I^\alpha)_n \tag{6.2.30}$$

In addition to that, the placement of the center of mass of the α-th body with respect to the inertial frame $\{\boldsymbol{e}_I\}$ is given by

$$\boldsymbol{\varphi}_{n+1}^\alpha = \boldsymbol{\varphi}_{n+1}^0 + \sum_{k=1}^{\alpha} \left((\boldsymbol{\varrho}^{k-1,k})_{n+1} - (\boldsymbol{\varrho}^{k,k})_{n+1} + (u_n^k + u^k)\boldsymbol{n}_{n+1}^{k-1} \right) \tag{6.2.31}$$

6.2.3 Closed kinematic chains

Unlike for open kinematic chains, where any combination of the lower kinematic pairs described in Section 6.1 can be combined to a movable kinematic chain, the question how many degrees of freedom a closed kinematic chain has, is much more challenging. Generally, it cannot be determined by investigation of the topology of the chain alone (see e.g. [Ange 88]).

The investigation of closed kinematic chains as sketched in Figure 6.21 usually starts with the associated open kinematic chain in Figure 6.19, which is subject to m_{ext}^c loop closure conditions

$$\boldsymbol{g}_{ext}^c(\boldsymbol{q}) = \boldsymbol{0} \tag{6.2.32}$$

connecting the first body with the last one in the open chain.

For general closed loop systems, it is often hard or even impossible to find an explicit representation of a continuous null space matrix by analysis of the independent generalised velocities or in terms of a reparametrisation of the constraint manifold (see Section 2.3.4). If one succeeds in finding an explicit representation, it is very unlikely that a midpoint evaluation serves as a viable discrete null space matrix or that the necessary modifications to a midpoint evaluations can be detected, see Remark 3.2.8. Consequently, one has to revert to the implicit representation of the discrete null space matrix described in Example 3.2.9, relying on the decomposition of $\mathbb{R}^n$, which is relatively expensive. Thus it is reasonable to make use of the explicit representation of the discrete null space matrix $\mathbf{P}^o(\boldsymbol{q}_n, \boldsymbol{q}_{n+1})$ in (6.2.27) by the introduction of a multiplicative decomposition of the closed kinematic chain's discrete null space matrix

$$\mathbf{P}^c(\boldsymbol{q}_n, \boldsymbol{q}_{n+1}) = \mathbf{P}^o(\boldsymbol{q}_n, \boldsymbol{q}_{n+1}) \cdot \mathbf{P}^c_{ext}(\boldsymbol{q}_n, \boldsymbol{q}_{n+1}) \tag{6.2.33}$$

into that of the associated open kinematic chain $\mathbf{P}^o(\boldsymbol{q}_n, \boldsymbol{q}_{n+1})$ and the discrete null space matrix $\mathbf{P}^c_{ext}(\boldsymbol{q}_n, \boldsymbol{q}_{n+1})$ pertaining to the loop closure condition (6.2.32). Inspection of the design condition of discrete null space matrices (3.2.30) yields

$$\mathbf{G}^c(\boldsymbol{q}_n, \boldsymbol{q}_{n+1}) \cdot \mathbf{P}^c(\boldsymbol{q}_n, \boldsymbol{q}_{n+1}) = \left[\begin{array}{c} \mathbf{G}^o(\boldsymbol{q}_n, \boldsymbol{q}_{n+1}) \cdot \mathbf{P}^o(\boldsymbol{q}_n, \boldsymbol{q}_{n+1}) \\ \mathbf{G}^c_{ext}(\boldsymbol{q}_n, \boldsymbol{q}_{n+1}) \cdot \mathbf{P}^o(\boldsymbol{q}_n, \boldsymbol{q}_{n+1}) \end{array} \right] \cdot \mathbf{P}^c_{ext}(\boldsymbol{q}_n, \boldsymbol{q}_{n+1}) \tag{6.2.34}$$

Assuming that the associated open loop system has been treated appropriately, the upper entry in the matrix in (6.2.34) equals the $m^o \times (n - m^o)$ zeros matrix. Then the nodal reparametrisation of the configuration variable $\boldsymbol{q}_{n+1} = \boldsymbol{F}_{\boldsymbol{q}_n}(\boldsymbol{\mu}^o) \in C \subset \mathbb{R}^{12(N+1)}$ in terms of the independent incremental unknowns of the open kinematic chain $\boldsymbol{\mu}^o = (\boldsymbol{u}^0_\varphi, \boldsymbol{\theta}^0, \vartheta^1, \ldots, \vartheta^N) \in \mathbb{R}^{N+6}$ is used to define the reduced $(n - m^o - m^c_{ext})$-dimensional constraint manifold

$$\widetilde{C} = \left\{ \boldsymbol{\mu}^o \in \mathbb{R}^{n-m^o} \,\middle|\, \boldsymbol{g}^o(\boldsymbol{F}_{\boldsymbol{q}_n}(\boldsymbol{\mu}^o)) = \mathbf{0}, \, \boldsymbol{g}^c_{ext}(\boldsymbol{F}_{\boldsymbol{q}_n}(\boldsymbol{\mu}^o)) = \mathbf{0} \right\} \tag{6.2.35}$$

According to the procedure described in Example 3.2.9, an implicit representation of the $(n - m^o) \times (n - m^o - m^c_{ext})$ discrete null space matrix $\mathbf{P}^c_{ext}(\boldsymbol{q}_n, \boldsymbol{q}_{n+1})$ relies on a decomposition

$$\mathbb{R}^{n-m^o} = T\widetilde{C} \oplus \left(T\widetilde{C} \right)^\perp \tag{6.2.36}$$

that can be found using the QR-decomposition of $(\boldsymbol{G}^c_{ext}(\boldsymbol{q}_n) \cdot \boldsymbol{P}^o(\boldsymbol{q}_n))^T$.

Remark 6.2.6 (Semi-explicit discrete null space matrix) Insertion of the implicit representation of $\mathbf{P}^c_{ext}(\boldsymbol{q}_n, \boldsymbol{q}_{n+1})$ and the explicit representation of $\mathbf{P}^o(\boldsymbol{q}_n, \boldsymbol{q}_{n+1})$ in (6.2.33) yields a semi-explicit representation of the discrete null space matrix pertaining to the closed kinematic chain.

Remark 6.2.7 (Computational costs) The complexity of the QR-decomposition of a $n \times m$ matrix is of the order nm^2. Since the number of constraints in the open kinematic chain $m^o = m_{int} + m^o_{ext}$ is usually higher than the number of closure conditions m^c_{ext}, i.e. $m^o \gg m^c_{ext}$, the decomposition of $\mathbb{R}^{n-m^o}$ relying on the QR-decomposition of the $(n - m^o) \times m^c_{ext}$ matrix $(\boldsymbol{G}^c_{ext}(\boldsymbol{q}_n) \cdot \boldsymbol{P}^o(\boldsymbol{q}_n))^T$ is substantially cheaper, than the decomposition of $\mathbb{R}^n$ based on the QR-decomposition of the $n \times m = n \times (m^o + m^c_{ext})$ matrix $\boldsymbol{G}^T(\boldsymbol{q}_n)$.
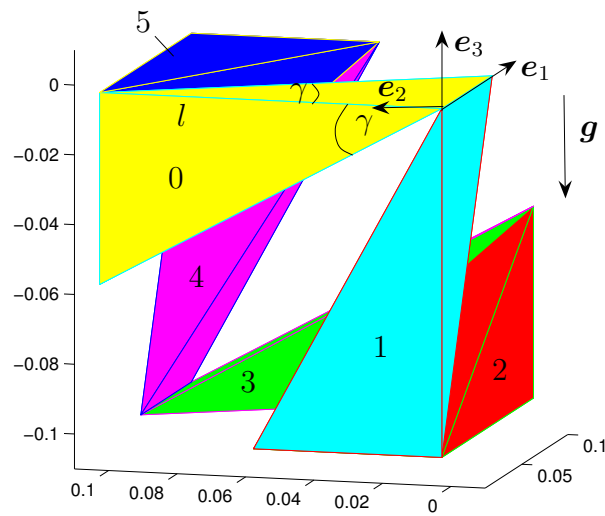
Figure 6.22: Initial configuration of the six-body linkage.

6.2.4 Numerical example: six-body linkage

As an example of a closed loop system, the simple closed kinematic chain consisting of six rigid bodies interconnected by revolute joints in Figure 6.22 is considered. This example has been analysed kinematically in [Witt 77, Lerb 05]. Simulations of the oscillation of the six-body linkage, whereby the initial configuration as well as the configuration at the turning point lie in one branch of the angle relation in Figure 6.25, have been reported by [Fuhr 88, Kim 86]. In [Kreu 79], the reduced equation of motion is deduced symbolically and its sectionwise integration is proposed. A similar problem consisting of six bars is investigated in [Ange 86, Ange 89]. Some historical remakrs on this 'invertible cube' and on Paul Schatz's interesting interpretation of the features of its motion can be found in Appendix F.

The initial configuration of the six-body linkage forms a cube of side length l (see Figure 6.22). Bodies $0, 2$ and 4 are identical and bodies $1, 3$ and 5 are identical. Furthermore, body 1 is a mirror image of body 0. Accordingly, it suffices to provide the details of body 0. Detailed investigation of the multibody's kinematics and symmetries reveals that the linkage moves without collision of contiguous bodies provided that the angle γ does not exceed $\pi/6$ (see [Witt 77]). Body 0 has density $\varrho = 1000$, length $l = 0.1$ and angle $\gamma = 0.16\pi$. Setting $a = \tan\gamma$, in the initial configuration the center of mass of body 0 with respect to the inertial frame $\{e_I\}$ is given by

$$\boldsymbol{\varphi}^0 = \varphi_i^0 \boldsymbol{e}_i \qquad [\varphi_i^0] = \begin{bmatrix} al/4 \\ l/2 \\ -al/4 \end{bmatrix} \tag{6.2.37}$$

In the inertial frame, the corners of this tetrahedral have the coordinates

$$[c_i^1] = \begin{bmatrix} -al/4 \\ -l/2 \\ al/4 \end{bmatrix} \qquad [c_i^2] = \begin{bmatrix} 3al/4 \\ -l/2 \\ al/4 \end{bmatrix} \qquad [c_i^3] = \begin{bmatrix} -al/4 \\ l/2 \\ al/4 \end{bmatrix} \qquad [c_i^4] = \begin{bmatrix} -al/4 \\ l/2 \\ -3al/4 \end{bmatrix} \quad (6.2.38)$$

and the mass of body 0 is given by $M_\varphi = \varrho a^2 l^3/6$. Furthermore, the inertia tensor of body 0 with respect to its center of mass in the initial configuration can be written as

$$\boldsymbol{J}^0 = J_{ij}^0 \boldsymbol{e}_i \otimes \boldsymbol{e}_j \tag{6.2.39}$$

with

$$[J_{ij}^0] = \frac{\varrho\, l^5\, a^2}{40} \begin{bmatrix} 1/3 + a^2/4 & a/6 & -a^2/12 \\ a/6 & a^2/2 & a/6 \\ -a^2/12 & a/6 & 1/3 + a^2/4 \end{bmatrix} \tag{6.2.40}$$

The principal values of the inertia tensor with respect to the center of mass are given by

$$[J_i^0] = \frac{a^2 l^5}{120} \left[(a^2 + 1), \frac{2a^2 + 1 + \sqrt{a^4 + 1}}{2}, \frac{2a^2 + 1 - \sqrt{a^4 + 1}}{2} \right] \tag{6.2.41}$$

With these preliminaries, the constant symmetric positive definite mass matrix for rigid body 0 can be inferred from (4.3.8). For simplicity, the director frame is assumed to coincide with the corresponding principal axes. Their directions relative to the inertial frame are characterised by

$$[(\tilde{\boldsymbol{d}}_1^0)_i] = [-1, 0, 1] \quad [(\tilde{\boldsymbol{d}}_2^0)_i] = [1, \frac{a^2 - 1 + \sqrt{a^4 + 1}}{a}, 1] \quad [(\tilde{\boldsymbol{d}}_3^0)_i] = [1, \frac{a^2 - 1 - \sqrt{a^4 + 1}}{a}, 1] \tag{6.2.42}$$

Then the director frame $\{\boldsymbol{d}_I^0\}$ of body 0 is gained by normalisation. Together with the placement of the center of mass given in (6.2.37), the 12-dimensional configuration variable $\boldsymbol{q}^0$ is defined. Subsequent mirroring at the diagonal planes of the cube configuration yields the other components $\boldsymbol{q}^1, \ldots, \boldsymbol{q}^5$ of the redundant configuration vector $\boldsymbol{q} \in \mathbb{R}^n$ of the six body linkage with $n = 72$. Let all revolute axes $\boldsymbol{n}^\alpha$, $\alpha = 0, \ldots, 5$ be directed inwards the cube and let θ^α, $\alpha = 1, \ldots, 6$ be defined as the angle through which body α is rotated relative to body $\alpha - 1$ in the positive sense about the axis $\boldsymbol{n}^{\alpha-1}$ of the α-th revolute joint. All angles are zero in the cube configuration. Note that body 6 equals body 0.

In the associated open kinematic chain, the revolute joint connecting body 5 to body 0 is cut, thus six rigid bodies are interconnected by five revolute joints with external constraints $\boldsymbol{g}_{ext}^\alpha([\boldsymbol{q}^{\alpha-1}, \boldsymbol{q}^\alpha]^T)$, $\alpha = 1, \ldots, 5$ of the form (6.1.67). The independent generalised velocities are given in (6.2.22). Body 0 is fixed totally in space at its center of mass. The corresponding constraints read

$$\boldsymbol{g}_{ext}^f(\boldsymbol{q}) \begin{bmatrix} \boldsymbol{\varphi}^0 - \boldsymbol{c} \\ \boldsymbol{e}_1^T \cdot \boldsymbol{d}_1^0 - \eta_1^0 \\ \boldsymbol{e}_2^T \cdot \boldsymbol{d}_2^0 - \eta_2^0 \\ \boldsymbol{e}_3^T \cdot \boldsymbol{d}_3^0 - \eta_3^0 \end{bmatrix} \tag{6.2.43}$$

where the constant $\boldsymbol{c} \in \mathbb{R}^3$ can be inferred from (6.2.37). This reduces the independent generalised velocities of the open loop system to the $n - m^o = 5$ relative angular velocities in the hinges $\boldsymbol{\nu}^o = [\dot{\theta}^1, \ldots, \dot{\theta}^5]^T$ and the independent incremental unknowns of the associated open loop system to $\boldsymbol{\mu}^o = [\theta^1, \ldots, \theta^5]^T$. An explicit representation of the continuous 72×5 null space matrix $\boldsymbol{P}^o(\boldsymbol{q})$ and the discrete null space matrix $\mathbf{P}^o(\boldsymbol{q}_n, \boldsymbol{q}_{n+1})$ for the pure R chain is derived in Section 6.2.2 in Example 6.2.1 and Example 6.2.3 respectively. Note that $\dot{\boldsymbol{q}}^0 = \boldsymbol{0} \in \mathbb{R}^{12}$ due to the total fixing in space of body 0 and therefore the first 12 rows in the 72×5 null space matrices equal the 12×5 zero matrix.

The open loop system is subject to the $m_{ext}^c = 5$ additional loop closure constraint $\boldsymbol{g}_{ext}^c(\boldsymbol{q}) = \boldsymbol{0}$, in particular, similar to (6.1.67) the closure condition reads

$$
\boldsymbol{g}_{ext}^c(\boldsymbol{q}) \begin{bmatrix} \boldsymbol{\varphi}^5 - \boldsymbol{\varphi}^0 + \boldsymbol{\varrho}^{5,6} - \boldsymbol{\varrho}^{0,6} \\ (\boldsymbol{n}^5)^T \cdot \boldsymbol{d}_1^0 - \eta_1^0 \\ (\boldsymbol{n}^5)^T \cdot \boldsymbol{d}_2^0 - \eta_2^0 \end{bmatrix} \tag{6.2.44}
$$

The orthonormality conditions (4.3.3) on each body's director triad constitute $m_{int} = 36$ internal constraints. According to Table 6.1, each revolute joint gives rise to 5 external constraints. Together with the fixing in space of body 0, the number of external constraints is $m_{ext} = 36$, thus the total number of constraints $m = m_{int} + m_{ext} = n$ and it is not clear whether the system has any degree of freedom. To answer this question, the dependency of the constraints combined to $\boldsymbol{g}(\boldsymbol{q}) \in \mathbb{R}^m$ has to be investigated. To this end it has to be examined whether all configurations in the constraint manifold

$$
C = \{\boldsymbol{q} \in \mathbb{R}^{72} \big|\ \begin{matrix} \boldsymbol{g}_{int}^\alpha(\boldsymbol{q}^\alpha) & = \boldsymbol{0}, & \alpha = 0, \ldots, 5, & \boldsymbol{g}_{ext}^f(\boldsymbol{q}) = \boldsymbol{0}, \\ \boldsymbol{g}_{ext}^\alpha(\boldsymbol{q}) & = \boldsymbol{0}, & \alpha = 1, \ldots, 5, & \boldsymbol{g}_{ext}^c(\boldsymbol{q}) = \boldsymbol{0}\} \end{matrix} \tag{6.2.45}
$$

are regular points (see A.27), i.e. the rank of the 72×72 constraint Jacobian $\boldsymbol{G}(\boldsymbol{q})$ has to be calculated for all kinematically admissible configurations $\boldsymbol{q} \in C$. It turns out, that only 71 constraints are independent. Therefore, the number of independent constraints is $\tilde{m} = 71$ and the system has $n - \tilde{m} = 1$ relative configurational degree of freedom.

Remark 6.2.8 (Lagrange multiplier method) For the use of the Lagrange multiplier method leading to the continuous constrained Hamiltonian equations presented in Section 2.3, it is required that the constraint Jacobian has maximal rank. Consequently 71 independent constraints must be used and one constraint equation is omitted.

The relative configurational degree of freedom can be chosen in $\{\theta^1, \ldots, \theta^5\}$. For reasons of symmetry, only two relative angles of the system are nonequal. The following relations hold

$$
\theta^1 = \theta^3 = \theta^5 \qquad \theta^2 = \theta^4 = \theta^6 \tag{6.2.46}
$$

Then the relationship

$$
\sin(\theta^1)(1 + \sin(\theta^2)) = \sin(\theta^2) \tag{6.2.47}
$$

can be inferred form the formulation of the closure constraints (6.2.44) in the relative degrees of freedom of the associated open loop system, see [Witt 77]. Together

with the conditions $|\sin(\theta^1)| \leq 1$ and $|\sin(\theta^2)| \leq 1$, (6.2.47) yields $\theta^1 \in [-\frac{7\pi}{6}, \frac{\pi}{6}]$ and $\theta^2 \in [-\frac{\pi}{6}, \frac{7\pi}{6}]$. Figure 6.25 shows the relation between θ^1 and θ^2 for a full revolution of the six-body linkage which bears two problems. First of all, it is ambiguous and secondly, it involves vertical tangents. Therefore, the reparametrisation of the relative angles in one independent relative degree of freedom must be partitioned according to the different periods of the motion as indicated in Figure 6.25.

$$
\begin{aligned}
s = 1 \quad & \theta^1 \in [-\frac{\pi}{2}, 0] \quad \theta^2(\theta^1) = \arcsin\left(\frac{\sin(\theta^1)}{1 - \sin(\theta^1)}\right) && \in [-\frac{\pi}{6}, 0] \\[2mm]
s = 2 \quad & \theta^2 \in [0, \frac{\pi}{2}] \quad\ \ \theta^1(\theta^2) = \arcsin\left(\frac{\sin(\theta^2)}{1 + \sin(\theta^2)}\right) && \in [0, \frac{\pi}{6}] \\[2mm]
s = 3 \quad & \theta^1 \in [-\frac{\pi}{2}, 0] \quad \theta^2(\theta^1) = \pi - \arcsin\left(\frac{\sin(\theta^1)}{1 - \sin(\theta^1)}\right) && \in [\frac{\pi}{2}, \frac{7\pi}{6}] \\[2mm]
s = 4 \quad & \theta^2 \in [0, \frac{\pi}{2}] \quad\ \ \theta^1(\theta^2) = -\pi - \arcsin\left(\frac{\sin(\theta^2)}{1 + \sin(\theta^2)}\right) && \in [-\frac{7\pi}{6}, -\frac{\pi}{2}]
\end{aligned}
\tag{6.2.48}
$$

A consistent reparametrisation of the all relative rotational degrees of freedom of the associated open kinematic chain $\boldsymbol{\mu}^o \in \mathbb{R}^5$ reads

$$
\begin{aligned}
&s \in \{1, 3\} && s \in \{2, 4\} \\[2mm]
&\boldsymbol{\mu}^o = \boldsymbol{F}^s(\theta^1) = \begin{bmatrix} \theta^1 \\ \theta^2(\theta^1) \\ \theta^1 \\ \theta^2(\theta^1) \\ \theta^1 \end{bmatrix}
&& \boldsymbol{\mu}^o = \boldsymbol{F}^s(\theta^2) = \begin{bmatrix} \theta^1(\theta^2) \\ \theta^2 \\ \theta^1(\theta^2) \\ \theta^2 \\ \theta^1(\theta^2) \end{bmatrix}
\end{aligned}
\tag{6.2.49}
$$

Thus the independent generalised velocities of the closed kinematic chain are given by $\nu^c = \dot{\theta}^1$ for $s \in \{1, 3\}$ and $\nu^c = \dot{\theta}^2$ for $s \in \{2, 4\}$.

The Jacobian of the reparametrisation (6.2.49) plays the role of a null space matrix in the temporal continuous setting, see Remark 2.3.10. This yields

$$
\begin{aligned}
&s \in \{1, 3\} && s \in \{2, 4\} \\[2mm]
&\boldsymbol{\nu}^o = \boldsymbol{P}_{ext}^{c,s} \dot{\theta}^1 && \boldsymbol{\nu}^o = \boldsymbol{P}_{ext}^{c,s} \dot{\theta}^2 \\[2mm]
&\boldsymbol{P}_{ext}^{c,s} = \begin{bmatrix} 1 \\ D_{\theta^1}\theta^2 \\ 1 \\ D_{\theta^1}\theta^2 \\ 1 \end{bmatrix}
&& \boldsymbol{P}_{ext}^{c,s} = \begin{bmatrix} D_{\theta^2}\theta^1 \\ 1 \\ D_{\theta^2}\theta^1 \\ 1 \\ D_{\theta^2}\theta^1 \end{bmatrix}
\end{aligned}
\tag{6.2.50}
$$

Using the null space matrix pertaining to the associated open loop system in (6.2.22), a continuous null space matrix for the six-body linkage at hand is given by

$$
\boldsymbol{P}^c = \boldsymbol{P}^o(\boldsymbol{q}) \cdot \boldsymbol{P}_{ext}^c
\tag{6.2.51}
$$

Remark 6.2.9 The closed form reparametrisation (6.2.49) is feasible because the system under consideration possesses such distinct symmetry properties as given in (6.2.46) and

(6.2.47). A major drawback of the reparametrisation (6.2.49) is that the dependence is highly nonlinear. Furthermore its Jacobian includes the angle θ^1 or θ^2. Therefore the continuous null space matrix for the six-body linkage (6.2.51) cannot be used to infer a temporal discrete null space matrix by midpoint evaluation or slight modifications of that, see Remark 3.2.8.

An alternative continuous null space matrix involving only the configuration variable $\boldsymbol{q}$ of the six-body linkage and being at most quadratic in it, can be derived as follows. Considering the associated open kinematic chain, with regard to (6.2.13), the twist of the body 5 can be expressed as

$$\boldsymbol{t}^5 = \boldsymbol{P}_{ext}^{5,0}(\boldsymbol{q}) \cdot \boldsymbol{t}^0 + \sum_{k=1}^{5} \boldsymbol{P}_{ext}^{5,k}(\boldsymbol{q})\dot{\theta}^k \tag{6.2.52}$$

On the other hand, the 6-th revolute joint interconnecting body 0 with its neighbour body 5 relates their twists and the relative angular velocity associated with the 6-th revolute joints according to formula (6.2.8). Accounting for the interchanged order of the neighbouring pairs, this relation reads

$$\boldsymbol{t}^5 = \boldsymbol{P}_{ext}^{5,(R),a}(\boldsymbol{q}) \cdot \boldsymbol{t}^0 + \boldsymbol{P}_{ext}^{5,(R),b}(\boldsymbol{q}) \cdot (-\dot{\theta}^6) \tag{6.2.53}$$

where

$$\boldsymbol{P}_{ext}^{5,(R),a}(\boldsymbol{q}) = \begin{bmatrix} \boldsymbol{I} & \widehat{\boldsymbol{\varrho}^{5,6} - \boldsymbol{\varrho}^{0,6}} \\ \boldsymbol{0} & \boldsymbol{I} \end{bmatrix} \qquad \boldsymbol{P}_{ext}^{5,(R),b}(\boldsymbol{q}) = \begin{bmatrix} \boldsymbol{\varrho}^{5,6} \times \boldsymbol{n}^5 \\ \boldsymbol{n}^5 \end{bmatrix} \tag{6.2.54}$$

Equating (6.2.52) and (6.2.53) yields the loop closure condition in the form

$$(\boldsymbol{P}_{ext}^{5,0}(\boldsymbol{q}) - \boldsymbol{P}_{ext}^{5,(R),a}(\boldsymbol{q})) \cdot \boldsymbol{t}^0 + \sum_{k=1}^{6} \boldsymbol{P}_{ext}^{5,k}(\boldsymbol{q})\dot{\theta}^k = \boldsymbol{0} \tag{6.2.55}$$

where $\boldsymbol{P}_{ext}^{5,6}(\boldsymbol{q}) = \boldsymbol{P}_{ext}^{5,(R),b}(\boldsymbol{q})$ has been set. With regard to $\boldsymbol{P}_{ext}^{5,0}(\boldsymbol{q})$ given in (6.2.16) and $\boldsymbol{P}_{ext}^{5,(R),a}(\boldsymbol{q})$ given in (6.2.54), it can be easily verified that $\boldsymbol{P}_{ext}^{5,0}(\boldsymbol{q}) - \boldsymbol{P}_{ext}^{5,(R),a}(\boldsymbol{q}) = \boldsymbol{0}$, since

$$\sum_{k=0}^{5} (\boldsymbol{\varrho}^{k,k} - \boldsymbol{\varrho}^{k,k+1}) = \boldsymbol{0} \tag{6.2.56}$$

with $\boldsymbol{\varrho}^{0,0} = \boldsymbol{\varrho}^{0,6}$ (see Figure 6.21, where the corresponding relation for a closed chain consisting of four rigid bodies can be observed). Accordingly, from condition (6.2.55), it remains

$$\sum_{k=1}^{6} \boldsymbol{P}_{ext}^{5,k}(\boldsymbol{q})\dot{\theta}^k = \boldsymbol{0} \tag{6.2.57}$$

which can be written more explicitly as

$$
\begin{bmatrix} \boldsymbol{g}^{5,1} \times \boldsymbol{n}^0 & \boldsymbol{g}^{5,2} \times \boldsymbol{n}^1 & \boldsymbol{g}^{5,3} \times \boldsymbol{n}^2 & \boldsymbol{g}^{5,4} \times \boldsymbol{n}^3 & \boldsymbol{g}^{5,5} \times \boldsymbol{n}^4 & \boldsymbol{\rho}^{5,6} \times \boldsymbol{n}^5 \\ \boldsymbol{n}^0 & \boldsymbol{n}^1 & \boldsymbol{n}^2 & \boldsymbol{n}^3 & \boldsymbol{n}^4 & \boldsymbol{n}^5 \end{bmatrix} \cdot \begin{bmatrix} \dot{\theta}^1 \\ \dot{\theta}^2 \\ \dot{\theta}^3 \\ \dot{\theta}^4 \\ \dot{\theta}^5 \\ \dot{\theta}^6 \end{bmatrix} = \boldsymbol{0}
$$

$$(6.2.58)$$

where (6.2.17) and (6.2.18) have been used.

Remark 6.2.10 According to the treatment of closed kinematic chains in [Ange 88], the nullity of the matrix in (6.2.58) equals the number of degrees of freedom of the closed kinematic chain. Since its nullity equals one, only one relative joint velocity can be chosen, the other five can then be determined similar to (6.2.50). This coincides with the former consideration of the constraint Jacobian $\boldsymbol{G}(\boldsymbol{q})$, whose rank deficiency turned out to be equal to one.

Taking the symmetry of the system given in (6.2.46) into account, equation (6.2.58) yields

$$\boldsymbol{p}_1 \dot{\theta}^1 + \boldsymbol{p}_2 \dot{\theta}^2 = \boldsymbol{0} \tag{6.2.59}$$

with

$$
\begin{aligned}
\boldsymbol{p}_1 &= \boldsymbol{P}_{ext}^{5,1}(\boldsymbol{q}) + \boldsymbol{P}_{ext}^{5,3}(\boldsymbol{q}) + \boldsymbol{P}_{ext}^{5,5}(\boldsymbol{q}) \\
\boldsymbol{p}_2 &= \boldsymbol{P}_{ext}^{5,2}(\boldsymbol{q}) + \boldsymbol{P}_{ext}^{5,4}(\boldsymbol{q}) + \boldsymbol{P}_{ext}^{5,6}(\boldsymbol{q})
\end{aligned} \tag{6.2.60}
$$

Thus from (6.2.59) the following relation of $\dot{\theta}^1$ and $\dot{\theta}^2$ can be deduced

$$\dot{\theta}^2 = -\frac{\boldsymbol{p}_1^T \cdot \boldsymbol{p}_2}{\boldsymbol{p}_2^T \cdot \boldsymbol{p}_2} \dot{\theta}^1 \tag{6.2.61}$$

Now by velocity analysis equation (6.2.50) can be rewritten as

$$\boldsymbol{\nu}^o = \boldsymbol{P}_{ext}^c(\boldsymbol{q}) \dot{\theta}^1 \tag{6.2.62}$$

which holds throughout the motion of the six-body linkage. It involves the continuous null space matrix pertaining to the closure of the linkage

$$
\boldsymbol{P}_{ext}^c(\boldsymbol{q}) = \begin{bmatrix} 1 \\ -\dfrac{\boldsymbol{p}_1^T \cdot \boldsymbol{p}_2}{\boldsymbol{p}_2^T \cdot \boldsymbol{p}_2} \\ 1 \\ -\dfrac{\boldsymbol{p}_1^T \cdot \boldsymbol{p}_2}{\boldsymbol{p}_2^T \cdot \boldsymbol{p}_2} \\ 1 \end{bmatrix} \tag{6.2.63}
$$

Analogous to (6.2.51), a continuous null space matrix for the closed six-body linkage is given by

$$\boldsymbol{P}^c(\boldsymbol{q}) = \boldsymbol{P}^o(\boldsymbol{q}) \cdot \boldsymbol{P}_{ext}^c(\boldsymbol{q}) \tag{6.2.64}$$

Remark 6.2.11 The deduction of this null space matrix relies on the dependence of the columns in the matrix in (6.2.58). More specific, it relies on the assumption, that the columns of (6.2.58) can be combined into two linearly dependent vectors, i.e. it as assumed that a linear combination with only two coefficients, namely 1 and $-(\boldsymbol{p}_1^T \cdot \boldsymbol{p}_2)/(\boldsymbol{p}_2^T \cdot \boldsymbol{p}_2)$ equals zero. This is the case for configurations $\boldsymbol{q} \in C$, where all constraints are fulfilled. Thus the matrix in (6.2.63) qualifies as null space matrix pertaining to the loop closure condition in the temporal continuous case. However, at intermediate configurations, e.g. at the midpoint $\boldsymbol{q}_{n+\frac{1}{2}} \notin C$, the columns of (6.2.58) are linearly dependent, but more than two different coefficients are needed for a linear combination that equals zero.

Neither the continuous null space matrix (6.2.51) deduced by reparametrisation of the constraint manifold (6.2.49) nor that in (6.2.64) obtained from the velocity analysis (6.2.62) serves as a basis for an explicit representation of a discrete null space matrix. Thus the semi-explicit construction procedure for the discrete null space matrix described in Section 6.2.3 (see Remark 6.2.6) must be used. To this end the one-dimensional constraint manifold in (6.2.45) is written in reduced form corresponding to (6.2.35) using the reparametrisation given in Example 6.2.4.

$$\widetilde{C} = \left\{ \boldsymbol{\mu}^o \in \mathbb{R}^5 \,\middle|\, \boldsymbol{g}^o(\boldsymbol{F}\boldsymbol{q}_n(\boldsymbol{\mu}^o)) = \boldsymbol{0},\, \boldsymbol{g}^c_{ext}(\boldsymbol{F}\boldsymbol{q}_n(\boldsymbol{\mu}^o)) = \boldsymbol{0} \right\} \tag{6.2.65}$$

According to (6.2.36) the decomposition of the $\mathbb{R}^5$ into the tangent space to the reduced constraint manifold and its orthogonal complement can be accomplished using the evaluation at $\boldsymbol{q}_n$ of the 5×5 matrix $\boldsymbol{G}^c_{ext}(\boldsymbol{q}) \cdot \boldsymbol{P}^o(\boldsymbol{q})$ which reads

$$\begin{bmatrix} \boldsymbol{n}^0 \times \boldsymbol{r}^1 & \boldsymbol{n}^1 \times \boldsymbol{r}^2 & \boldsymbol{n}^2 \times \boldsymbol{r}^3 & \boldsymbol{n}^3 \times \boldsymbol{r}^4 & \boldsymbol{n}^4 \times \boldsymbol{r}^5 \\ (\boldsymbol{d}_1^1)^T \cdot (\boldsymbol{n}^5 \times \boldsymbol{n}^0) & (\boldsymbol{d}_1^1)^T \cdot (\boldsymbol{n}^5 \times \boldsymbol{n}^1) & (\boldsymbol{d}_1^1)^T \cdot (\boldsymbol{n}^5 \times \boldsymbol{n}^2) & (\boldsymbol{d}_1^1)^T \cdot (\boldsymbol{n}^5 \times \boldsymbol{n}^4) & (\boldsymbol{d}_1^1)^T \cdot (\boldsymbol{n}^5 \times \boldsymbol{n}^4) \\ (\boldsymbol{d}_2^1)^T \cdot (\boldsymbol{n}^5 \times \boldsymbol{n}^0) & (\boldsymbol{d}_2^1)^T \cdot (\boldsymbol{n}^5 \times \boldsymbol{n}^1) & (\boldsymbol{d}_2^1)^T \cdot (\boldsymbol{n}^5 \times \boldsymbol{n}^2) & (\boldsymbol{d}_2^1)^T \cdot (\boldsymbol{n}^5 \times \boldsymbol{n}^4) & (\boldsymbol{d}_2^1)^T \cdot (\boldsymbol{n}^5 \times \boldsymbol{n}^4) \end{bmatrix}$$

$$\tag{6.2.66}$$

where $\boldsymbol{r}^k = \boldsymbol{\varrho}^{5,6} - \boldsymbol{g}^{5,k}$ and $\boldsymbol{g}^{5,k}$ is given in (6.2.18).

Remark 6.2.12 (Discrete null space matrix) Similar to the rank deficiency of the full 72×72 constraint Jacobian $\boldsymbol{G}(\boldsymbol{q})$, the matrix in (6.2.66) has rank 4. Thus 4 independent rows of $(\boldsymbol{G}^c_{ext}(\boldsymbol{q}_n) \cdot \boldsymbol{P}^o(\boldsymbol{q}_n))^T$ must be chosen for the QR-decomposition leading to the implicit representation of $\mathbf{P}^c_{ext}(\boldsymbol{q}_n, \boldsymbol{q}_{n+1})$ form which the semi-explicit representation of the discrete null space matrix pertaining to the six-body linkage can be calculated (see Remark 6.2.6).

Remark 6.2.13 (Explicit discrete null space matrix) To reduce the computational costs, an explicit representation of the discrete null space matrix is naturally preferable. If one succeeds in finding the QR-decomposition of $(\boldsymbol{G}^c_{ext}(\boldsymbol{q}_n) \cdot \boldsymbol{P}^o(\boldsymbol{q}_n))^T$ explicitly, formula (3.2.38) yields the desired explicit representation of the discrete null space matrix $\mathbf{P}^c_{ext}(\boldsymbol{q}_n, \boldsymbol{q}_{n+1})$. For the simple example of a double spherical pendulum treated by the discrete null space matrix in Section 4.2.4, an explicit representation of a discrete null space matrix could be achieved in this way.

Numerical results

Consistent initial velocities $\dot{\boldsymbol{q}} \in \mathbb{R}^{72}$ follow from $\dot{\boldsymbol{q}} = \boldsymbol{P}^c \dot{\theta}^1$ using one of the continuous null space matrices given in (6.2.51) or (6.2.63). In the numerical example $\dot{\theta}^1 = 30$ has been chosen. Gravity is acting on the system with $g = -9.81$.

Figure 6.24 gives an impression of the motion by showing snapshots at consecutive instances. Algorithmic conservation of the total energy for the present conservative problem is corroborated in Figure 6.23. Due to the presence of gravitation and the total fixing in space of body 0, no component of the angular momentum is a first integral of the motion. The evolution of the coordinates $\theta^1(t)$ and $\theta^2(t)$ is depicted in Figure 6.25 as well as the relation of $\theta^2(\theta^1)$ described in (6.2.48). A characteristic of the motion of the six-body linkage is that the distances $\sigma_1, \sigma_2, \sigma_3$ between opposite corner nodes (the three space diagonals in the initial cube configuration) remain constant (see [Scha 98]). Figure 6.26 verifies the algorithmic conservation of these distances. Note that due to the magnitude of the initial angular velcity, the six-body linkage performs full revolutions. This can be considered as an amelioration to the simulation of oscillations reproted in the existing literature. Table 6.5 shows a comparison of the simulations of the motion of the six-body linkage using the constrained scheme (3.2.7) and the d'Alembert-type scheme with nodal reparametrisation (3.2.44) respectively. Although a 143-dimensional system of equations has to be solved using the constrained scheme, approximately the same computational time is needed as for the setup and solution of the one equation in the d'Alembert-type scheme with nodal reparametrisation, since the implicit representation of the discrete null space matrix pertaining to the closure condition has been used. Concerning the conditioning issue, the advantageous properties of the advocated discrete null space method are obvious in view of Table 6.5.
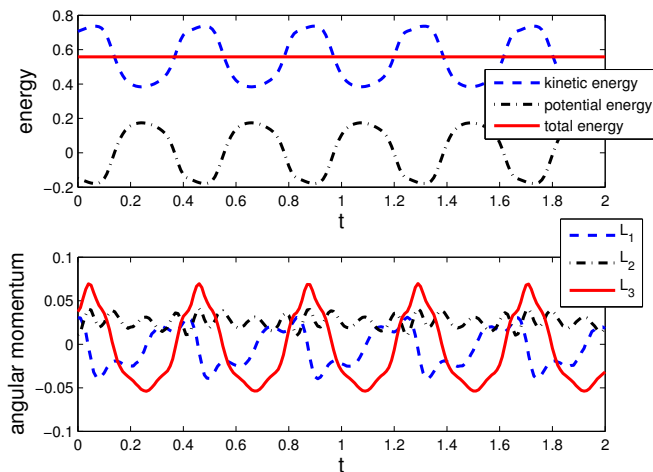
Figure 6.23: Six-body linkage: energy and components of angular momentum vector $\boldsymbol{L} = L_i \boldsymbol{e}_i$ ($h = 0.01$).

PSfrag replacements

$t = 0.04$
$t = 0.08$
$t = 0.09$
$t = 0.13$
$t = 0.26$

$t = 0.02$

PSfrag replacements

$t = 0.02$

$t = 0.08$
$t = 0.09$
$t = 0.13$
$t = 0.26$

$t = 0.04$

PSfrag replacements

$t = 0.02$
$t = 0.04$

$t = 0.09$
$t = 0.13$
$t = 0.26$

$t = 0.08$

PSfrag replacements

$t = 0.02$
$t = 0.04$
$t = 0.08$

$t = 0.13$
$t = 0.26$

$t = 0.09$

PSfrag replacements

$t = 0.02$
$t = 0.04$
$t = 0.08$
$t = 0.09$

$t = 0.26$

$t = 0.13$

PSfrag replacements

$t = 0.02$
$t = 0.04$
$t = 0.08$
$t = 0.09$
$t = 0.13$

$t = 0.26$
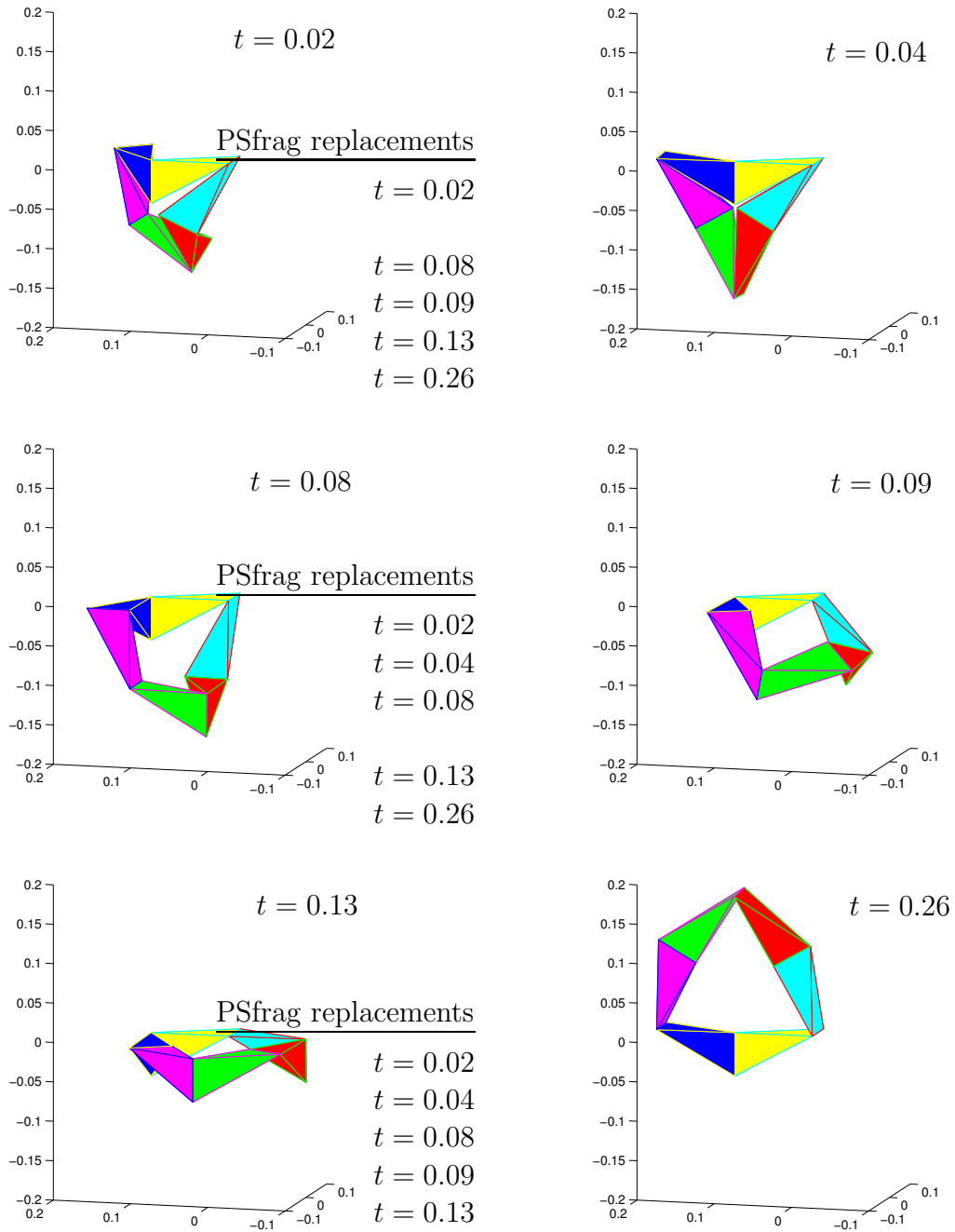
Figure 6.24: Six-body linkage: snapshots of the motion at $t \in \{0.02, 0.04, 0.08, 0.09, 0.13, 0.26\}$.
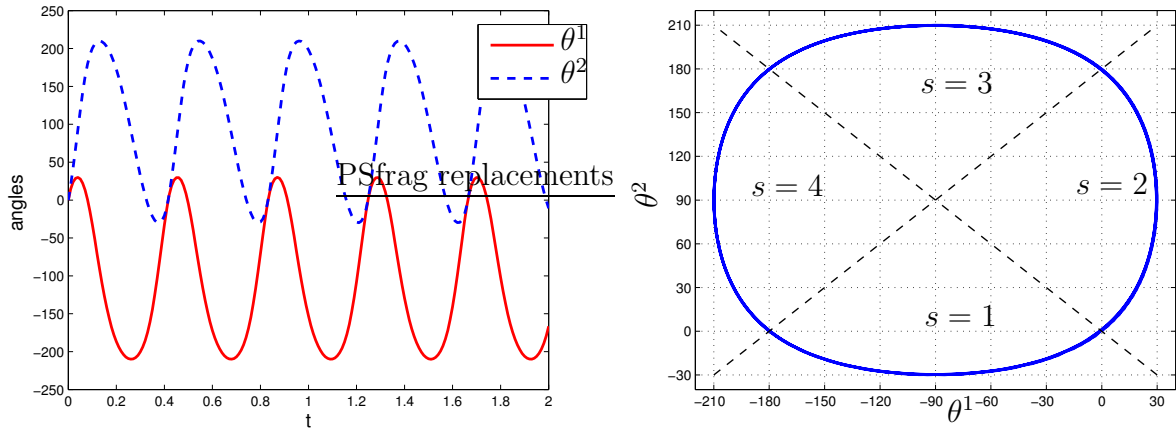
Figure 6.25: Six-body linkage: relative coordinates $\theta^1(t)$ and $\theta^2(t)$ ($h = 0.01$) and angle relation $\theta^2(\theta^1)$.
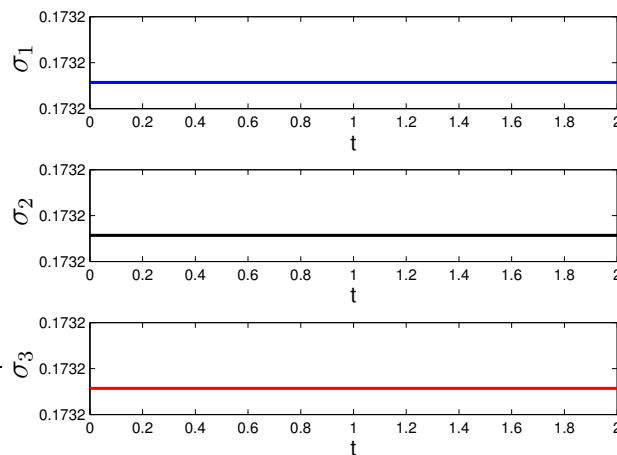
Figure 6.26: Six-body linkage: distance between opposite corner nodes ($h = 0.01$).

Table 6.5: Comparison of constrained scheme to d'Alembert-type scheme with nodal reparametrisation for the example 'six-body linkage'.

	constrained	d'Alembert
number of unknowns $n = 72$ $m = 71$	143	1
CPU-time	1	1
condition number $h = 10^{-2}$	10^5	1
$h = 10^{-3}$	10^8	1
$h = 10^{-4}$	10^{11}	1

6.3 Flexible multibody system dynamics

The description of rigid bodies and spatially discretised geometrically exact beams as constrained continua in terms of the configuration variables given in (4.3.2) and (5.3.2) respectively allows their coupling to a multibody system consisting of rigid and elastic components in a systematic way. As a generalisation of (5.3.2), (6.1.1) and (6.2.3), their configuration vectors are combined into the general configuration vector $\boldsymbol{q}(t) \in \mathbb{R}^n$ where n equals twelve times the actual number of nodes present in the system. As already mentioned in Remark 5.4.6, a spatially discretised beam can be interpreted as a chain of n_{node} rigid bodies for which the interconnections are prescribed by the connectivity of the spatial finite element method. Furthermore, a rigid body can be considered as a 'one-node structure', i.e. it is a special case of a geometrically exact beam, for which the spatial distribution is degenerate to a single point. Two examples of multibody systems comprising elastic components are given in the sequel before the general procedure for the treatment of arbitrary multibody systems by the discrete null space method is outlined in Section 6.3.1.
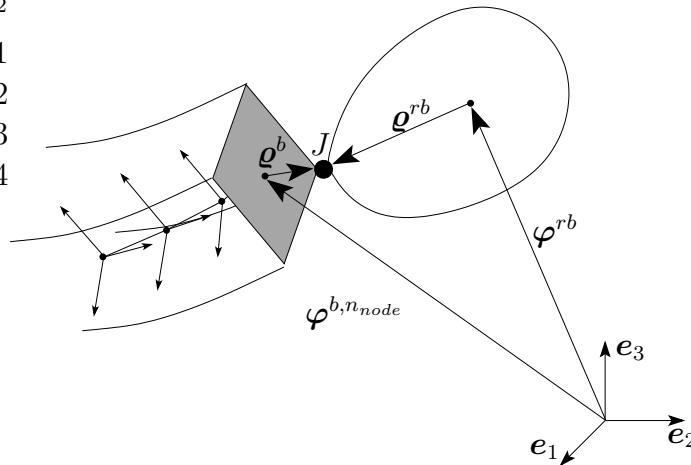
Figure 6.27: Coupling of a beam to a rigid body.

Example 6.3.1 (Coupling of a beam to a rigid body) The configuration variable of the multibody system in Figure 6.27 reads

$$
\boldsymbol{q}(t) = \begin{bmatrix} \boldsymbol{q}^1(t) \\ \vdots \\ \boldsymbol{q}^{n_{node}}(t) \\ \boldsymbol{q}^{rb}(t) \end{bmatrix} \in \mathbb{R}^{12(n_{node}+1)} \tag{6.3.1}
$$

It is subject to the internal constraints of the form (4.3.3) respectively (5.3.6) and the external constraints representing the coupling by a specific joint expatiated in Section 6.1. Interconnecting e.g. the last beam node to a rigid body by means of a specific joint $J \in \{R, P, C, S, E\}$ reduces the relative motion of the rigid body with respect to the beam to the $r^{(J)}$ joint velocities $\boldsymbol{\tau}^{(J)}$ (see Table 6.1). Similar to (6.1.11), the motion of the multibody system is characterised by the independent generalised velocities

$\boldsymbol{\nu} \in \mathbb{R}^{6n_{node}+r^{(J)}}$ with

$$\boldsymbol{\nu} = \begin{bmatrix} \boldsymbol{t}^1 \\ \vdots \\ \boldsymbol{t}^{n_{node}} \\ \boldsymbol{\tau}^{(J)} \end{bmatrix} \tag{6.3.2}$$

The $12(n_{node}+1)$-dimensional redundant velocity vector of the multibody system can then be expressed via

$$\dot{\boldsymbol{q}} = \boldsymbol{P}(\boldsymbol{q}) \cdot \boldsymbol{\nu} = \boldsymbol{P}_{int}(\boldsymbol{q}) \cdot \boldsymbol{P}_{ext}(\boldsymbol{q}) \cdot \boldsymbol{\nu} \tag{6.3.3}$$

The $12(n_{node} + 1) \times 6(n_{node} + 1)$ internal null space matrix is given by

$$\boldsymbol{P}_{int}(\boldsymbol{q}) = \begin{bmatrix} \boldsymbol{P}_{int}^1(\boldsymbol{q}^1) & \boldsymbol{0} & \cdots & \boldsymbol{0} & \boldsymbol{0} \\ \boldsymbol{0} & \boldsymbol{P}_{int}^2(\boldsymbol{q}^2) & \cdots & \boldsymbol{0} & \boldsymbol{0} \\ \vdots & \vdots & \ddots & \vdots & \vdots \\ \boldsymbol{0} & \boldsymbol{0} & \cdots & \boldsymbol{P}_{int}^{n_{node}}(\boldsymbol{q}^{n_{node}}) & \boldsymbol{0} \\ \boldsymbol{0} & \boldsymbol{0} & \cdots & \boldsymbol{0} & \boldsymbol{P}_{int}^{rb}(\boldsymbol{q}^{rb}) \end{bmatrix} \tag{6.3.4}$$

with $\boldsymbol{P}_{int}^\alpha(\boldsymbol{q}^\alpha)$ given in (6.1.10) for $\alpha = 1, \ldots, n_{node}, rb$ and $\boldsymbol{0}$ denoting the 12×6 zero matrix. From (6.1.14) it can be inferred that the $6(n_{node} + 1) \times (6n_{node} + r^{(J)})$ external null space matrix reads

$$\boldsymbol{P}_{ext}(\boldsymbol{q}) = \begin{bmatrix} \boldsymbol{I} & \boldsymbol{0} & \cdots & \boldsymbol{0} & \boldsymbol{0}_{6 \times r^{(J)}} \\ \boldsymbol{0} & \boldsymbol{I} & \cdots & \boldsymbol{0} & \boldsymbol{0}_{6 \times r^{(J)}} \\ \vdots & \vdots & \ddots & \vdots & \vdots \\ \boldsymbol{0} & \boldsymbol{0} & \cdots & \boldsymbol{I} & \boldsymbol{0}_{6 \times r^{(J)}} \\ \boldsymbol{0} & \boldsymbol{0} & \cdots & \boldsymbol{P}_{ext}^{2,(J)}(\boldsymbol{q}) \end{bmatrix} \tag{6.3.5}$$

Here $\boldsymbol{I}$ and $\boldsymbol{0}$ denote the 6×6 identity and zero matrices respectively. Different forms of the external null space matrix $\boldsymbol{P}_{ext}^{2,(J)}(\boldsymbol{q})$ accounting for specific joints can be found in Section 6.1.

Example 6.3.2 (Rigid connection of two beams) A rigid connection between the node $b_1 \in \{1, \ldots, n_{node}^1\}$ with nodal configuration vector $\boldsymbol{q}^{1,b_1} \in \mathbb{R}^{12}$ in the first beam (which contains n_{node}^1 nodes) and the node $b_2 \in \{1, \ldots, n_{node}^2\}$ with nodal configuration vector $\boldsymbol{q}^{2,b_2}$ in the second beam (which contains n_{node}^2 nodes) gives rise to the following six constraint functions

$$\boldsymbol{g}_{ext}^{(F)}(\boldsymbol{q}) = \begin{bmatrix} \boldsymbol{\varphi}^{2,b_2} - \boldsymbol{\varphi}^{1,b_1} + \boldsymbol{\varrho}^{b_2} - \boldsymbol{\varrho}^{b_1} \\ (\boldsymbol{d}_1^{1,b_1})^T \cdot \boldsymbol{d}_2^{2,b_2} - \eta_1 \\ (\boldsymbol{d}_2^{1,b_1})^T \cdot \boldsymbol{d}_3^{2,b_2} - \eta_2 \\ (\boldsymbol{d}_3^{1,b_1})^T \cdot \boldsymbol{d}_1^{2,b_2} - \eta_3 \end{bmatrix} \tag{6.3.6}$$

where $\boldsymbol{\varrho}^{b_1}$ and $\boldsymbol{\varrho}^{b_2}$ point from $\boldsymbol{\varphi}^{1,b_1}$ respectively $\boldsymbol{\varphi}^{2,b_2}$ to the rigidly connected point.

Thus there are no relative degrees of freedom of the node b_2 with respect to the node b_1 and its twist can be calculated in terms of the twist of the node b_1 via

$$\boldsymbol{t}^{2,b_2} = \boldsymbol{P}_{ext}^{2,(F)}(\boldsymbol{q}) \cdot \boldsymbol{t}^{1,b_1} \tag{6.3.7}$$

with the 6×6 null space matrix pertaining to the rigid connection

$$\boldsymbol{P}_{ext}^{2,(F)}(\boldsymbol{q}) = \begin{bmatrix} \boldsymbol{I} & \widehat{\boldsymbol{\varrho}^{b_2} - \boldsymbol{\varrho}^{b_1}} \\ \boldsymbol{0} & \boldsymbol{I} \end{bmatrix} \tag{6.3.8}$$

Then the mapping $\boldsymbol{t} = \boldsymbol{P}_{ext}(\boldsymbol{q}) \cdot \boldsymbol{\nu}$ of the independent generalised velocities $\boldsymbol{\nu} \in \mathbb{R}^{6(n_{node}^1 + n_{node}^2 - 1)}$ to the twist of the multibody system $\boldsymbol{t} \in \mathbb{R}^{6(n_{node}^1 + n_{node}^2)}$ via the external null space matrix $\boldsymbol{P}_{ext}(\boldsymbol{q})$ reads explicitly

$$\begin{bmatrix} \boldsymbol{t}^{1,1} \\ \vdots \\ \boldsymbol{t}^{1,b_1} \\ \vdots \\ \boldsymbol{t}^{1,n_{node}^1} \\ \boldsymbol{t}^{2,1} \\ \vdots \\ \boldsymbol{t}^{2,b_2} \\ \vdots \\ \boldsymbol{t}^{2,n_{node}^2} \end{bmatrix} = \begin{bmatrix} \boldsymbol{I} & \cdots & \boldsymbol{0} & \cdots & \boldsymbol{0} & \boldsymbol{0} & \cdots & \boldsymbol{0} & \boldsymbol{0} & \cdots & \boldsymbol{0} \\ \vdots & \ddots & \vdots & \ddots & \vdots & \vdots & \ddots & \vdots & \vdots & \ddots & \vdots \\ \boldsymbol{0} & \cdots & \boldsymbol{I} & \cdots & \boldsymbol{0} & \boldsymbol{0} & \cdots & \boldsymbol{0} & \boldsymbol{0} & \cdots & \boldsymbol{0} \\ \vdots & \ddots & \vdots & \ddots & \vdots & \vdots & \ddots & \vdots & \vdots & \ddots & \vdots \\ \boldsymbol{0} & \cdots & \boldsymbol{0} & \cdots & \boldsymbol{I} & \boldsymbol{0} & \cdots & \boldsymbol{0} & \boldsymbol{0} & \cdots & \boldsymbol{0} \\ \boldsymbol{0} & \cdots & \boldsymbol{0} & \cdots & \boldsymbol{0} & \boldsymbol{I} & \cdots & \boldsymbol{0} & \boldsymbol{0} & \cdots & \boldsymbol{0} \\ \vdots & \ddots & \vdots & \ddots & \vdots & \vdots & \ddots & \vdots & \vdots & \ddots & \vdots \\ \boldsymbol{0} & \cdots & \boldsymbol{P}_{ext}^{2,(F)} & \cdots & \boldsymbol{0} & \boldsymbol{0} & \cdots & \boldsymbol{0} & \boldsymbol{0} & \cdots & \boldsymbol{0} \\ \vdots & \ddots & \vdots & \ddots & \vdots & \vdots & \ddots & \vdots & \vdots & \ddots & \vdots \\ \boldsymbol{0} & \cdots & \boldsymbol{0} & \cdots & \boldsymbol{0} & \boldsymbol{0} & \cdots & \boldsymbol{0} & \boldsymbol{0} & \cdots & \boldsymbol{I} \end{bmatrix} \cdot \begin{bmatrix} \boldsymbol{t}^{1,1} \\ \vdots \\ \boldsymbol{t}^{1,b_1} \\ \vdots \\ \boldsymbol{t}^{1,n_{node}^1} \\ \boldsymbol{t}^{2,1} \\ \vdots \\ \boldsymbol{t}^{2,b_2-1} \\ \boldsymbol{t}^{2,b_2+1} \\ \vdots \\ \boldsymbol{t}^{2,n_{node}^2} \end{bmatrix} \tag{6.3.9}$$

6.3.1 General treatment by the discrete null space method

A further generalisation to multibody systems consisting of several elastic and rigid components can be accomplished in a straightforward way. Specific nodal configuration vectors $\boldsymbol{q}^\alpha, \boldsymbol{q}^\beta \in \mathbb{R}^{12}$ are coupled according to the procedure described for kinematic pairs, regardless whether they represent a node in a spatially discretised beam or a rigid body's configuration. The order in which the nodal configuration vectors are combined to the configuration vector of the multibody system (see e.g. (6.3.1)), defines the positions of the node-specific block-matrices in the internal null space matrix (see e.g. (6.3.4)). It also prescribes the assembly of the external null space matrices representing specific couplings in the total external null space matrix (see e.g. (6.3.5) and (6.3.9)).

A general procedure for the treatment of multibody systems consisting of rigid and elastic components by the discrete null space method comprises the steps described in Table 6.6. All alternatives for the construction of the discrete null space matrix in step (iii) yield equivalent results, but they differ significantly in the arising computational costs (see Remark 6.2.7). From the computational point of view, the explicit representation in **alternative iii.1** is most desirable. If it is not feasible for the problem at hand (e.g. for most closed loop systems) the semi-explicit representation in **alternative iii.3** states a reasonable compromise while the implicit representation in **alternative iii.2** requires the highest computational costs.

Table 6.6: General procedure for the treatment of flexible multibody systems by the discrete null space method.

(i) definition of the order in which the nodal configuration variables (regardless whether they represent a node in a spatially discretised beam or a rigid body's configuration) are combined to the configuration variable of the multibody system $\boldsymbol{q} \in \mathbb{R}^n$

(ii) identification of independent constraint functions and full-rank Jacobian; comprising m_{int} internal constraint functions and m_{ext} external constraint functions corresponding to n_c couplings or bearings

$$
\boldsymbol{g}(\boldsymbol{q}) = \begin{bmatrix} \boldsymbol{g}_{int}(\boldsymbol{q}) \\ \boldsymbol{g}_{ext}^1(\boldsymbol{q}) \\ \vdots \\ \boldsymbol{g}_{ext}^{n_c}(\boldsymbol{q}) \end{bmatrix} \in \mathbb{R}^m \qquad \boldsymbol{G}(\boldsymbol{q}) = \begin{bmatrix} \boldsymbol{G}_{int}(\boldsymbol{q}) \\ \boldsymbol{G}_{ext}^1(\boldsymbol{q}) \\ \vdots \\ \boldsymbol{G}_{ext}^{n_c}(\boldsymbol{q}) \end{bmatrix} \in \mathbb{R}^{m \times n}
$$

where $m = m_{int} + m_{ext} = m_{int} + m_{ext}^1 + \ldots + m_{ext}^{n_c}$

(iii) construction of a full-rank discrete null space matrix $\mathbf{P}(\boldsymbol{q}_n, \boldsymbol{q}_{n+1}) \in \mathbb{R}^{n \times (n-m)}$ fulfilling $\mathbf{G}(\boldsymbol{q}_n, \boldsymbol{q}_{n+1}) \cdot \mathbf{P}(\boldsymbol{q}_n, \boldsymbol{q}_{n+1}) = \mathbf{0}$ by employing one of the alternatives outlined in the sequel

alternative iii.1 (explicit representation)
construction of a continuous null space matrix $\boldsymbol{P}(\boldsymbol{q}) \in \mathbb{R}^{n \times (n-m)}$ fulfilling $\boldsymbol{G}(\boldsymbol{q}) \cdot \boldsymbol{P}(\boldsymbol{q}) = \mathbf{0}$ by a) or b)

    a) velocity analysis (see Section 2.3.4): successive reduction of the redundant velocities $\dot{\boldsymbol{q}} \in \mathbb{R}^n$ to the independent generalised velocities $\boldsymbol{\nu} \in \mathbb{R}^{n-m}$

        • internal constraints: $\dot{\boldsymbol{q}} = \boldsymbol{P}_{int}(\boldsymbol{q}) \cdot \boldsymbol{t}, \quad \boldsymbol{t} \in \mathbb{R}^{n-m_{int}}$

        • first external coupling or bearing:
        $\dot{\boldsymbol{q}} = \boldsymbol{P}_{int}(\boldsymbol{q}) \cdot \boldsymbol{P}_{ext}^1(\boldsymbol{q}) \cdot \boldsymbol{\nu}^1, \quad \boldsymbol{\nu}^1 \in \mathbb{R}^{n-m_{int}-m_{ext}^1}$

        $\vdots$

        • last external coupling or bearing:
        $\dot{\boldsymbol{q}} = \boldsymbol{P}_{int}(\boldsymbol{q}) \cdot \boldsymbol{P}_{ext}^1(\boldsymbol{q}) \cdot \ldots \cdot \boldsymbol{P}_{ext}^{n_c}(\boldsymbol{q}) \cdot \boldsymbol{\nu}, \quad \boldsymbol{\nu} \in \mathbb{R}^{n-m}$

        • $\boldsymbol{P}(\boldsymbol{q}) = \boldsymbol{P}_{int}(\boldsymbol{q}) \cdot \boldsymbol{P}_{ext}^1(\boldsymbol{q}) \cdot \ldots \cdot \boldsymbol{P}_{ext}^{n_c}(\boldsymbol{q})$

    b) explicit analytical QR-decomposition of the transposed constraint Jacobian in terms of $\boldsymbol{q}$: $\boldsymbol{G}^T = [\boldsymbol{Q}_1, \boldsymbol{Q}_2] \cdot \boldsymbol{R}$ yields $\boldsymbol{P}(\boldsymbol{q}) = \boldsymbol{Q}_2(\boldsymbol{q})$ (see Section 2.3.4)

midpoint evaluation of the continuous null space matrix $\boldsymbol{P}(\boldsymbol{q}_{n+\frac{1}{2}})$ or slight modification of the midpoint evaluation yields $\mathbf{P}(\boldsymbol{q}_n, \boldsymbol{q}_{n+1})$ (see Remark 3.2.8)

alternative iii.2 (implicit representation)
QR-decomposition of $\boldsymbol{G}^T(\boldsymbol{q}_n)$ yields the necessary submatrices to infer $\mathbf{P}(\boldsymbol{q}_n, \boldsymbol{q}_{n+1})$ via formula (3.2.38) (see Example 3.2.9)

alternative iii.3 (semi-explicit representation)

- explicit representation of internal discrete null space matrix:
  $\mathbf{P}_{int}(\boldsymbol{q}_n, \boldsymbol{q}_{n+1}) = \boldsymbol{P}_{int}(\boldsymbol{q}_{n+\frac{1}{2}})$

- if possible: $\mathbf{P}_{ext}^c(\boldsymbol{q}_n, \boldsymbol{q}_{n+1})$ is obtained explicitly by midpoint evaluation $\boldsymbol{P}_{ext}^c(\boldsymbol{q}_{n+\frac{1}{2}})$ for $c = 1, \ldots, n_c$ or by slight modification of that (see Remark 3.2.8)

- if not possible: QR-decomposition of
  $\left(\boldsymbol{G}_{ext}^c(\boldsymbol{q}_n) \cdot \boldsymbol{P}_{int}(\boldsymbol{q}_n) \cdot \boldsymbol{P}_{ext}^1(\boldsymbol{q}_n) \cdot \ldots \cdot \boldsymbol{P}_{ext}^{c-1}(\boldsymbol{q}_n) \right)^T$ yields implicitly $\mathbf{P}_{ext}^c(\boldsymbol{q}_n, \boldsymbol{q}_{n+1})$ for $c = 1, \ldots, n_c$ via formula (3.2.38) (see Remark 6.2.6 and Example 3.2.9)

- $\mathbf{P}(\boldsymbol{q}_n, \boldsymbol{q}_{n+1}) = \mathbf{P}_{int}(\boldsymbol{q}_n, \boldsymbol{q}_{n+1}) \cdot \mathbf{P}_{ext}^1(\boldsymbol{q}_n, \boldsymbol{q}_{n+1}) \cdot \ldots \cdot \mathbf{P}_{ext}^{n_c}(\boldsymbol{q}_n, \boldsymbol{q}_{n+1})$

(iv) solution of the resulting nonlinear algebraic system by applying one of the alternatives outlined in the sequel

alternative iv.1 (d'Alembert-type scheme)
solution of time-stepping scheme (3.2.33) for $\boldsymbol{q}_{n+1} \in \mathbb{R}^n$

alternative iv.2 (d'Alembert-type scheme with nodal reparametrisation)
nodal reparametrisation (3.2.42) $\boldsymbol{q}_{n+1} = \boldsymbol{F}_{\boldsymbol{q}_n}(\boldsymbol{\mu})$; solution of time-stepping scheme (3.2.44) for $\boldsymbol{\mu} \in \mathbb{R}^{n-m}$

6.3.2 Numerical example: spatial slider-crank mechanism
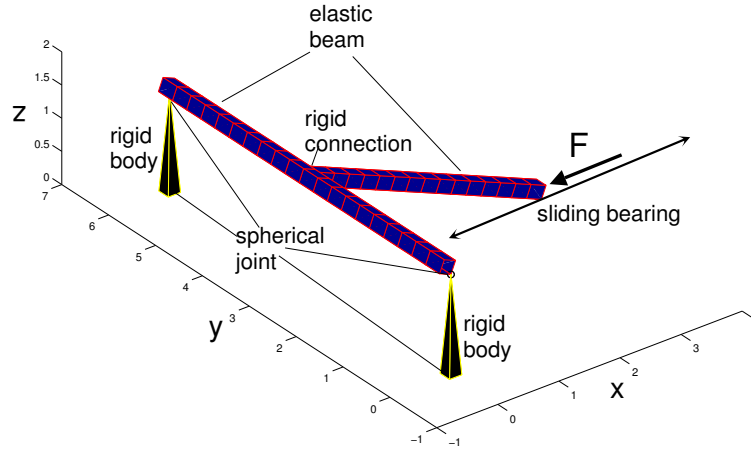
Figure 6.28: Initial configuration of the spatial slider-crank mechanism.

The multibody system under consideration is a three-dimensional slider-crank mechanism. The initial configuration is depicted in Figure 6.28. It consists of a horizontal elastic beam of length 6, which is discretised by 20 linear beam elements and characterised by the axial and shear stiffness $EA = GA = 10^5$ and bending and torsional stiffness $EI = EJ = 10^4$. The middle node (node 11) is rigidly connected (see Example 6.3.2) to the first node of the elastic slider of length 4, which is discretised by 15 linear beam elements and characterised by the axial and shear stiffness $EA = GA = 10^6$ and bending and torsional stiffness $EI = EJ = 10^5$. The hyperelastic material behaviour of the beams is specified in Example 5.3.3. The end of the slider is supported by a sliding bearing (see Section 4.3.5) which allows it to slide parallel to the x-axis in the xy-plane. The inertia properties of both elastic beams are characterised by the mass density per reference length $A_\rho = 20$ and the principal mass moments of inertia of the cross-section $M_\rho^1 = M_\rho^2 = 10$. The ends of the horizontal beam are connected via spherical joints to rigid bodies (see Example 6.3.1), which are modelled as pyramids of height $H = 1.5$ with square bases of edge length $A = 0.2$ and total mass $M = 1$ respectively. To allow true three-dimensional motion, both rigid bodies are supported by spherical joints fixed in space (see Section 4.3.5). A force parallel to the x-axis $\boldsymbol{F}(t) = f(t)\boldsymbol{e}_1$ with

$$
f(t) = \begin{cases} 1000 \sin(\pi t) & \text{for} \quad t \le 2 \\ 0 & \text{for} \quad t > 2 \end{cases} \tag{6.3.10}
$$

is applied at the end of the slider with a sinusoidal time variation for the first two seconds of motion. After the force is removed the system undergoes free vibration, since no other external loads are present. The results presented in the sequel have been obtained by

solving the d'Alembert-type scheme with nodal reparametrisation (3.2.44). Figure 6.29 shows a series of snapshots of the motion and deformation of the slider-crank mechanism during the first and second revolution. The cuboids of the initially horizontal beam are coloured by a linear interpolation of the norm of the resulting momenta $\left\|\boldsymbol{m}_e\right\|$ in the elements whereas the slider is coloured by the norm of the resultant forces $\left\|\boldsymbol{n}_e\right\|$. Thereby blue represents zero while red represents 3000. The deformations depicted in Figure 6.29 are the original deformations, they have not been scaled for the illustration.

The orbit of the rigid connection point between the beams in Figure 6.30 also emphasises the large deformation the system is undergoing. It starts as a circle but soon leaves that path due to the large bending of the initially horizontal beam. The diagrams in Figure 6.31 show the stress resultants in the rigidly connected elements for the horizontal beam on the left and for the slider on the right hand side. One can see that the horizontal beam undergoes much bending deformation whereas in the slider the axial and shear forces dominate. Figure 6.32 shows that after the removal of the external forces at $t = 2$ the total energy is conserved exactly. It also reveals that the strain energy amounts a substantial part of the total energy.

Comparison

The same problem has been calculated using the constrained scheme (3.2.7). The schemes are equivalent, consequently the solutions are identical and both schemes fulfil the constraints exactly. Table 6.7 summarises the simulations using both schemes. A remarkable difference is in the dimensions of the system of equations of motion. For the present problem, the constrained scheme requires the solution of 722 equations whereas the system for the d'Alembert-type scheme with nodal reparametrisation is 214-dimensional. This has a big impact on the computational costs, the constrained scheme requires more than twice the CPU-time than the d'Alembert-type scheme with nodal reparametrisation to simulate 10 seconds of motion and deformation of the slider-crank mechanism. For the time-step $h = 10^{-2}$ the condition number of the constrained scheme is of the order 10^{10} and it increases substantially for decreasing time-steps, whereas it is of the order 10^4 or less for arbitrary time-steps in the d'Alembert-type scheme.
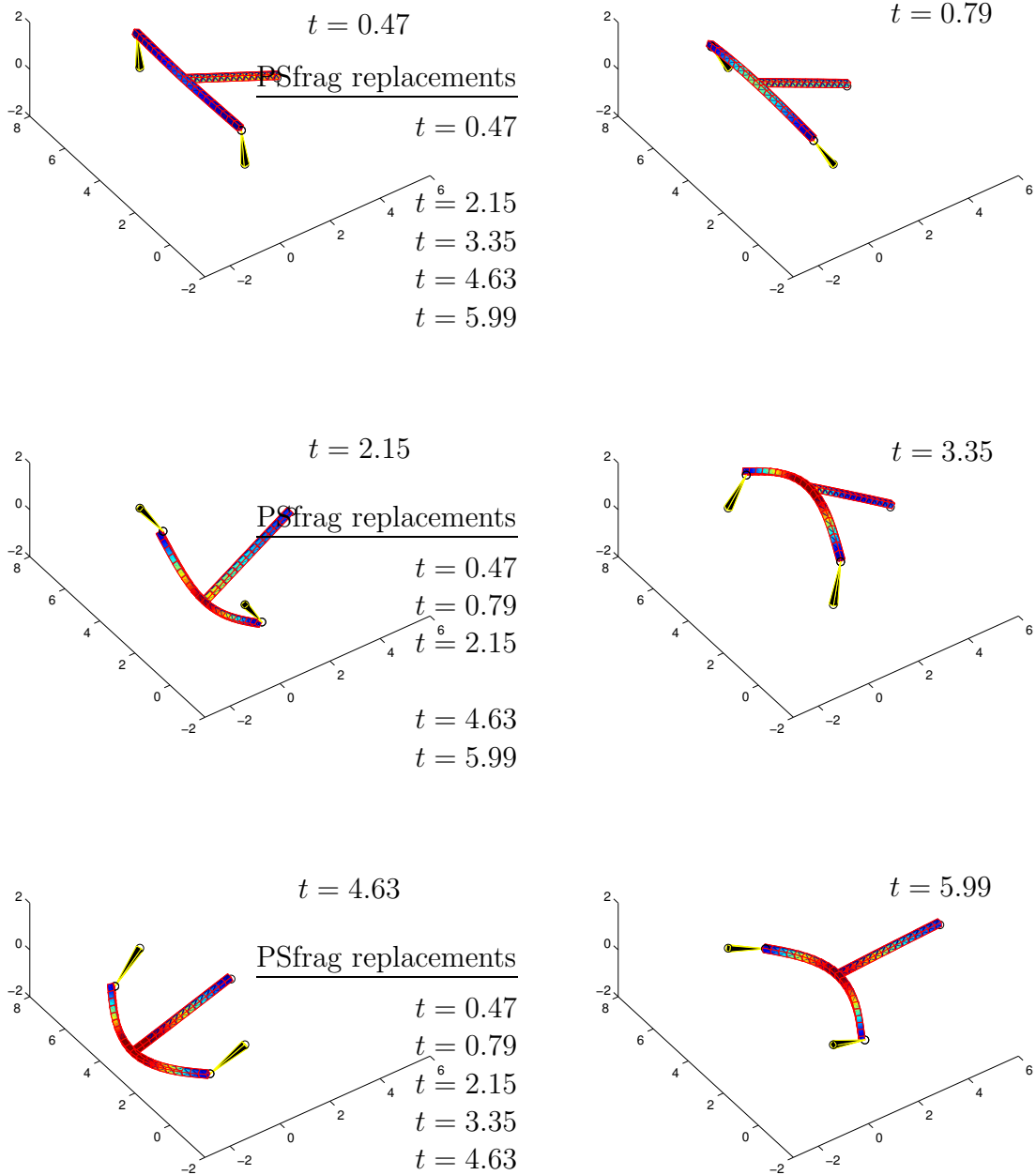
Figure 6.29: Spatial slider-crank mechanism: snapshots of the motion and deformation at $t \in \{0.47, 0.79, 2.15, 3.35, 4.63, 5.99\}$.
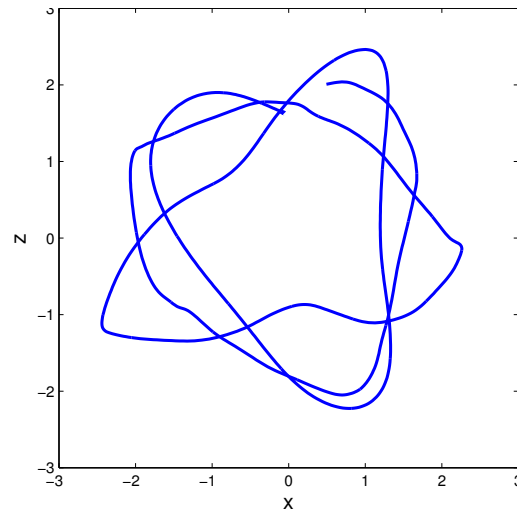
Figure 6.30: Spatial slider-crank mechanism: orbit of the rigid connection point in the xz-plane.
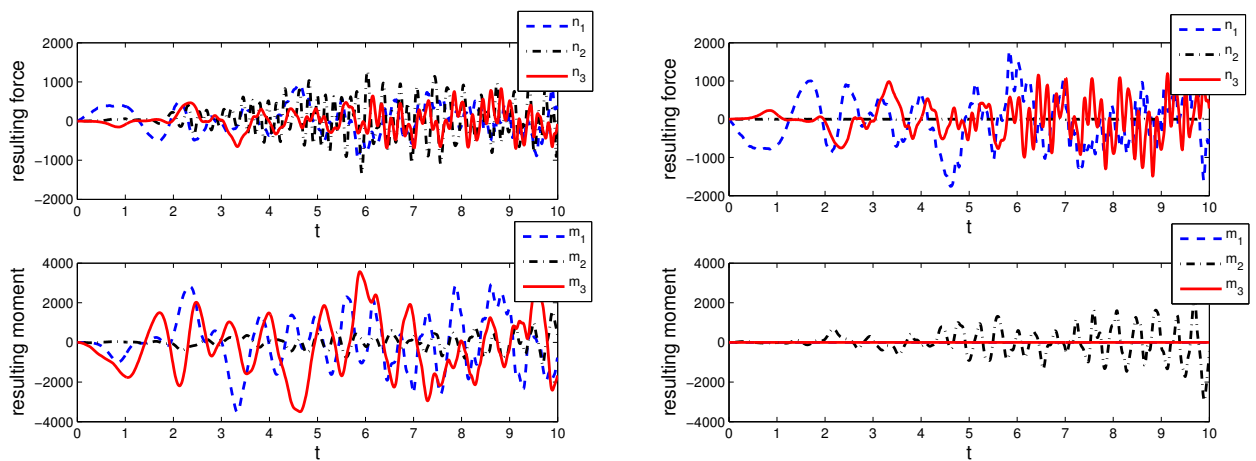
Figure 6.31: Spatial slider-crank mechanism: stress resultants in rigidly connected elements in the initially horizontal beam (left) and in the slider (right) ($h = 0.01$).
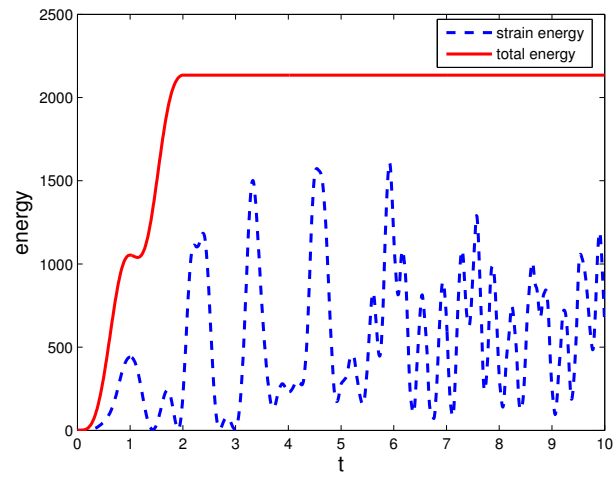
Figure 6.32: Spatial slider-crank mechanism: energy ($h = 0.01$).

Table 6.7: Comparison of constrained scheme to d'Alembert-type scheme with nodal reparametrisation for the example 'spatial slider-crank mechanism'.

	constrained	d'Alembert
number of unknowns $n = 468 \quad m = 254$	722	214
CPU-time	2.3	1
condition number $h = 10^{-2}$ $h = 10^{-3}$ $h = 10^{-4}$	10^{10} 10^{11} 10^{14}	10^4 10^3 10^3

7 Conclusions

Energy-momentum conserving time-stepping schemes emanating from the use of different methods for the constraint enforcement have been deduced from scratch in this work. The derived algorithms have been compared by means of theoretical investigations as well as with the help of examples. Particular emphasis has been placed on their robustness, accuracy and efficiency for the simulation of flexible multibody dynamics. It turned out that the Lagrange multiplier method can be applied in a straight-forward manner to complex settings. However this approach requires the solution of the augmented system of DAEs which yields exact constraint fulfilment on the one hand, but on the other hand becomes computationally expensive for large problems subject to a high number of constraints and, moreover, is subject to severe conditioning problems. The Lagrange multiplier method yields accurate solutions but is neither robust nor efficient. Using the penalty method, the high sensitivity of the constraint fulfilment to the choice of the penalty parameter is troublesome. While proper enforcement of the constraints requires high penalty parameters, the system becomes increasingly stiff. The dependence of the condition number on the time-step and the penalty parameter is clearly demonstrated in the example of the double spherical pendulum. Although the penalty method can perform relatively accurate, this property is negatived by high condition numbers or high computational costs as a consequence of a small time-step balancing the high penalty parameter. The most striking property of the augmented Lagrange method is its immensely high computational effort which disqualifies it in the competition with the other methods. It has been shown by theoretical analysis and numerical examples that the discrete null space method with nodal reparametrisation performs excellently in all respects. This approach yields accurate results – the constraints are fulfilled exactly, the computational costs are comparatively low since the system of equations has the minimal possible dimension and it is robust due to the independence of the condition number on the time-step. Therefore, this method is investigated in detail in this work.

The construction of a discrete null space matrix lies at the heart of the discrete null space method. The key properties of a discrete null space matrix are summarised in Remark 3.2.7, based on the necessary and sufficient condition (3.2.30). With its help the Lagrange multipliers are eliminated from the temporally discretised constrained scheme and the systems dimension is reduced. The primary question 'How can a discrete null space matrix for a specific problem be found?' is answered explicitly for general flexible multibody dynamics. It can be stated that an explicit representation of the discrete null space matrix is generally desirable, since it minimises the computational costs. Such an explicit representation is feasible for most applications, e.g. for the examples in this work comprising mass point systems, rigid body dynamics, open kinematic chains and flexible multibody dynamics. Solely the simulation of the dynamics of the closed loop system

requires special treatment, involving an implicit representation of a discrete null space matrix.

The explicit representation of a discrete null space matrix can be inferred from a corresponding continuous null space matrix either by midpoint evaluation at $\boldsymbol{q}_{n+\frac{1}{2}}$ or by slight modification of the midpoint evaluation, see Remark 3.2.8. The necessary continuous null space matrix can also be constructed in two different ways, either via velocity analysis or by performing an explicit QR-decomposition of the transposed continuous constraint Jacobian in terms of the configuration variable, see Section 2.3.4. The latter approach has been used for the example of the double spherical pendulum while all other continuous null space matrices have been constructed via velocity analysis. The third possibility to obtain a continuous null space matrix as the Jacobian of the reparametrisation of the constraint manifold in terms of generalised coordinates mentioned in Remark 2.3.10 cannot be used to construct an explicit discrete null space matrix by midpoint evaluation or slight modification of that, since it involves generalised coordinates. This fact is shown exemplarily for the six-body linkage, see Remark 6.2.9. The six-body linkage constitutes an example, for which it is not possible to construct a continuous null space matrix in terms of the configuration variable, from which an explicit discrete null space matrix can be inferred. Thus the discrete null space matrix has to be constructed implicitly.

The implicit construction of a discrete null space matrix, based on the QR-decomposition of the transposed constraint Jacobian at every time-step, is always feasible, see Example 3.2.9. However, to reduce the computational effort, it is recommendable to use a semi-explicit representation of the discrete null space matrix as proposed in Remark 6.2.6 for closed kinematic chains. Its construction is based on the idea of identifying those constraints which impede the construction of an explicit discrete null space matrix (typically these are the closure constraints) and to set up an explicit discrete null space matrix corresponding to the remaining constraints. Then the null space matrix pertaining to the identified (closure) constraints can be obtained implicitly and a semi-explicit representation of the total null space matrix is gained by multiplication of the explicit and the implicit discrete null space matrices, see Section 6.2.3.

An instructive outline for the treatment of general multibody systems by the discrete null space method is given in Section 6.3.1, providing a new robust, accurate and efficient integrator for flexible multibody dynamics. Thereby, particular use can be made of the discrete null space matrices pertaining to the internal constraints for rigid bodies and spatially discretised beams and of the discrete null space matrices pertaining to the external constraints arising from the interconnection of kinematic pairs by joints which are given explicitly in this work.

7.1 Outlook

This study is of course by no means considered to close the rather active field of research on computational methods for flexible multibody dynamics. Various topics seem to be attractive for future investigations.

- The considerations in this work are restricted to holonomic constraints on the configuration level. In [Bets 04] the discrete null space method has been generalised to

nonholonomic equality constraints and applied to a rigid ball, rolling on an inclined plane. This can be considered as the foundation for a systematic construction of discrete null space matrices pertaining to the integrable holonomic constraints on the momentum level, arising from temporal differentiation of internal or external configurational constraints.

- Flexible structures considered in this work are elastic beams, discretised using structural finite beam elements. The discrete null space method could also be applied to other structural elements like shells or plates and their coupling to multibody systems. Furthermore, the application to flexible bodies which are discretised by continuum finite elements and coupled to other bodies are of interest.

- The discrete null space method could be extended to inequality constraints occurring e.g. in contact problems.

- It is of interest to test the discrete null space method in conjunction with other temporal discretisation methods, e.g. variational integrators leading to symplectic-momentum conserving time-stepping schemes.

- A very important field of application of multibody dynamics are actuated systems. An extension of the discrete null space method to optimal control problems seems to be a challenging and worthwhile task.

A Definitions

The following standard definitions can be found in a variety of books. The list includes parts of the representations in [Abra 78], [Mars 94], [Bern 98], [Agri 01], [Choq 77], [Arno 78], [Luen 84]:

Definition A.1 (Differentiable manifold) Let M be a connected, topological Hausdorff space. A *chart* on M is a pair (ψ, U), where U is an open set in a Banach space X and ψ is a bijection of U onto some subset of M,

$$\psi : U \to \psi(U) \subset M$$

If two charts (ψ, U) and (ψ', U') have an overlapping image in M, then $V := (\psi)^{-1} \left(\psi(U) \cap \psi'(U') \right)$ and $V' := (\psi')^{-1} \left(\psi(U) \cap \psi'(U') \right)$ are open sets in X. Hence the mapping $(\psi')^{-1} \circ \psi : V \to V'$ is defined. The two charts are called *compatible* if this mapping is C^∞. A union of compatible charts is called *atlas*, and two atlases are *equivalent* if their union is also an atlas.
M is called *differentiable manifold* if M has an atlas. If every chart has domain in an n-dimensional vector space, M is called n-manifold. In other words, M is covered by a union of compatible charts, and the differentiable structure on M is an equivalence class of atlases.

Definition A.2 (Bundle, fibre) A *bundle* is a triple (E, B, τ) consisting of two topological spaces E and B and a continuous, surjective mapping $\tau : E \to B$. B is called the *base*. If for all $x \in B$ the topological spaces $\tau^{-1}(x)$ are homeomorphic to a space F, then $\tau^{-1}(x)$ is called *fibre* at x.

Definition A.3 (Tangent vector, tangent space, tangent bundle, cotangent bundle) Two curves $\boldsymbol{c}_1, \boldsymbol{c}_2 : \mathbb{R} \to M$ in an n-manifold M are called *equivalent at x*, if

$$\boldsymbol{c}_1(0) = \boldsymbol{c}_2(0) = x \quad \text{and} \quad (\psi^{-1} \circ \boldsymbol{c}_1)'(0) = (\psi^{-1} \circ \boldsymbol{c}_2)'(0)$$

in some chart ψ. This definition is chart independent. A *tangent vector $\boldsymbol{v}$* to a manifold M at $\boldsymbol{x} \in M$ is an equivalence class of curves at $\boldsymbol{x}$. Let U be a chart of an atlas for M with coordinates $\boldsymbol{x} = (x_1, \ldots, x_n)$. The components of the tangent vector $\boldsymbol{v}$ to the curve $(\psi^{-1} \circ \boldsymbol{c}) : \mathbb{R} \to \mathbb{R}^n$ are defined by

$$v^i = \frac{d}{dt}(\psi^{-1} \circ \boldsymbol{c})^i|_{t=0} \quad \text{where } i = 1, \ldots, n$$

The set of tangent vectors to M at $\boldsymbol{x}$ forms a vector space, called the *tangent space* to M at $\boldsymbol{x}$, denoted by $T_{\boldsymbol{x}} M$.

The union of the tangent spaces $T_{\boldsymbol{x}}M$ to M at all points $\boldsymbol{x} \in M$ is the differentiable manifold

$$TM = \bigcup_{\boldsymbol{x} \in M} T_{\boldsymbol{x}}M$$

Together with the *natural projection* $\tau_M : TM \to M$, which takes a tangent vector $\boldsymbol{v} \in T_{\boldsymbol{x}}M \subset TM$ to the point $\boldsymbol{x}$, the *tangent bundle* (TM, M, τ_M) is defined. If the base and the projection are clear from the circumstances, the tangent bundle is denoted by TM.

Let $\boldsymbol{x} = (x_1, \ldots, x_n)$ be local coordinates on M and let $\boldsymbol{v} = (v_1, \ldots, v_n)$ be components of a tangent vector in this coordinate system. Then $(\boldsymbol{x}, \boldsymbol{v}) = (x_1, \ldots, x_n, v_1, \ldots, v_n)$ give a local coordinates system on TM.

If each vector space $T_{\boldsymbol{x}}M$ is replaced with its dual $T_{\boldsymbol{x}}^*M$, and the canonical projection $\pi_Q : T^*M \to M$ is introduced analogously to τ_M, one obtains the *cotangent bundle* (T^*M, M, π_M), which is often simply denoted by T^*M.

Definition A.4 (Derivative) Let M and N be differentiable manifolds (see A.1) and $f : M \to N$ a map. f is called *differentiable*, if f is given by differentiable functions in local coordinates on M and N. The *derivative* (or *tangent lift*) at any point $\boldsymbol{x} \in M$ is the linear map

$$T_{\boldsymbol{x}}f : T_{\boldsymbol{x}}M \to T_{f(\boldsymbol{x})}N$$

constructed in the following way: for $\boldsymbol{v} \in T_{\boldsymbol{x}}M$ choose a curve $\boldsymbol{c} :] -\epsilon, \epsilon[\to M$ with $\boldsymbol{c}(0) = \boldsymbol{x}$ and velocity vector $\boldsymbol{c}'(0) = \boldsymbol{v}$. Then $T_{\boldsymbol{x}}f \cdot \boldsymbol{v}$ is the velocity vector at $t = 0$ of the curve $f \circ \boldsymbol{c} : \mathbb{R} \to N$, i.e.

$$T_{\boldsymbol{x}}f \cdot \boldsymbol{v} = \frac{d}{dt}f\left(c(t)\right)|_{t=0}$$

If M and N are finite dimensional, the derivative is also denoted by Df and called the *Jacobian*. If $N = \mathbb{R}$ and identifying the tangent space of $\mathbb{R}$ at any point with itself (as it is usually done with vector spaces), one gets the linear map $\boldsymbol{d}f(\boldsymbol{x}) : T_{\boldsymbol{x}}M \to \mathbb{R}$. That is $\boldsymbol{d}f(\boldsymbol{x}) \in T_{\boldsymbol{x}}^*M$ and reads in coordinates

$$\boldsymbol{d}f(\boldsymbol{x}) \cdot \boldsymbol{v} = \frac{\partial f}{\partial x^i}v^i$$

$\boldsymbol{d}f$ is called *differential* of f. Using the operators $\dfrac{\partial}{\partial x^i}$ one can identify a basis of $T_{\boldsymbol{x}}M$ by $\left(\dfrac{\partial}{\partial x^1}, \ldots, \dfrac{\partial}{\partial x^n}\right)$. The dual basis to $\dfrac{\partial}{\partial x^i}$ is dx^i, thus

$$\boldsymbol{d}f(\boldsymbol{x}) = \frac{\partial f}{\partial x^i}dx^i$$

holds for any smooth function $f : M \to \mathbb{R}$.

Definition A.5 (Functional derivative) Let P be a smooth infinite-dimensional manifold. Moreover assume that P is a subset of an infinite-dimensional linear space V with interior product $\langle \cdot, \cdot \rangle : V \times V \to \mathbb{R}$. The functional derivative of a smooth functional $f : P \to \mathbb{R}$ at $\varphi \in P$, denoted by $\dfrac{\delta f}{\delta \varphi}$, is the unique element of V, if it exists, satisfying

$$\langle \frac{\delta f}{\delta \varphi}, v \rangle = T_\varphi f \quad \text{for all } v \in T_\varphi P$$

Definition A.6 (Cotangent lift) Let M and N be two manifolds, and let $f : M \to N$ be a diffeomorphism. The *cotangent lift* of $T^*f : T^*N \to T^*M$ of f is defined by

$$\langle T^*f(\boldsymbol{a_s}), \boldsymbol{v} \rangle = \langle \boldsymbol{a_s}, Tf \cdot \boldsymbol{v} \rangle$$

where $\boldsymbol{a_s} \in T^*_{\boldsymbol{q}}N$, $\boldsymbol{v} \in T_{\boldsymbol{r}}M$, $\boldsymbol{r} \in M$, $\boldsymbol{s} \in N$ and $\boldsymbol{s} = f(\boldsymbol{r})$.

Definition A.7 (k-form) A *two-form* ω on M is a function $\omega_{\boldsymbol{x}} : T_{\boldsymbol{x}}M \times T_{\boldsymbol{x}}M \to \mathbb{R}$ that assigns to each point $\boldsymbol{x} \in M$ a skew-symmetric bilinear form from the tangent space $T_{\boldsymbol{x}}M$ to M at $\boldsymbol{x}$.
More generally, a k-form α on M is a function $\omega_{\boldsymbol{x}} : T_{\boldsymbol{x}}M \times \ldots \times T_{\boldsymbol{x}}M \to \mathbb{R}$ that assigns to each point $\boldsymbol{x} \in M$ a skew-symmetric k-multilinear form from the tangent space $T_{\boldsymbol{x}}M$ to M at $\boldsymbol{x}$.

Definition A.8 (Interior product) Let α be a k-form on a manifold M and $X : M \to TM$ be a vector field. The *interior product* $\mathrm{i}_X\alpha$ of X and α (sometimes called *contraction* and denoted by $\mathrm{i}(X)\alpha$) is the $(k-1)$-form

$$(\mathrm{i}_X\alpha)_{\boldsymbol{x}}(v_2, \ldots, v_k) = \alpha_{\boldsymbol{x}}(X(\boldsymbol{x}), v_2, \ldots, v_k)$$

for $\boldsymbol{x} \in M$ and $(v_2, \ldots, v_k) \in T_{\boldsymbol{x}}M$.

Definition A.9 (Exterior derivative) The *exterior derivative* $\boldsymbol{d}\alpha$ of a k-form α on M is the $(k+1)$-form on M, which is uniquely determined by the following properties:

(i)   If α is a 0-form, i.e. $\alpha = f \in \mathcal{C}^\infty(M)$, then $\boldsymbol{d}\alpha$ is the one-form which is the differential of f.

(ii) $\boldsymbol{d}\alpha$ is linear in α.

(iii) $\boldsymbol{d}\alpha$ satisfies the product rule, that is

$$\boldsymbol{d}(\alpha \wedge \beta) = \boldsymbol{d}\alpha \wedge \beta + (-1)^k \alpha \wedge \boldsymbol{d}\beta$$

where α is a k-form and β is a l-form.

(iv) $\boldsymbol{d}^2 = 0$, i.e. $\boldsymbol{d}(\boldsymbol{d}\alpha) = 0$ for any k-form α.

(v) $\boldsymbol{d}$ is a local operator, i.e. $\boldsymbol{d}\alpha(\boldsymbol{x})$ only depends on α restricted to any open neighborhood of $\boldsymbol{x}$. If $U \subset M$ is open, then

$$\boldsymbol{d}(\alpha|_U) = (\boldsymbol{d}\alpha)|_U$$

Definition A.10 (Symplectic manifold) A *symplectic manifold* is a pair (P, ω) where P is a manifold (see A.1) and ω is a *symplectic form*, i.e. ω is a closed, (weakly) nondegenerate two-form (see A.7) on P.

ω is called *closed* if $\boldsymbol{d}\omega = 0$, where $\boldsymbol{d}$ is the exterior derivative (see A.9), and it is called *weakly nondegenerate* if for $\boldsymbol{z} \in P$ the induced map $\omega_{\boldsymbol{z}}^{b} : T_{\boldsymbol{z}}P \to T_{\boldsymbol{z}}^{*}P$ with $\omega_{\boldsymbol{z}}^{b}(\boldsymbol{x})(\boldsymbol{y}) = \omega_{\boldsymbol{z}}(\boldsymbol{x}, \boldsymbol{y})$ is injective, i.e. let $\boldsymbol{x} \in T_{\boldsymbol{z}}P$, if $\omega_{\boldsymbol{z}}(\boldsymbol{x}, \boldsymbol{y}) = 0$ for all $\boldsymbol{y} \in T_{\boldsymbol{z}}P$ then $\boldsymbol{x} = \boldsymbol{0}$. In the case of strong nondegeneracy $\omega_{\boldsymbol{z}}^{b}$ is an isomorphism.

If P is finite dimensional, weak nondegeneracy and strong degeneracy are equivalent.

Definition A.11 (Pull back, push forward) Let $f : M \to N$ be a $\mathcal{C}^{\infty}$-map between the manifolds (see A.1) M and N and α be a k-form on N. The *pull back* $f^{*}\alpha$ of α by f is the k-form on M given by

$$(f^{*}\alpha)_{\boldsymbol{x}}(v_1, \ldots, v_k) = \alpha_{f(\boldsymbol{x})}(T_{\boldsymbol{x}}f \cdot v_1, \ldots, T_{\boldsymbol{x}}f \cdot v_k)$$

for $\boldsymbol{x} \in M$, $v_1, \ldots v_k \in T_{\boldsymbol{x}}M$ and $T_{\boldsymbol{x}}f$ the derivative (see A.4) of f.

If $Y : N \to TN$ is a vector field on N and f is a diffeomorphism, the *pull back* $f^{*}Y$ is a vector field on M defined by

$$(f^{*}Y)(\boldsymbol{x}) = T_{\boldsymbol{x}}f^{-1} \circ Y \circ f$$

where $\boldsymbol{x} \in M$ and $T_{\boldsymbol{x}}f^{-1}$ the derivative (see A.4) of f^{-1}.

If f is a diffeomorphism, the *push forward* f_{*} is defined by $f_{*} = (f^{-1})^{*}$.

Definition A.12 (Symplectic/canonical transformation) A differentiable map $f : P_1 \to P_2$ between symplectic manifolds (P_1, ω_1) and (P_2, ω_2) (see A.10) is called *symplectic* (or *canonical transformation*) if

$$f^{*}\omega_2 = \omega_1$$

That is, by definition of the pull back of a 2-form (see A.11)

$$(f^{*}\omega_2)_{\boldsymbol{z}}(\boldsymbol{x}, \boldsymbol{y}) = \omega_{2_{f(\boldsymbol{z})}}(T_{\boldsymbol{z}}f(\boldsymbol{x}), T_{\boldsymbol{z}}f(\boldsymbol{y})) = \omega_{1_{\boldsymbol{z}}}(\boldsymbol{x}, \boldsymbol{y})$$

for each $\boldsymbol{z} \in P_1$ and all $(\boldsymbol{x}, \boldsymbol{y}) \in T_{\boldsymbol{z}}P_1$, with the derivative (see A.4) $T_{\boldsymbol{z}}f : T_{\boldsymbol{z}}P_1 \to T_{f(\boldsymbol{z})}P_2$.

Definition A.13 (Jacobi-Lie bracket) Let M be a smooth $\mathcal{C}^{\infty}$ manifold, $f \in \mathcal{F}(M)$ and $X, Y : M \to TM$ two vector fields on M. Then the *derivation*

$$f \to X[Y[f]] - Y[X[f]]$$

where $X[f] = \boldsymbol{d}f \cdot X$ determines a unique vector field denoted by $[X, Y]$ and is called *Jacobi-Lie bracket* of X and Y.

Thus $\mathfrak{X}(M)$ (the set of vector fields on M) coincides with the set of derivatives on $\mathcal{F}(M)$.

Definition A.14 (Lie derivative) Let α be a k-form (see A.7) on M and let $X : M \to TM$ be a vector field with flow $\varphi : \mathbb{R} \times M \to M$. The *Lie derivative* of α along X is given by

$$\mathcal{L}_X \alpha = \lim_{t \to 0} \frac{1}{t}\left((\varphi_t^{*}\alpha) - \alpha\right) = \frac{d}{dt}\varphi_t^{*}\alpha|_{t=0}$$

Let $f : M \to \mathbb{R}$ be a real-valued function and $X : M \to TM$ a vector field on M. The Lie derivative of f along X is the directional derivative

$$\mathcal{L}_X f = X[f] = \boldsymbol{d}f \cdot X$$

If M is finite dimensional

$$\mathcal{L}_X f = X_i \frac{\partial f}{\partial x^i}$$

Let $Y : M \to TM$ be a vector field on M. Defining

$$\mathcal{L}_X Y = [X, Y]$$

where $[X, Y]$ is the Jacobi-Lie bracket (see A.13) gives the *Lie derivative* of Y along X.

Theorem A.15 (Lie derivative theorem) *Let α, X, Y and φ be defined as in (A.14) and recall the definition of the pull back (see A.11). Then the following statements hold:*

$$\frac{d}{dt} \varphi_t^* \alpha = \varphi_t^* \mathcal{L}_X \alpha \qquad and \qquad \frac{d}{dt} \varphi_t^* Y = \varphi_t^* \mathcal{L}_X Y$$

Definition A.16 (Hamiltonian vector field) Let (P, ω) be a symplectic manifold (see A.10). A vector field $X : P \to TP$ is called *Hamiltonian vector field* if there exists a function $H : P \to \mathbb{R}$ such that

$$\mathsf{i}_X \omega = \boldsymbol{d}H$$

where i_X is the interior product (see A.8) and $\boldsymbol{d}$ the exterior derivative (see A.9). Then X is denoted by X_H and is called Hamiltonian vector field of H with respect to ω.
The relation between Hamiltonian vector fields and 2-forms can also be expressed in terms of the Lie derivative (see A.14) by demanding

$$L_{X_H} \omega = 0$$

since Carton's formula states $L_X = \boldsymbol{d}\,\mathsf{i}_X + \mathsf{i}_X \boldsymbol{d}$, by definition $\boldsymbol{d}\boldsymbol{d}H = 0$ and ω is closed (see A.10).

Definition A.17 (Lie group) A *Lie group* is a group G and at the same time it is a differentiable manifold (see A.1). The group structure must be compatible with the manifold structure in the sense that the group operations

$$
\begin{array}{ll}
G \times G \to G & G \to G \\
(g, h) \mapsto gh & g \mapsto g^{-1}
\end{array}
$$

are $\mathcal{C}^\infty$ maps.

Definition A.18 (Lie algebra) Let V be a vector space and $[.,.] : V \times V \to V$ a *Lie bracket*, i.e. it is a bilinear, skew-symmetric map which fulfils the Jacobi-identity:

$$[A, [B, C]] + [B, [C, A]] + [C, [A, B]] = 0 \text{ for all } A, B, C \in V$$

Then the pair $(V, [.,.])$, is called *Lie algebra*.

More specific, every Lie group G induces a Lie algebra: the vector space $\mathfrak{X}_L(G)$ of left invariant vector fields on G is isomorphic to the tangential space T_eG to G at the neutral element e. Define the Lie bracket for $\xi, \eta \in T_eG$ by

$$[\xi, \eta] := [X_\xi, X_\eta](e)$$

where X_ξ, X_η are the vector fields induced by ξ and η respectively and $[X_\xi, X_\eta]$ is the Jacobi-Lie bracket (see A.13) of vector fields. This makes T_eG into a Lie algebra. It is denoted by $\mathfrak{g} = \text{Lie}(G)$ and is called *Lie algebra of G*.

Definition A.19 (Exponential map) Let G be a Lie group (see A.17). For all $\xi \in \mathfrak{g} = \text{Lie}(G)$ (see A.18) let $\gamma_\xi : \mathbb{R} \to G$ denote the integral curve of the left-invariant vector field X_ξ on G induced by ξ, which is defined uniquely by claiming

$$X_\xi(e) = \xi \qquad \gamma_\xi(0) = e$$

$$\dot{\gamma}_\xi(t) = X_\xi(\gamma_\xi(t)) \quad \text{for all } t \in \mathbb{R}$$

The map

$$\exp : \mathfrak{g} \to G$$
$$\exp(\xi) = \gamma_\xi(1)$$

is called *exponential map* of the Lie algebra $\mathfrak{g}$ in G.

Definition A.20 (Action, infinitesimal generator) Let G be a Lie group (see A.17) and P be a symplectic manifold (see A.10). Corresponding to $\xi \in \mathfrak{g} = \text{Lie}(G)$ (see A.18) the *action* $\phi^\xi : \mathbb{R} \times P \to P$ is defined by

$$\phi^\xi(s, \boldsymbol{z}) = \phi(\exp(s\xi), \boldsymbol{z})$$

where $\boldsymbol{z} \in P$. Thus ϕ^ξ is a flow on P. The corresponding vector field ξ_P on P is given by

$$\xi_P(\boldsymbol{z}) := \frac{d}{ds}\phi(\exp(s\xi), \boldsymbol{z})|_{s=0}$$

and is called the *infinitesimal generator* of the action corresponding to ξ.

Definition A.21 (Momentum map) Let the Lie algebra $\mathfrak{g}$ (see A.18) act canonically (see A.20, A.12) on the symplectic manifold P (see A.10). Suppose there is a linear map $J : \mathfrak{g} \to \mathcal{F}(P)$, such that the vector field belonging to the smooth function $J(\xi) : P \to \mathbb{R}$

$$X_{J(\xi)} = \xi_P \quad \text{for all } \xi \in \mathfrak{g}$$

The map $\boldsymbol{J} : P \to \mathfrak{g}^*$ defined by

$$\langle \boldsymbol{J}(\boldsymbol{z}), \xi \rangle = J(\xi)(\boldsymbol{z})$$

for all $\xi \in \mathfrak{g}$ and $\boldsymbol{z} \in P$ is called *momentum map* of the action.

Definition A.22 (Liouville measure) Let (P, ω) be an $2n$-dimensional symplectic manifold (see A.10). Then the *Liouville volume* is defined by

$$\Lambda = \frac{(-1)^{\frac{n}{2}}}{n!} \underbrace{\omega \wedge \ldots \wedge \omega}_{n \text{ times}}$$

In canonical coordinates $(q^1, \ldots, q^n, p_1, \ldots, p_n)$, Λ has the expression

$$\Lambda = dq^1 \wedge \ldots \wedge dq^n \wedge dp_1 \wedge \ldots \wedge dp_n$$

The measure associated to Λ is called *Liouville measure.*

Definition A.23 (Poisson bracket) Let (P, ω) be a symplectic manifold (see A.10) and $F, G \in \mathcal{F}(P)$ with the corresponding Hamiltonian vector fields X_F, X_G (see A.16). Then the *Poisson bracket* is defined by

$$\{F, G\}(\boldsymbol{z}) = \omega_{\boldsymbol{z}}(X_F(\boldsymbol{z}), X_G(\boldsymbol{z}))$$

where $\boldsymbol{z} \in P$.

Definition A.24 (Hat map) The Lie algebra $\mathfrak{so}(3)$ (see A.18) of the Lie group $SO(3)$ (see A.17) can be identified with $\mathbb{R}^3$ via the isomorphism $\hat{} : \mathbb{R}^3 \to \mathfrak{so}(3)$ (called *hat map*), defined by

$$\boldsymbol{a} = [a_1, a_2, a_3] \mapsto \widehat{\boldsymbol{a}} = \begin{bmatrix} 0 & -a_3 & a_2 \\ a_3 & 0 & -a_1 \\ -a_2 & a_1 & 0 \end{bmatrix}$$

Definition A.25 (Regular value) Let M, N be differentiable manifolds (see A.1) and $f : M \to N$ be of class $\mathcal{C}^1$. A point $n \in N$ is called *regular value* of f if for each $m \in f^{-1}(\{n\})$, $T_m f$ is surjective.

Proposition A.26 *Let M, N be differentiable manifolds (see A.1) and $f : M \to N$ be of class $\mathcal{C}^\infty$. Suppose that $n \in N$ is a regular value of f. Then $f^{-1}(n) = \{m | m \in M, f(m) = n\}$ is a submanifold in M.*

Definition A.27 (Regular point) Let $f : \mathbb{R}^n \to \mathbb{R}^m$ be of class $\mathcal{C}^1$. A point $\boldsymbol{x} \in \mathbb{R}^n$ satisfying $f(\boldsymbol{x}) = 0$ is called *regular point* of f if the differentials (see A.4) $\boldsymbol{d}f_i(\boldsymbol{x})$, $i = i, \ldots, m$ are linearly independent.

Proposition A.28 *At a regular point $\boldsymbol{x} \in \mathbb{R}^n$ of the $\mathcal{C}^1$-function $f : \mathbb{R}^n \to \mathbb{R}^m$, the tangent plane to the surface $S = \{\boldsymbol{x} \in \mathbb{R}^n | f(\boldsymbol{x}) = 0\}$ is equal to $T = \{\boldsymbol{y} \in \mathbb{R}^n | Df(\boldsymbol{x}) \cdot \boldsymbol{y} = 0\}$.*

B Linearisation of the d'Alembert-type scheme

The residual $\boldsymbol{R}(\boldsymbol{q}_{n+1}) \in \mathbb{R}^n$ of the d'Alembert-type time-stepping scheme is the nonlinear equation in terms of the configuration variable $\boldsymbol{q}_{n+1} \in \mathbb{R}^n$ given in (3.2.33). Linearisation of the residual by truncation of its Taylor expansion after the linear term yields the familiar linear equation

$$\boldsymbol{R}(\boldsymbol{q}_{n+1}^l) + D\boldsymbol{R}(\boldsymbol{q}_{n+1}^l) \cdot \Delta\boldsymbol{q}_{n+1} = \boldsymbol{0} \tag{B.1}$$

which is solved for $\Delta\boldsymbol{q}_{n+1} = \boldsymbol{q}_{n+1}^{l+1} - \boldsymbol{q}_{n+1}^l$ repeatedly until $\|\boldsymbol{R}(\boldsymbol{q}_{n+1}^{l_{max}})\| < \varepsilon$, where ε is some prescribed tolerance.

With regard to (3.2.33) the tangent matrix assumes the following form which is deduced explicitly in [Bets 05].

$$D\boldsymbol{R}(\boldsymbol{q}_{n+1}) = \left[\begin{array}{c} \mathsf{P}^T(\boldsymbol{q}_n, \boldsymbol{q}_{n+1}) \cdot \boldsymbol{S}(\boldsymbol{q}_{n+1}) \\ \boldsymbol{G}(\boldsymbol{q}_{n+1}) \end{array} \right] \tag{B.2}$$

Here $\boldsymbol{S}(\boldsymbol{q}_{n+1})$ is given by

$$
\begin{aligned}
\boldsymbol{S}(\boldsymbol{q}_{n+1}) &= D\boldsymbol{T}(\boldsymbol{q}_{n+1}) - \frac{\partial \mathsf{G}^T(\boldsymbol{q}_n, \boldsymbol{q}_{n+1})}{\partial \boldsymbol{q}_{n+1}} \cdot \boldsymbol{l}(\boldsymbol{q}_{n+1}) \\
&= D\boldsymbol{T}(\boldsymbol{q}_{n+1}) - \sum_{b=1}^{m} l_b(\boldsymbol{q}_{n+1}) \frac{\partial (\mathsf{d}^G g_b(\boldsymbol{q}_n, \boldsymbol{q}_{n+1}))}{\partial \boldsymbol{q}_{n+1}}
\end{aligned} \tag{B.3}
$$

and the abbreviations

$$\boldsymbol{T}(\boldsymbol{q}_{n+1}) = \frac{2}{h}\boldsymbol{M} \cdot (\boldsymbol{q}_{n+1} - \boldsymbol{q}_n) - 2\boldsymbol{p}_n + h\mathsf{d}^G V(\boldsymbol{q}_n, \boldsymbol{q}_{n+1}) \tag{B.4}$$

and

$$\boldsymbol{l}(\boldsymbol{q}_{n+1}) = \left(\boldsymbol{G}^T(\boldsymbol{q}_n) \cdot (\mathsf{G}(\boldsymbol{q}_n, \boldsymbol{q}_{n+1}) \cdot \boldsymbol{G}^T(\boldsymbol{q}_n))^{-1} \right)^T \cdot \boldsymbol{T}(\boldsymbol{q}_{n+1}) \tag{B.5}$$

have been introduced.

B.1 Linearisation of the d'Alembert-type scheme with nodal reparametrisation

For the reparametrisation $\boldsymbol{q}_{n+1} = \boldsymbol{F}_{\boldsymbol{q}_n}(\boldsymbol{u})$ with $\boldsymbol{u} \in \mathbb{R}^{n-m}$ introduced in (3.2.42), in the context of an iterative solution procedure for the system of nonlinear algebraic equations (3.2.44) one can distinguish between two types of unknowns. In both cases the tangent matrix includes the $(n-m) \times n$ matrix

$$D\boldsymbol{R}(\boldsymbol{F}_{\boldsymbol{q}_n}(\boldsymbol{u})) = \mathsf{P}^T(\boldsymbol{q}_n, \boldsymbol{F}_{\boldsymbol{q}_n}(\boldsymbol{u})) \cdot \boldsymbol{S}(\boldsymbol{F}_{\boldsymbol{q}_n}(\boldsymbol{u})) \tag{B.6}$$

where $\boldsymbol{S}$ can be calculated from (B.3).

B.1.1 Iterative unknowns

Using iterative unknowns, the configuration variable is updated in each step of the Newton-Raphson iteration according to $\boldsymbol{q}_{n+1}^{l+1} = \boldsymbol{F}_{\boldsymbol{q}_{n+1}^l}(\boldsymbol{u})$ such that the constraints are fulfilled. Truncation of the Taylor expansion of this reparametrisation after the linear term reads

$$
\begin{aligned}
\boldsymbol{q}_{n+1}^{l+1} &= \boldsymbol{F}_{\boldsymbol{q}_{n+1}^l}(\boldsymbol{0}) &+& \frac{d}{d\epsilon}[\boldsymbol{F}_{\boldsymbol{q}_{n+1}^l}(\epsilon\boldsymbol{u})]_{|\epsilon=0} \\
&= \boldsymbol{q}_{n+1}^l &+& D\boldsymbol{F}_{\boldsymbol{q}_{n+1}^l}(\boldsymbol{0}) \cdot \boldsymbol{u}
\end{aligned}
\tag{B.7}
$$

Insertion into (B.1) yields the $(n-m)$-dimensional linear system, which has to be solved for the iterative unknowns $\boldsymbol{u}$

$$
\boldsymbol{R}(\boldsymbol{q}_{n+1}^l) + D\boldsymbol{R}(\boldsymbol{q}_{n+1}^l) \cdot D\boldsymbol{F}_{\boldsymbol{q}_{n+1}^l}(\boldsymbol{0}) \cdot \boldsymbol{u} = \boldsymbol{0}
\tag{B.8}
$$

B.1.2 Incremental unknowns

Alternatively, a configuration variable fulfilling the constraints can be expressed as $\boldsymbol{q}_{n+1}^{l+1} = \boldsymbol{F}_{\boldsymbol{q}_n}(\boldsymbol{u}^{l+1})$, with $\boldsymbol{u}^{l+1} \in \mathbb{R}^{n-m}$.
Then its linearisation reads

$$
\begin{aligned}
\boldsymbol{q}_{n+1}^{l+1} &= \boldsymbol{F}_{\boldsymbol{q}_n}(\boldsymbol{u}^l) &+& \frac{d}{d\epsilon}[\boldsymbol{F}_{\boldsymbol{q}_n}(\boldsymbol{u}^l + \epsilon\Delta\boldsymbol{u})]_{|\epsilon=0} \\
&= \boldsymbol{q}_{n+1}^l &+& D\boldsymbol{F}_{\boldsymbol{q}_n}(\boldsymbol{u}^l) \cdot \Delta\boldsymbol{u}
\end{aligned}
\tag{B.9}
$$

and the $(n-m)$-dimensional linear system to be solved for $\Delta\boldsymbol{u}$ reads

$$
\boldsymbol{R}(\boldsymbol{q}_{n+1}^l) + D\boldsymbol{R}(\boldsymbol{q}_{n+1}^l) \cdot D\boldsymbol{F}_{\boldsymbol{q}_n}(\boldsymbol{u}^l) \cdot \Delta\boldsymbol{u} = \boldsymbol{0}
\tag{B.10}
$$

In each iteration, the reduced unknowns are updated according to $\boldsymbol{u}^{l+1} = \boldsymbol{u}^l + \Delta\boldsymbol{u}$ and in each time-step (after the iteration is complete, i.e. $l = l_{max}$), the configuration variable is determined by $\boldsymbol{q}_{n+1} = \boldsymbol{F}_{\boldsymbol{q}_n}(\boldsymbol{u}^{l_{max}})$.

C Conditioning issues

C.1 Lagrange multiplier method

The constrained $(n+m)$-dimensional time-stepping scheme (3.2.7) which has to be solved for $\boldsymbol{q}_{n+1}, \boldsymbol{\lambda}_{n+1}$ suffers from conditioning problems. For decreasing time-steps, the system becomes more and more ill-conditioned. In particular the following calculations prove, that the condition number of the iteration matrix for the solution of the nonlinear system of equations is of the order $\mathcal{O}(h^{-3})$.

The iteration matrix of the residual (3.2.7) takes the form

$$DR = \begin{bmatrix} \boldsymbol{N} & h\mathbf{G}^T \\ \boldsymbol{G} & \mathbf{0} \end{bmatrix} \tag{C.1}$$

where the $n \times n$ matrix $\boldsymbol{N}$ reads more explicitly

$$\boldsymbol{N} = \frac{2}{h}\boldsymbol{M} + h\boldsymbol{X} \tag{C.2}$$

with

$$\boldsymbol{X} = \frac{\partial \left(\mathsf{d}^G V(\boldsymbol{q}_n, \boldsymbol{q}_{n+1}) + \mathbf{G}^T(\boldsymbol{q}_n, \boldsymbol{q}_{n+1}) \cdot \boldsymbol{\lambda}_{n+1} \right)}{\partial \boldsymbol{q}_{n+1}} \tag{C.3}$$

Accordingly the order of the blocks of DR is

$$\begin{bmatrix} \mathcal{O}(h^{-1}) & \mathcal{O}(h) \\ 1 & 0 \end{bmatrix} \tag{C.4}$$

This yields $\left\| DR \right\| = \mathcal{O}(h^{-1})$ in an arbitrary matrix norm $\left\| . \right\|$. Using Gaussian elimination, the inverse of DR can be computed as

$$(DR)^{-1} = \begin{bmatrix} \boldsymbol{N}^{-1} - \boldsymbol{N}^{-1} \cdot \mathbf{G}^T \cdot \tilde{\boldsymbol{N}}^{-1} \cdot \boldsymbol{G} \cdot \boldsymbol{N}^{-1} & \boldsymbol{N}^{-1} \cdot \mathbf{G}^T \cdot \tilde{\boldsymbol{N}}^{-1} \\ h^{-1}\tilde{\boldsymbol{N}}^{-1} \cdot \boldsymbol{G} \cdot \boldsymbol{N}^{-1} & -h^{-1}\tilde{\boldsymbol{N}}^{-1} \end{bmatrix} \tag{C.5}$$

where $\tilde{\boldsymbol{N}} = \left(\boldsymbol{G} \cdot \boldsymbol{N}^{-1} \cdot \mathbf{G}^T \right)$. Let $\boldsymbol{M} = \boldsymbol{M}_L \cdot \boldsymbol{M}_U$ be the LU-factorisation of $\boldsymbol{M}$. Then (C.2) can be rewritten as

$$\boldsymbol{N} = \frac{2}{h}\boldsymbol{M}_L \cdot \left(\boldsymbol{I} + \frac{h^2}{2}\boldsymbol{M}_L^{-1} \cdot \boldsymbol{X} \cdot \boldsymbol{M}_U^{-1} \right) \cdot \boldsymbol{M}_U \tag{C.6}$$

and $\boldsymbol{N}^{-1}$ reads

$$\boldsymbol{N}^{-1} = \frac{h}{2}\boldsymbol{M}_U^{-1} \cdot \left(\boldsymbol{I} + \frac{h^2}{2}\boldsymbol{M}_L^{-1} \cdot \boldsymbol{X} \cdot \boldsymbol{M}_U^{-1} \right)^{-1} \cdot \boldsymbol{M}_L^{-1} \tag{C.7}$$

For sufficiently small time-steps, $\left\|\frac{h^2}{2}\boldsymbol{M}_L^{-1} \cdot \boldsymbol{X} \cdot \boldsymbol{M}_U^{-1}\right\| < 1$ holds. Then application of the Neumann series expansion (see e.g. [Deuf 03]) leads to

$$\left(\boldsymbol{I} + \frac{h^2}{2}\boldsymbol{M}_L^{-1} \cdot \boldsymbol{X} \cdot \boldsymbol{M}_U^{-1}\right)^{-1} = \sum_{k=0}^{\infty} \left(-\frac{h^2}{2}\boldsymbol{M}_L^{-1} \cdot \boldsymbol{X} \cdot \boldsymbol{M}_U^{-1}\right)^k \tag{C.8}$$

Cutting the expansion after the second term yields

$$\boldsymbol{N}^{-1} = \frac{h}{2}\left(\boldsymbol{M}^{-1} - \frac{h^2}{2}\boldsymbol{M}^{-1} \cdot \boldsymbol{X} \cdot \boldsymbol{M}^{-1}\right) \tag{C.9}$$

Similarly, it can be shown that $\tilde{\boldsymbol{N}}^{-1} = \left(\boldsymbol{G} \cdot \boldsymbol{N}^{-1} \cdot \mathbf{G}^T\right)^{-1}$ can be written as

$$\tilde{\boldsymbol{N}}^{-1} = \frac{2}{h}\left(\tilde{\boldsymbol{M}}^{-1} + \frac{h^2}{2}\tilde{\boldsymbol{M}}^{-1} \cdot \tilde{\boldsymbol{X}} \cdot \tilde{\boldsymbol{M}}^{-1}\right) \tag{C.10}$$

where $\tilde{\boldsymbol{M}} = \boldsymbol{G} \cdot \boldsymbol{M}^{-1} \cdot \mathbf{G}^T$ and $\tilde{\boldsymbol{X}} = \boldsymbol{G} \cdot \boldsymbol{X} \cdot \mathbf{G}^T$. Substitution of (C.9) and (C.10) into (C.5) shows that the order of the blocks of $(D\boldsymbol{R})^{-1}$ is

$$\begin{bmatrix} \mathcal{O}(h) & 1 \\ \mathcal{O}(h^{-1}) & \mathcal{O}(h^{-2}) \end{bmatrix} \tag{C.11}$$

Consequently, $\left\|(D\boldsymbol{R})^{-1}\right\| = \mathcal{O}(h^{-2})$ and the condition number of the iteration matrix of the constrained scheme is given by

$$\kappa(D\boldsymbol{R}) = \left\|D\boldsymbol{R}\right\|\left\|(D\boldsymbol{R})^{-1}\right\| = \mathcal{O}(h^{-3}) \tag{C.12}$$

C.2 Discrete null space method with nodal reparametrisation

The $(n-m)$-dimensional d'Alembert-type time-stepping scheme with nodal reparametrisation (3.2.44) is unconditionally well-conditioned. The following calculations show, that the condition number of the iteration matrix is independent of the time-step, regardless whether iterative or incremental unknowns are in use. From (B.8) and (B.10), the iteration matrix of the residual (3.2.44) can be inferred to be

$$D\boldsymbol{R} \cdot D\boldsymbol{F}_{\boldsymbol{q}_n} = \frac{2}{h}\boldsymbol{X} + h\boldsymbol{Y} + \boldsymbol{Z} \tag{C.13}$$

with

$$\begin{aligned} \boldsymbol{X} &= \mathbf{P}^T(\boldsymbol{q}_n, \boldsymbol{q}_{n+1}) \cdot \boldsymbol{M} \cdot D\boldsymbol{F}_{\boldsymbol{q}_n}(\boldsymbol{u}) \\ \boldsymbol{Y} &= \mathbf{P}^T(\boldsymbol{q}_n, \boldsymbol{q}_{n+1}) \cdot \frac{\partial\left(\mathsf{d}^G V(\boldsymbol{q}_n, \boldsymbol{q}_{n+1})\right)}{\partial \boldsymbol{q}_{n+1}} \cdot D\boldsymbol{F}_{\boldsymbol{q}_n}(\boldsymbol{u}) \\ \boldsymbol{Z} &= -\mathbf{P}^T(\boldsymbol{q}_n, \boldsymbol{q}_{n+1}) \cdot \frac{\partial \mathbf{G}^T(\boldsymbol{q}_n, \boldsymbol{q}_{n+1})}{\partial \boldsymbol{q}_{n+1}} \cdot \boldsymbol{l}(\boldsymbol{q}_{n+1}) \cdot D\boldsymbol{F}_{\boldsymbol{q}_n}(\boldsymbol{u}) \end{aligned} \tag{C.14}$$

This yields $\left\| D\boldsymbol{R} \cdot D\boldsymbol{F}_{\boldsymbol{q}_n} \right\| = \mathcal{O}(h^{-1})$. Let $\boldsymbol{X} = \boldsymbol{X}_L \cdot \boldsymbol{X}_U$ be the LU-factorisation of $\boldsymbol{X}$. Then (C.13) can be rewritten as

$$
D\boldsymbol{R} \cdot D\boldsymbol{F}_{\boldsymbol{q}_n} = \frac{2}{h}\boldsymbol{X}_L \cdot \left(\boldsymbol{I} + \boldsymbol{X}_L^{-1} \cdot \left(\frac{h^2}{2}\boldsymbol{Y} + \frac{h}{2}\boldsymbol{Z} \right) \cdot \boldsymbol{X}_U^{-1} \right) \cdot \boldsymbol{X}_U \tag{C.15}
$$

and its inverse reads

$$
\left(D\boldsymbol{R} \cdot D\boldsymbol{F}_{\boldsymbol{q}_n} \right)^{-1} = \frac{h}{2}\boldsymbol{X}_U^{-1} \cdot \left(\boldsymbol{I} + \boldsymbol{X}_L^{-1} \cdot \left(\frac{h^2}{2}\boldsymbol{Y} + \frac{h}{2}\boldsymbol{Z} \right) \cdot \boldsymbol{X}_U^{-1} \right)^{-1} \cdot \boldsymbol{X}_L^{-1} \tag{C.16}
$$

For sufficiently small time-steps, $\left\| \boldsymbol{X}_L^{-1} \cdot \left(\frac{h^2}{2}\boldsymbol{Y} + \frac{h}{2}\boldsymbol{Z} \right) \cdot \boldsymbol{X}_U^{-1} \right\| < 1$ holds. Analogous to the procedure in Section C.1, application of the Neumann series expansion (see e.g. [Deuf 03]) leads to

$$
\left(\boldsymbol{I} + \boldsymbol{X}_L^{-1} \cdot \left(\frac{h^2}{2}\boldsymbol{Y} + \frac{h}{2}\boldsymbol{Z} \right) \cdot \boldsymbol{X}_U^{-1} \right)^{-1} = \sum_{k=0}^{\infty} \left(-\boldsymbol{X}_L^{-1} \cdot \left(\frac{h^2}{2}\boldsymbol{Y} + \frac{h}{2}\boldsymbol{Z} \right) \cdot \boldsymbol{X}_U^{-1} \right)^k \tag{C.17}
$$

Cutting this expansion after the second term yields

$$
\left(D\boldsymbol{R} \cdot D\boldsymbol{F}_{\boldsymbol{q}_n} \right)^{-1} = \frac{h}{2} \left(\boldsymbol{X}^{-1} - \boldsymbol{X}^{-1} \cdot \left(\frac{h^2}{2}\boldsymbol{Y} + \frac{h}{2}\boldsymbol{Z} \right) \cdot \boldsymbol{X}^{-1} \right) \tag{C.18}
$$

and consequently $\left\| \left(D\boldsymbol{R} \cdot D\boldsymbol{F}_{\boldsymbol{q}_n} \right)^{-1} \right\| = \mathcal{O}(h)$ and the condition number of the iteration matrix of the d'Alembert-type scheme with nodal reparametrisation is independent of the time-step

$$
\kappa(D\boldsymbol{R} \cdot D\boldsymbol{F}_{\boldsymbol{q}_n}) = \left\| D\boldsymbol{R} \cdot D\boldsymbol{F}_{\boldsymbol{q}_n} \right\| \left\| \left(D\boldsymbol{R} \cdot D\boldsymbol{F}_{\boldsymbol{q}_n} \right)^{-1} \right\| \approx 1 \tag{C.19}
$$

More precisely, $\kappa(D\boldsymbol{R} \cdot D\boldsymbol{F}_{\boldsymbol{q}_n}) = c$ where $c \in \mathbb{R}$ is a problem dependent constant.

C.3 Discrete null space method

Although the d'Alembert-type scheme (3.2.33) can be implemented directly using the iteration matrix in (B.2), the there given form is not suitable for the conditioning considerations. As described in [Bets 05], using the decomposition (3.2.34) in conjunction with the matrices $\boldsymbol{W}_n, \boldsymbol{U}_n$ given in (2.3.23) implies

$$
\begin{aligned}
\boldsymbol{q}_{n+1}^l &= \boldsymbol{q}_n + \boldsymbol{U}_n \cdot \boldsymbol{u}^l + \boldsymbol{W}_n \cdot \boldsymbol{w}^l \\
\Delta\boldsymbol{q}_{n+1} &= \boldsymbol{U}_n \cdot \Delta\boldsymbol{u} + \boldsymbol{W}_n \cdot \Delta\boldsymbol{w}
\end{aligned} \tag{C.20}
$$

Insertion into (B.1) results in two equations including $\boldsymbol{S}$ and $\boldsymbol{T}$ given in (B.3) and (B.4) respectively. Multiplying the second resulting equation by $\mathbf{P}^T \cdot \boldsymbol{S} \cdot \boldsymbol{W}_n \cdot (\boldsymbol{G} \cdot \boldsymbol{W}_n)^{-1}$ and subtracting it from the first resulting equation yields

$$
\begin{aligned}
\boldsymbol{K}_u(\boldsymbol{q}_{n+1}^l) \cdot \Delta\boldsymbol{u} &= -\boldsymbol{R}_u(\boldsymbol{q}_{n+1}^l) \\
\boldsymbol{K}_w(\boldsymbol{q}_{n+1}^l) \cdot \Delta\boldsymbol{w} &= -\boldsymbol{R}_w(\boldsymbol{q}_{n+1}^l)
\end{aligned} \tag{C.21}
$$

with

$$
\begin{aligned}
\boldsymbol{K}_u(\boldsymbol{q}_{n+1}^l) &= \mathsf{P}^T(\boldsymbol{q}_n, \boldsymbol{q}_{n+1}^l) \cdot \boldsymbol{S}(\boldsymbol{q}_{n+1}^l) \cdot \left[\boldsymbol{I} - \boldsymbol{W}_n \cdot \left(\boldsymbol{G}(\boldsymbol{q}_{n+1}^l) \cdot \boldsymbol{W}_n \right)^{-1} \cdot \boldsymbol{G}(\boldsymbol{q}_{n+1}^l) \right] \cdot \boldsymbol{U}_n \\
\boldsymbol{R}_u(\boldsymbol{q}_{n+1}^l) &= \mathsf{P}^T(\boldsymbol{q}_n, \boldsymbol{q}_{n+1}^l) \cdot \left[\boldsymbol{T}(\boldsymbol{q}_{n+1}^l) - \boldsymbol{S}(\boldsymbol{q}_{n+1}^l) \cdot \boldsymbol{W}_n \cdot \left(\boldsymbol{G}(\boldsymbol{q}_{n+1}^l) \cdot \boldsymbol{W}_n \right)^{-1} \cdot \boldsymbol{g}(\boldsymbol{q}_{n+1}^l) \right] \\
\boldsymbol{K}_w(\boldsymbol{q}_{n+1}^l) &= \boldsymbol{G}(\boldsymbol{q}_{n+1}^l) \cdot \boldsymbol{W}_n \\
\boldsymbol{R}_w(\boldsymbol{q}_{n+1}^l) &= \boldsymbol{g}(\boldsymbol{q}_{n+1}^l) + \boldsymbol{G}(\boldsymbol{q}_{n+1}^l) \cdot \boldsymbol{U}_n \cdot \Delta\boldsymbol{u}
\end{aligned}
\tag{C.22}
$$

Since $\boldsymbol{K}_w(\boldsymbol{q}_{n+1}^l)$ is obviously independent of the time-step

$$
\kappa(\boldsymbol{K}_w) = \left\| \boldsymbol{K}_w \right\| \left\| \boldsymbol{K}_w^{-1} \right\| \approx 1
\tag{C.23}
$$

holds. More precisely, $\kappa(\boldsymbol{K}_w) = c_w$ where $c_w \in \mathbb{R}$ is a problem dependent constant. Among the matrices composing $\boldsymbol{K}_u(\boldsymbol{q}_{n+1}^l)$, only $\boldsymbol{S}(\boldsymbol{q}_{n+1}^l)$ given in (B.3) depends on the time-step. Analogous to (C.13), it can be written as $\boldsymbol{K}_u = \frac{2}{h}\boldsymbol{X} + h\boldsymbol{Y} + \boldsymbol{Z}$ and

$$
\kappa(\boldsymbol{K}_u) = \left\| \boldsymbol{K}_u \right\| \left\| \boldsymbol{K}_u^{-1} \right\| \approx 1
\tag{C.24}
$$

or more precisely $\kappa(\boldsymbol{K}_u) = c_u$ with the problem dependent constant $c_u \in \mathbb{R}$ can be shown in the same way.

C.4 Penalty method

Besides the time-step, the n-dimensional penalty system's (3.2.20) condition number is influenced by the penalty parameter μ. In the sequel it is shown, that the condition number of the iteration matrix is of the order $\mathcal{O}(h^2\mu)$, thus for well balanced time-steps and penalty parameters, the penalty system is well-conditioned. In particular the use of relatively high penalty parameters, leading to acceptable constraint fulfilment, requires the use of relatively small time-steps. In this case, the system has the property of being stiff, see [Hair 96].
The iteration matrix of the residual (3.2.20) takes the form

$$
D\boldsymbol{R} = \frac{2}{h}\boldsymbol{M} + h\boldsymbol{X} + h\mu\boldsymbol{Y}
\tag{C.25}
$$

with

$$
\begin{aligned}
\boldsymbol{X} &= \frac{\partial \left(\mathsf{d}^G V(\boldsymbol{q}_n, \boldsymbol{q}_{n+1}) \right)}{\partial \boldsymbol{q}_{n+1}} \\
\boldsymbol{Y} &= \frac{\partial \mathsf{d}^G R(\boldsymbol{g}(\boldsymbol{q}_n, \boldsymbol{q}_{n+1}))}{\partial \boldsymbol{q}_{n+1}}
\end{aligned}
\tag{C.26}
$$

Under the reasonable assumptions of relatively small time-steps $h \ll 1$ and relatively large penalty parameters $\mu \gg 1$ which are necessary for an adequately accurate solution, the first and last terms in (C.25) are leading and obviously $\left\| D\boldsymbol{R} \right\| = \mathcal{O}(h^{-1} + h\mu)$ holds. Let $\boldsymbol{M} = \boldsymbol{M}_L \cdot \boldsymbol{M}_U$ be the LU-factorisation of $\boldsymbol{M}$. Then (C.13) can be rewritten as

$$
D\boldsymbol{R} = \frac{2}{h}\boldsymbol{M}_L \cdot \left(\boldsymbol{I} + \boldsymbol{M}_L^{-1} \cdot \left(\frac{h^2}{2}\boldsymbol{X} + \frac{h^2\mu}{2}\boldsymbol{Y} \right) \cdot \boldsymbol{M}_U^{-1} \right) \cdot \boldsymbol{M}_U
\tag{C.27}
$$

Assuming further that h^2 is decreasing quicker than μ is increasing, i.e. μ is of the order $\mathcal{O}(h^{-2})$, for sufficiently small time-steps, $\left\| \boldsymbol{M}_L^{-1} \cdot \left(\frac{h^2}{2}\boldsymbol{X} + \frac{h^2\mu}{2}\boldsymbol{Y} \right) \cdot \boldsymbol{M}_U^{-1} \right\| < 1$ holds. Analogous to the procedure using the Neumann series expansion in Section C.3 it can be shown here, that the inverse iteration matrix reads

$$(D\boldsymbol{R})^{-1} = \frac{h}{2} \left(\boldsymbol{M}^{-1} - \boldsymbol{M}^{-1} \cdot \left(\frac{h^2}{2}\boldsymbol{X} + \frac{h^2\mu}{2}\boldsymbol{Y} \right) \cdot \boldsymbol{M}^{-1} \right) \tag{C.28}$$

This yields $\left\|(D\boldsymbol{R})^{-1}\right\| = \mathcal{O}(h + h^3\mu)$ and consequently

$$\kappa(D\boldsymbol{R}) = \left\|D\boldsymbol{R}\right\|\left\|(D\boldsymbol{R})^{-1}\right\| = \mathcal{O}(h^2\mu) \tag{C.29}$$

C.5 Augmented Lagrange method

As for the penalty scheme, the condition number of the iteration matrix of the n-dimensional augmented Lagrange time-stepping scheme (3.2.29) is of the order $\mathcal{O}(h^2\mu)$. But in contrast to the penalty scheme, the parameter μ can remain of moderate magnitude and the constraint fulfilment is achieved through an extra iteration. Thus for small time-steps, the augmented Lagrange scheme is well-conditioned.
The iteration matrix of the residual (3.2.29) takes the form

$$D\boldsymbol{R} = \frac{2}{h}\boldsymbol{M} + h\boldsymbol{X} + h\mu\boldsymbol{Y} \tag{C.30}$$

with

$$\begin{aligned} \boldsymbol{X} &= \frac{\partial \left(\mathsf{d}^G V(\boldsymbol{q}_n, \boldsymbol{q}_{n+1}) + \boldsymbol{G}^T(\boldsymbol{q}_n, \boldsymbol{q}_{n+1}^k) \cdot \boldsymbol{\lambda}_{n+1}^k \right)}{\partial \boldsymbol{q}_{n+1}} \\ \boldsymbol{Y} &= \frac{\partial \mathsf{d}^G R(\boldsymbol{g}(\boldsymbol{q}_n, \boldsymbol{q}_{n+1}))}{\partial \boldsymbol{q}_{n+1}} \end{aligned} \tag{C.31}$$

Analogous to the procedure for the penalty scheme in Section C.4, it can be shown that that

$$\kappa(D\boldsymbol{R}) = \left\|D\boldsymbol{R}\right\|\left\|(D\boldsymbol{R})^{-1}\right\| = \mathcal{O}(h^2\mu) \tag{C.32}$$

D Configuration dependent mass matrix of the double spherical pendulum
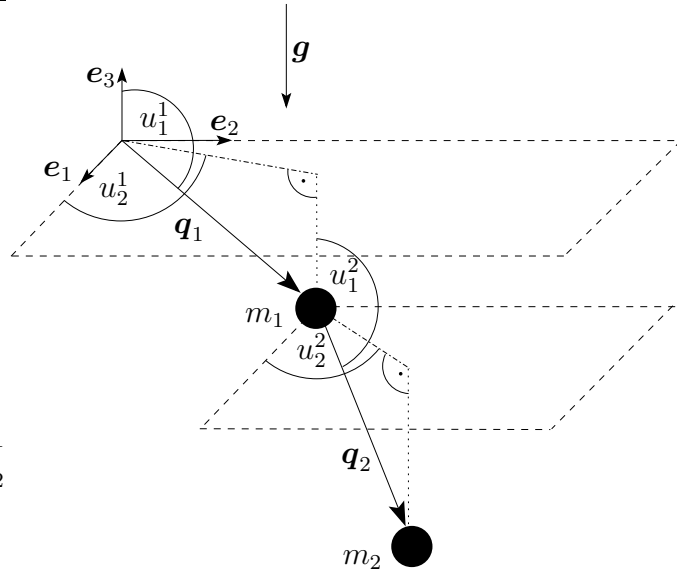
Figure D.1: Double spherical pendulum.

A description of the double spherical pendulum in Figure 4.1 in terms of generalised coordinates $\boldsymbol{u} = [u_1^1, u_2^1, u_1^2, u_2^2]^T \in \mathbb{R}^4$ relies on the angles

$$u_1^\alpha = \sphericalangle\,(\boldsymbol{e}_3, \boldsymbol{q}^\alpha) \qquad u_2^\alpha = \sphericalangle\,\big(\boldsymbol{e}_1, \boldsymbol{\Pi}_{(\boldsymbol{e}_1, \boldsymbol{e}_2)}(\boldsymbol{q}^\alpha)\big) \qquad \alpha = 1, 2 \tag{D.1}$$

where $\boldsymbol{\Pi}_{(\boldsymbol{e}_1, \boldsymbol{e}_2)}$ is the projection to the $(\boldsymbol{e}_1, \boldsymbol{e}_2)$-plane, and for $\alpha = 2$ the origin is moved to the position of the first mass, see Figure D.1.

Then the reparametrisation of the constraint manifold $C = S_{l_1}^2 \times S_{l_2}^2$ introduced in (2.3.26) reads

$$\boldsymbol{F}(\boldsymbol{u}) = \begin{bmatrix} l_1\,\sin(u_1^1)\sin(u_2^1) \\ l_1\,\cos(u_1^1) \\ l_1\,\sin(u_1^1)\cos(u_2^1) \\ l_2\,\sin(u_1^2)\sin(u_2^2) \\ l_2\,\cos(u_1^2) \\ l_2\,\sin(u_1^2)\cos(u_2^2) \end{bmatrix} \tag{D.2}$$

Corresponding to the kinetic and potential energy of the double spherical pendulum in (4.1.1), the reparametrisation of the Hamiltonian in generalised coordinates is given by

$\tilde{H} : T^*C \to \mathbb{R}$ with

$$\tilde{H}(\boldsymbol{u}, \boldsymbol{y}) = \frac{1}{2}\boldsymbol{y}^T \cdot \left(\tilde{\boldsymbol{M}}(\boldsymbol{u})\right)^{-1} \cdot \boldsymbol{y} + V(\boldsymbol{F}(\boldsymbol{u})) \tag{D.3}$$

with the configuration-dependent reduced mass matrix $\tilde{\boldsymbol{M}}(\boldsymbol{u}) = D^T\boldsymbol{F}(\boldsymbol{u}) \cdot \boldsymbol{M} \cdot D\boldsymbol{F}(\boldsymbol{u})$. Insertion of $\boldsymbol{M}$ from (4.1.3) and the Jacobian of the transformation (D.2) yields

$$\tilde{\boldsymbol{M}}(\boldsymbol{u}) = \begin{bmatrix} \tilde{\boldsymbol{m}}_1 & \tilde{\boldsymbol{m}}_2 & \tilde{\boldsymbol{m}}_3 & \tilde{\boldsymbol{m}}_4 \end{bmatrix} \tag{D.4}$$

with

$$\tilde{\boldsymbol{m}}_1 = \begin{bmatrix} l_1^2\,(m_1 + m_2) \\ 0 \\ l_1 m_2 l_2\,(\sin(u_1^1)\sin(u_1^2) + \cos(u_1^1)\cos(u_2^1)\cos(u_1^2)\cos(u_2^2)) \\ l_1\cos(u_1^1)m_2 l_2\,(\sin(u_2^1)\sin(u_1^2)\cos(u_2^2) - \cos(u_2^1)\sin(u_1^2)\sin(u_2^2)) \end{bmatrix}$$

$$\tilde{\boldsymbol{m}}_2 = \begin{bmatrix} 0 \\ -l_1^2\left(-1 + (\cos(u_1^1))^2\right)(m_1 + m_2) \\ -l_1\sin(u_1^1)\sin(u_2^1)m_2 l_2\cos(u_1^2)\cos(u_2^2) \\ l_1\sin(u_1^1)m_2 l_2\,(\cos(u_2^1)\sin(u_1^2)\cos(u_2^2) + \sin(u_2^1)\sin(u_1^2)\sin(u_2^2)) \end{bmatrix}$$

$$\tilde{\boldsymbol{m}}_3 = \begin{bmatrix} l_1 m_2 l_2\,(\sin(u_1^1)\sin(u_1^2) + \cos(u_1^1)\cos(u_2^1)\cos(u_1^2)\cos(u_2^2)) \\ -l_1\sin(u_1^1)\sin(u_2^1)m_2 l_2\cos(u_1^2)\cos(u_2^2) \\ l_2^2 m_2\left(1 - (\cos(u_1^2))^2 + (\cos(u_1^2))^2(\cos(u_2^2))^2\right) \\ -l_2^2\cos(u_1^2)\cos(u_2^2)m_2\sin(u_1^2)\sin(u_2^2) \end{bmatrix}$$

$$\tilde{\boldsymbol{m}}_4 = \begin{bmatrix} l_1\cos(u_1^1)m_2 l_2\,(\sin(u_2^1)\sin(u_1^2)\cos(u_2^2) - \cos(u_2^1)\sin(u_1^2)\sin(u_2^2)) \\ l_1\sin(u_1^1)m_2 l_2\,(\cos(u_2^1)\sin(u1_1^2)\cos(u_2^2) + \sin(u_2^1)\sin(u_1^2)\sin(u_2^2)) \\ -l_2^2\cos(u_1^2)\cos(u_2^2)m_2\sin(u_1^2)\sin(u_2^2) \\ -l_2^2 m_2\left((\cos(u_2^2))^2(\cos(u_1^2))^2 - 1 + (\cos(u_1^2))^2 - (\cos(u_1^2))^2(\cos(u_2^2))^2\right) \end{bmatrix}$$

The presence of highly nonlinear entries in $\tilde{\boldsymbol{M}}(\boldsymbol{u})$ causes a temporal discretisation of Hamilton's equations in terms of generalised coordinates (2.3.28) to be very involved.

E Discrete derivative of the stored energy function

For clearness of exposition, the dependence of the stored energy function of the geometrically exact beam W_{int} on the bending strain measures $\boldsymbol{K}$ is ignored. Also the integration over the arc-length is not indicated, since it is not relevant for the following purpose.

Then corresponding to (5.2.3), the potential energy pertaining to the internal elastic deformation reads $V_{int}(\boldsymbol{q}) = W_{int}(\boldsymbol{\Gamma}(\boldsymbol{q}))$. According to (5.2.4), $\boldsymbol{\Gamma}$ is quadratic in the configuration variable $\boldsymbol{q}$. Consequently, after reparametrisation in the quadratic invariants $\boldsymbol{\pi}(\boldsymbol{z})$ given in (5.4.5), the strain measures $\tilde{\boldsymbol{\Gamma}}(\boldsymbol{\pi}(\boldsymbol{z}))$ in (5.4.9) are linear in $\boldsymbol{\pi}$.

Despite the formal differences, the following two alternatives to apply the discrete derivative in Example 3.1.6 to the beams stored energy function are equal. In particular, the terms in equal colours coincide.

Alternative 1

Defining $f = W_{int} \circ \tilde{\boldsymbol{\Gamma}}$ and using $\boldsymbol{\pi}$ from (5.4.5), the G-equivariant discrete derivative of the potential energy pertaining to the internal elastic deformation reads

$$\mathsf{D}^G V_{int}(\boldsymbol{z}_n, \boldsymbol{z}_{n+1}) = \mathsf{D}_{\boldsymbol{\pi}} \tilde{W}(\tilde{\boldsymbol{\Gamma}}(\boldsymbol{\pi}(\boldsymbol{z}_n), \boldsymbol{\pi}(\boldsymbol{z}_{n+1}))) \cdot D\boldsymbol{\pi}(\boldsymbol{z}_{n+\frac{1}{2}}) =$$

$$D_{\tilde{\boldsymbol{\Gamma}}} \tilde{W} \left(\tilde{\boldsymbol{\Gamma}} \left(\frac{1}{2}(\boldsymbol{\pi}(\boldsymbol{z}_{n+1}) + \boldsymbol{\pi}(\boldsymbol{z}_n)) \right) \right) \cdot D_{\boldsymbol{\pi}} \tilde{\Gamma} \left(\frac{1}{2}(\boldsymbol{\pi}(\boldsymbol{z}_{n+1}) + \boldsymbol{\pi}(\boldsymbol{z}_n)) \right) \cdot D\boldsymbol{\pi}(\boldsymbol{z}_{n+\frac{1}{2}}) +$$

$$\left[\frac{\tilde{W}\left(\tilde{\boldsymbol{\Gamma}}(\boldsymbol{\pi}(\boldsymbol{z}_{n+1})) \right) - \tilde{W}\left(\tilde{\boldsymbol{\Gamma}}(\boldsymbol{\pi}(\boldsymbol{z}_n)) \right)}{\left\| \boldsymbol{\pi}(\boldsymbol{z}_{n+1}) - \boldsymbol{\pi}(\boldsymbol{z}_n) \right\|^2} - \right.$$

$$\left. \frac{\left(D_{\tilde{\boldsymbol{\Gamma}}} \tilde{W}\left(\tilde{\boldsymbol{\Gamma}} \left(\frac{1}{2}(\boldsymbol{\pi}(\boldsymbol{z}_{n+1}) + \boldsymbol{\pi}(\boldsymbol{z}_n)) \right) \right) \right) \cdot D_{\boldsymbol{\pi}} \tilde{\Gamma} \left(\frac{1}{2}(\boldsymbol{\pi}(\boldsymbol{z}_{n+1}) + \boldsymbol{\pi}(\boldsymbol{z}_n)) \right) \cdot (\boldsymbol{\pi}(\boldsymbol{z}_{n+1}) - \boldsymbol{\pi}(\boldsymbol{z}_n))}{\left\| \boldsymbol{\pi}(\boldsymbol{z}_{n+1}) - \boldsymbol{\pi}(\boldsymbol{z}_n) \right\|^2} \right]$$

$$(\boldsymbol{\pi}(\boldsymbol{z}_{n+1}) - \boldsymbol{\pi}(\boldsymbol{z}_n)) \cdot D\boldsymbol{\pi}(\boldsymbol{z}_{n+\frac{1}{2}})$$

Alternative 2

Defining $f = W_{int}$ and replacing $\boldsymbol{\pi}$ in Example 3.1.6 by $\tilde{\boldsymbol{\Gamma}} \circ \boldsymbol{\pi}$, the G-equivariant discrete derivative of the potential energy pertaining to the internal elastic deformation reads

$$\mathsf{D}^G V_{int}(\boldsymbol{z}_n, \boldsymbol{z}_{n+1}) = \mathsf{D}_{\tilde{\boldsymbol{\Gamma}}} \tilde{W}\left(\tilde{\boldsymbol{\Gamma}}(\boldsymbol{\pi}(\boldsymbol{z}_n)), \tilde{\boldsymbol{\Gamma}}(\boldsymbol{\pi}(\boldsymbol{z}_{n+1})) \right) \cdot D_{\boldsymbol{z}} \left(\tilde{\boldsymbol{\Gamma}}(\boldsymbol{\pi}(\boldsymbol{z}_{n+\frac{1}{2}})) \right) =$$

$$D_{\tilde{\boldsymbol{\Gamma}}} \tilde{W} \left(\frac{1}{2} \left(\tilde{\boldsymbol{\Gamma}}(\boldsymbol{\pi}(\boldsymbol{z}_{n+1})) + \tilde{\boldsymbol{\Gamma}}(\boldsymbol{\pi}(\boldsymbol{z}_n)) \right) \right) \cdot D_{\boldsymbol{\pi}} \tilde{\boldsymbol{\Gamma}} \left(\boldsymbol{\pi}(\boldsymbol{z}_{n+\frac{1}{2}}) \right) \cdot D\boldsymbol{\pi}(\boldsymbol{z}_{n+\frac{1}{2}}) +$$

$$\left[\frac{\tilde{W}\left(\tilde{\boldsymbol{\Gamma}}(\boldsymbol{\pi}(\boldsymbol{z}_{n+1})) \right) - \tilde{W}\left(\tilde{\boldsymbol{\Gamma}}(\boldsymbol{\pi}(\boldsymbol{z}_n)) \right)}{\left\| \tilde{\boldsymbol{\Gamma}}(\boldsymbol{\Pi}(\boldsymbol{z}_{n+1})) - \tilde{\boldsymbol{\Gamma}}(\boldsymbol{\pi}(\boldsymbol{z}_n)) \right\|^2} - \right.$$

$$\left. \frac{D_{\tilde{\boldsymbol{\Gamma}}} \tilde{W} \left(\frac{1}{2} \left(\tilde{\boldsymbol{\Gamma}}(\boldsymbol{\pi}(\boldsymbol{z}_{n+1})) + \tilde{\boldsymbol{\Gamma}}(\boldsymbol{\pi}(\boldsymbol{z}_n)) \right) \right) \cdot \left(\tilde{\boldsymbol{\Gamma}}(\boldsymbol{\pi}(\boldsymbol{z}_{n+1})) - \tilde{\boldsymbol{\Gamma}}(\boldsymbol{\pi}(\boldsymbol{z}_n)) \right)}{\left\| \tilde{\boldsymbol{\Gamma}}(\boldsymbol{\Pi}(\boldsymbol{z}_{n+1})) - \tilde{\boldsymbol{\Gamma}}(\boldsymbol{\pi}(\boldsymbol{z}_n)) \right\|^2} \right]$$

$$\left(\tilde{\boldsymbol{\Gamma}}(\boldsymbol{\pi}(\boldsymbol{z}_{n+1})) - \tilde{\boldsymbol{\Gamma}}(\boldsymbol{\pi}(\boldsymbol{z}_n)) \right) \cdot D_{\boldsymbol{\pi}} \tilde{\boldsymbol{\Gamma}} \left(\boldsymbol{\pi}(\boldsymbol{z}_{n+\frac{1}{2}}) \right) \cdot D\boldsymbol{\pi}(\boldsymbol{z}_{n+\frac{1}{2}})$$

F Invertible cube by Paul Schatz

The mechanism treated as an example of a six-body linkage in Section 6.2.4 is an invention of the artist, inventor and technician Paul Schatz. The following abridgement of his biography has partly been taken from the web pages of the Paul Schatz-Stiftung http://www.paul-schatz.ch and from http://www.fzk.at, where Franz Zahaurek offers a detailed report on the invertible cube and programmes for the simulation of its motion.

Paul Schatz was born in Constance on December 22nd, 1898. Already during his teenage years, he was an ardent admirer of those days aviation pioneers. After World War I, he began to study mathematics, mechanical engineering, and philosophy at the Munich College of Technology. Alike many of his contemporaries, he was seeking a connection of technics and arts. Between 1924 and 1927, he worked as a sculptor of wood and at the same time, he studied intensively anthroposophy. In 1927 he published the book [Scha 27], whose title has been translated as 'A Quest of Art Based on the Strength of Perception'. In the same year, he and his wife, Emmy Schatz-Witt, moved to Dornach (Switzerland), where he lived and worked until his death on March 7th, 1979.

In 1975, his second book [Scha 98] was published, wherein the first of two parts is devoted entirely to the invertible cube. On page 40, it is explained, that when the first model of the invertible cube was released in 1930, it could be observed that the way people 'invert' the cube gives information on their personality. Extrovert natures put it over in an outward direction, as depicted in Figure 6.24, while introvert people put it over in the opposite direction. The specialty about the invertible cubes motion is the rhythmically pulsatile kinematics. It consists of the interplay of diastole (expansion) and systole (contraction) which is characteristic for the inversion. Furthermore, the ratio of four pulsations per one full revolution is associated with the ratio of pulse and breathing of the human organism, which is considered to be of great 'dynamical relevance'.

A requirement for the 'preforced motion' (i.e. motion having only one degree of freedom) in both directions, is the composition of the cube by pairwise laterally reversed bodies. The principle can be generalised to an invertible cuboid or an invertible rhombus, where the neighbouring revolute axes are skew. Invertible bodies are frequently applied in industrial processes of mixing and agitation, e.g. the 'turbula' and the 'inversina' are inventions by Paul Schatz which have a long history of development in engineering.

A model of the invertible cube can be built by cutting out the contour in Figure F.2 and gluing it together according to the letter's guidance.

The timeform of the invertible cube (i.e. the space, where the invertible cube passes through during a full revolution) yields the so-called oloid. It correlates with the convex

hull of two circles in orthogonal planes, each containing the center of the other one, see Figure F.1. Its motion is qualitatively resembling that of a fish's fin. With minimal energy input, it can circulate large volumina of fluids, thus it is used widely in sewage preparation.

Figure F.1: Timeform of the invertible cube: oloid.

Der **umstülpbare Würfel** nach **Paul Schatz**

© 2000 Franz Zahaurek <http://www.fzk.at>
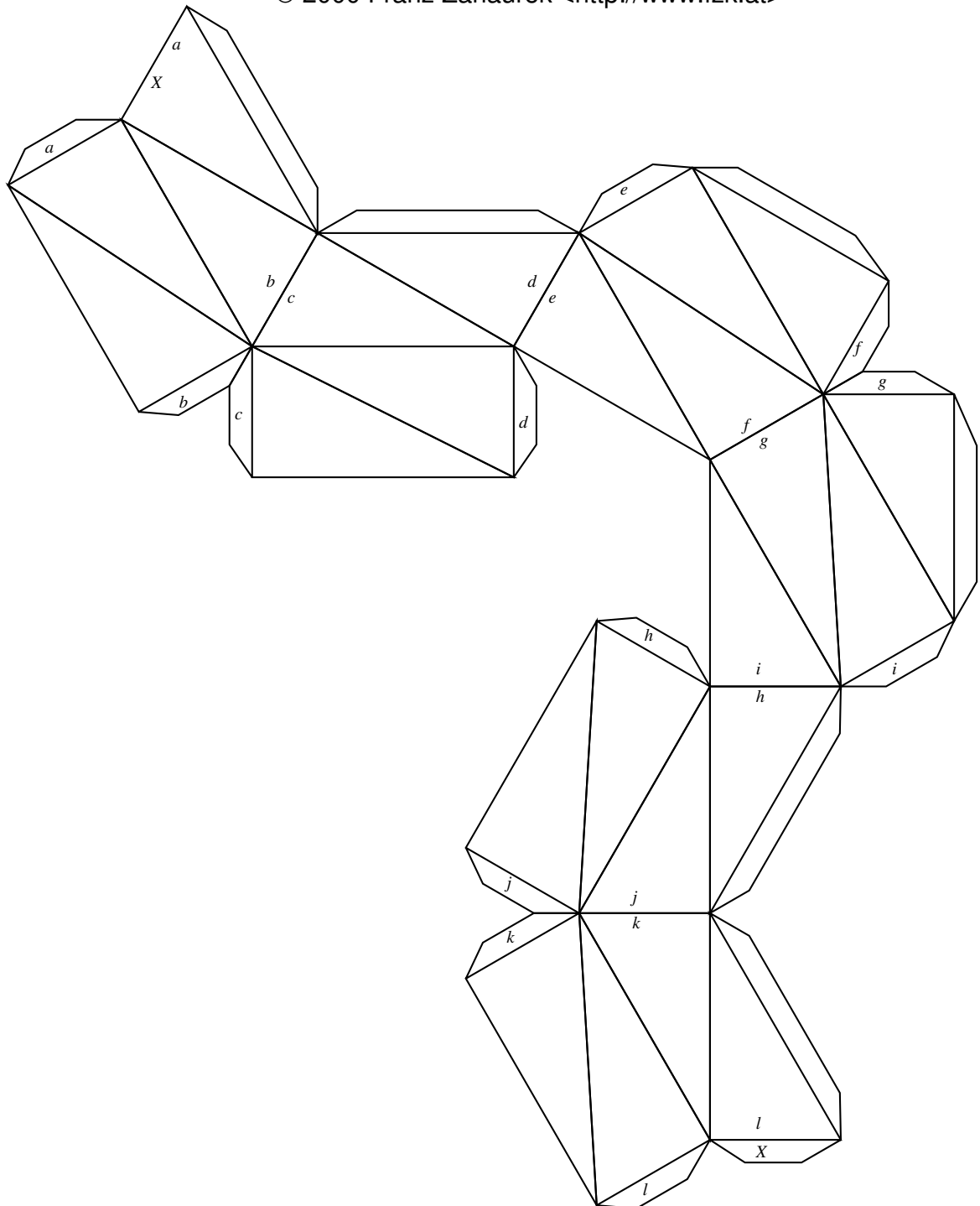
Figure F.2: Model to build an invertible cube.

Bibliography

[Abra 78]   R. Abraham and J. Marsden. *Foundations of Mechanics*. The Benjamin/Cummings publishing company, 1978.

[Abra 88]   R. Abraham, J. Marsden, and T. Ratiu. *Manifolds, Tensor Analysis, and Applications*. Vol. 75 of Applied Mathematical Sciences, Springer, 1988.

[Agri 01]   I. Agricola and T. Friedrich. *Globale Analysis. Differentialformen in Analysis, Geometrie und Physik*. Vieweg, 2001.

[Ange 86]   J. Angeles. "Iterative Kinematic Inversion of General Five-Axis Robot Manipulators". *The International Journal of Robotics Research*, Vol. 4, No. 4, pp. 59–70, 1986.

[Ange 88]   J. Angeles. *Rational Kinematics*. Springer, 1988.

[Ange 89]   J. Angeles and S. Lee. "The modelling of holonomic mechanical systems using a natural orthogonal complement". *Trans. Canadian Society of Mechanical Engineers*, Vol. 13, No. 4, pp. 81–89, 1989.

[Ange 97]   J. Angeles. *Fundamentals of Robotic Mechanical Systems*. Springer, 1997.

[Anit 04]   M. Anitescu and G. Hart. "A constraint-stabilized time-stepping approach for rigid multibody dynamics with joints, contact and friction". *Int. J. Numer. Meth. Engng.*, Vol. 60, No. 14, pp. 2335–2371, 2004.

[Antm 95]   S. Antmann. *Nonlinear Problems in Elasticity*. Springer, 1995.

[Arev 02]   C. Arevalo, C. Führer, and M. Selva. "Variable stepsize extensions of multistep formulas – a review and new approaches". *Appl. Num. Math.*, Vol. 42, No. 3-4, pp. 1–16, 2002.

[Arme 01a] F. Armero and I. Romero. "On the formulation of high-frequency dissipative time-stepping algorithms for nonlinear dynamics. Part I: low-order methods for two model problems and nonlinear elastodynamics". *Comput. Methods Appl. Mech. Engrg.*, Vol. 190, pp. 2603–2649, 2001.

[Arme 01b] F. Armero and I. Romero. "On the formulation of high-frequency dissipative time-stepping algorithms for nonlinear dynamics. Part II: second-order methods". *Comput. Methods Appl. Mech. Engrg.*, Vol. 190, pp. 6783–6824, 2001.

[Arme 03]   F. Armero and I. Romero. "Energy-dissipative momentum-conserving time stepping algorithms for the dynamics of nonlinear Cosserat rods". *Comput. Mech.*, Vol. 31, pp. 3–26, 2003.

[Arno 05]   M. Arnold, A. Fuchs, and C. Führer. "Efficient corrector iteration for DAE time integration in multibody dynamics". *Comp. Meth. Appl. Mech. Eng.*, 2005. in press.

[Arno 78]   V. Arnold. *Mathematical Methods of Classical Mechanics*. Springer, 1978.

[Bart 96]   E. Barth and B. Leimkuhler. "Sympletic methods for conservative multibody systems". *Fields Institute Commun.*, Vol. 10, pp. 25–43, 1996.

[Bart 98]   E. Barth, B. Leimkuhler, and S. Reich. "A Time-Reversible Variable-Stepsize Integrator for Constrained Dynamics". *Konrad-Zuse-Zentrum für Informationstechnik Berlin*, 1998.

[Bauc 03a] O. Bauchau, C. Bottasso, and Trainelli L. "Robust integration schemes for flexible multibody systems". *Comput. Methods Appl. Mech. Engrg.*, Vol. 192, pp. 395–420, 2003.

[Bauc 03b] O. Bauchau and L. Trainelli. "The Vectorial Parameterization of Rotation". *Nonlin. Dynamics*, Vol. 1, pp. 71–92, 2003.

[Bauc 96]   O. Bauchau and N. Theron. "Energy decaying scheme for non-linear beam models". *Comput. Methods Appl. Mech. Engrg.*, Vol. 134, pp. 37–56, 1996.

[Bauc 99a] O. Bauchau. "On the Modeling of Friction and Rolling in Flexible Multi-Body Systems". *Multibody System Dynamics*, Vol. 3, pp. 209–239, 1999.

[Bauc 99b] O. Bauchau and L. Bottasso. "On the Design of Energy Preserving and Decaying Schemes for Flexible, Nonlinear Multi-Body Systems". *Comput. Methods Appl. Mech. Engrg.*, Vol. 169, pp. 61–79, 1999.

[Beck 75]   E. Becker and W. Bürger. *Kontinuumsmechanik*. Teubner, 1975.

[Bely 01]   T. Belytschko, W. Liu, and B. Moran. *Nonlinear Finite Elements for Continua and Structures*. Prentice-Hall, 2001.

[Benz 05]   M. Benzi, G. Golub, and J. Liesen. "Numerical solution of saddle point problems". *Acta Numerica*, pp. 1–137, 2005.

[Bern 98]   R. Berndt. *Einführung in die symplektische Geometrie*. Vieweg, 1998.

[Bert 95]   D. Bertsekas. *Nonlinear Programming*. Athena Scientific, 1995.

[Bets 00a] P. Betsch and P. Steinmann. "Conserving properties of a time FE method – Part I: time-stepping schemes for N-body problems". *Int. J. Numer. Meth. Engng.*, Vol. 49, pp. 599–638, 2000.

[Bets 00b] P. Betsch and P. Steinmann. "Inherently Energy Conserving Time Finite Elements for Classical Mechanics". *J. Comput. Phys.*, Vol. 160, pp. 88–116, 2000.

[Bets 01a] P. Betsch and P. Steinmann. "Conserving properties of a time FE method – Part II: Time-stepping schemes for non-linear elastodynamics". *Int. J. Numer. Meth. Engng.*, Vol. 50, pp. 1931–1955, 2001.

[Bets 01b] P. Betsch and P. Steinmann. "Constrained integration of rigid body dynamics". *Comput. Methods Appl. Mech. Engrg.*, Vol. 191, pp. 467–488, 2001.

[Bets 02a]   P. Betsch. *Computational Methods for Flexible Multibody Dynamics*. Habilitationsschrift, Lehrstuhl für Technische Mechanik, Universität Kaiserslautern, 2002.

[Bets 02b]   P. Betsch and P. Steinmann. "Conserving properties of a time FE method – Part III: Mechanical systems with holonomic constraints". *Int. J. Numer. Meth. Engng.*, Vol. 53, pp. 2271–2304, 2002.

[Bets 02c]   P. Betsch and P. Steinmann. "A DAE Approach to Flexible Multibody Dynamics". *Multibody System Dynamics*, Vol. 8, pp. 367–391, 2002.

[Bets 02d]   P. Betsch and P. Steinmann. "Frame-indifferent beam finite elements based upon the geometrically exact beam theory". *Int. J. Numer. Meth. Engng.*, Vol. 54, pp. 1775–1788, 2002.

[Bets 03]   P. Betsch and P. Steinmann. "Constrained dynamics of geometrically exact beams". *Comput. Mech.*, Vol. 31, pp. 49–59, 2003.

[Bets 04]   P. Betsch. "A unified approach to the energy consistent numerical integration of nonholonomic mechanical systems and flexible multibody dynamics". *GAMM Mitteilungen*, Vol. 27, No. 1, pp. 66–87, 2004.

[Bets 05]   P. Betsch. "The discrete null space method for the energy consistent integration of constrained mechanical systems. Part I: Holonomic constraints". *Comput. Methods Appl. Mech. Engrg.*, Vol. 194, No. 50-52, pp. 5159–5190, 2005.

[Bets 06]   P. Betsch and S. Leyendecker. "The discrete null space method for the energy consistent integration of constrained mechanical systems. Part II: Multibody dynamics". *Int. J. Numer. Meth. Engng.*, 2006. in press.

[Bets 98]   P. Betsch, A. Menzel, and E. Stein. "On the parametrization of finite rotations in computational mechanics; A classification of concepts with application to smooth shells". *Comput. Methods Appl. Mech. Engrg.*, Vol. 155, pp. 273–305, 1998.

[Blaj 02]   W. Blajer. "Augmented Lagrangian Formulation: Geometrical Interpretation and Application to Systems with Singularities and Redundancy". *Multibody System Dynamics*, Vol. 8, pp. 141–159, 2002.

[Bone 97]   J. Bonet and R. Wood. *Nonlinear Continuum Mechanics for Finite Element Analysis*. Cambridge University Press, 1997.

[Born 96]   F. Bornemann and C. Schütte. "Homogenization of Hamiltonian systems with a strong constraining potential". *Physica D*, Vol. 102, pp. 57–77, 1996.

[Bott 02a]   C. Bottasso, O. Bauchau, and J. Choi. "An energy decaying scheme for nonlinear dynamics of shells". *Comput. Methods Appl. Mech. Engrg.*, Vol. 191, pp. 3099–3121, 2002.

[Bott 02b]   C. Bottasso, M. Borri, and L. Trainelli. "Geometric invariance". *Comput. Mech.*, Vol. 29, pp. 163–169, 2002.

[Bott 05]   C. Bottasso and O. Bauchau. "Time-step-size-independent conditioning and sensitivity to perturbations in the numerical solution of index three differential algebraic equations". *preprint*, 2005.

[Brem 04]   H. Bremer. "Robotik I". Vorlesung und Arbeitsgrundlage für weitere Vertiefungsstudien, Johannes Keppler Universität Linz, 2004.

[Bren 96]   L. Brenan, S. Campbell, and L. Petzold. *Numerical Solution of Initial-Value Problems in Differential-Algebraic Equations*. SIAM, 1996.

[Butc 87]   J. Butcher. *The Numerical Analysis of Ordinary Differential Equations. Runge-Kutta and General Linear Methods*. John Wiley & Sons, 1987.

[Card 89]   A. Cardona and M. Geradin. "Time integration of the equations of motion in mechanism analysis". *Comput. Struct.*, Vol. 33, pp. 801–820, 1989.

[Choq 77]   Y. Choquet-Bruhat, C. De Witt-Morett, and M. Dillard-Bleick. *Analysis, Manifolds and Physics*. North-Holland, 1977.

[Cris 96]   M. Crisfield and J. Shi. "An Energy Conserving Co-Rotational Procedure for Non-Linear Dynamics with Finite Elements". *Nonlin. Dynamics*, Vol. 9, pp. 37–52, 1996.

[Cris 99]   M. Crisfield and G. Jelenić. "Objectivity of strain measures in the geometrically exact three-dimensional beam theory and its finite-element implementation". *Proc. R. Soc. Lond. A*, Vol. 455, pp. 1125–1147, 1999.

[Deuf 00]   P. Deuflhard and F. Bornemann. *Scientific Computing with Ordinary Differential Equations*. Springer, 2000.

[Deuf 03]   P. Deuflhard and A. Hohmann. *Numerical Analysis in Modern Scientific Computing*. Springer, 2003.

[Diaz 03]   J. Dìaz and C. Führer. "A wavelet semidiscretisation of elastic multibody systems". *ZAMM*, Vol. 83, No. 10, pp. 677–689, 2003.

[Dira 50]   P. Dirac. "On generalized Hamiltonian dynamics". *Can. J. Meth.*, Vol. 2, pp. 129–148, 1950.

[Eich 98]   E. Eich-Soellner and C. Führer. *Numerical Methods in Multibody Dynamics*. Teubner, 1998.

[Fisc 97]   G. Fischer. *Lineare Algebra*. Vieweg, 1997.

[Fuhr 88]   C. Führer. *Differential-algebraische-Gleichungssysteme in mechanischen Mehrkörpersystemen. Theorie, numerische Ansätze und Anwendungen*. PhD thesis, Technische Universität München, 1988.

[Fuhr 91]   C. Führer and B. Leimkuhler. "Numerical Solution of Differential-Algebraic Equations for Constrained Mechanical Motion". *Numer. Math.*, Vol. 59, pp. 55–69, 1991.

[Ge 88]   Z. Ge and J. Marsden. "Lie-Poisson Hamilton-Jacobi Theory and Lie-Poisson integrators". *Physics Letters A*, Vol. 133, No. 3, pp. 134–139, 1988.

[Gear 85]   C. Gear, G. Gupta, and B. Leimkuhler. "Automatic integration of the Euler-Lagrange equations with constraints". *J. Comp. Appl. Math.*, Vol. 12, pp. 77–90, 1985.

[Gera 01]   M. Géradin and A. Cardona. *Flexible Multibody Dynamics*. John Wiley & Sons, 2001.

[Gold 85]   H. Goldstein. *Klassische Mechanik*. Aula, 1985.

[Gonz 00]   O. Gonzalez. "Exact Energy-Momentum Conserving Algorithms for General Models in Nonlinear Elasticity". *Comput. Methods Appl. Mech. Engrg.*, Vol. 190, pp. 1763–1783, 2000.

[Gonz 96a]   O. Gonzalez. *Design and analysis of conserving integrators for nonlinear Hamiltonian systems with symmetry*. PhD thesis, Stanford University, 1996.

[Gonz 96b]   O. Gonzalez. "On the Stability of Symplectic and Energy-Momentum Algorithms for Nonlinear Hamiltonian systems with Symmetry". *Comput. Methods Appl. Mech. Engrg.*, Vol. 134, pp. 197–222, 1996.

[Gonz 96c]   O. Gonzalez. "Time Integration and Discrete Hamiltonian Systems". *J. Nonlinear Sci.*, Vol. 6, pp. 449–467, 1996.

[Gonz 99]   O. Gonzalez. "Mechanical Systems Subject to Holonomic Constraints: Differential-Algebraic Formulations and Conservative Integration". *Physica D*, Vol. 132, pp. 165–174, 1999.

[Grah 02]   E. Graham, G. Jelenic, and M. A. Crisfield. "A note on the equivalence of two recent time-integration schemes for N-body problems". *Commun. Numer. Methods Engng.*, Vol. 18, pp. 615–620, 2002.

[Gree 88]   D. Greenwood. *Principles of Dynamics*. Prentice-Hall, 1988.

[Gros 00]   M. Groß, P. Betsch, and P. Steinmann. "Comparison of Galerkin Methods applied to Classical Mechanics". UKL/LTM report J00-07, 2000.

[Gros 04]   M. Groß. *Conserving Time Integrators for Nonlinear Elastodynamics*. PhD thesis, Universität Kaiserslautern, 2004.

[Gros 05]   M. Groß, P. Betsch, and P. Steinmann. "Conservation properties of a time FE method. Part IV: Higher order energy and momentum conserving schemes". *Int. J. Numer. Methods Engng.*, Vol. 63, pp. 1849–1897, 2005.

[Hair 00]   E. Hairer and C. Lubich. "Long-time energy conservation of numerical methods for oscillatory differential equations". *SIAM J. Numer. Anal.*, Vol. 38, pp. 414–441, 2000.

[Hair 04]   E. Hairer, G. Wanner, and C. Lubich. *Geometric Numerical Integration: Structure-Preserving Algorithms for Ordinary Differential Equations*. Springer, 2004.

[Hair 89]   E. Hairer, C. Lubich, and M. Roche. *The numerical solution of differential algebraic equations by Runge-Kutta methods*. Springer, 1989.

[Hair 93]   E. Hairer, S. Nørsett, and G. Wanner. *Solving Ordinary Differential Equations I. Nonstiff Problems*. Vol. 8 of *Springer Series in Computational Mathematics*, Springer, 1993.

[Hair 96]   E. Hairer and G. Wanner. *Solving Ordinary Differential Equations II. Stiff and Differential-Algebraic Problems.* Vol. 14 of *Springer Series in Computational Mathematics*, Springer, 1996.

[Hilb 77]   H. Hilber, T. Hughes, and R. Taylor. "Improved Numerical Dissipation for Time Integration Algorithms in Structural Dynamics". *Earthquake Engineering and Structural Dynamics*, Vol. 5, pp. 283–292, 1977.

[Hofe 94]   H. Hofer and E. Zehnder. *Symplectic Invariants and Hamiltonian Dynamics.* Birkhäuser, 1994.

[Holz 00]   G. Holzapfel. *Nonlinear Solid Mechanics.* Wiley, 2000.

[Hugh 00]   T. Hughes. *The Finite Element Method. Linear Static and Dynamic Finite Element Analysis.* Dover, 2000.

[Hugh 78]   T. Hughes, T. Caughey, and W. Liu. "Finite-Element Methods for Nonlinear Elastodynamics Which Conserve Energy". *ASME J. Appl. Mech.*, Vol. 45, pp. 366–370, 1978.

[Ibra 00a] A. Ibrahimbegović and S. Mamouri. "On rigid components and joint constraints in nonlinear dynamics of flexible multibody systems employing 3d geometrically exact beam model". *Comp. Meth. Appl. Mech. Engrg.*, Vol. 188, pp. 805–831, 2000.

[Ibra 00b] A. Ibrahimbegović, S. Mamouri, R. Taylor, and A. Chen. "Finite element method in dynamics of flexible multibody systems: Modeling of holonomic constraints and energy conserving integration schemes". *Multibody System Dynamics*, Vol. 4, pp. 195–223, 2000.

[Ibra 02a] A. Ibrahimbegović and S. Mamouri. "Energy consering/decaying implicit time-stepping scheme for nonlinear dynamics of three-dimensional beams undergoing finite rotations". *Comput. Methods Appl. Mech. Engrg.*, pp. 4241–4258, 2002.

[Ibra 02b] A. Ibrahimbegović and R. Taylor. "On the role of frame-invariance in structural mechanics models at finite rotations". *Comput. Methods Appl. Mech. Engrg.*, pp. 5159–5176, 2002.

[Ibra 03]   A. Ibrahimbegović, R. Taylor, and H. Lim. "Non-linear dynamics of flexible multibody systems". *Comput. Struct.*, Vol. 81, pp. 1113–1132, 2003.

[Ibra 95]   A. Ibrahimbegović, F. Frey, and I. Kozar. "Computational aspects of vector-like parametrization of three-dimensional finite rotations". *Int. J. Numer. Meth. Engng.*, Vol. 38, pp. 3653–3673, 1995.

[Ibra 97]   A. Ibrahimbegović. "On the joice of finite rotation parameters". *Comput. Methods Appl. Mech. Engrg.*, Vol. 149, pp. 49–71, 1997.

[Ibra 98]   A. Ibrahimbegović and S. Mamouri. "Finite rotations in dynamics of beams and implicit time-stepping schemes". *Int. J. Numer. Meth. Engng.*, Vol. 41, pp. 781–814, 1998.

[Ibra 99]   A. Ibrahimbegović and S. Mamouri. "Nonlinear dynamics of flexible beams in planar motion: formulation and time-stepping scheme for stiff problems". *Comput. Struct.*, Vol. 70, pp. 1–22, 1999.

[Jay 96]   L. Jay. "Symplectic Partitioned Runge-Kutta Methods for Constrained Hamiltonian Systems". *SIAM J. Numer. Anal.*, Vol. 33, No. 1, pp. 368–387, 1996.

[Jele 01]   G. Jelenić and M. Crisfield. "Dynamic analysis of 3D beams with joints in presence of large rotations". *Comput. Methods Appl. Mech. Engrg.*, Vol. 190, pp. 4195–4230, 2001.

[Jele 02]   G. Jelenić and M. Crisfield. "Problems associated with the use of Cayley transform and tangent scaling for conserving energy and momenta in the Reissner-Simo beam theory". *Commun. Numer. Meth. Engng.*, Vol. 18, pp. 711–720, 2002.

[Jele 96]   G. Jelenić and M. Crisfield. "Non-linear 'master-slave' relationships for joints in 3D beams with large rotations". *Comp. Meth. Appl. Mech. Engrg.*, Vol. 135, pp. 211–228, 1996.

[Jele 98]   G. Jelenić and M. Crisfield. "Interpolation of rotational variables in non-linear dynamics of 3D beams". *Int. J. Numer. Meth. Engng.*, Vol. 43, pp. 1193–1222, 1998.

[Jele 99]   G. Jelenić and M. Crisfield. "Geometrically exact 3D beam theory: implementation of a strain-invariant finite element for statics and dynamics". *Comput. Methods Appl. Mech. Engrg.*, Vol. 171, pp. 141–171, 1999.

[Kane 00]   C. Kane, J. Marsden, M. Ortiz, and M. West. "Variational Integrators and the Newmark Algorithm for Conservative and Dissipative Mechanical Systems". *Int. J. Numer. Meth. Engng.*, Vol. 49, pp. 1295–1325, 2000.

[Kim 86]   S. Kim and M. Vanderploeg. "QR decomposition for state space representation of constrained mechanical dynamic systems". *J. Mech. Trans. Auto. Des.*, Vol. 108, pp. 183–188, 1986.

[Kreu 79]   E. Kreuzer. *Symbolische Berechnung der Bewegungsgleichungen von Mehrkörpersystemen.* Vol. 11, Fortschrittsbericht der VDI Zeitschriften, 1979.

[Krys 05a]   P. Krysl. "Direct time integration of rigid body motion with discrete-impulse midpoint approximation: explicit Newmark algorithms". *preprint*, 2005.

[Krys 05b]   P. Krysl. "Explicit momentum-conserving integrator for dynamics of rigid bodies approximationg the midpoint Lie algorithm". *Int. J. Numer. Meth. Engng.*, Vol. 63, pp. 2171–2193, 2005.

[Kuyp 03]   F. Kuypers. *Klassische Mechanik.* Wiley, 2003.

[LaBu 76a]   R. A. LaBudde and D. Greenspan. "Energy and Momentum Conserving Methods of Arbitrary Order for the Numerical Integration of Equations of Motion, I. Motion of a Single Particle". *Numer. Math.*, Vol. 25, pp. 323–346, 1976.

[LaBu 76b]   R. A. LaBudde and D. Greenspan. "Energy and Momentum Conserving Methods of Arbitrary Order for the Numerical Integration of Equations of Motion, II. Motion of a System of Particles". *Numer. Math.*, Vol. 26, pp. 1–16, 1976.

[Laue]   S. Lauer. "Numerical Integration Methods that Preserve Mechanical Invariants and Holonomic Constraints". Diplomarbeit, Universität Kaiserslautern, 2002.

[Leim 04]   B. Leimkuhler and S. Reich. *Simulating Hamiltonian Dynamics*. Cambridge University Press, 2004.

[Leim 94]   B. Leimkuhler and S. Reich. "Symplectic integration of constrained Hamiltonian systems". *Mathematics of Computations*, Vol. 63, pp. 589–605, 1994.

[Leim 96]   B. Leimkuhler and G. Patrick. "A Sympletic Integrator for Riemannian Manifolds". *J. Nonlinear Sci.*, pp. 1–19, 1996.

[Lerb 05]   J. Lerbet. "Coordinate-free kinematic analysis of overconstrained mechanisms with mobility one". *ZAMM*, Vol. 85, No. 10, pp. 740–747, 2005.

[Lew 03]   A. Lew, J. Marsden, M. Ortiz, and M. West. "Asynchronous Variational Integrators". *Arch. Rational Mech. Anal.*, Vol. 167, pp. 85–146, 2003.

[Leye 04]   S. Leyendecker, P. Betsch, and P. Steinmann. "Energy-conserving integration of constrained Hamiltonian systems – a comparison of approaches". *Comput. Mech.*, Vol. 33, pp. 174–185, 2004.

[Leye 06]   S. Leyendecker, P. Betsch, and P. Steinmann. "Objective energy-momentum conserving integration for the constrained dynamics of geometrically exact beams". *Comput. Methods Appl. Mech. Engrg.*, Vol. 195, pp. 2313–2333, 2006.

[Lian 87]   C. Liang and G. Lance. "A differentiable null space method for constrained dynamic analysis". *J. Mech. Trans. Auto. Des.*, Vol. 109, pp. 405–411, 1987.

[Luen 84]   D. Luenberger. *Linear and Nonlinear Programming*. Addison-Wesley, 1984.

[Magn 71]   K. Magnus. *Kreisel, Theorie und Anwendungen*. Springer, 1971.

[Mars 01]   J. Marsden and M. West. "Discrete mechanics and variational integrators". *Acta Numerica*, pp. 357–514, 2001.

[Mars 83]   J. Marsden and T. Hughes. *Mathematical Foundations of Elasticity*. Dover, 1983.

[Mars 92]   J. Marsden. *Lectures on Mechanics*. Cambridge University Press, 1992.

[Mars 94]   J. Marsden and T. Ratiu. *Introduction to Mechanics and Symmetry. A Basic Exposition of Classical Mechanical Systems. Texts in Applied Mathematics 17*, Springer, 1994.

[Mars 99]   J. Marsden, C. Kane, and M. Ortiz. "Symplectic-energy-momentum preserving variational integrators". *J. Math. Phys.*, Vol. 40, No. 7, pp. 3353–3371, 1999.

[Noel 04a]   L. Noels, L. Stainier, and J. P. Ponthot. "An energy-momentum conserving algorithm for non-linear hypoelastic constitutive models". *Int. J. Numer. Meth. Engng.*, No. 59, pp. 83–114, 2004.

[Noel 04b]   L. Noels, L. Stainier, and J. P. Ponthot. "On the use of large time steps with an energy momentum conserving algorithm for non-linear hypoelastic constitutive models". *Int. J. Numer. Meth. Engng.*, No. 41, pp. 663–693, 2004.

[Nolt 02]   W. Nolting. *Grundkurs Theoretische Physik 2: Analytische Mechnaik*. Springer, 2002.

[Olve 86]   P. Olver. *Applications of Lie Groups to Differential Equations. Graduate Texts in Mathematics*, Springer, 1986.

[Olve 95]   P. Olver. *Equivalence, Invariants and Symmetry.* Cambridge University Press, 1995.

[Pesk 95]   M. Peskin and D. Schroeder. *An Introduction to Quantum Field Theory.* Addison-Wesley, 1995.

[Petz 86]   L. Petzold and P. Loetstedt. "Numerical Solution of Nonlinear Differential Equations with Algebraic Constraints II: Practical Implications". *SIAM J. Sci. Comput.*, Vol. 7, No. 3, pp. 720–733, 1986.

[Reic 94]   S. Reich. "Momentum conserving symplectic integrations". *Physica D*, Vol. 76, No. 4, pp. 375–383, 1994.

[Reic 95]   S. Reich. "Enhancing energy conserving methods". *BIT*, Vol. 36, pp. 122–134, 1995.

[Reic 96]   S. Reich. "Symplectic integrators for systems of rigis bodies". *Fields Institute Commun.*, Vol. 10, pp. 181–191, 1996.

[Rhei 84]   W. Rheinboldt. "Differential-Algebraic Systems as Differential Equations on Manifolds". *Mathematics of Computation*, Vol. 43, No. 168, pp. 473–482, 1984.

[Rhei 91]   W. Rheinboldt. "On the Existence and Uniqueness of Solutions of Nonlinear Semi-implicit Differential-Algebraic Equations". *Nonlinear Anal. Theor. Methods Appl*, Vol. 16, No. 7-8, pp. 647–661, 1991.

[Rhei 96]   W. Rheinboldt. "MANPAK: A Set of Algorithms for Computations on Implicitly Defined Manifolds". *Computers Math. Applic.*, Vol. 32, No. 12, pp. 15–28, 1996.

[Rhei 97]   W. Rheinboldt. "Solving Algebraically Explicit DAEs with the MANPAK-Manifold-Algorithms". *Computers Math. Applic.*, Vol. 33, No. 3, pp. 31–43, 1997.

[Rome 02a]   I. Romero and F. Armero. "Numerical integration of the stiff dynamics of geometrically exact shells: an energy-dissipative momentum-conserving scheme". *Int. J. Numer. Meth. Engng.*, Vol. 54, pp. 1043–1086, 2002.

[Rome 02b]   I. Romero and F. Armero. "An objective finite element approximation of the kinematics of geometrically exact rods and its use in the formulation of an energy-momentum scheme in dynamics". *Int. J. Numer. Meth. Engng.*, Vol. 54, pp. 1683–1716, 2002.

[Rome 04]   I. Romero. "The interpolation of rotations and its application to finite element models of geometrically exact rods". *Comput. Mech.*, Vol. 34, pp. 121–133, 2004.

[Rubi 57]   H. Rubin and P. Ungar. "Motion under a strong constraining force". *Commun. Pure Appl. Math.*, Vol. 10, No. 1, pp. 65–87, 1957.

[Saha 99]   S. Saha. "Dynamic modelling of serial multi-body systems using the decoupled natural orthogonal complement matrices". *ASME J. Appl. Mech.*, Vol. 66, pp. 986–996, 1999.

[Sans 03]   C. Sansour and W. Wagner. "Multiplicative updating of the rotation tensor in the finite element analysis of rods and shells – a path independent approach". *Comp. Mech.*, Vol. 31, pp. 153–162, 2003.

[Scha 27]   P. Schatz. *Der Weg zur künstlerischen Gestaltung in der Kraft des Bewusstseins.* Eigenverlag, 1927.

[Scha 98]   P. Schatz. *Rhythmusforschung und Technik*. Verlag Freies Geistesleben, 2., erweiterte Auflage 1998.

[Schi 86]   W. Schiehlen. *Technische Dynamik*. Teubner, 1986.

[Seil 99]   W. Seiler. "Numerical Integration of Constrained Hamiltonian Systems using Dirac Brackets". *Mathematics of Computation*, Vol. 68, No. 226, pp. 661–681, 1999.

[Simo 85]   J. Simo. "A finite strain beam formulation. The three-dimensional dynamic problem. Part I". *Comput. Methods Appl. Mech. Engrg.*, Vol. 49, pp. 55–70, 1985.

[Simo 86a]   J. Simo and T. Hughes. "On the Variational Foundations of Assumed Strain Methods". *ASME J. Appl. Mech.*, Vol. 53, pp. 51–54, 1986.

[Simo 86b]   J. Simo and L. Vu-Quoc. "A three-dimensional finite-strain rod model. Part II: Computational Aspects". *Comput. Methods Appl. Mech. Engrg.*, Vol. 58, pp. 79–116, 1986.

[Simo 88]   J. Simo and L. Vu-Quoc. "On the dynamics in space of rods undergoing large motions – A geometrically exact approach". *Comput. Methods Appl. Mech. Engrg.*, Vol. 66, pp. 125–161, 1988.

[Simo 91a]   J. Simo, D. Lewis, and J. Marsden. "Stability of Relative Equilibria. Part I: The Reduced Energy-Momentum Method". *Arch. Rational Mech. Anal.*, Vol. 115, pp. 15–59, 1991.

[Simo 91b]   J. Simo and K. Wong. "Unconditionally Stable Algorithms For Rigid Body Dynamics That Exactly Preserve Energy and Momentum". *Int. J. Numer. Methods Engrg.*, Vol. 31, pp. 19–52 and 1321–1323, 1991.

[Simo 92a]   J. Simo and N. Tarnow. "The discrete energy-momentum method. Conserving algorithms for nonlinear elastodynamics". *ZAMP*, Vol. 43, 1992.

[Simo 92b]   J. Simo, N. Tarnow, and K. Wong. "Exact Energy-Momentum Conserving Algorithms and Symplectic Schemes for Nonlinear Dynamics". *Comput. Methods Appl. Mech. Engrg.*, No. 100, pp. 1–56, 1992.

[Simo 93]   J. Simo and O. Gonzalez. "Assessment of Energy-Momentum and Symplectic Schemes for Stiff Dynamical Systems". In: *American Society of Mechanical Engineers*, ASME Winter Annual Meeting, New Orleans, Louisiana, 1993.

[Simo 94]   J. Simo and N. Tarnow. "A new energy and momentum conserving algorithm for the non-linear dynamics of shells". *Int. J. Numer. Meth. Engng.*, Vol. 37, pp. 2527–2549, 1994.

[Simo 95]   J. Simo, N. Tarnow, and M. Doblare. "Non-linear dynamics of three-dimensional rods: Exact energy and momentum conserving algorithms". *Int. J. Numer. Meth. Engng.*, Vol. 38, pp. 1431–1473, 1995.

[Toro 00]   J. Török. *Analytical Mechanics with an Introduction to Dynamical Systems*. John Wiley & Sons, 2000.

[Warb 76]   G. Warburton. *The Dynamical Behaviour of Structures*. Pergamon, 1976.

[Wend 97]   J. Wendlandt and J. Marsden. "Mechanical Integrators Derived from a Discrete Variational Principle". *Physica D*, Vol. 106, pp. 223–246, 1997.

[Witt 77]   J. Wittenburg. *Dynamics of systems of rigid bodies*. Teubner, 1977.

[Wrig 01]   P. Wriggers. *Nichtlineare Finite-Elemente-Methoden*. Springer, 2001.

[Yen 98]   J. Yen and L. Petzold. "An Efficient Newton-Type Iteration for Numerical Solution of Highly Oscillatory Constrained Multibody Dynamic Systems". *SIAM J. Sci. Comput.*, Vol. 19, No. 5, pp. 1510–1534, 1998.

[Zien 92]   O. Zienkiewicz and R. Taylor. *The Finite Element Method, Volume 2*. McGraw-Hill, 1992.

[Zien 94]   O. Zienkiewicz and R. Taylor. *The Finite Element Method, Volume 1*. McGraw-Hill, 1994.

Curriculum vitae

name	Sigrid Leyendecker
date of birth	05.07.1977
place of birth	Kaiserslautern, Germany

professional development

since 08.02	research associate at Chair of Applied Mechanics, University of Kaiserslautern
11.98 - 02.02	student work contract at Fraunhofer-Institut für Techno- und Wirtschaftsmathematik (ITWM, Institute for Industrial Mathematics), Kaiserslautern
08.99 - 11.99	vocational training at Commonwealth Scientific and Industrial Research Organisation (CSIRO), Sydney, Australia

education and qualifications

10.96 - 07.02	Technomathematics, University of Kaiserslautern; Diploma
03.99 - 07.02	European Consortium for Mathematics in Industry (ECMI) certification of Postgraduate Programme: Mathematics for Industry
08.87 - 06.96	Gymnasium am Rittersberg, Kaiserslautern; general qualification for university entrance (Abitur)